Gastroenterology Research and Practice

Drug Discovery and Mechanism Exploration by Targeting Hepatic Dysfunction

Lead Guest Editor: Xiude Fan
Guest Editors: Changli Zhou and Enfa Zhao

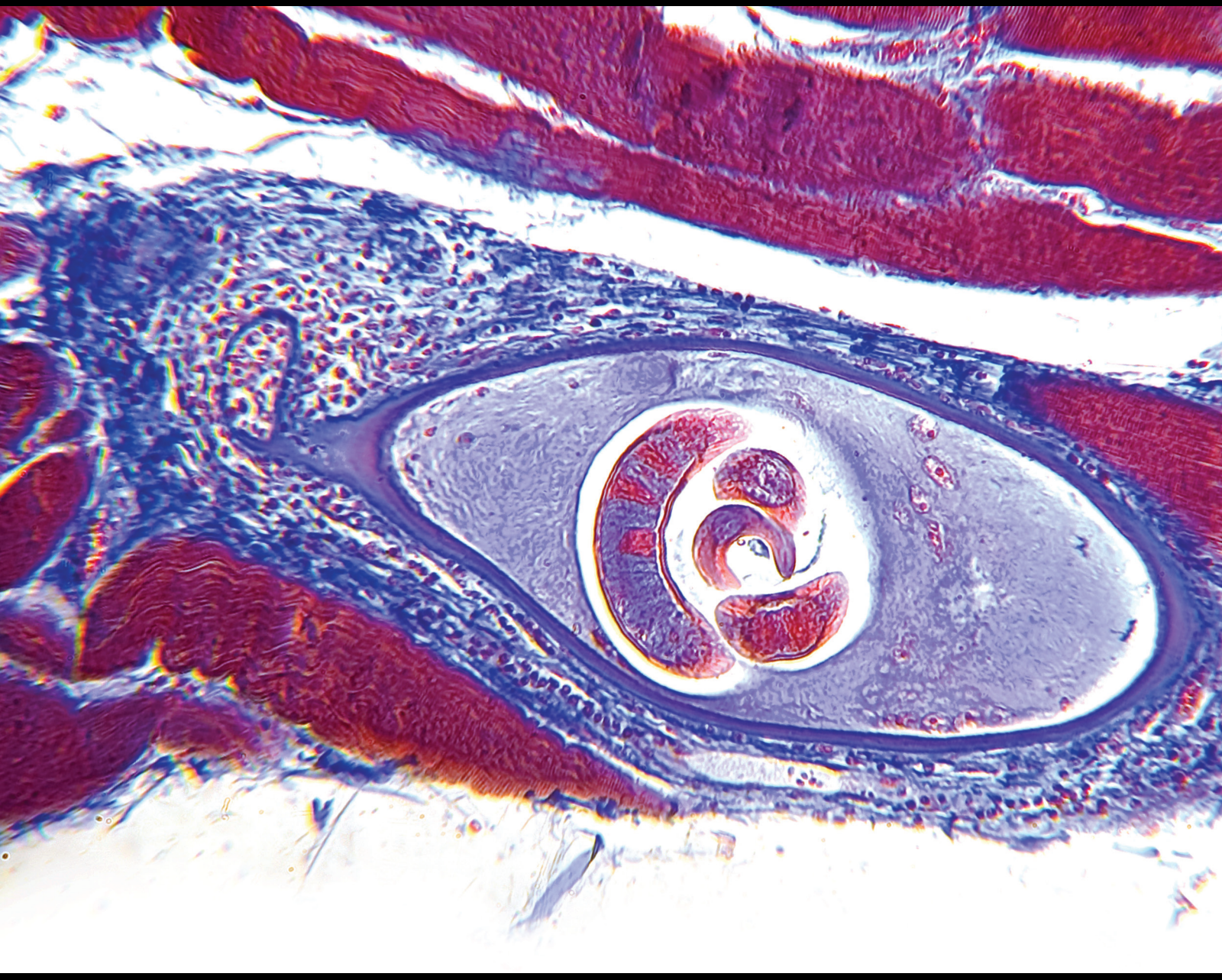

Drug Discovery and Mechanism Exploration by Targeting Hepatic Dysfunction

Gastroenterology Research and Practice

Drug Discovery and Mechanism Exploration by Targeting Hepatic Dysfunction

Lead Guest Editor: Xiude Fan
Guest Editors: Changli Zhou and Enfa Zhao

Contents

Hindawi
Gastroenterology Research and Practice
Volume 2023, Article ID 2479192, 17 pages
https://doi.org/10.1155/2023/2479192

Research Article

EMP1 as a Potential Biomarker in Liver Fibrosis: A Bioinformatics Analysis

Xuchen Chen,[1] Xinliang Lv,[2] Manman Han,[1] Yexiao Hu,[1] Wanqiong Zheng,[1] Haibo Xue,[3] Zhuokai Li,[2] Kui Li,[4] and Wei Tan[2]

[1]*Department of General Surgery, Wenzhou Hospital of Integrated Traditional Chinese and Western Medicine Wenzhou, Zhejiang, China*
[2]*Department of Hepatobiliary and Pancreatic Surgery, Lishui Municipal Central Hospital, The Fifth Affiliated Hospital of Wenzhou Medical University Lishui, Zhejiang, China*
[3]*Department of Gastroenterology, The First Affiliated Hospital of Wenzhou Medical University Wenzhou, Zhejiang, China*
[4]*Department of Blood Transfusion, Lishui Central Hospital, Fifth Affiliated Hospital of Wenzhou Medical College Lishui, Zhejiang, China*

Correspondence should be addressed to Wei Tan; tanwei112854@163.com

Received 6 May 2022; Revised 16 July 2022; Accepted 5 September 2022; Published 22 March 2023

Academic Editor: Enfa Zhao

Liver fibrosis is a wound-healing response to chronic injury, which may result in cirrhosis and liver failure. Studies have been carried on the mechanisms and pathogenesis of liver fibrosis. However, the potential cell-specific expressed marker genes involved in fibrotic processes remain unknown. In this study, we combined a publicly accessible single-cell transcriptome of human liver with microarray datasets to evaluate the cell-specific expression patterns of differentially expressed genes in the liver. We noticed that *EMP1* (epithelial membrane protein 1) is significantly active not only in CCl_4 (carbon tetrachloride)-treated mouse liver fibrosis but also in BDL (bile duct ligation)-induced liver fibrosis and even in human fibrotic liver tissues such as alcoholic hepatitis, NASH (nonalcoholic steatohepatitis), and advanced stage liver fibrosis. Furthermore, we demonstrated that EMP1 is a specific fibrotic gene expressed in HSCs (hepatic stellate cells) and endothelial cells using the Protein Atlas single-cell transcriptome RNA-sequencing clustering. Its expression was significantly elevated in fibrotic HSCs or CCl_4 and NASH-induced fibroblasts. Previous research revealed that *EMP1* plays a role in proliferation, migration, metastasis, and tumorigeneses in different cancers via a variety of mechanisms. Because HSC activation and proliferation are two important steps following liver injury, it would be interesting to investigate the role of EMP1 in these processes. All of this information suggested that EMP1 could be used as a novel fibrotic liver marker and a possible target in the future.

1. Introduction

Liver fibrosis is an abnormal accumulation of extracellular matrix (ECM) proteins, such as collagen, that occurs in the majority of chronic liver disease, and cirrhosis, liver failure, and portal hypertension are all symptoms of advanced liver fibrosis [1]. Liver inflammation is caused by chronic liver damage that disrupts the physiological architecture of the liver tissue [2]. During the injury, hepatocytes apoptosis and emit damage-associated patterns, which recruit and activate lymphocytes and macrophages, as well as promote pro-fibrotic myofibroblast activation [3]. These myofibroblasts are primarily derived from transdifferentiation resident hepatic stellate cells (HSCs) [4]. However, the fate of liver might either be an anti-fibrotic, scar-dissolving stage, or an unconstrained fibrosis-promoting stage by liver non-parenchymal cells [5]. A number of pathways and mediators, such as autophagy, endoplasmic reticulum stress, oxidative stress, retinol and cholesterol metabolism, epigenetics, and receptor-mediated signals, demonstrate the complexities of HSC activation [6, 7]. The novel possible marker genes that may be important in these processes, on the other hand, remain unexplored.

Table 1: The characteristics of the included datasets.

Datasets	Species	Samples
GSE141821	Mice	$N = 36$, 18 CCl4 induced liver injury and 18 control
GSE55747	Mice	$N = 17$, 13 CCl4 induced liver fibrosis and 18 control
GSE80601	Mice	$N = 10$, 5 CCl4 induced liver fibrosis and 5 control
GSE103580	Human	$N = 86$, 67 cirrhosis samples and 19 control
GSE139994	Rat	$N = 9$, 6 CCl4 induced liver fibrosis and 3 control
GSE27640	Mice	$N = 4$, 2 CCl4 induced liver fibrosis and 2 control
GSE28619	Human	$N = 22$, 15 alcoholic hepatitis and 7 control
GSE40041	Mice	$N = 24$, 12 CCl4 induced liver fibrosis and 12 control
GSE73499	Rat	$N = 12$, 12 rat model of liver cirrhosis

In this study, we combined single-cell RNA sequence data from liver samples with a conventional microarray dataset from public database to identify marker genes that are expressed in HSCs and respond during the fibrotic process. We discovered that *EMP1* (epithelial membrane protein 1) is significantly activated not only in CCl_4 (carbon tetrachloride)-treated mice liver, but also in BDL (bile duct ligation)-induced mice liver fibrosis and even in human fibrotic liver tissues such as alcoholic hepatitis, NASH (non-alcoholic steatohepatitis), and also liver with advanced stage disease. Furthermore, we proved *EMP1* is a particular fibrotic gene expressed in HSCs and endothelial cells (EC) utilizing the single-cell transcriptome RNA-sequencing clustering result from ProtinAtlas database, and its expression was dramatically elevated in both CCl_4 and NASH-induced fibroblasts. Previous studies found that *EMP1* regulates cancer cell migration and proliferation, and we suspect it has a similar role in activated HSCs [8, 9]. The epithelial membrane proteins (EMPs) are encoded by the peripheral myelin protein 22 kDa (PMP22) gene family, and involved in tumor cell migration, growth, and differentiation. EMP1 is also known as CL-40, tumor-associated membrane protein. The EMP1 protein consists of 157 amino acids and is a glycoprotein containing four highly conserved hydrophobic transmembrane domains localized on the membrane. All of this information showed that EMP1 might be employed as a novel fibrotic liver marker and could be a potential target in the future.

2. Materials and Methods

2.1. Gene Expression Profile Data. All gene expression microarray matrix were collected from the NCBI (National Center for Biotechnology Information) GEO (Gene Expression Omnibus), which is a database repository of high throughput gene expression data and hybridization arrays, chips, and microarrays [10].

2.2. Differentially Expressed Gene (DEG) Analysis. The expression matrix from microarray dataset GSE141821 [11], GSE55747, and GSE80601 [12] downloaded from GEO was automatically loaded into R statistical software (version 3.8.0, https://www.r-project.org/) and DEGs was generated using the limma package (version 3.46.0) [13]. Genes are considered to be differentially expressed if they have an absolute log2 fold change of >1 at FDR of <0.05. For all the other microarray dataset including GSE103580 [14], GSE139994 [15], GSE27640 [16], GSE28619 [17], GSE40041 [18], GSE49541 [19], and GSE73499 [20], the GEO2R analysis was used to acquire EMP1 expression values and construct differential expressions [21]. All the datasets related information could be found in the GEO database. The dataset information is shown in Table 1.

2.3. Function Enrichment Analysis. We uploaded the DEGs into Metascape (https://metascape.org/) and conducted Gene Ontology (GO), Kyoto Encyclopedia of Genes and Genomes (KEGG) enrichment analyses, and Minimal Common Oncology Data Elements (MCODE) enrichment analysis [22]. The results of GO and KEGG analysis were visualized in the R ggplot2 package (v 3.3.3). Meanwhile, DEGs were submitted into the STRING (Search Tool for the Retrieval of Interacting Genes/Proteins) database (v11.0) using the medium confidence (interaction score >0.400) parameter [23]. Functional annotation enrichment was also performed in STRING and top enriched pathways were visualized in R using ggplot2 package (v 3.3.3).

2.4. Liver Tissue Single-Cell Analysis. Because numerous cells are involved in the course of liver fibrosis, the expression of common genes in these cells was examined to see if they induce fibrosis by controlling the function (migration) of these cells. In this study, we used the Protein Atlas [24] and PanglaoDB databases [25] to investigate for specific expression patterns of *EMP1*. Protein Atlas is an interactive open-access database (http://www.proteinatlas.org/) to allow genome-wide exploration of the impact of individual proteins on clinical outcomes. PanglaoDB (https://panglaodb.se/) is a database for the scientific community interested in investigating single-cell RNA-sequencing research from mice and humans.

2.5. GEPIA Database Analysis. The GEPIA (Gene Expression Profiling Interactive Analysis) [26] is a website that contains the sequenced RNA expression data of 9736 cancers and 8587 normal samples from the TCGA and GTEx (the genotype-tissue expression) projects (http://gepia.cancer-pku.cn). Pearson's correlation was utilized to validate the strong positive correlations of EMP1 with other fibrotic-related genes,

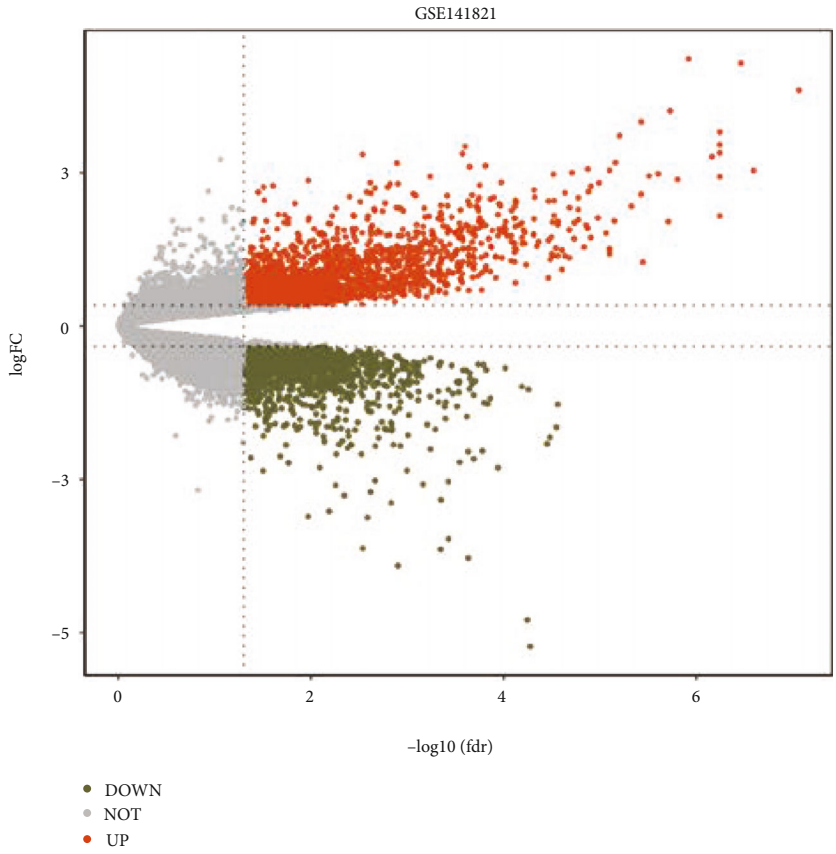

(a)

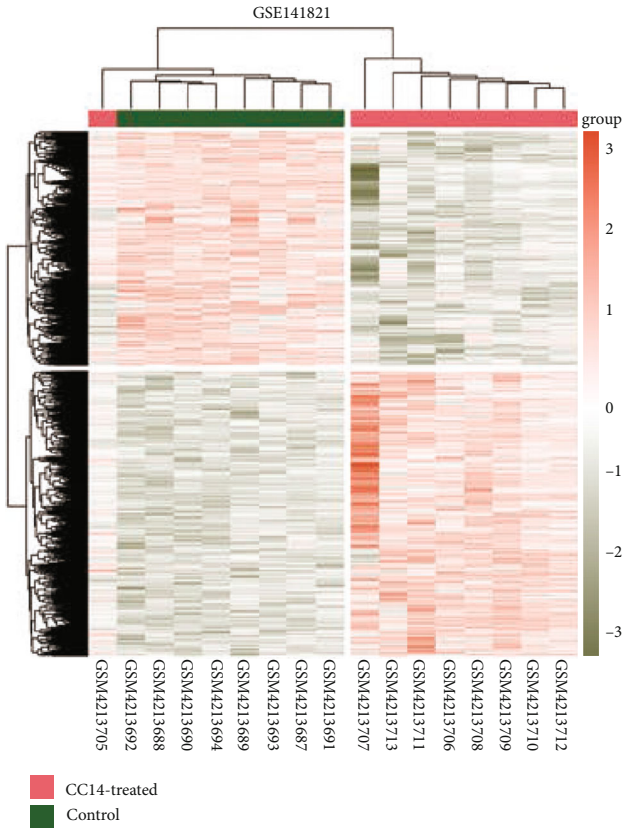

(b)

Figure 1: Continued.

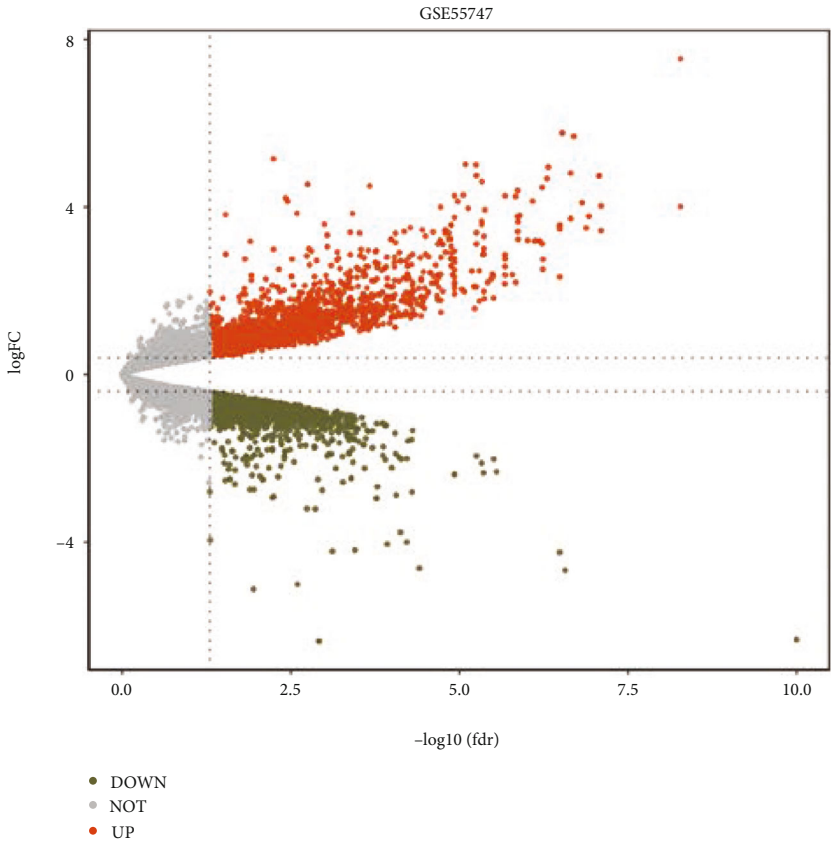

(c)

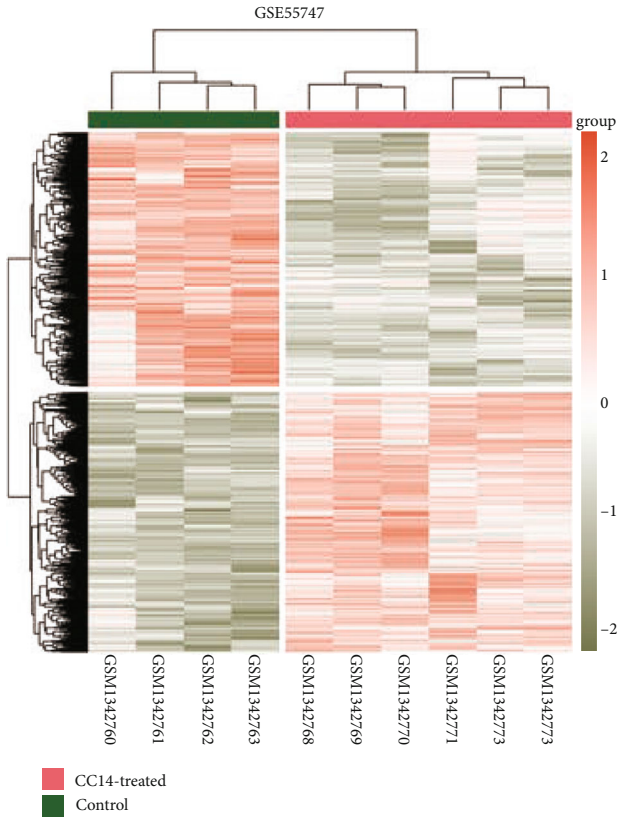

(d)

Figure 1: Continued.

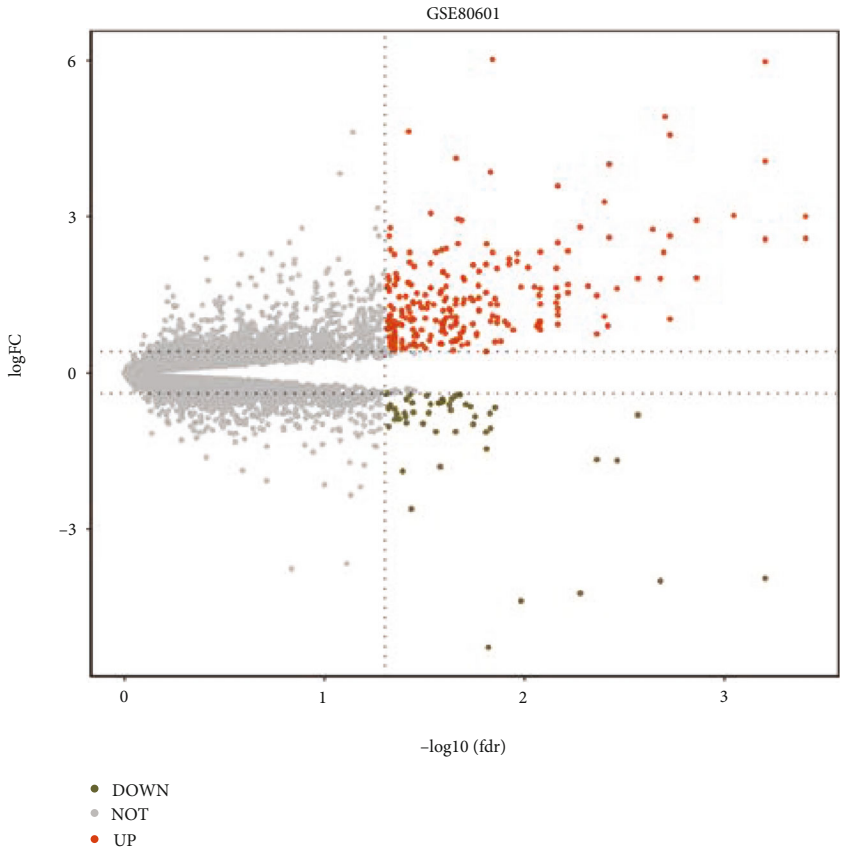

(e)

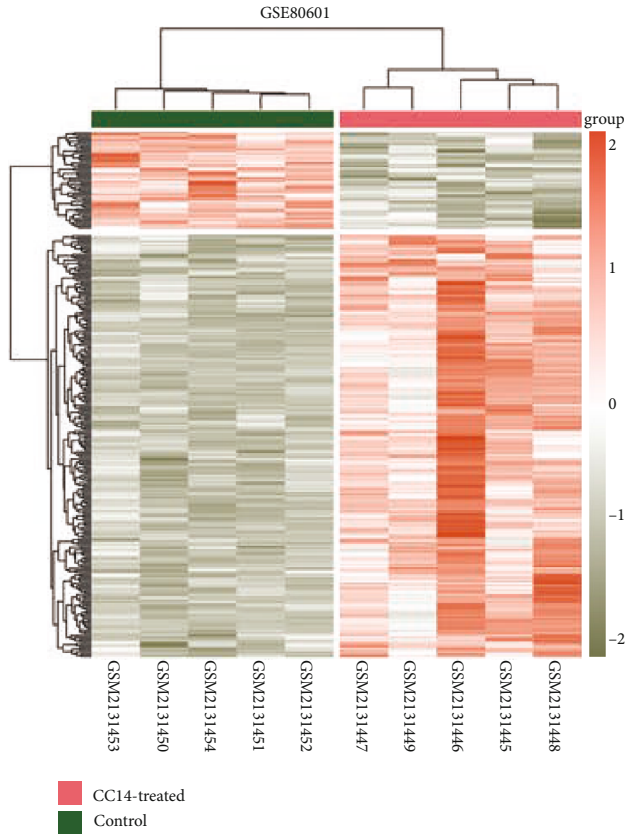

(f)

Figure 1: Continued.

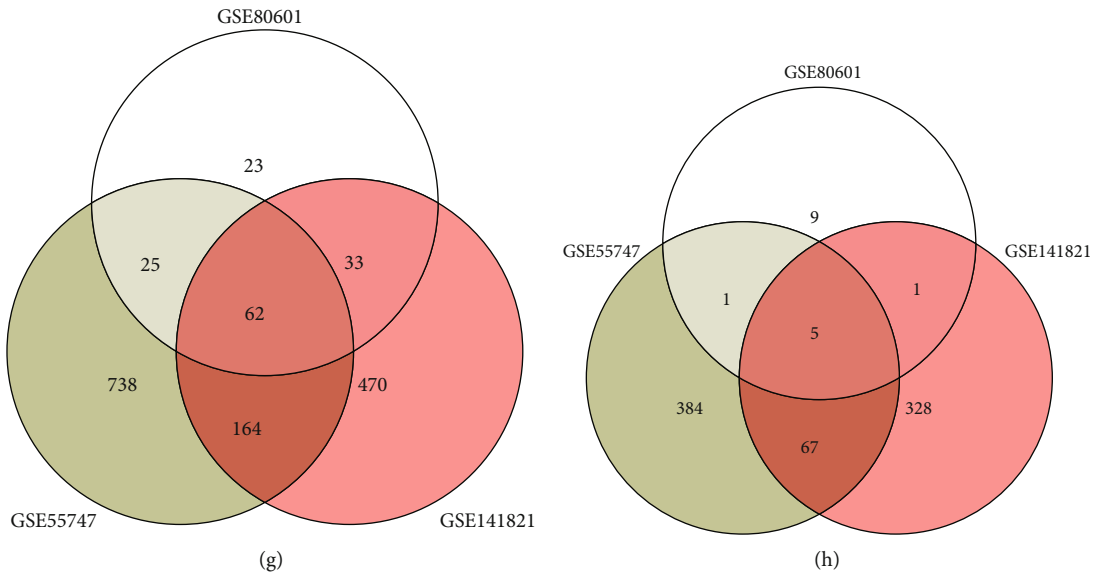

Figure 1: Identification of DEGs in CCl_4-treated mouse liver samples. DEGs were obtained by comparing untreated and CCl4-induced fibrotic mouse liver tissues from three GEO datasets: GSE14182, GSE55747, and GSE80601. (a)–(c)) Volcano plot of the distribution of all DEGs between untreated control and CCl_4-treated liver samples from GSE14182, GSE55747, and GSE80601, respectively, with a threshold of $|\log_2(\text{foldchange})| > 1$ and adjusted $P < 0.05$ (the brick red, upregulated DEGs; grass green: downregulated DEGs; grey: unchanged). (d)–(f) The heatmap plot of DEGs across the samples (CCl_4-treated vs Control) from GSE14182, GSE55747, and GSE80601, respectively. Colors above the heatmap indicate sample groups. Each row of the heatmap represents the normalized expression values of one differentially expressed gene across all samples (grass green, low expression; brick red, high expression). (g) and (h) Venn diagram of DEGs from 3 different microarray dataset. CCl_4, carbon tetrachloride; DEG, differential expressed genes; GEO, Gene Expression Omnibus.

as well as the expression matrix of normal liver tissues from GTEx [27].

3. Results

3.1. Fibrotic-Related Gene Expression Patterns in CCl_4-Induced Mouse Liver Samples. To investigate the mechanisms of liver fibrosis, we analyzed the DEGs in three GEO datasets between CCl_4-induced fibrotic and control samples. In GSE141821, 45 upregulated and 7 downregulated DEGs were found (|log2 (foldchange)| >1, adjusted $P = 0.05$; Figure 1(a) and 1(b)). On the other hand, Figure 1(c) and 1(d) demonstrate that in GSE55747 fibrotic mouse liver samples, there were 1817 upregulated and 1778 downregulated DEGs with a |log2 (foldchange)| > 1 and adjusted $P < 0.05$. In GSE80601, following analysis, 1778 downregulated and 1817 upregulated DEGs were found in CCl4-induced fibrotic liver tissues (|log2 (foldchange)| > 1, adjusted $P < 0.05$; Figures 1(e) and 1(f)). We identified 62 upregulated genes and 5 downregulated genes by intersecting the DEGs from three datasets (Figures 1(g) and 1(h)). These genes encode a number of ECM proteins, including *Col3a1*, *Col4a1*, and *Col1a1*. In the meanwhile, genes encoding ECM degrading enzymes including *Timp2*, *Mmp2*, and *Adamts5* were considerably upregulated. Acute-phase protein expression of *Saa3* (serum amyloid A3) significantly elevates in response to acute and chronic inflammatory stimuli. This finding highlights the fact that the ECM is altered after CCl_4 treatment. Also, *Cd14*, *Cd53*, and *Cd68*, which are markers for monocytes and macrophages, were considerably increased. It implies an increase of macrophage contents and increased immune filtration level following the injury. Cytochrome P450 gene family members, such as *Cyp7b1* and *Cyp2d40* are among downregulated genes. In addition, after the injury, *Hsd3b5* (hydroxy-delta-5-steroid dehydrogenase, 3 beta- and steroid delta-isomerase 5) was down regulated. The function of normal liver cells is impacted by liver injury. The upregulated and downregulated DEGs were shown using Venn diagrams (Figures 1(g) and 1(h), respectively).

The enrichment analysis was performed by Metascape (Figure 2(a)). Pathways involved includes ECM organization (GO: 0030198), positive regulation of cell migration (GO: 0030335), collagen degradation (R-MMU-1442490), and positive regulation of response to external stimuli (GO: 0032103). Figure 2(b) depicts the MCODE analysis for PPI (protein–protein interaction) models by Metascape. The ECM protein cluster is part of the core PPI interaction network (*Col1a1*, *Col3a1*, *Col4a1*, *Col6a1*, *Lum*, and *Sparc*; Figure 2(b)). Furthermore, we used STRING for functional annotation enrichment, and the top enriched pathways were displayed in R using the ggplot2 tool (v 3.3.3). GO:BP enrichment indicated that pathways, such as stress response and cytokine are altered (Figure 2(c)), whilst KEGG enrichment indicated an alteration in actin cytoskeleton regulation and leukocyte transendothelial activation (Figure 2(d)). These enrichment pathway findings are mostly consistent with the fibrosis process in the liver.

3.2. EMP1 Is a Marker Gene for CCl_4-Treated Liver Samples. We noticed that CCl_4 treatment caused a rapid increase in *Emp1* expression in mouse liver tissues from various datasets (Figures 3(a)–3(d)). The GSE80601 expression profiles of

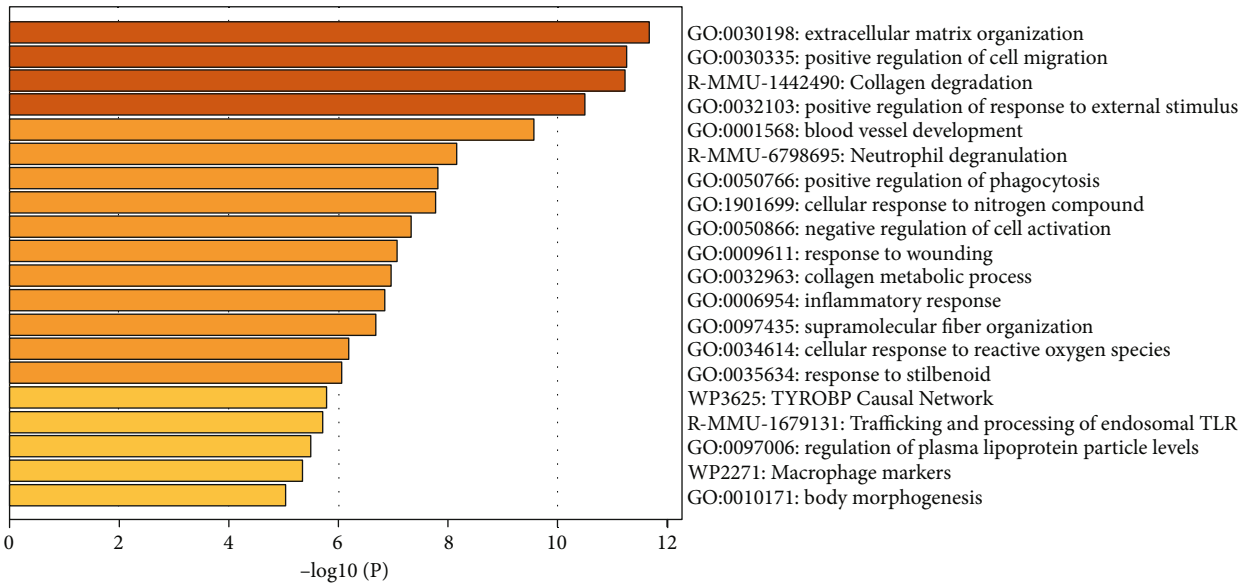

(a)

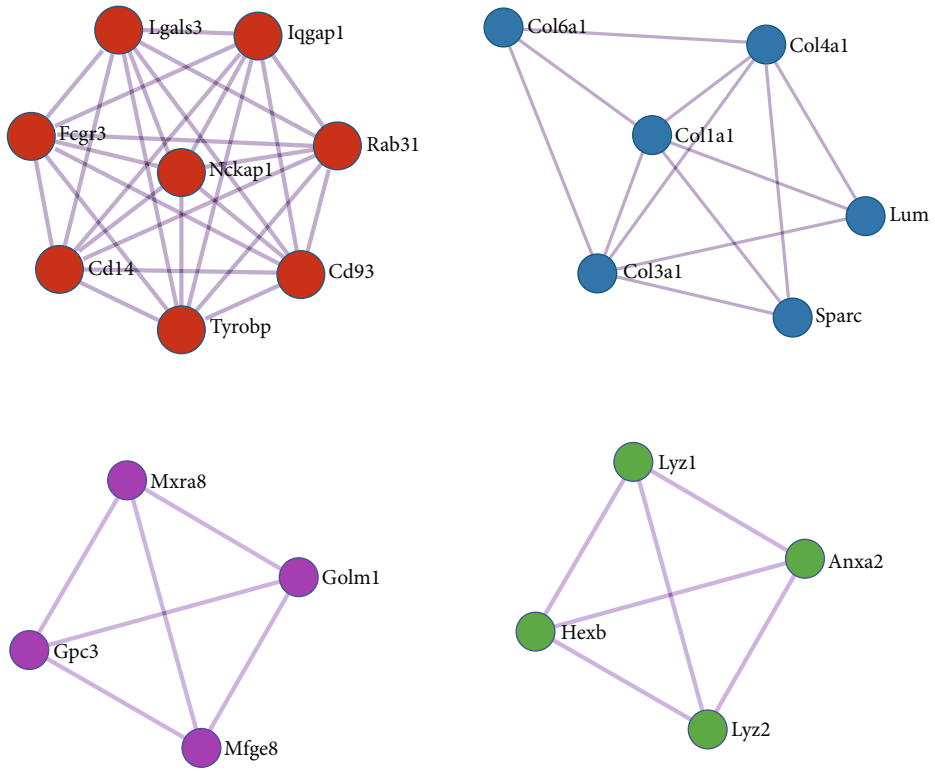

(b)

Figure 2: Continued.

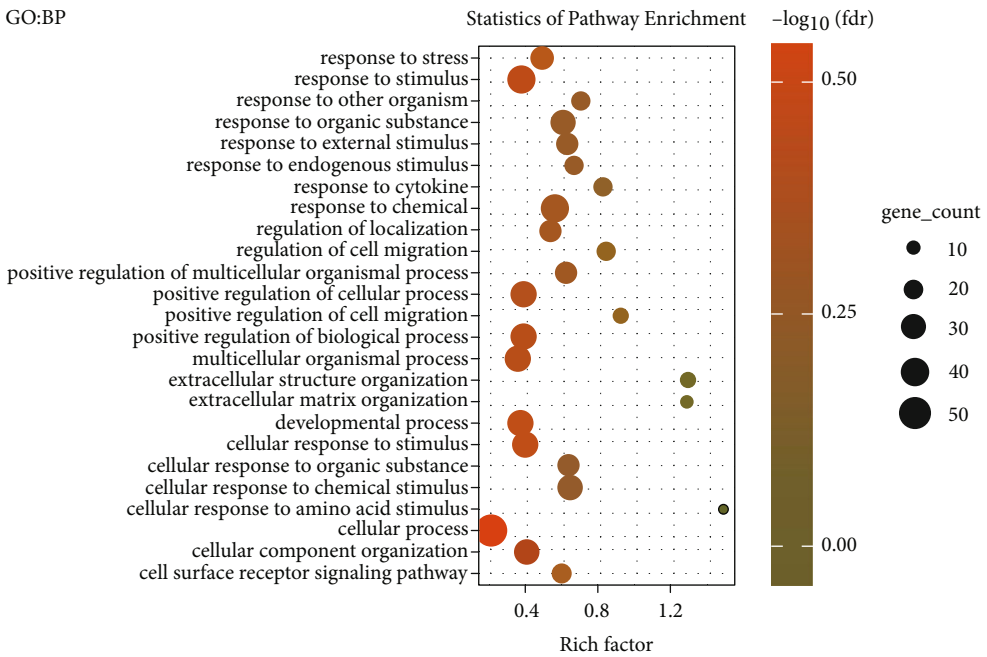

(c)

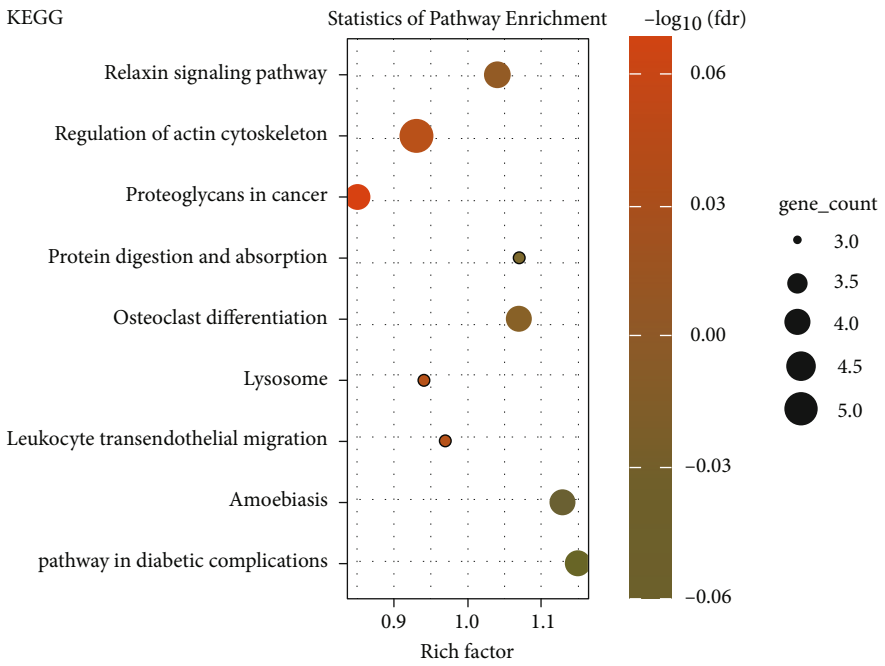

(d)

Figure 2: Functional enrichment analysis of DEGs. (a) Bar chart of clustered enrichment ontology categories (including both GO and KEGG terms) by Metascape (colored by P-values; minimum overlap: 3; $P < 0.01$; minimum enrichment: 1.5). (b) MCODE enrichment analysis of PPI network by Metascape. Functional enrichment analysis of GO: BP (c) and KEGG (d) using PPI generated by STRING. DEGs were imported into the STRING database to generate a PPI network with a 0.4 minimum necessary interaction score. GO, Gene Ontology; KEGG, Kyoto Encyclopedia of Genes and Genomes; MCODE, Molecular Complex Detection; PPI: protein–protein interaction.

liver tissues treated with CCl_4 (n =6) and control liver tissues ($n = 5$) treated with oil for both 6 weeks from Balb/c mice revealed that *Emp1* expression significantly increased following CCl_4 treatment ($\log_2FC = 2.461$, $P = 2.39 \times 10^{-4}$; Figure 3(a)). In GSE27640 after 18 weeks of CCl_4 treatment in the mouse model, the *Emp1* gene was significantly upregulated ($\log_2FC = 1.673$, $P = 2.61 \times 10^{-3}$) compared to normal control liver tissues. Erlotinib, an EGF receptor inhibitor that can reduce liver fibrosis and the development of hepatocellular carcinoma, suppressed the increased expression of *Emp1* in GSE27640 (Figure 3(b)). Meanwhile, in GSE73499 following 3, 6, and 9 weeks of CCl_4 administration, the expression of the *Emp1* gene

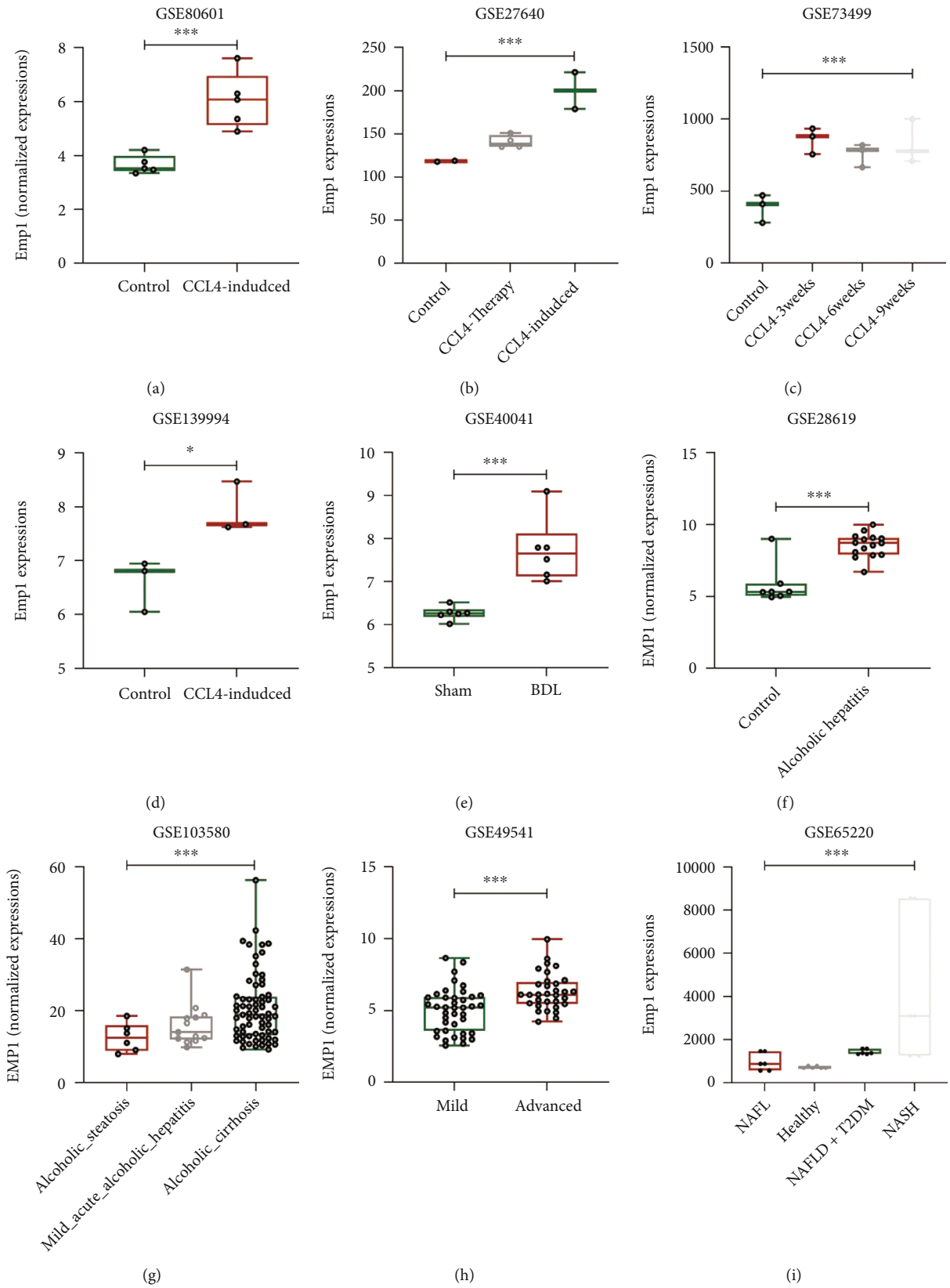

Figure 3: *EMP1* is a marker gene for fibrotic liver in both animal and human samples. *Emp1* upregulation in CCl_4-treated mouse liver samples compared with normal tissues in GSE80601 (a), GSE27640 (b), GSE73499 (c), and GSE139994 (d). *Emp1* expression elevation in mice BDL model compared with sham group (e). Positive association of *EMP1* expression with alcoholic hepatitis (GSE28619) (f) and alcoholic cirrhosis (GSE103580) samples (g). Increased expression of *EMP1* in liver samples with advanced stage of fibrosis (stage 3–4) compared with mild (stage 0–1) (h). In the rat model, *Emp1* expression is greatest in the NASH group compared to the NAFL, NAFLD + T2DM, and healthy control groups. BDL, bile duct ligation (i); CCl_4, carbon tetrachloride; EMP1, epithelial membrane protein 1; NAFL, nonalcoholic fatty liver; NAFLD, nonalcoholic fatty liver disease; NASH, nonalcoholic steatohepatitis; T2DM, type 2 diabetes; $^{*}P < 0.05$ and $^{***}P < 0.01$.

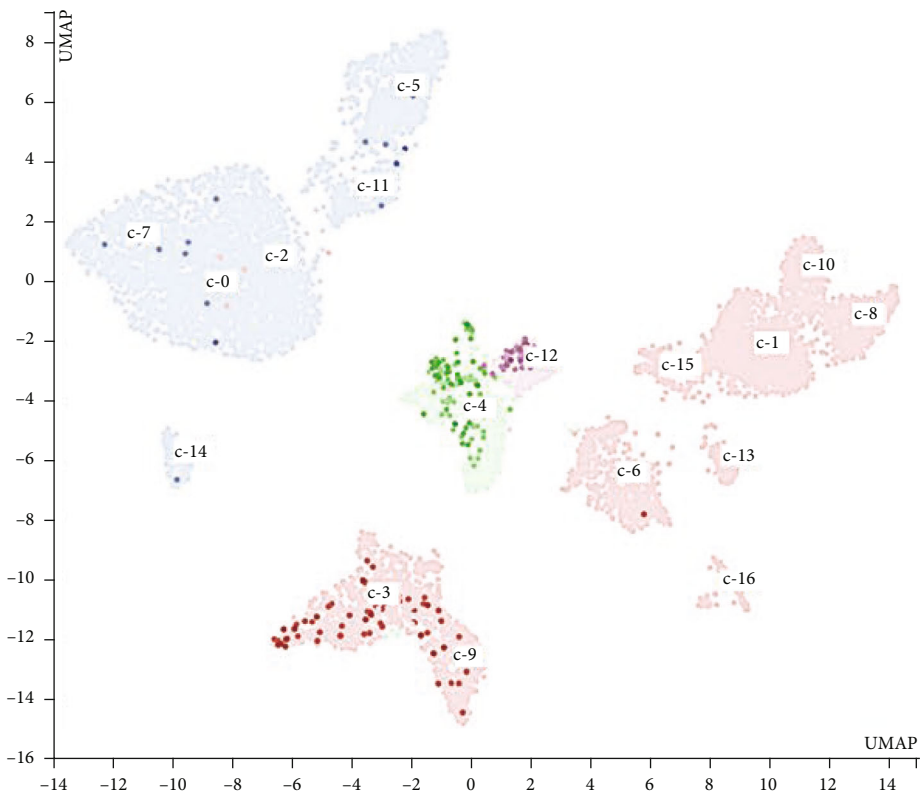

(a)

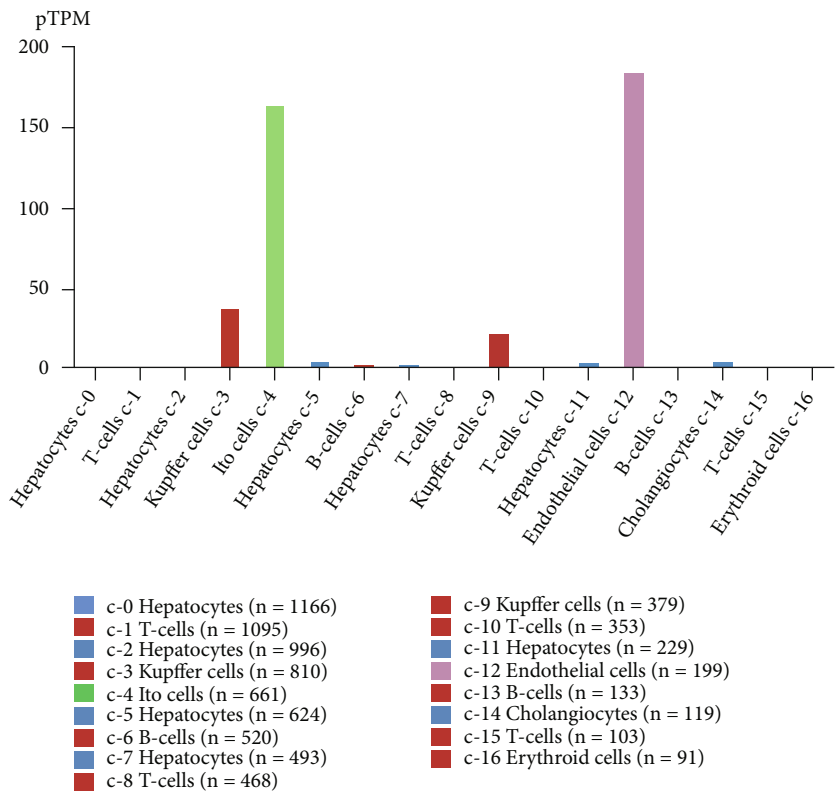

(b)

Figure 4: Continued.

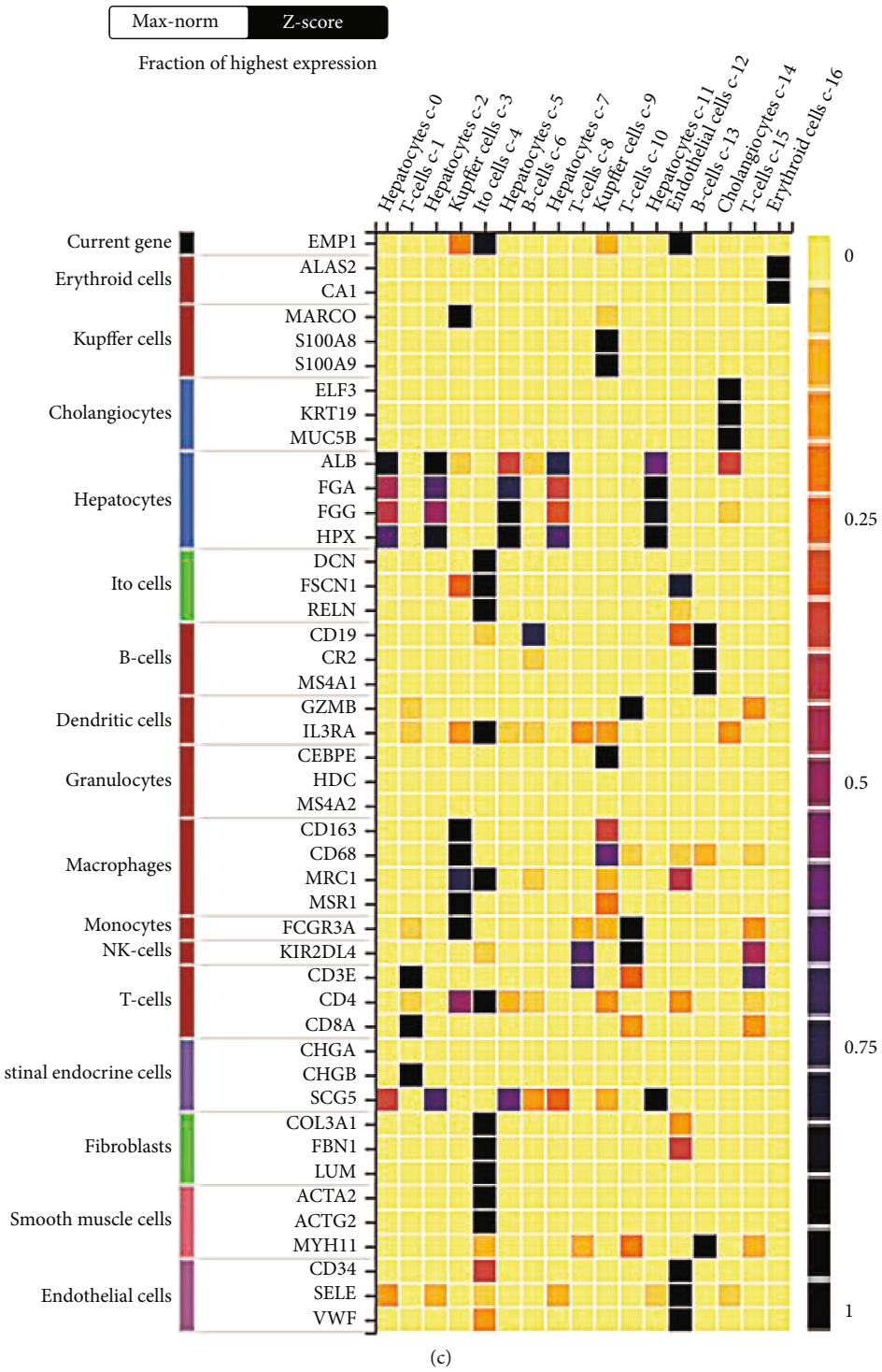

(c)

Figure 4: Continued.

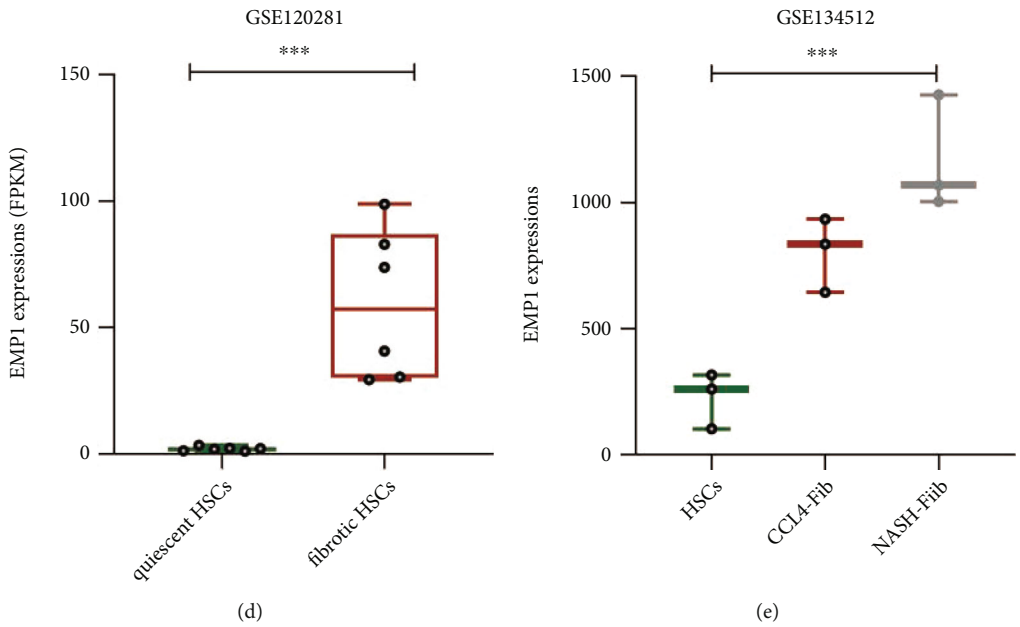

Figure 4: *EMP1* is expressed in activated fibrotic hepatic stellate. The cell type atlas given by Protein Atlas (https://www.proteinatlas.org/) validated the expression of *EMP1* in liver tissues. (a) Feature plot of *EMP1* overlaid with the UMAP projection of liver samples. (b) Bar plot showing the TPM expression of *EMP1* across different cell type clusters including hepatocytes, Ito cells, T cells, Kupfer cells, B cells, and others. (c) Heatmap plot of normalized *EMP1* expressions along with other marker genes across the different cell types in liver tissues. Significant positive association of *EMP1* expression with fibrotic HSCs (GSE120281) (d) and activated fibroblast introduced by either CCl_4 treatment or Western diet-fed NASH model (GSE134512) samples (e). CCl_4, carbon tetrachloride; EMP1, epithelial membrane protein 1; NASH, nonalcoholic steatohepatitis; TPM, transcripts per million; UMAP, Uniform Manifold Approximation and Projection. $P < 0.05$ and $^{***}P < 0.01$.

was also significantly upregulated in the rat liver cirrhosis model ($\log_2FC = 1.117$, $P = 6.13 \times 10^{-3}$) (Figure 3(c)). When compared to samples of rat livers treated with a control vehicle, the expression of Emp1 in the liver tissue of rats treated with CCl_4 was significantly upregulated ($\log_2FC = 1.416$, $P = 0.035$) in GSE139994. Taken together, these findings suggested that the liver tissues response to CCl_4-induced acute and chronic injury triggers a rapid increase in *Emp1* in mouse model.

3.3. EMP1 Is a Marker Gene for Fibrotic Liver Samples. Aside from the CCl_4-treatment model, similar findings have been made in other liver fibrosis models, including human clinical fibrotic liver samples caused by conditions like NAFLD (nonalcoholic fatty liver [NAFL] disease). For instance, when compared to the control group, *Emp1* is rapidly activated in GSE40041 in acute or chronic damage mouse models by sham or BDL for either 48 hours or 28 days, respectively ($\log_2FC = 1.152$, $P = 3.26 \times 10^{-4}$; Figure 3(e)). According to the GSE28619 dataset, hepatic gene expression profiling was examined by microarray in patients with alcoholism ($n = 15$) and normal livers ($n = 7$), and *EMP1* is considerably higher in alcoholic hepatitis tissues (GSE28619; $\log_2FC = 2.73$, $P = 1.08 \times 10^{-5}$; Figure 3(f)). *EMP1* is also substantially more highly expressed in alcoholic steatosis and cirrhosis than in moderate acute alcoholic hepatitis, according to the set of data (GSE103580; ($\log_2FC = 0.325$, $P = 0.032$; Figure 3(g)). Moreover, *EMP1* is greater higher expressed in samples of NAFLD liver biopsy tissues recovered from advanced (fibrotic stage 3–4) compared to moderate samples (fibrotic stage 0–1) in GSE49541 ($\log_2FC = 1.152$, $P = 3.26 \times 10^{-4}$; Figure 3(h)). Furthermore, in the different stages of rat fibrotic liver from GSE65220, Emp1 has the highest expression in NASH compared to other stages, such as healthy, NAFL, and NAFLD with T2DM (type 2 diabetes; $\log_2FC = 2.157$, $P = 9.92 \times 10^{-3}$; Figure 3(i)). All of this evidence suggests that EMP1 expression increased with the severity of the fibrotic liver malignancy and that it may play a role in the regulation of the liver injury response.

3.4. Dominant Expression of EMP1 in HSCs from Liver Single-Cell Transcriptome. Using The Human Protein Atlas (https://www.proteinatlas.org/), we investigated the expression profiles of different cell types in liver tissues to determine which cell type expresses EMP1 the most. We discovered that *EMP1* is exclusively expressed in EC (purple c-12 cluster) as well as Ito (perisinusoidal fat-storing cells, also known as stellate cells) of the liver as mesenchymal cells (grass green c-4 cluster) in the single-cell transcriptome clustering results for normal liver tissues. The data was displayed in a UMAP (Uniform Manifold Approximation and Projection plot; Figure 4(a)). According to the clustering results, *EMP1* expression is lower in Kupffer cells (brick red c-3 and c-6 clusters) and other cell types including immune cells and hepatocytes (c-2; Figure 4(a)). Ito cells had an average expression value TPM (transcripts per kilobase) of 161.3, while EC had an average TPM of 181.9, and *EMP1* expression is low in all other cell types (Figure 4(b)). The heatmap

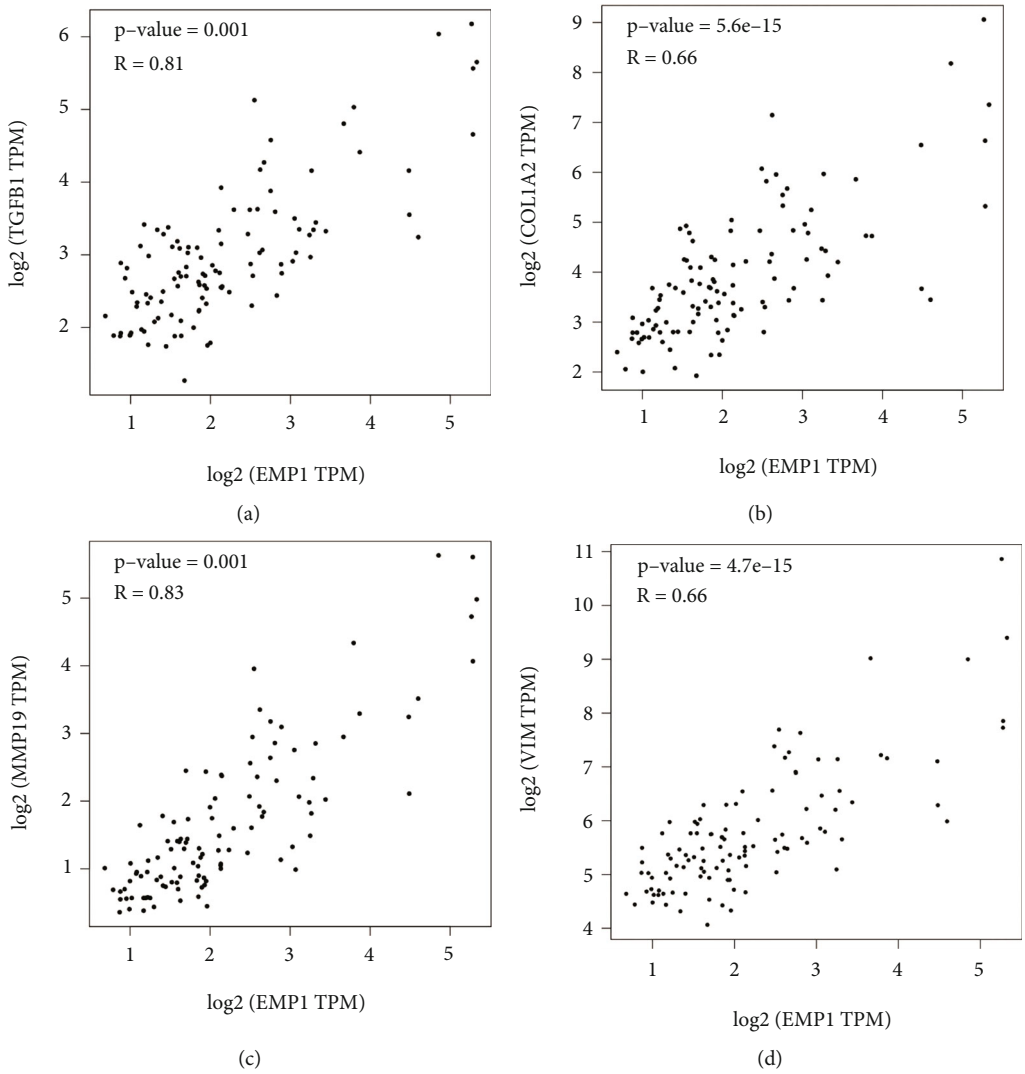

Figure 5: Continued.

Summary of search results

Gene	Description	Type	No. samples	No. cell clusters
EMP1	epithelial membrane protein 1	protein-coding gene	363	1487

Barplot of cell clusters (Y-axis) and cell types (X-axis) where the gene is expressed.

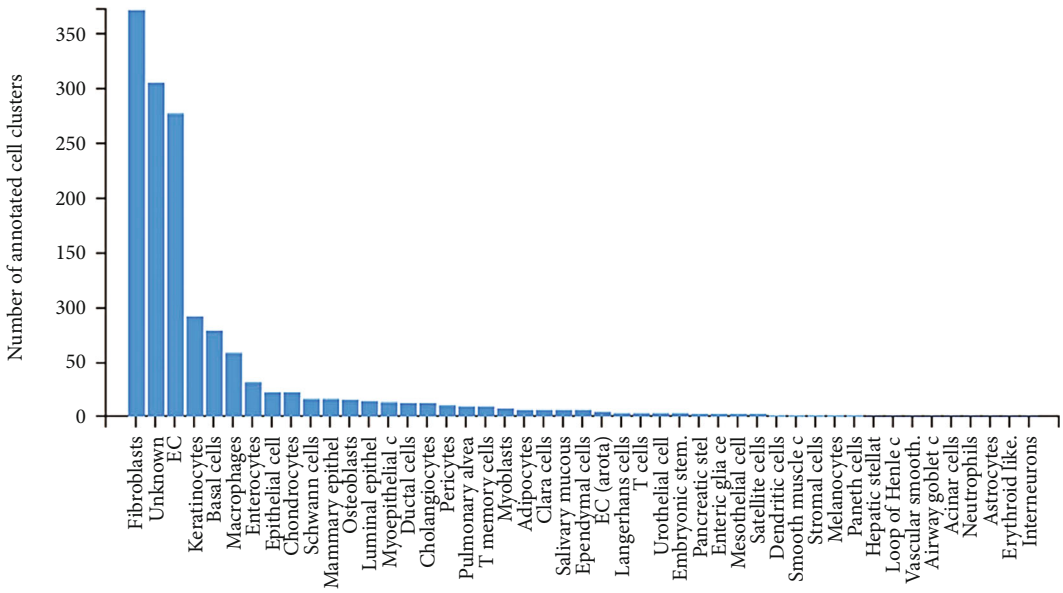

(e)

Figure 5: EMP1 expression positively correlated with fibrotic-related genes in liver. Significant positive correlations of *EMP1* expression with fibrotic-related genes including *TGFB1* (a), *COL1A2* (b), *MMP9* (c), and *VIM* (d), according to the expression profile from GTEx normal liver RNA-sequencing matrix in GEPIA2. (e) Barplot of cell clusters (*y*-axis) and cell types (*x*-axis) where the gene is expressed. Expression enrichment of *EMP1* in different cell types from 363 scRNA-seq samples and 1487 cell clusters according to PanglaoDB. COL1A2, collagen type *i* alpha 2 chain; EMP1, epithelial membrane protein 1; GEPIA2, Gene Expression Profiling Interactive Analysis; GTEx, Genotype-Tissue Expression; MMP9, matrix metallopeptidase 9; scRNA-seq, single-cell RNA sequencing; TGFB1, transforming growth factor beta 1; VIM, vimentin.

depicts the highest levels of EMP1 gene expression as well as other marker genes from various cell types, such as *CD34* for EC, *CD3E* for T cells, and *CD163* for macrophages. *EMP1* and *FSCN1* (Fascin actin-bundling protein 1) have the most similar expression patterns according to the dataset (Figure 4(c)).

3.5. EMP1 Expression Elevated in Activated HSCs and Liver Fibroblast. Since we know that the activation of HSCs into proliferative, fibrogenic myofibroblasts has long been recognized as the primary cause of hepatic fibrosis in both experimental and human liver injury. GSE120281, an mRNA profile of quiescent (Q) or fibrotic (F) HSC and liver sinusoidal EC (SEC) generated by RNA sequencing in control or CCl_4-treated mice, was investigated. In fibrotic HSCs, compared to quiescent HSCs, *Emp1* expression is markedly increased in response to CCl_4 treatment ($\log_2 FC = 4.895$, $P = 0.0008$; Figure 4(d)). GSE134512 dataset that analyzed the transcriptome of activated fibroblasts from NASH livers and discovered that *Emp1* was significantly elevated in both CCl_4-induced and NASH-induced fibroblasts when compared to activated HSCs ($\log_2 FC = 2.116$, $P = 0.00228$; Figure 4(e)).

3.6. EMP1 Expression Correlated with ECM Proteins. GEPIA was used to confirm the significantly positive association of *EMP1* expression with *COL1A2* (collagen type I alpha 2 chain), *TGFB1* (transforming growth factor beta 1), *MMP19* (matrix metallopeptidase 19), and *VIM* (vimentin) in normal liver samples ($r > 0.60$, $P < 0.05$; Figure 5(a)–5(d)). Then, we double-checked our findings using the PanglaoDB database. *EMP1* was shown to be highly expressed in fibroblasts, EC, followed by keratinocytes, but not in HSCs (Figure 5(e)). These results indicate that EMP1 may assist in the fibrotic progression after activation and transdifferentiation of HSCs in the development of liver fibrosis, therefore increasing liver fibrosis.

4. Discussion

The fundamental cause of liver fibrosis is the activation of HSCs, which then transform from quiescent, vitamin-A-storing cells into proliferative, fibrogenic myofibroblasts [28]. Deactivation of HSCs by Tcf21 (transcription factor 21), has been proved to suppress hepatic fibrosis progression in mice [29]. However, HSCs activation is a rather complex process that has yet to be fully understood.

In this work, we first demonstrated that EMP1 is one of the most elevated genes after CCl_4-induced liver damage in mouse model. Then, we discovered that *EMP1* levels are also elevated in various liver samples after injury, such as the

BDL model and alcoholic hepatitis in humans. EMP1 is expressed in fibroblasts and EC, according to single-cell transcriptome study of liver tissues. Furthermore, we observed that EMP1 expression was much greater in activated fibrogenic fibroblasts and was associated with typical fibrotic genes. The EMPs, which includes *EMP1*, *EMP2*, and *EMP3* are encoded by the growth arrest-specific 3 (GAS3)/peripheral myelin protein 22 kDa (PMP22) gene family [9]. The EMPs family has four putative transmembrane domains with about 160 amino acid residues [30]. Although the genes in this family are commonly implicated in cancer cell migration, proliferation, and differentiation, few studies have demonstrated their role in fibrosis. He et al. previously discovered that abnormal upregulation of *PMP22* in TGF-β-activated HSCs and CCl_4-induced hepatic fibrosis model in mice, as well as the pro-fibrotic role of *PMP22* through aggravating TGF-β-induced HSC activation [31]. It would be interesting to look into and compare the role of the entire gene family in fibrotic processes in the liver.

Extensive research has been conducted into the role of EMP1 in pathogenesis and tumorigenesis of various cancer. In breast cancer, for example, EMP1 functions as a new marker for lobular and ductal invasive breast carcinoma differentiation, as well as a putative link with breast cancer invasion promotion [32]. With increasing histologic grade, the expression of EMP1, EMP2, and EMP3 decreases in the epithelial component and increases in the stromal component of phyllodes tumors [33]. In prostate cancer, *EMP1* is highly expressed in patients with a higher Gleason score, and increasing EMP1 levels significantly increases cancer cell migration, resulting in tumor metastasis, implying that EMP1 may play an important role as a positive regulator of tumor metastasis [8]. In ovarian cancer, *EMP1* was discovered to play a critical role as a negative regulator in ovarian serous tumors, and decreased EMP1 expression in serous tumors associated with increased disease severity [34]. EMP1 is also a biomarker of gefitinib resistance, and it has been linked to a lack of complete or partial response to gefitinib in lung cancer patient samples, as well as clinical progression to secondary gefitinib resistance [35]. In acute lymphoblastic leukemia, *EMP1* is a novel poor prognostic factor in pediatric leukemia that regulates prednisolone resistance, cell proliferation, migration, and adhesion [36]. In glioma, EMP1 regulates the cell proliferation, migration, and stemness through PI3K-AKT signaling and CD44 [37]. Given that the majority of research agree that EMP1 can enhance tumor growth, invasion, and migration, we hypothesize that EMP1 could also promote activated HSC proliferation and migration following injury. Stellate cell activation is characterized by proliferation and migration [38], and reducing proliferation may modify hepatic fibrosis, according to many published results [39–42]. However, further validating tests are required in the future to validate the hypothesis.

In our enriched analysis, the pathways involved includes ECM organization, positive regulation of cell migration, collagen degradation, and positive regulation of response to external stimuli. The enrichment analysis indicated that pathways such as stress response and cytokine are altered, whilst KEGG enrichment indicated an alteration in actin cytoskeleton regulation and leukocyte transendothelial activation. These enrichment pathway findings are mostly consistent with the fibrosis process in the liver.

There were several limitations in the present study. First, the included datasets were based on mice; we lack validation in human samples. Second, we did not perform the analysis to study the expression of EMP1 in different subgroups by different clinical factors such as sex and age. Third, lack of experiments to verify, and our analysis was performed using data sets from public databases but was not validated in larger data sets.

Taken together, these bioinformatic data imply that EMP1 might be used as a marker gene during liver fibrosis after injury and may have a potential role in HSCs, however additional validating experiments is needed in the future.

Data Availability

The simulation experiment data supporting this research article are available from the corresponding author or first author on reasonable request.

Conflicts of Interest

The authors declare that they have no conflicts of interest.

References

[1] Z. Zhan, Y. Chen, Y. Duan et al., "Identification of key genes, pathways and potential therapeutic agents for liver fibrosis using an integrated bioinformatics analysis," *PeerJ*, vol. 7, article e6645, 2019Epub 2019/03/30.

[2] Y. Zhang, W. Lu, X. Chen, Y. Cao, and Z. Yang, "A bioinformatic analysis of correlations between polymeric immunoglobulin receptor (PIGR) and liver fibrosis progression," *BioMed Research International*, vol. 2021, 2021Epub 2021/05/04.

[3] O. Krenkel and F. Tacke, "Liver macrophages in tissue homeostasis and disease," *Nature Reviews Immunology*, vol. 17, no. 5, pp. 306–321, 2017.

[4] N. Roehlen, E. Crouchet, and T. F. Baumert, "Liver fibrosis: mechanistic concepts and therapeutic perspectives," *Cell*, vol. 9, no. 4, p. 875, 2020.

[5] P. Ramachandran, A. Pellicoro, M. A. Vernon et al., "Differential Ly-6C expression identifies the recruited macrophage phenotype, which orchestrates the regression of murine liver fibrosis," *Proceedings of the National Academy of Sciences of the United States of America*, vol. 109, no. 46, pp. E3186–E3195, 2012.

[6] T. Tsuchida and S. L. Friedman, "Mechanisms of hepatic stellate cell activation," *Nature Reviews Gastroenterology & Hepatology*, vol. 14, no. 7, pp. 397–411, 2017.

[7] L. Campana and J. P. Iredale, "Regression of liver fibrosis," *Seminars in Liver Disease*, vol. 37, no. 1, pp. 1–10, 2017.

[8] M. K. B. Ahmat Amin, A. Shimizu, D. P. Zankov et al., "Epithelial membrane protein 1 promotes tumor metastasis by enhancing cell migration via copine-III and Rac1," *Oncogene*, vol. 37, no. 40, pp. 5416–5434, 2018.

[9] Y. W. Wang, H. L. Cheng, Y. R. Ding, L. H. Chou, and N. H. Chow, "EMP1, EMP 2, and EMP3 as novel therapeutic targets

in human cancer," *Biochimica Et Biophysica Acta - Reviews on Cancer*, vol. 1868, no. 1, pp. 199–211, 2017.

[10] R. Edgar, M. Domrachev, and A. E. Lash, "Gene expression omnibus: NCBI gene expression and hybridization array data repository," *Nucleic Acids Research*, vol. 30, no. 1, pp. 207–210, 2002.

[11] P. Lefebvre, F. Lalloyer, E. Baugé et al., "Interspecies NASH disease activity whole-genome profiling identifies a fibrogenic role of PPARα-regulated dermatopontin," *JCI Insight*, vol. 2, no. 13, article e92264, 2017.

[12] K. Zhang, X. Han, Z. Zhang et al., "The liver-enriched lncLFAR1 promotes liver fibrosis by activating TGFβ and notch pathways," *Nature Communications*, vol. 8, no. 1, p. 144, 2017.

[13] M. E. Ritchie, B. Phipson, D. Wu et al., "Limma powers differential expression analyses for RNA-sequencing and microarray studies," *Nucleic Acids Research*, vol. 43, no. 7, article e47, 2015.

[14] E. Trépo, N. Goossens, N. Fujiwara et al., "Combination of gene expression signature and model for end-stage liver disease score predicts survival of patients with severe alcoholic hepatitis," *Gastroenterology*, vol. 154, no. 4, pp. 965–975, 2018.

[15] L. Yang, B. Han, M. Zhang et al., "Activation of BK channels prevents hepatic stellate cell activation and liver fibrosis through the suppression of TGFβ1/SMAD3 and JAK/STAT3 profibrotic signaling pathways," *Frontiers in Pharmacology*, vol. 11, p. 165, 2020.

[16] B. C. Fuchs, Y. Hoshida, T. Fujii et al., "Epidermal growth factor receptor inhibition attenuates liver fibrosis and development of hepatocellular carcinoma," *Hepatology*, vol. 59, no. 4, pp. 1577–1590, 2014.

[17] S. Affò, M. Dominguez, J. J. Lozano et al., "Transcriptome analysis identifies TNF superfamily receptors as potential therapeutic targets in alcoholic hepatitis," *Gut*, vol. 62, no. 3, pp. 452–460, 2013.

[18] G. Zhao, M. Hatting, Y. A. Nevzorova et al., "Jnk1 in murine hepatic stellate cells is a crucial mediator of liver fibrogenesis," *Gut*, vol. 63, no. 7, pp. 1159–1172, 2014.

[19] S. K. Murphy, H. Yang, C. A. Moylan et al., "Relationship between methylome and transcriptome in patients with nonalcoholic fatty liver disease," *Gastroenterology*, vol. 145, no. 5, pp. 1076–1087, 2013.

[20] G. Wang, S. Chen, C. Zhao et al., "Comparative analysis of gene expression profiles of OPN signaling pathway in four kinds of liver diseases," *Journal of Genetics*, vol. 95, no. 3, pp. 741–750, 2016.

[21] S. Davis and P. S. Meltzer, "GEOquery: a bridge between the gene expression omnibus (GEO) and BioConductor," *Bioinformatics*, vol. 23, no. 14, pp. 1846–1847, 2007.

[22] Y. Zhou, B. Zhou, L. Pache et al., "Metascape provides a biologist-oriented resource for the analysis of systems-level datasets," *Nature Communications*, vol. 10, no. 1, p. 1523, 2019.

[23] D. Szklarczyk, A. L. Gable, D. Lyon et al., "STRING v11: protein-protein association networks with increased coverage, supporting functional discovery in genome-wide experimental datasets," *Nucleic Acids Research*, vol. 47, no. D1, pp. D607–D613, 2019.

[24] M. Uhlen, C. Zhang, S. Lee et al., "A pathology atlas of the human cancer transcriptome," *Science*, vol. 357, no. 6352, article eaan2507, 2017.

[25] O. Franzén, L. M. Gan, and J. L. M. Björkegren, "PanglaoDB: a web server for exploration of mouse and human single-cell RNA sequencing data," *Database: The Journal of Biological Databases and Curation*, vol. 2019, article baz046, 2019.

[26] Z. Tang, B. Kang, C. Li, T. Chen, and Z. Zhang, "GEPIA2: an enhanced web server for large-scale expression profiling and interactive analysis," *Nucleic Acids Research*, vol. 47, no. W1, pp. W556–W560, 2019.

[27] "The genotype-tissue expression (GTEx) pilot analysis: multitissue gene regulation in humans," *Science*, vol. 348, no. 6235, pp. 648–660, 2015.

[28] Y. A. Lee, M. C. Wallace, and S. L. Friedman, "Pathobiology of liver fibrosis: a translational success story," *Gut*, vol. 64, no. 5, pp. 830–841, 2015.

[29] Y. Nakano, A. Kamiya, H. Sumiyoshi, K. Tsuruya, T. Kagawa, and Y. Inagaki, "A deactivation factor of fibrogenic hepatic stellate cells induces regression of liver fibrosis in mice," *Hepatology*, vol. 71, no. 4, pp. 1437–1452, 2020.

[30] M. K. B. Ahmat Amin, A. Shimizu, and H. Ogita, "The pivotal roles of the epithelial membrane protein family in cancer invasiveness and metastasis," *Cancers*, vol. 11, no. 11, p. 1620, 2019.

[31] C. He, B. Shu, Y. Zhou, R. Zhang, and X. Yang, "The miR-139-5p/peripheral myelin protein 22 axis modulates TGF-β-induced hepatic stellate cell activation and CCl_4-induced hepatic fibrosis in mice," *Life Sciences*, vol. 276, article 119294, 2021.

[32] G. Turashvili, J. Bouchal, K. Baumforth et al., "Novel markers for differentiation of lobular and ductal invasive breast carcinomas by laser microdissection and microarray analysis," *BMC Cancer*, vol. 7, no. 1, p. 55, 2007.

[33] Y. J. Cha and J. S. Koo, "Expression of EMP1, EMP2, and EMP3 in breast phyllodes tumors," *PLoS One*, vol. 15, no. 8, article e0238466, 2020.

[34] Y. Liu, Y. Ding, Y. Nie, and M. Yang, "EMP1 promotes the proliferation and invasion of ovarian cancer cells through activating the MAPK pathway," *Oncotargets and Therapy*, vol. - Volume 13, pp. 2047–2055, 2020.

[35] A. Jain, C. A. Tindell, I. Laux et al., "Epithelial membrane protein-1 is a biomarker of gefitinib resistance," *Proceedings of the National Academy of Sciences of the United States of America*, vol. 102, no. 33, pp. 11858–11863, 2005.

[36] I. M. Ariës, I. S. Jerchel, R. E. van den Dungen et al., "EMP1, a novel poor prognostic factor in pediatric leukemia regulates prednisolone resistance, cell proliferation, migration and adhesion," *Leukemia*, vol. 28, no. 9, pp. 1828–1837, 2014.

[37] J. Wang, X. Li, H. Wu et al., "EMP1 regulates cell proliferation, migration, and stemness in gliomas through PI3K-AKT signaling and CD44," *Journal of Cellular Biochemistry*, vol. 120, no. 10, pp. 17142–17150, 2019.

[38] J. E. Puche, Y. Saiman, and S. L. Friedman, "Hepatic stellate cells and liver fibrosis," *Comprehensive Physiology*, vol. 3, no. 4, pp. 1473–1492, 2013.

[39] J. Fu, B. Wu, S. Zhong, W. Deng, and F. Lin, "miR-29a-3p suppresses hepatic fibrosis pathogenesis by modulating hepatic stellate cell proliferation via targeting PIK3R3 gene expression," *Biochemical and Biophysical Research Communications*, vol. 529, no. 4, pp. 922–929, 2020.

[40] W. Chen, X. Yan, A. Yang, A. Xu, T. Huang, and H. You, "miRNA-150-5p promotes hepatic stellate cell proliferation and sensitizes hepatocyte apoptosis during liver fibrosis," *Epigenomics*, vol. 12, no. 1, pp. 53–67, 2020.

[41] D. Zheng, Y. Jiang, C. Qu et al., "Pyruvate kinase M2 tetramerization protects against hepatic stellate cell activation and liver fibrosis," *The American Journal of Pathology*, vol. 190, no. 11, pp. 2267–2281, 2020.

[42] Y. Xu, F. Fang, H. Jiao et al., "Activated hepatic stellate cells regulate MDSC migration through the SDF-1/CXCR4 axis in an orthotopic mouse model of hepatocellular carcinoma," *Cancer Immunology, Immunotherapy*, vol. 68, no. 12, pp. 1959–1969, 2019.

Hindawi
Gastroenterology Research and Practice
Volume 2023, Article ID 1269504, 12 pages
https://doi.org/10.1155/2023/1269504

Research Article

The Efficacy of Surgical Resection versus Radiofrequency Ablation for the Treatment of Single Hepatocellular Carcinoma: A SEER-Based Study

Fang Wu,[1] **Chao Wei**,[2] **Shicun Zhang**,[3] **Shanshan Jia**,[4] **and Jidong Zhang**[4]

[1]*Department of Gastroenterology, School of Clinical Medical, Jiamusi University, Jiamusi, 154007, Heilongjiang Province, China*
[2]*Department of Medical Oncology, The Seventh Hospital of Qiqihar, Qiqihar, 161000, Heilongjiang Province, China*
[3]*Department of Neurology, The Second Affiliated Hospital of Qiqihar Medical University, Qiqihar, 161000, Heilongjiang Province, China*
[4]*Department of Gastroenterology, The First Hospital of Qiqihar, Qiqihar, 161000, Heilongjiang Province, China*

Correspondence should be addressed to Jidong Zhang; zjd2022@qqhrdyyy.com.cn

Received 15 June 2022; Accepted 18 August 2022; Published 21 February 2023

Academic Editor: Enfa Zhao

Background. There is controversy regarding whether patients with single hepatocellular carcinoma (HCC) should be offered radiofrequency ablation (RFA) as a first-line treatment option. Thus, this study compared overall survival after surgical resection (SR) and RFA for single HCC. *Methods*. The Surveillance, Epidemiology, and End Results (SEER) database was used for this retrospective study. The study included 30- to 84-year-old patients diagnosed with HCC from 2000 to 2018. Selection bias was reduced via propensity score matching (PSM). The study compared the overall survival (OS) and cancer-specific survival (CSS) of patients with single HCC who were treated with SR and RFA. *Results*. Before and after PSM, the median OS and median CSS were significantly longer in the SR group than in the RFA group ($p < 0.05$). In the subgroup analysis, the median OS and median CSS for male and female patients with male and female patients with tumor sizes <3, 3–5, and>5 cm, age at diagnosis between 60 and 84 years, and grades I–IV tumors were longer than in the SR group than in the RFA group ($p < 0.05$). Similar results were reported for patients who received chemotherapy ($p < 0.05$). Univariate and multivariate analyses revealed that compared with RFA, SR was an independent favorable factor for OS and CSS ($p < 0.05$) before and after PSM. *Conclusion*. Patients with SR who had a single HCC showed higher OS and CSS compared with patients who received RFA. Hence, SR should be used as a first-line treatment in cases of single HCC.

1. Introduction

According to the 2018 Global Cancer Statistics, hepatocellular carcinoma (HCC) was the sixth most prevalent cancer in the world and the fourth leading cause of cancer-related deaths [1]. Worldwide, the number of HCC deaths is approximately the same as the incidence, with the incidence being higher among men. A liver cancer diagnosis occurs in 1 in 45 men and in 1 in 113 women before age 79 years [2]. A history of chronic alcohol abuse, non-alcoholic fatty liver disease, cirrhosis, or hepatitis B or C virus infection is most commonly associated with HCC development [3], and HCC has a poor prognosis historically. The current Barcelona-Clinic Liver Cancer staging system recommends liver transplantation (LT), surgical resection (SR), and radiofrequency ablation (RFA) as treatment methods for HCC patients with single tumors <5 cm or with three or less tumors <3 cm, without lymph node invasion or distant metastasis [4]. For early single HCC, LT is the best treatment. However, since donors are in short supply, both SR and RFA are considered effective treatments [5].

Regarding treatment for very early hepatocellular carcinomas, it is unclear which treatment is more effective between SR and RFA. Previous studies have shown that

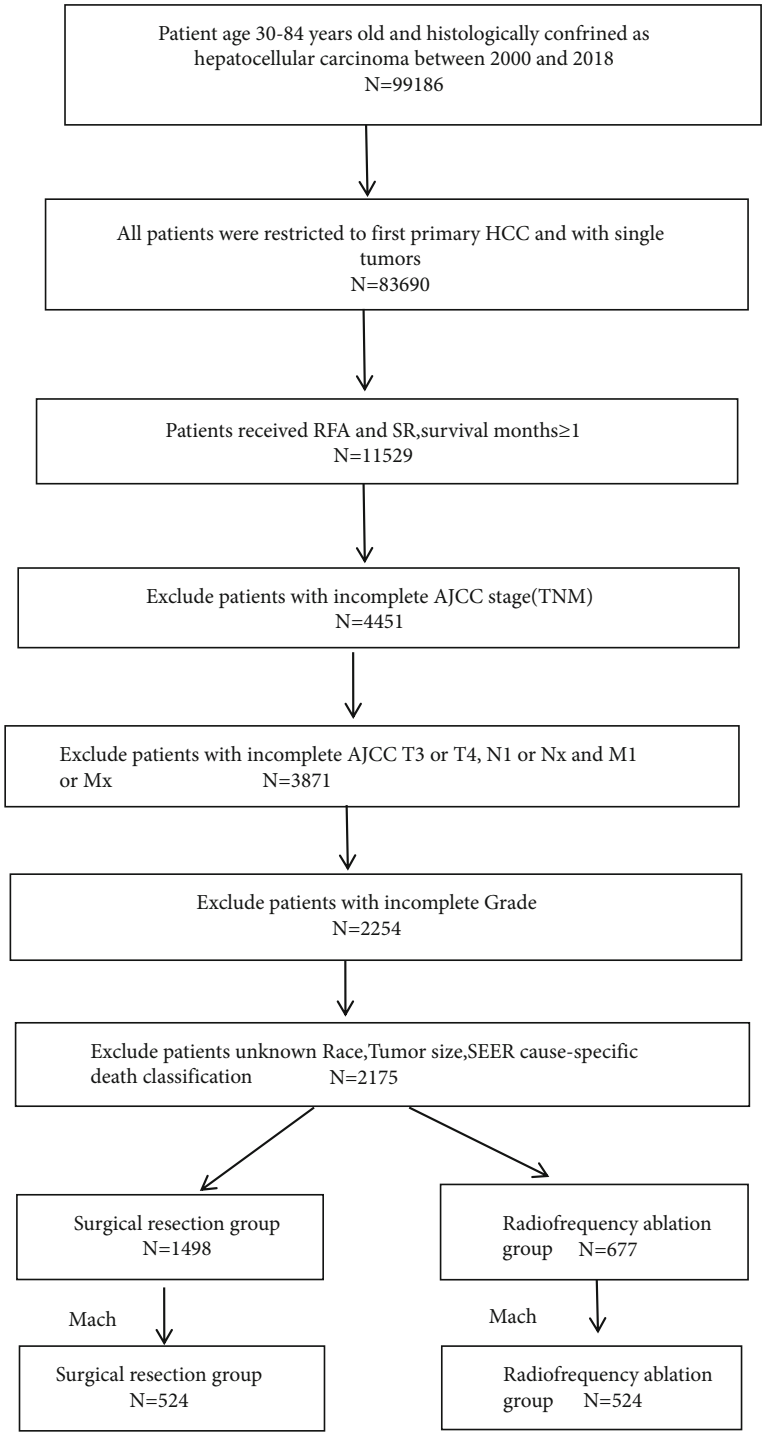

Figure 1: Flowchart of patient selection. HCC: hepatocellular carcinoma; RFA: radiofrequency ablation; SR: surgical resection. AJCC: American Joint Committee on Cancer (7th); SEER: the surveillance, epidemiology, and end results.

RFA is as effective as SR for treating small liver tumors [6–8]. The results of recent studies indicate that SR is associated with a better overall survival rate (OS) than RFA for patients with a single small HCC [9, 10]. However, it is unclear which therapy provides a better prognosis for patients with single HCC. Our study aimed to compare overall survival after SR or RFA for single HCC.

2. Materials and Methods

2.1. Patients. Data from the Surveillance, Epidemiology, and End Results (SEER)*stat software (version 8.4.0) were used for the study after SEER-approval (the reference ID: 23587-Nov2020). Patients with the relevant site code (C22.0) and pathological diagnosis (ICD-O-3 histology

Table 1: Characteristics of patients.

Characteristics	Before PSM ($N = 2175$)				After PSM ($N = 1048$)			
	SR ($N = 1498$)	RFA ($N = 677$)	P	SMD	SR ($N = 524$)	RFA ($N = 524$)	P	SMD
Age of diagnosis (%)			0.528	0.030			0.653	0.032
30–59 years	530 (35.4)	230 (34.0)			193 (36.8)	185 (35.3)		
60–84 years	968 (64.6)	447 (66.0)			339 (64.7)	331 (63.2)		
Gender (%)			0.434	0.039			0.615	0.035
Male	1085 (72.4)	502 (74.2)			392 (74.8)	400 (76.3)		
Female	413 (27.6)	175 (27.6)			132 (25.2)	124 (23.7)		
Race (%)			<0.001	0.322			0.674	0.002
White	808 (54.0)	463 (68.4)			345 (65.8)	349 (66.6)		
Black	207 (13.8)	75 (11.1)			66 (12.6)	57 (10.9)		
Others	483 (32.2)	139 (20.5)			113 (21.6)	118 (22.5)		
Grade (%)			<0.001	0.474			0.851	0.017
I	326 (21.8)	267 (39.4)			179 (34.2)	179 (34.2)		
II	821 (54.8)	334 (49.3)			283 (54.0)	276 (52.7)		
III	324 (21.6)	74 (11.0)			59 (11.3)	67 (12.8)		
IV	27 (1.8)	2 (0.3)			3 (0.5)	2 (0.3)		
SEER stage (%)			<0.001	0.147			1	<0.001
Localized	1381 (92.2)	591 (87.3)			481 (91.8)	481 (91.8)		
Regional	117 (7.8)	86 (12.7)			43 (8.2)	43 (8.2)		
Chemotherapy (%)			<0.001	0.340			0.440	0.044
No	1343 (89.7)	507 (74.9)			449 (85.7)	439 (83.8)		
Yes	155 (10.3)	170 (25.1)			75 (14.3)	85 (16.2)		
Tumor size (%)			<0.001	0.951			0.067	0.034
<3 cm	388 (25.9)	368 (54.4)			277 (52.9)	254 (48.5)		
3–5 cm	566 (37.8)	266 (39.3)			193 (36.8)	228 (43.5)		
>5 cm	544 (36.3)	43 (6.3)			54 (10.3)	42 (8.0)		
AJCC T (%)			0.643	0.023			1	0.004
T1	1082 (72.2)	482 (71.2)			407 (77.7)	408 (77.9)		
T2	416 (27.8)	195 (28.8)			117 (22.3)	116 (22.1)		

codes: 8170-8175) were included in the analysis. All cases were restricted to the first primary HCC. The surgery codes used were: RFA-16 and SR-20 to 25, 30, 36, 37, 50, 51, and 52. The inclusion criteria were as follows: (1) diagnosis of the patient was between 2000 and 2018; (2) patient age 30–84 years; (3) presence of a single tumor that had not invaded the lymph nodes or spread to distant sites; (4) availability of complete survival data; and (5) history of RFA or SR. The exclusion criteria comprised (1) incomplete AJCC 7th TNM stage; (2) AJCC stages T3 or T4, N1 or NX, and M1 or MX; (3) incomplete grade; (4) unknown patient race; (5) unknown tumor size; and (6) missing/unknown cause-specific death classification (Figure 1).

2.2. Statistical Analyses. We extracted patient information from the SEER database. We converted all continuous variables to categorical variables were analyzed using the chi-square test or Fisher exact test. The median OS and median cause-specific survival (CSS) were determined using Kaplan–Meier survival curves and compared with the log-rank test. Before and after propensity score matching (PSM), Cox-proportional hazards model was used to identify OS and CSS predictors. Multivariate analysis was conducted using variables with p-values <0.1 in the univariate analysis. Age at diagnosis, sex, race, tumor size, grade, SEER stage, chemotherapy, and AJCC T stage were included into the PSM analysis. We set the optimal caliper at 0.01, and a total of 524 pairs of matched nearest neighbors were found. Values of $p < 0.05$ were considered to indicate statistical significance in all tests, which were two-sided. Statistics were analyzed using SPSS v22.0 (IBM, Armonk, NY, USA).

3. Results

3.1. Baseline Characteristics. The study included 2175 (1587 male and 588 female) patients, with 677 in the RFA group and 1498 in the SR group. Prior to PSM, the RFA group had more white patients and tumors sized <3 cm compared

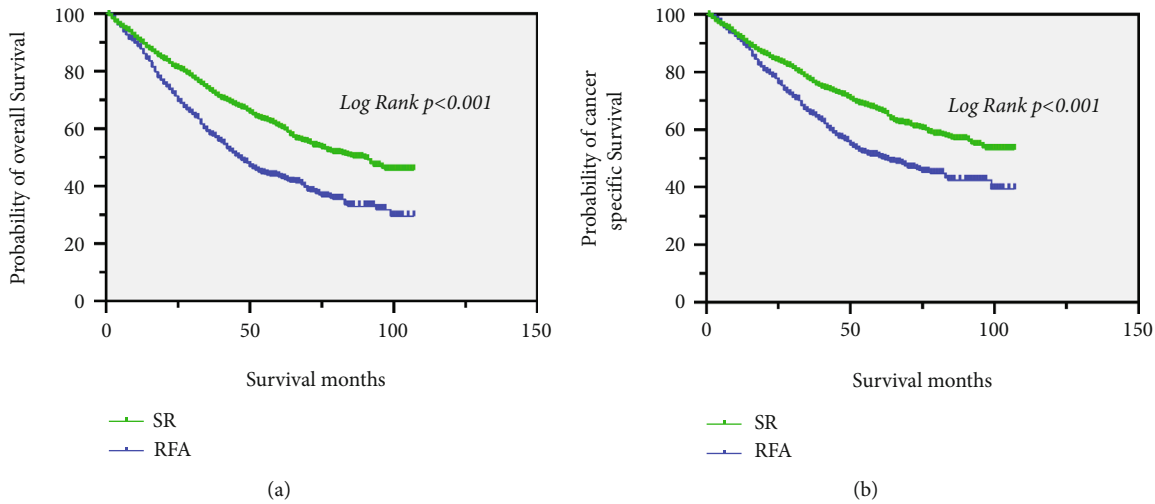

Figure 2: The Kaplan–Meier curve for OS (a) and CSS (b) before PSM for patients with SR and RFA.

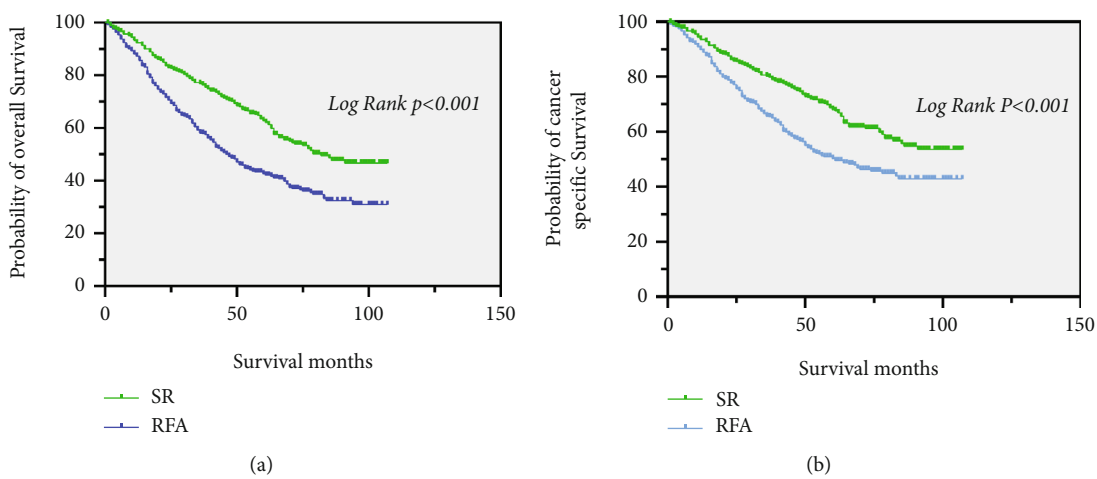

Figure 3: The Kaplan–Meier curve for OS (a) and CSS (b) after PSM for patients with SR and RFA.

to the SR group ($p < 0.001$). The SR group had more cases without chemotherapy, and more moderately differentiated and more localized cancer cases than the RFA group ($p < 0.001$) (Table 1). After PSM, the characteristics of the two groups did not significantly differ (all $p > 0.05$) (Table 1).

3.2. Efficacy. Prior to PSM, the median OS of the SR group (86 months) was significantly longer than that of the RFA group (46 months) ($p < 0.001$; Figure 2(a)). The median CSS of patients in the SR was significantly better than that in the RFA group ($p < 0.001$; Figure 2(b)).

After PSM, patients in the SR group (82 months) had a higher median OS than those in the RFA group (46 months) ($p < 0.001$; Figure 3(a)). The SR group had a higher median CSS than those the RFA group ($p < 0.001$; Figure 3(b)).

Among patients who received chemotherapy, the median OS was significantly longer in the SR group (64 months) than in the RFA group (41 months) ($p = 0.004$; Figure 4(a)). The median CSS was also significantly longer in the SR group (66 months) than in the RFA group (42 months) ($p = 0.018$; Figure 4(b)).

In those with tumor size <3 cm, the median OS and median CSS of patients in the SR group were significantly better than in the RFA group ($p = 0.001$ and $p = 0.007$, respectively) (Figure 4(c) and 4(d)).

Regarding patients with a single tumor size of 3–5 cm, the median OS was significantly longer in the SR group (71 months) than in the RFA group (39 months) ($p < 0.001$; Figure 4(e)). The median CSS of patients in the SR was significantly better than in the RFA group ($p < 0.001$; Figure 4(f)).

Similar results were noted in patients with tumor sizes >5 cm. The median OS and median CSS were significantly

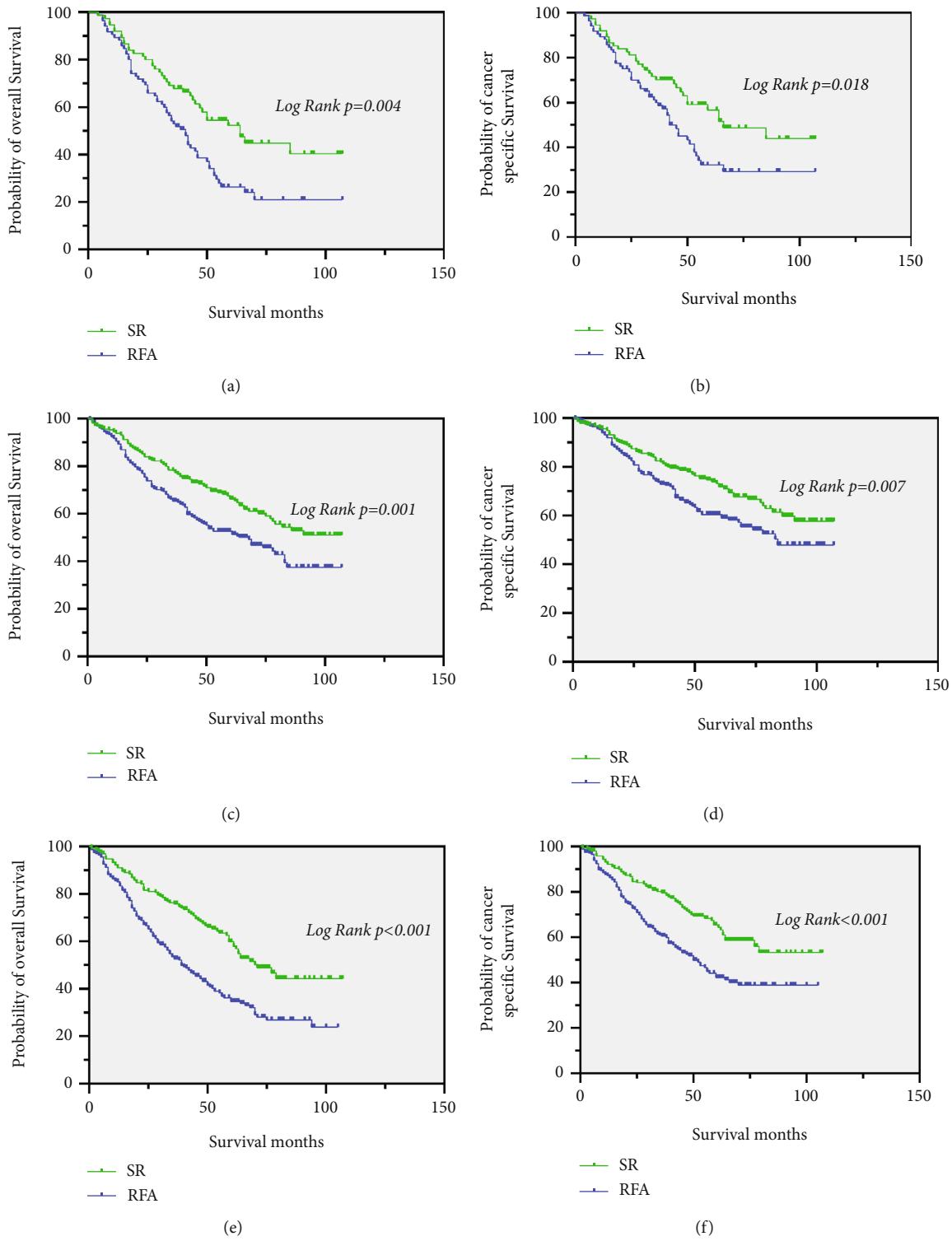

Figure 4: Continued.

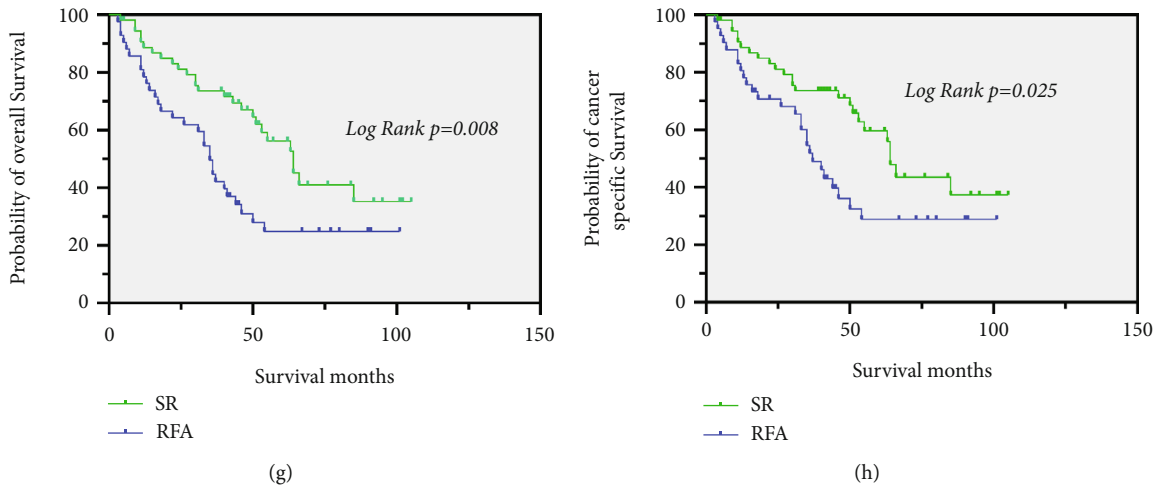

Figure 4: Kaplan–Meier curve of OS and CSS in patients with SR and RFA after PSM—(a and b) patients who received chemotherapy; (c and d) patients with tumor size ≤3 cm; (e and f) patients with tumor size 3–5 cm; (g, h) patients with tumor size >5 cm.

longer in the SR group (64 months, 64 months, respectively) than in the RFA group (35 months, 37 months, respectively) ($p = 0.008$ and $p = 0.025$, respectively) (Figure 4(g) and 4(h)).

In patients with age of diagnosis between 30–59 years, the median OS was significantly longer in the SR group (85 months) than in the RFA group (60 months) ($p = 0.021$). The median CSS was also significantly longer in the SR group than in the RFA group ($p = 0.214$), it is no statistical (Figure 5(a) and 5(b)).

For those with an age at diagnosis between 60 and 84 years, male patients and female patients, the median OS in the SR group (79 months, 79 months, and 82 months, respectively) were longer than that in the RFA group (43 months, 49 months and 34 months, respectively) ($p < 0.05$; Figure 5(c), 5(e), and 5(g)). Meanwhile, the median CSS of these patients in the SR group was significantly better than in the RFA group ($p < 0.05$; Figure 5(d), 5(f), and 5(h)).

For patients with grade I tumors and grade II tumors, the median OS in the SR group (82 months, 78 months, respectively) were longer than that in the RFA group (63 months, 45 months, respectively) ($p < 0.05$; Figure 6(a) and 6(c)). The median CSS of these patients in the SR group was significantly better than in the RFA group ($p < 0.05$; Figure 6(b) and 6(d)).

The results of the analysis showed that patients with grade III and grade IV tumors had longer the median OS and median CSS in the SR group than in the RFA group ($p < 0.001$; Figure 6(e) and 6(f)).

3.3. Predictors of OS and CSS. Prior to PSM, univariate analysis suggested that compared with RFA, SR was an independent favorable factor for OS (hazard ratio [HR]: 1.628, 95% CI: 1.434–1.847, $p < 0.001$) (Table 2) and CSS (HR: 1.557; 95% CI: 1.351–1.794, $p < 0.001$) (Table 2). Multivariate analysis also showed that compared to RFA, SR was an independent favorable factor for OS (HR: 1.799, 95% CI: 1.523–2.125, $p < 0.001$) (Table 2) and CSS (HR: 1.799; 95% CI: 1.523–2.125, $p < 0.001$) (Table 2). After PSM, similar results were obtained and the univariate analysis showed that compared with RFA, SR was an independent favorable factor for OS (HR: 1.755; 95% CI: 1.470–2.095, $p < 0.001$) (Table 3) and CSS (HR: 1.667; 95% CI: 1.368–2.031, $p < 0.001$) (Table 3). Multivariate analysis showed that compared with RFA, SR was an independent favorable factor for OS (HR: 1.761; 95% CI: 1.474–2.104, $p < 0.001$) (Table 3) and CSS (HR: 1.686; 95% CI: 1.382–2.057, $p < 0.001$) (Table 3).

3.4. Prognostic Factors for OS and CSS after PSM. Univariate analysis showed that race, grade, seer stage, chemotherapy, tumor size, AJCC T stage, and treatment was strongly related to OS (Table 3). Multivariate Cox regression analysis showed that the others race (non-black, non-white) (HR: 0.491, 95% CI: 0.382–0.630; $p < 0.001$), grade III (HR: 1.507; 95% CI: 1.137–1.998; $p = 0.004$), grade IV (HR: 3.235; 95% CI: 1.015–10.316; $p = 0.047$), tumor 3–5 cm (HR: 1.340; 95% CI: 1.112–1.614; $p = 0.002$), tumor >5 cm (HR: 1.636; 95% CI: 1.198–2.236; $p = 0.002$), AJCC T stage (HR: 1.606; 95% CI: 1.298–1.986; $p < 0.001$), and treatment modality (HR: 1.761; 95% CI: 1.474–2.104; $p < 0.001$) were significantly associated with OS (Table 3).

In the univariate analysis, age at diagnosis, race, grade, seer stage, chemotherapy, tumor size, AJCC T stage, and treatment were significantly associated with CSS (Table 3). The multivariate Cox regression analysis showed that the others race (HR: 0.519, 95% CI: 0.394–0.683; $p < 0.001$), grade III (HR: 1.566; 95% CI: 1.146–2.142; $p = 0.005$), grade IV (HR: 3.644; 95% CI: 1.130–11.750; $p = 0.030$), tumors of 3–5 cm (HR: 1.329; 95% CI: 1.076–1.641; $p = 0.008$), tumors >5 cm (HR: 1.787; 95% CI: 1.273–2.509; $p = 0.001$), AJCC T

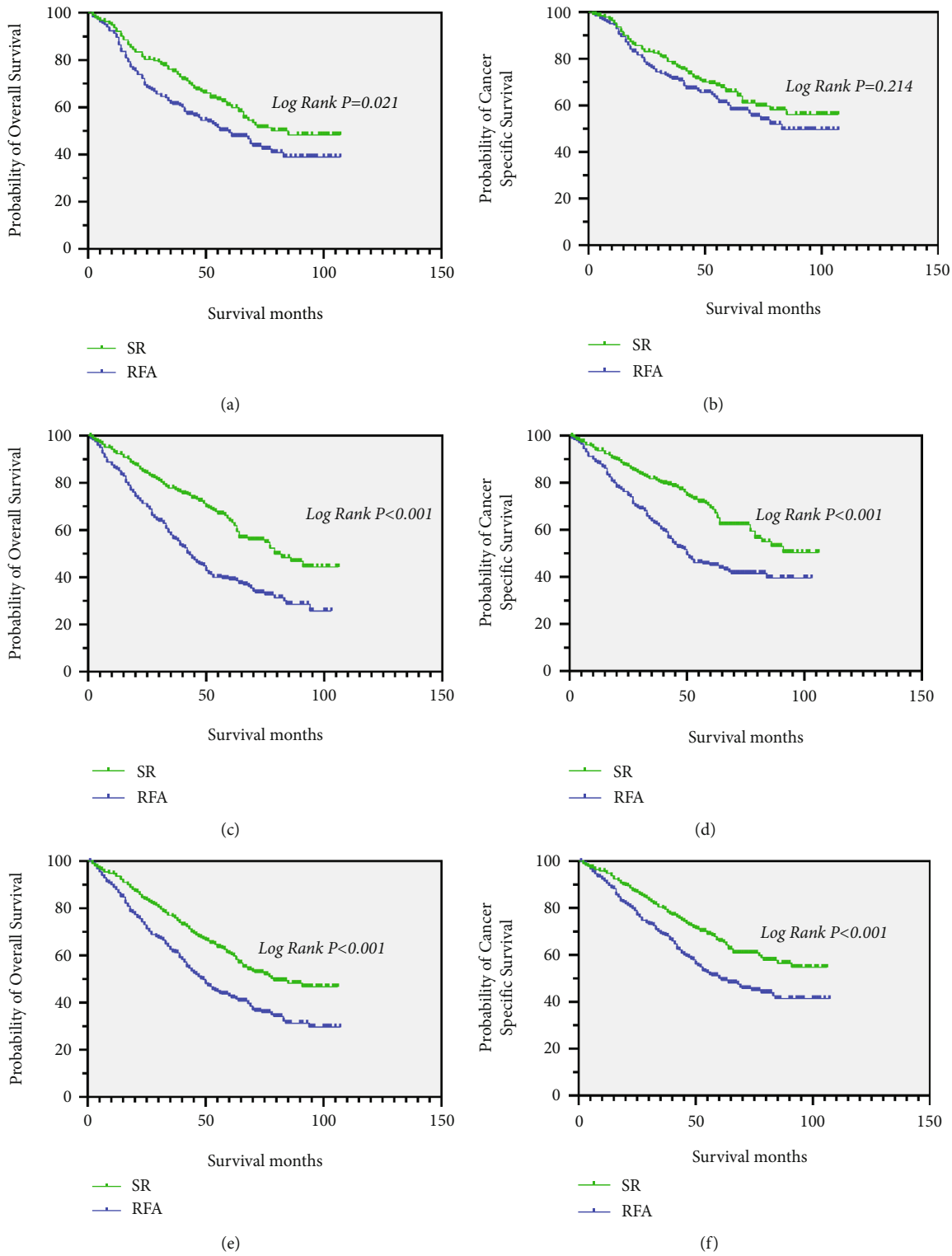

Figure 5: Continued.

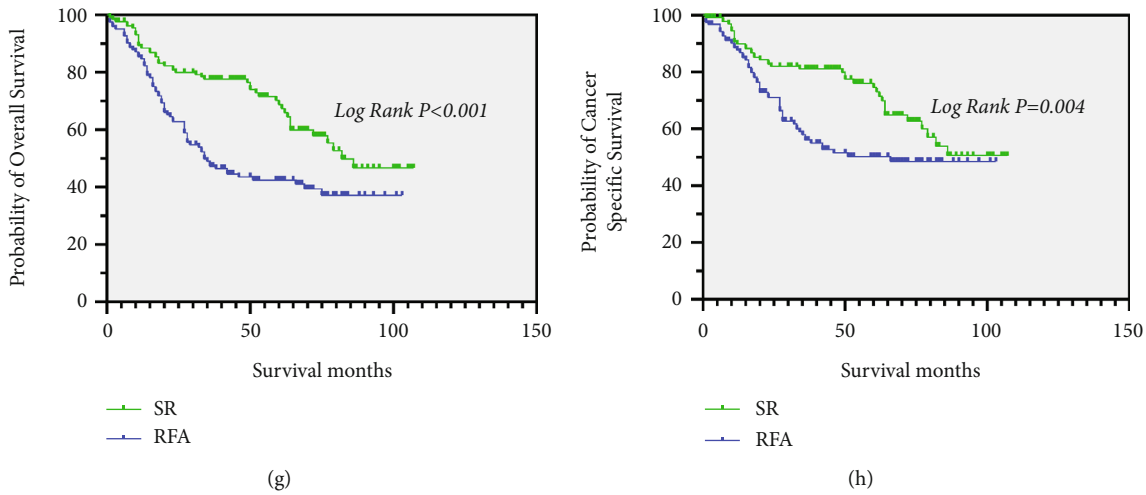

Figure 5: Kaplan–Meier curve of OS and CSS in patients with SR and RFA after PSM—(a and b) patients with an age at diagnosis between 30 and 59 years; (c and d) patients with an age at diagnosis between 60 and 84 years; (e and f) male patients; (g and h) female patients.

stage (HR: 1.718; 95% CI: 1.355–2.178; $p < 0.001$), and treatment (HR: 11.686; 95% CI: 1.382–2.057; $p < 0.001$) were significantly associated with CSS (Table 3).

4. Discussion

Our study showed that before and after PSM, SR demonstrated better median OS and CSS than RFA. The results showed that the median OS and median CSS of male and female SR patients were longer than those of RFA patients with tumor sizes <3, 3–5, and >5 cm, age at diagnosis 60–84 years, and grades I–IV tumors. A similar result was also observed in those who received chemotherapy. Several previous studies have recorded similar results, with SR being associated with a longer OS than RFA for patients with small HCC [9, 10]. Mills et al. noted that patients with HCC who undergo SR have a better chance of surviving than those who undergo RFA [11]. Nathan et al. recorded improved survival rates in patients with early HCC who underwent SR [12].

In this study, age at diagnosis, gender, race, grade, seer stage, chemotherapy, tumor size, AJCC T stage, and treatment modality were included in the Cox proportional-hazards model. Before PSM, age at diagnosis, gender, race, grade, chemotherapy, tumor size, AJCC T stage, and treatment modality influenced OS and CSS. After PSM, OS and CSS were only associated with race, grade, tumor size, AJCC T stage, and treatment modality. Thus, we concluded that patients who had single HCCs that were poorly differentiated, with higher AJCC T stages and greater sizes, had worse prognoses, and this is in agreement with other population-based studies [13]. Margonis et al. indicated that in lesions with poorly differentiated HCC, the prognosis might be less favorable [14]. A prospective study by Camma et al. showed that patients with HCC whose tumors were <3 cm had better outcomes after treatment [15]. Likewise, our study showed that tumor size <3 cm was associated with superior survival compared to tumor size of 3–5 cm. The prognosis of most solid tumors is predicted based on the AJCC TNM system [16], as our results reflect. Citterio et al. noted that in patients with single HCC and no lymph nodes or distant metastases, SR is frequently performed [17]. SR is recommended as the first-line treatment for patients with very early-stage HCC since it has a better OS than RFA [9]. The results of our study are similar to some previous studies [18, 19] that showed that SR provides better therapeutic effect than RFA for small single HCC. The present study has some limitations. First, due to its retrospective design, selection bias was inevitable. Thus, we attempted to reduce the selection bias by PSM, which ensured a better balance in the baseline characteristics between the two groups. Second, the hepatic function and health of the patients were unknown because the SEER database did not contain this information. This lack of information might have influenced the results. However, previous studies have shown that those with a single HCC who undergo SR had better survival outcomes compared with those who received RFA [20]. The results of our study are similar to those of previous studies, but the SEER database did not contain HCC predisposing factors, such as hepatitis or steatohepatitis. There was only macroscopic information regarding the treatment methods in the SEER database, which did not include chemotherapy regimens and surgery programs. Considering this, it is necessary to conduct a prospective randomized trial to confirm these results in future work.

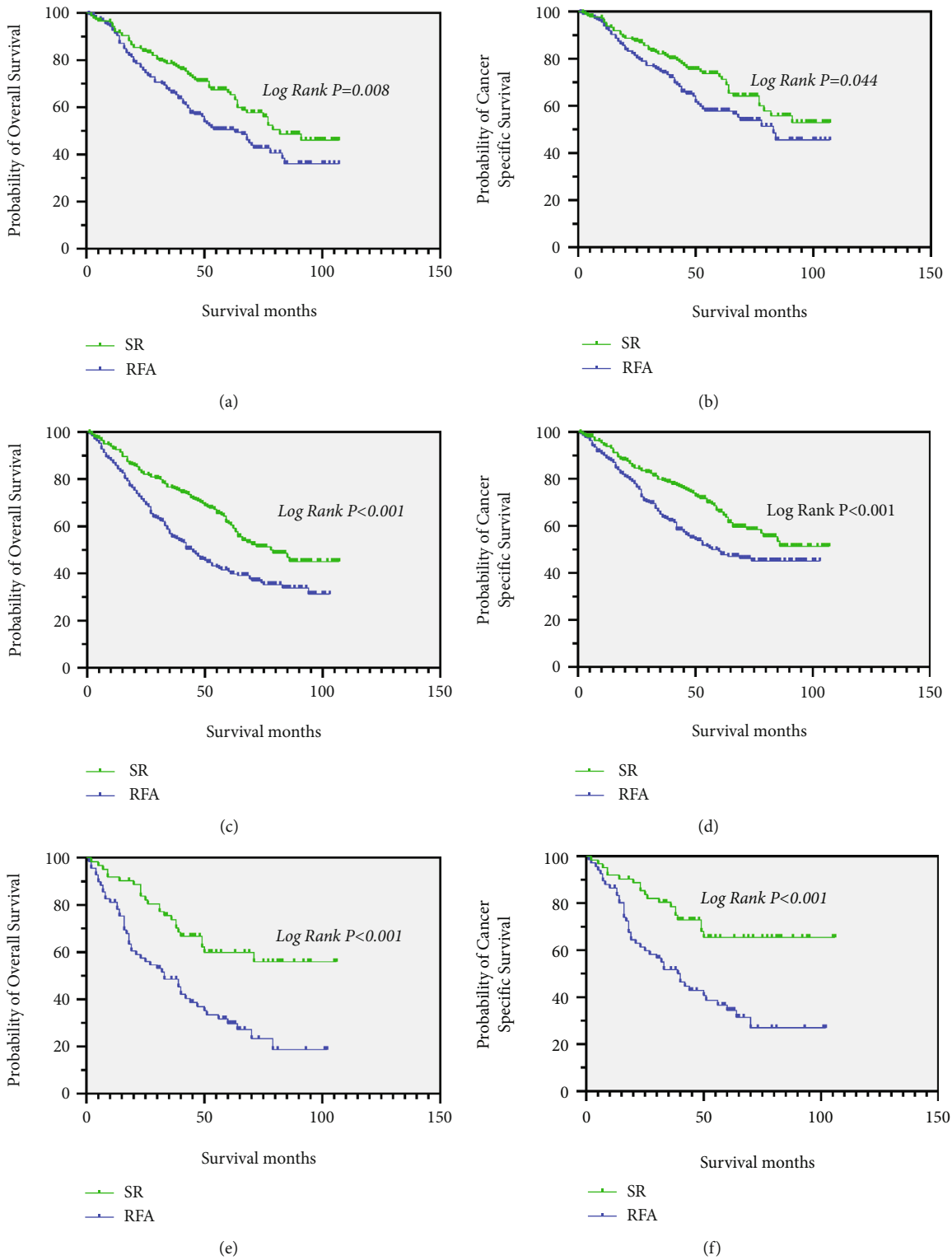

Figure 6: Kaplan–Meier curve of OS and CSS in patients with SR and RFA after PSM—(a and b) patients with Grade I tumors; (c and d) patients with Grade II tumors; (e, f) patients with Grade III and Grade IV tumors.

Table 2: Predictors for overall survival and cancer-specific survival prior to PSM.

	Overall survival				Cancer-specific survival			
	Univariate analysis		Multivariate Analysis		Univariate analysis		Multivariate analysis	
Characteristics	HR (95% CI)	*P*	HR (95% CI)	*P*	HR (95% CI)	*P*	HR (95% CI)	*P*
Age of diagnosis								
30–59 years	Reference		Reference		Reference		Reference	
60–84 years	1.228 (1.075, 1.402)	0.002	1.186 (1.038, 1.357)	0.012	1.235 (1.065, 1.433)	0.005	1.189 (1.024, 1.381)	0.023
Gender								
Male	Reference		Reference		Reference		Reference	
Female	0.816 (0.705, 0.943)	0.006	0.832 (0.719, 0.964)	0.014	0.815 (0.693, 0.958)	0.013	0.826 (0.702, 0.972)	0.022
Race								
White	Reference		Reference		Reference		Reference	
Black	1.048 (0.877,1.251)	0.608	1.093 (0.914,1.306)	0.329	1.052 (0.862,1.283)	0.62	1.100 (0.901,1.342)	0.35
Others	0.576 (0.492, 0.674)	<0.001	0.601 (0.513, 0.704)	<0.001	0.611 (0.514, 0.725)	<0.001	0.633 (0.532, 0.754)	<0.001
Grade								
I	Reference		Reference		Reference		Reference	
II	1.098 (0.946, 1.275)	0.22	1.159 (0.996, 1.349)	0.057	1.122 (0.948, 1.328)	0.18	11.168 (0.985, 1.386)	0.075
III	1.371 (1.142, 1.647)	0.001	1.592 (1.318, 1.924)	<0.001	1.500 (1.225, 1.836)	<0.001	1.705 (1.383, 2.102)	<0.001
IV	1.329 (0.790, 2.237)	0.284	1.523 (0.897, 2.586)	0.12	1.478 (0.843, 2.590)	0.172	1.571 (0.888, 2.782)	0.121
SEER stage								
Localized	Reference		Reference		Reference		Reference	
Regional	1.417 (1.164, 1.725)	0.001	1.109 (0.900, 1.366)	0.331	1.569 (1.272, 1.937)	<0.001	1.204 (0.963, 1.505)	0.103
Chemotherapy								
No	Reference		Reference		Reference		Reference	
Yes	1.538 (1.315, 1.797)	<0.001	1.186 (1.007, 1.397)	0.041	1.667 (1.407, 1.975)	<0.001	1.273 (1.065, 1.521)	0.008
Tumor size								
<3 cm	Reference		Reference		Reference		Reference	
3–5 cm	1.194 (1.030, 1.383)	0.018	1.319 (1.134, 1.535)	<0.001	1.218 (1.031, 1.439)	0.02	1.335 (1.125, 1.583)	0.001
>5 cm	1.259 (1.074, 1.477)	0.005	1.616 (1.352, 1.931)	<0.001	1.401 (1.175, 1.671)	<0.001	1.783 (1.463, 2.171)	<0.001
AJCC T								
T1	Reference		Reference		Reference		Reference	
T2	1.527 (1.340, 1.740)	<0.001	1.436 (1.251, 1.648)	<0.001	1.657 (1.435, 1.912)	<0.001	1.528 (1.313, 1.777)	<0.001
Treatment								
Surgical resection	Reference		Reference		Reference		Reference	
Radiofrequency ablation	1.628 (1.434, 1.847)	<0.001	1.828 (1.577, 2.120)	<0.001	1.557 (1.351, 1.794)	<0.001	1.799 (1.523, 2.125)	<0.001

Table 3: Predictors for overall survival and cancer-specific survival after PSM.

	Overall survival				Cancer-specific survival			
	Univariate analysis		Multivariate analysis		Univariate analysis		Multivariate analysis	
Characteristics	HR (95% CI)	*P*	HR (95% CI)	*P*	HR (95% CI)	*P*	HR (95% CI)	*P*
Age of diagnosis								
30–59 years	Reference				Reference		Reference	
60–84 years	1.129 (0.941,1.354)	0.193			1.201 (0.977,1.476)	0.082	1.198 (0.971,1.477)	0.092
Gender								
Male	Reference				Reference			
Female	0.990 (0.807,1.215)	0.925			1.001 (0.796, 1.259)	0.993		
Race								
White	Reference		Reference		Reference		Reference	
Black	1.008 (0.777, 1.308)	0.952	1.005 (0.773, 1.306)	0.97	0.997 (0.742, 1.339)	0.982	0.984 (0.731, 1.324)	0.914
Others	0.506 (0.395, 0.648)	<0.001	0.491 (0.382, 0.630)	<0.001	0.541 (0.412, 0.710)	<0.001	00.519 (0.394, 0.683)	<0.001
Grade								
I	Reference	Reference	Reference	Reference				
II	1.171 (0.964, 1.423)	0.111	1.144 (0.941, 1.391)	0.178	1.185 (0.952, 1.476)	0.129	1.150 (0.922, 1.434)	0.214
III	1.407 (1.062, 1.863)	0.017	1.507 (1.137, 1.998)	0.004	1.491 (1.092, 2.035)	0.012	1.566 (1.146, 2.142)	0.005
IV	2.136 (0.681, 6.696)	0.193	3.235 (1.015, 10.316)	0.047	2.788 (0.887, 8.769)	0.079	3.644 (1.130, 11.750)	0.03
SEER stage								
Localized	Reference		Reference		Reference		Reference	
Regional	1.329 (0.993, 1.780)	0.056	0.942 (0.687, 1.290)	0.707	1.380 (0.999, 1.906)	0.051	0.932 (0.657, 1.322)	0.692
Chemotherapy								
No	Reference		Reference		Reference		Reference	
Yes	1.433 (1.149,1.786)	0.001	1.148 (0.908,1.451)	0.249	1.568 (1.233,1.994)	<0.001	1.242 (0.959,1.608)	0.1
Tumor size								
<3 cm	Reference		Reference		Reference		Reference	
3–5 cm	1.427 (1.187, 1.715)	<0.001	1.340 (1.112, 1.614)	0.002	1.450 (1.178, 1.785)	<0.001	1.329 (1.076, 1.641)	0.008
>5 cm	1.540 (1.149, 2.063)	0.004	1.636 (1.198, 2.236)	0.002	1.772 (1.294, 2.426)	<0.001	1.787 (1.273,2.509)	0.001
AJCC T								
T1	Reference		Reference		Reference		Reference	
T2	1.641 (1.354, 1.989)	<0.001	1.606 (1.298, 1.986)	<0.001	1.722 (1.390, 2.133)	<0.001	1.718 (1.355, 2.178)	<0.001
Treatment								
Surgical resection	Reference		Reference		Reference		Reference	
Radiofrequency ablation	1.755 (1.470, 2.095)	<0.001	1.761 (1.474, 2.104)	<0.001	1.667 (1.368, 2.031)	<0.001	1.686 (1.382, 2.057)	<0.001

5. Conclusion

In this population-based study, patients with single HCC who underwent SR had better OS and CSS compared to those who received RFA, indicating that SR should be used as a first-line treatment in such cases. The research showed that the prognosis was poorer for patients who had single HCC with poor differentiation, higher AJCC T stages, and greater tumor sizes.

Data Availability

All data were acquired from the SEER database.

Ethical Approval

For experiments on humans, our institution requires that we conduct all our work in accordance with the Helsinki Declaration (1964).

Consent

Since we obtained the data from the SEER database and did not conduct any human experiments, we did not need written informed consent.

Conflicts of Interest

There are no conflicts of interest regarding the publication of this article.

Acknowledgments

We thank the SEER database staff for the data provided.

References

[1] F. Bray, J. Ferlay, I. Soerjomataram, R. L. Siegel, L. A. Torre, and A. Jemal, "Global cancer statistics 2018: GLOBOCAN estimates of incidence and mortality worldwide for 36 cancers in 185 countries," *CA: A Cancer Journal for Clinicians*, vol. 68, no. 6, pp. 394–424, 2018.

[2] Global Burden of Disease Cancer Collaboration, C. Fitzmaurice, C. Allen et al., "Global, regional, and national cancer incidence, mortality, years of life lost, years lived with disability, and disability-adjusted life-years for 32 cancer groups, 1990 to 2015," *JAMA Oncology*, vol. 3, no. 4, pp. 524–548, 2017.

[3] J. Ferlay, M. Colombet, I. Soerjomataram et al., "Estimating the global cancer incidence and mortality in 2018: GLOBOCAN sources and methods," *International Journal of Cancer*, vol. 144, no. 8, pp. 1941–1953, 2019.

[4] M. Reig, A. Forner, J. Rimola et al., "BCLC strategy for prognosis prediction and treatment recommendation: the 2022 update," *Journal of Hepatology*, vol. 76, no. 3, pp. 681–693, 2022.

[5] F. Meng, H. Zhang, H. Peng, and S. Lu, "Comparison of 10-year survival outcomes for early single hepatocellular carcinoma following different treatments," *BioMed Research International*, vol. 2021, 2021.

[6] H. H. Hung, Y. Y. Chiou, C. Y. Hsia et al., "Survival rates are comparable after radiofrequency ablation or surgery in patients with small hepatocellular carcinomas," *Clinical Gastroenterology and Hepatology*, vol. 9, no. 1, pp. 79–86, 2011.

[7] D. Choi, H. K. Lim, H. Rhim et al., "Percutaneous radiofrequency ablation for early-stage hepatocellular carcinoma as a first-line treatment: long-term results and prognostic factors in a large single-institution series," *European Radiology*, vol. 17, no. 3, pp. 684–692, 2007.

[8] Y. K. Cho, J. K. Kim, W. T. Kim, and J. W. Chung, "Hepatic resection versus radiofrequency ablation for very early stage hepatocellular carcinoma: A Markov model analysis," *Hepatology*, vol. 51, no. 4, pp. 1284–1290, 2010.

[9] H. H. Chu, J. H. Kim, P. N. Kim et al., "Surgical resection versus radiofrequency ablation very early-stage HCC (≤2 cm Single HCC): a propensity score analysis," *Liver International*, vol. 39, no. 12, pp. 2397–2407, 2019.

[10] Y. C. Li, P. H. Chen, J. H. Yeh et al., "Clinical outcomes of surgical resection versus radiofrequency ablation in very-early-stage hepatocellular carcinoma: a propensity score matching analysis," *BMC Gastroenterology*, vol. 21, no. 1, p. 418, 2021.

[11] A. Mills, D. Thayer, C. Noda et al., "Thermal ablation versus surgical resection for localized hepatocellular carcinoma: a population study using the SEER database," *Future Oncology*, vol. 14, no. 7, pp. 631–645, 2018.

[12] H. Nathan, O. Hyder, S. C. Mayo et al., "Surgical therapy for early hepatocellular carcinoma in the modern era," *Annals of Surgery*, vol. 258, no. 6, pp. 1022–1027, 2013.

[13] B. Yan, B. B. Su, D. S. Bai et al., "A practical nomogram and risk stratification system predicting the cancer- specific survival for patients with early hepatocellular carcinoma," *Cancer Medicine*, vol. 10, no. 2, pp. 496–506, 2021.

[14] G. A. Margonis, K. Sasaki, N. Andreatos et al., "Prognostic impact of complications after resection of early stage hepatocellular carcinoma," *Journal of Surgical Oncology*, vol. 115, no. 7, pp. 791–804, 2017.

[15] C. Cammà, V. Di Marco, A. Orlando et al., "Treatment of hepatocellular carcinoma in compensated cirrhosis with radiofrequency thermal ablation (RFTA): a prospective study," *Journal of Hepatology*, vol. 42, no. 4, pp. 535–540, 2005.

[16] T. W. Leung, A. M. Tang, B. Zee et al., "Construction of the Chinese University Prognostic Index for hepatocellular carcinoma and comparison with the TNM staging system, the Okuda staging system, and the Cancer of the Liver Italian Program staging system," *Cancer*, vol. 94, no. 6, pp. 1760–1769, 2002.

[17] D. Citterio, A. Facciorusso, C. Sposito, R. Rota, S. Bhoori, and V. Mazzaferro, "Hierarchic interaction of factors associated with liver decompensation after resection for hepatocellular carcinoma," *JAMA Surgery*, vol. 151, no. 9, pp. 846–853, 2016.

[18] S. Lee, T. W. Kang, D. I. Cha et al., "Radiofrequency ablation _vs._ surgery for perivascular hepatocellular carcinoma: propensity score analyses of long-term outcomes," *Journal of Hepatology*, vol. 69, no. 1, pp. 70–78, 2018.

[19] D. H. Lee, J. W. Kim, J. M. Lee et al., "Laparoscopic liver resection versus percutaneous radiofrequency ablation for small single nodular hepatocellular carcinoma: comparison of treatment outcomes," *Liver Cancer*, vol. 10, no. 1, pp. 25–37, 2021.

[20] J. Huang, L. Yan, Z. Cheng et al., "A randomized trial comparing radiofrequency ablation and surgical resection for HCC conforming to the Milan criteria," *Annals of Surgery*, vol. 252, no. 6, pp. 903–912, 2010.

Hindawi
Gastroenterology Research and Practice
Volume 2022, Article ID 3200932, 13 pages
https://doi.org/10.1155/2022/3200932

Research Article

Differential Expression Profiles of mRNA and Noncoding RNA and Analysis of Competitive Endogenous RNA Regulatory Networks in Nonalcoholic Steatohepatitis

Mengjia Gao,[1,2,3,4] Jingxin Xin,[1,2,3,4] Xiaoling Li,[1,2,3,4] Ling Gao,[2,3,4,5] Shanshan Shao,[1,2,3,4] and Meng Zhao[1,2,3,4]

[1]*Department of Endocrinology, Shandong Provincial Hospital Affiliated to Shandong First Medical University, Jinan, Shandong 250021, China*
[2]*Shandong Clinical Research Center of Diabetes and Metabolic Diseases, Jinan, Shandong 250021, China*
[3]*Shandong Key Laboratory of Endocrinology and Lipid Metabolism, Jinan, Shandong 250021, China*
[4]*Shandong Prevention and Control Engineering Laboratory of Endocrine and Metabolic Diseases, Jinan, Shandong 250021, China*
[5]*Scientific Center, Shandong Provincial Hospital Affiliated to Shandong First Medical University, Jinan, Shandong 250021, China*

Correspondence should be addressed to Shanshan Shao; shaoshanshan11@126.com and Meng Zhao; zjsylpzm@163.com

Received 10 March 2022; Revised 19 June 2022; Accepted 21 June 2022; Published 7 July 2022

Academic Editor: Enfa Zhao

Nonalcoholic steatohepatitis (NASH) is a liver disease caused by multiple factors, and there is no approved pharmacotherapy. The pathogenesis of NASH remains underexplored. In this study, differentially expressed circular RNAs (circRNAs) were obtained by analyzing NASH-related circRNA datasets, and then, corresponding target microRNAs (miRNAs) and messenger RNAs (mRNAs) were predicted to construct a circRNA–miRNA–mRNA regulatory network. On this basis, a total of 38 circRNAs, 7 miRNAs, and 10 mRNAs were screened out. The present study reveals novel circRNA biomarkers of NASH and reports a potential competing endogenous RNA (ceRNA) regulatory network that might provide insights for further investigation into the underlying pathogenesis of NASH.

1. Introduction

Nonalcoholic fatty liver disease (NAFLD) is the most common liver disease worldwide and includes nonalcoholic fatty liver, nonalcoholic steatohepatitis (NASH), and cirrhosis. Nonalcoholic fatty liver (NAFL) is characterized by simple steatosis, whereas NASH is typically characterized by the presence of lobular inflammation and ballooning with or without perisinusoidal fibrosis in addition to steatosis [1]. NAFL is the nonprogressive form of NAFLD, while NASH is the progressive form of NAFLD and may advance to cirrhosis and hepatocellular carcinoma (HCC), which is the leading cause of end-stage liver disease or liver transplantation [2]. The prevalence of NASH has been gradually increasing worldwide in recent years, and worryingly, the liver-specific mortality rate for NASH is high [3]. However, the pathogenesis of NASH has not been fully elucidated.

In recent years, various noncoding RNAs (ncRNAs) acting as competing endogenous RNAs (ceRNAs) have become a major research hotspot for various diseases. MiRNAs and circRNAs are different kinds of ncRNAs [4]. Multiple lines of evidence indicate that other RNAs with miRNA target sites, such as circRNAs, can compete with mRNAs to bind miRNAs [5]. CircRNAs have become a focus of life science and medical research and have been identified as key regulators of many diseases. Studies have shown that circRNAs can act as ceRNAs or miRNA sponges by interacting with miRNAs to sequester these molecules and reduce their regulatory effect on target mRNAs [6]. The circRNA–miRNA–mRNA axis has also been shown to be involved in a variety

of cellular events, including apoptosis, vascularization, and metastasis. Studies have shown that the expression profile of circRNA can be a candidate for NASH diagnosis, and the circRNA–miRNA–mRNA pathway may provide clues for studying the pathogenesis of NASH [7, 8]. The exploration of circRNA expression patterns and the circRNA–miRNA–mRNA network in the pathogenesis of NAFLD has gradually been carried out. As the pathogenesis of NASH has not been fully elucidated, it appears to be multifactorial. Moreover, the clinical options for NASH are very limited, and many of the drugs in development have failed in both phase 2 and 3 clinical trials. Therefore, research on NASH still faces great challenges. The role of circRNAs in NASH is a new research field. There are few reports on circRNAs in NASH, so further research is needed. Exploring ncRNAs in NASH may provide useful clues to the pathogenesis of NASH.

Therefore, in this study, bioinformatics methods were used to analyze differentially expressed genes (DEGs) associated with NASH, and then, a ceRNA regulatory network involving circRNA, miRNA, and mRNA was constructed to explore some new circRNAs that might be used as ceRNAs to regulate gene expression in NASH.

2. Materials and Methods

2.1. Data Collection and Differentially Expressed circRNA (DEC) Identification. The Gene Expression Omnibus (GEO) is a public functional genomics data repository that supports MIAME-compliant data submissions. This database accepts data based on arrays and sequences. Tools are provided to help users query, locate, review, and download research and gene expression profiles [9]. We searched the dataset of NASH in the GEO database, and a series of related microarray datasets that provide circRNA expression profile data in NASH were acquired. We found raw microarray data for the circRNA expression profile GSE134146 and related GPL microarray gene annotation files [10]. DEC data were obtained by analyzing 4 cases of NASH and 4 controls included in the raw files of the GSE134146 dataset. All raw expression data were normalized by log2 transformation. Then, the online analysis tool GEO2R was used to analyze the differences in microarray data, and the DECs of the microarray dataset were determined with $P < 0.05$, Log2-fold change (FC) > 1 or Log2-fold change (FC) < −1 as the criteria.

2.2. Prediction of miRNAs. CircInteractome computationally identifies potential binding sites for RNA-binding proteins within circRNAs [11]. It maps RNA-binding protein (RBP) and miRNA-responsive element (MRE) sites on human circRNAs by searching some public databases of circRNAs, miRNAs, and RBPs. It uses the TargetScan prediction tool to predict miRNAs that may target circRNAs. miRNet is an easy-to-use web-based tool designed to create, customize, visually explore, and functionally interpret miRNA target interaction networks. It can be integrated into a powerful network visualization system by integrating multiple high-quality miRNA target data sources and advanced statistical methods [12]. The relevant target miRNAs of these selected DECs were predicted using two network tools, miRNet and CircInteractome. Overlapping miRNAs for both algorithms were predicted as potential target miRNAs for DECs.

The expression dataset GSE33857 of NASH-related miRNAs was retrieved from the GEO database and includes information for 7 NASH cases and 12 controls. The GSE33857 chip was analyzed by GEO2R, and the differentially expressed miRNAs that overlapped with the predicted targets were included in the next analysis.

2.3. Forecasting of miRNA-Targeted Genes. miRWalk is a comprehensive miRNA target gene database that includes the miRNA target gene information of humans, mice, rats, dogs, cows, and other species. It not only includes the full-length gene sequence record of the complete miRNA-binding site but is also compatible with the 12 existing miRNA target prediction programs (DIANA-microTv4.0, DIANA-microT-CDS, miRanda-rel2010, mirBridge, miRDB4.0, miRmap, miRNAMap, doRiNA, i.e., PicTar2, PITA RNA22v2, RNAhybrid2.1 and Targetscan6.2). This database can be used to predict the associated combined information set. The two databases miRWalk and miRNet were used to predict target mRNAs of differentially expressed miRNAs. Then, the overlapping DEGs were selected. The GSE24807 dataset is related to the gene expression profiles of NASH, and the raw data were also analyzed with GEO2R [13, 14]. Only the DEGs obtained by intersecting the genes of the dataset with the predicted target genes were included in the ceRNA network.

2.4. Functional Enrichment Analysis of Overlapping Genes and Establishment of the Protein–Protein Interaction (PPI) Network. The Database for Annotation, Visualization, and Integrated Discovery (DAVID) provides a comprehensive set of functional annotation tools for investigators to understand the biological meaning behind large lists of genes [15]. It was used to perform Gene Ontology (GO) analysis and Kyoto Encyclopedia of Genes and Genomes (KEGG) pathway enrichment analysis. The Search Tool for the Retrieval of Interacting Genes database (STRING) provides credible information on interactions between proteins and supplies detailed annotation [16].

2.5. Construction of circRNA–miRNA–mRNA Network. To reveal the relationships among circRNAs, miRNAs, and mRNAs, a circRNA–miRNA–mRNA network was constructed by combining circRNA–miRNA interactions with miRNA–mRNA interactions using Cytoscape.

3. Results

3.1. Identification of DECs in NASH. To construct the interaction network between circRNAs and miRNAs in NASH, DECs should be determined first. A microarray dataset GSE134146 was obtained from the GEO database, which includes 4 NASH cases and 4 controls. The gene chip was from the Agilent-074301 Arraystar Human CircRNA microarray V2 platform. The online analysis tool GEO2R was used to analyze a series of differentiated circRNAs, such as boxplots (Figure 1(a)). $P < 0.05$ and $|\log FC| > 1$ were used as

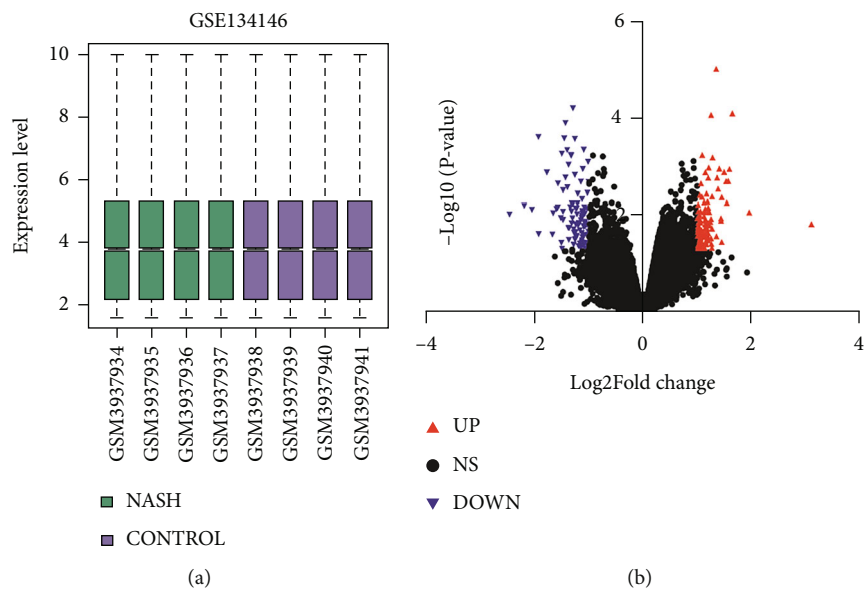

Figure 1: (a) Sample expression correction box diagram. Analysis of normalized GSE134146 data. (b) Volcano diagram of differentially expressed genes. The red dots represent significantly upregulated genes, and the blue dots represent significantly downregulated genes. Log FC > 1 or Log FC < −1, and $P < 0.05$.

the screening criteria in the GSE134146 dataset. There were 192 DECs, including 96 upregulated circRNAs and 96 downregulated circRNAs, between NASH patients and controls (Figure 1(b)). The expression differences of the top 50 circRNAs with the most significant differences in 4 NASH tissues and 4 control tissues are shown in Figure 2.

3.2. Identification of 54 circRNA–miRNA Interactions. Growing evidence indicates that circRNAs regulate gene expression via miRNA sponges. Therefore, some miRNAs related to the DECs we obtained were predicted based on this ceRNA theory. We collected and explored their potential miRNAs through the CircInteractome and miRNet online databases. Among them, 603 miRNAs were found in CircInteractome, and 640 miRNAs were found in miRNet. To ensure accuracy, we used the intersection of the two to obtain 58 overlapping predicted miRNAs. The gene chip dataset GSE33857 from the GEO database was used to verify the predicted miRNAs, and 8 miRNAs that interacted with circRNAs were obtained. According to the related regulatory relationship between circRNA–miRNAs, only 39 circRNAs (25 upregulated, 14 downregulated) and 8 miRNAs (3 upregulated, 5 downregulated) were included in the ceRNA network study. A total of 54 circRNA–miRNA interactions were identified (Table 1).

3.3. Analysis of miRNA–mRNA Interactions. We obtained 8 miRNAs associated with circRNAs. To explore the functions of these miRNAs in NASH, we used two databases, miRWalk and miRNet, to predict miRNA-related target genes. A total of 2738 folded predicted target genes were found in both databases. The GSE24807 dataset from the GEO database was used to verify the DEGs. A total of 3245 DEGs were obtained from the dataset. In addition, as shown in Figures 3, 448 overlapping genes were identified by intersecting miRNA target genes with DEGs in GEO. Based on the regulatory relationship between miRNAs and mRNAs, 291 genes were included in the list of ceRNAs. A circRNA–miRNA–mRNA regulatory network was constructed by using Cytoscape software (Table 1).

3.4. Functional Enrichment Analyses and PPI Network Construction. Terms related to the DEGs were divided into three functional groups, including biological processes (BP), molecular functions (MF), and cell compositions (CC), using DAVID. The values of the individual components in the GO analysis are shown in Figure 4. In the BP category, 291 DEGs were mainly involved in negative regulation of transcription from RNA polymerase II promoter, positive regulation of transcription from RNA polymerase II promoter, postembryonic development, wound healing, positive regulation of protein kinase B signaling, vascular endothelial growth factor receptor signaling pathway, regulation of defense response to virus by virus, positive regulation of cell proliferation, cell migration, cell motility, and other processes. In the MF category, the genes were mainly enriched in protein binding, growth factor binding, steroid hormone receptor activity, transcription factor binding, ATP binding, transcriptional activator activity, transcription factor activity, sequence-specific DNA binding, DNA binding, double-stranded DNA binding, 1-phosphatidylinositol-3-kinase activity, etc. In the CC category, the genes were mainly enriched in the nucleus, nucleoplasm, cytosol, Golgi apparatus, extracellular exosome, cytoplasm, plasma membrane, lamellipodium, cyclin-dependent protein kinase holoenzyme complex, chromatin, etc. KEGG signaling pathway showed that genes were mainly enriched in cellular senescence, human T cell leukemia virus 1 infection, PI3K-Akt signaling pathway, proteoglycans in cancer, adherens junction, p53 signaling pathway, osteoclast differentiation, pancreatic

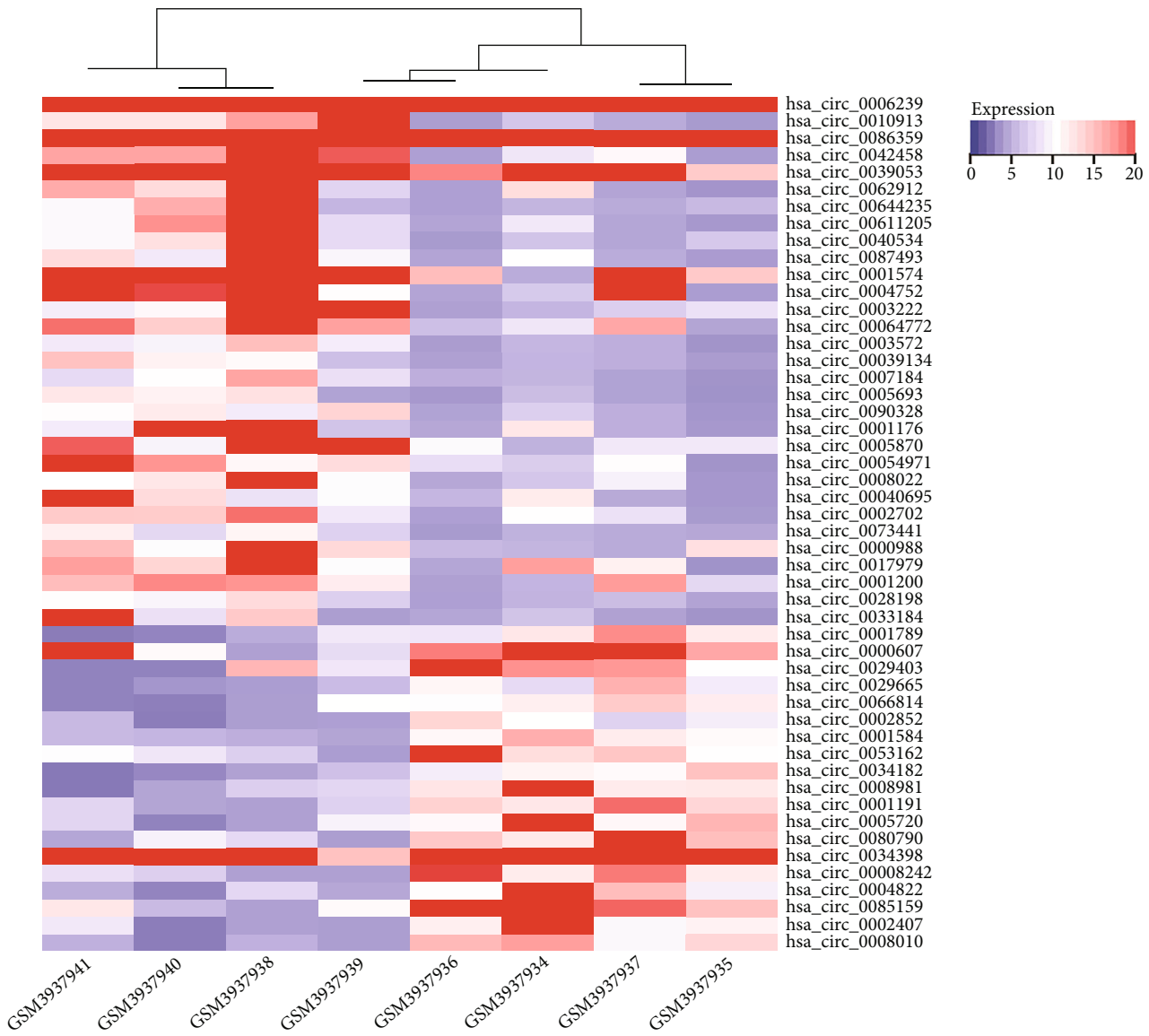

Figure 2: Sample clustering diagram. These are the 50 most significant differentially expressed circRNAs in GSE134146, and the change in color represents the difference in expression. Blue represents low expression; red represents high expression.

cancer, JAK-STAT signaling pathway, Wnt signaling pathway, ErbB signaling pathway, colorectal cancer, lipid and atherosclerosis, pathogenic Escherichia coli infection, oocyte meiosis, cGMP-PKG signaling pathway, T cell receptor signaling pathway, pathways in cancer, cholinergic synapse, axon guidance, MAPK signaling pathway, VEGF signaling pathway, Cushing syndrome, natural killer cell-mediated cytotoxicity, purine metabolism, TGF-beta signaling pathway, focal adhesion, prostate cancer, FoxO signaling pathway, viral carcinogenesis, etc. The results in the KEGG analysis are shown in Figure 5.

3.5. Construction of a circRNA–miRNA–mRNA Network. To further explore the effect of the circRNA–miRNA regulatory network on the expression levels of NASH genes, a PPI network was constructed, and 558 pairs of genes with interactions were found through the STRING database. The PPI network was imported into Cytoscape, and the cytoHubba plug-in was used to further screen hub genes according to the maximal clique centrality (MCC) algorithm. Then, a subnetwork with 10 nodes and 31 edges was selected, which revealed the critical roles of the ten genes (KDR, FYN, RAC1, MAPK1, ERBB2, CDKN1A, HSPA4, SMAD2, MCL1, and ESR1) in NASH (Figure 6). According to the negative regulatory relationship between ceRNAs, a total of 10 genes and miRNAs were included in the network. After this, a network about the association among these circRNA, miRNAs, and hub genes was built (Figure 7). It provided a visualization of the connections among the 38 DECs (hsa_circ_0000566, hsa_circ_0087493, hsa_circ_0082335, hsa_circ_0004196, hsa_circ_0002702, hsa_circ_0003362, hsa_circ_0006239, hsa_circ_0078605, hsa_circ_0001200, hsa_circ_0044235, hsa_circ_0042458, hsa_circ_0040534, hsa_circ_0003222, hsa_circ_0005935, hsa_circ_0000562, hsa_circ_

Table 1: NASH-related ceRNA regulatory network.

ceRNA regulatory network		ceRNA regulatory network	
hsa_circ_0000566	hsa-miR-885-5p	hsa-miR-142-3p	LOX
hsa_circ_0087493	hsa-miR-885-5p	hsa-miR-142-3p	BTNL9
hsa_circ_0082335	hsa-miR-885-5p	hsa-miR-142-3p	NUDT8
hsa_circ_0004196	hsa-miR-671-5p	hsa-miR-142-3p	NIN
hsa_circ_0002702	hsa-miR-671-5p	hsa-miR-142-3p	DUSP7
hsa_circ_0003362	hsa-miR-671-5p	hsa-miR-142-3p	PIK3CG
hsa_circ_0006239	hsa-miR-671-5p	hsa-miR-142-3p	XRCC1
hsa_circ_0078605	hsa-miR-671-5p	hsa-miR-142-3p	NCKAP1
hsa_circ_0001200	hsa-miR-671-5p	hsa-miR-142-3p	MMD
hsa_circ_0044235	hsa-miR-574-5p	hsa-miR-142-3p	AP4B1
hsa_circ_0042458	hsa-miR-574-5p	hsa-miR-142-3p	VKORC1
hsa_circ_0040534	hsa-miR-574-5p	hsa-miR-142-3p	CTTN
hsa_circ_0003222	hsa-miR-574-5p	hsa-miR-142-3p	KLHL24
hsa_circ_0005935	hsa-miR-574-5p	hsa-miR-142-3p	POLI
hsa_circ_0000562	hsa-miR-326	hsa-miR-142-3p	ATF5
hsa_circ_0005303	hsa-miR-326	hsa-miR-142-3p	ABCG2
hsa_circ_0000607	hsa-miR-326	hsa-miR-142-3p	CHST11
hsa_circ_0036272	hsa-miR-326	hsa-miR-142-5p	CD109
hsa_circ_0029403	hsa-miR-326	hsa-miR-142-5p	RMND5A
hsa_circ_0062762	hsa-miR-326	hsa-miR-142-5p	UHMK1
hsa_circ_0080790	hsa-miR-326	hsa-miR-142-5p	PCBP2
hsa_circ_0001191	hsa-miR-326	hsa-miR-142-5p	NFIB
hsa_circ_0008010	hsa-miR-326	hsa-miR-142-5p	RAB34
hsa_circ_0023598	hsa-miR-326	hsa-miR-142-5p	UBXN2A
hsa_circ_0092319	hsa-miR-326	hsa-miR-142-5p	LAPTM4A
hsa_circ_0071271	hsa-miR-326	hsa-miR-142-5p	KLHDC10
hsa_circ_0008981	hsa-miR-326	hsa-miR-142-5p	ZBTB20
hsa_circ_0021928	hsa-miR-326	hsa-miR-142-5p	PLEK
hsa_circ_0029665	hsa-miR-326	hsa-miR-142-5p	SCD
hsa_circ_0083789	hsa-miR-326	hsa-miR-142-5p	UBE2H
hsa_circ_0063583	hsa-miR-326	hsa-miR-142-5p	ZFP36L1
hsa_circ_0071511	hsa-miR-331-3p	hsa-miR-142-5p	VAPA
hsa_circ_0011914	hsa-miR-331-3p	hsa-miR-142-5p	ZNF248
hsa_circ_0080790	hsa-miR-331-3p	hsa-miR-142-5p	SH2B3
hsa_circ_0019917	hsa-miR-331-3p	hsa-miR-142-5p	TMEM98
hsa_circ_0067492	hsa-miR-331-3p	hsa-miR-142-5p	ZNF585B
hsa_circ_0001191	hsa-miR-331-3p	hsa-miR-142-5p	RHOC
hsa_circ_0023598	hsa-miR-331-3p	hsa-miR-142-5p	MYO1D
hsa_circ_0000926	hsa-miR-331-3p	hsa-miR-142-5p	ZNF614
hsa_circ_0063583	hsa-miR-331-3p	hsa-miR-142-5p	TAOK1
hsa_circ_0001971	hsa-miR-324-5p	hsa-miR-142-5p	TRIM66
hsa_circ_0029403	hsa-miR-324-5p	hsa-miR-142-5p	EEF1A1
hsa_circ_0001191	hsa-miR-324-5p	hsa-miR-142-5p	ARF6
hsa_circ_0056029	hsa-miR-324-5p	hsa-miR-142-5p	ATXN1
hsa_circ_0021928	hsa-miR-324-5p	hsa-miR-142-5p	SOX5
hsa_circ_0000562	hsa-miR-142-3p	hsa-miR-142-5p	IGF2
hsa_circ_0005303	hsa-miR-142-3p	hsa-miR-142-5p	APOL6
hsa_circ_0001191	hsa-miR-142-3p	hsa-miR-142-5p	C1orf21

Table 1: Continued.

ceRNA regulatory network		ceRNA regulatory network	
hsa_circ_0000562	hsa-miR-142-5p	hsa-miR-142-5p	FAM126B
hsa_circ_0005303	hsa-miR-142-5p	hsa-miR-142-5p	GABPB1
hsa_circ_0011898	hsa-miR-142-5p	hsa-miR-142-5p	STMN1
hsa_circ_0029403	hsa-miR-142-5p	hsa-miR-142-5p	MTHFD2
hsa_circ_0001191	hsa-miR-142-5p	hsa-miR-142-5p	CCNE1
hsa_circ_0063583	hsa-miR-142-5p	hsa-miR-142-5p	GXYLT1
hsa-miR-574-5p	ITPRIP	hsa-miR-142-5p	NAGK
hsa-miR-574-5p	EIF5	hsa-miR-142-5p	DENND4C
hsa-miR-574-5p	OSMR	hsa-miR-142-5p	FIGN
hsa-miR-574-5p	ZNF738	hsa-miR-142-5p	MIB1
hsa-miR-574-5p	LPP	hsa-miR-142-5p	PIK3C2A
hsa-miR-574-5p	RREB1	hsa-miR-142-5p	HELZ
hsa-miR-574-5p	FHL2	hsa-miR-142-5p	C5orf15
hsa-miR-574-5p	MAPK1	hsa-miR-142-5p	PLS1
hsa-miR-574-5p	ETV6	hsa-miR-142-5p	CREBRF
hsa-miR-574-5p	CD28	hsa-miR-142-5p	TNFSF13B
hsa-miR-574-5p	CD164	hsa-miR-142-5p	GPR65
hsa-miR-574-5p	ATP2B1	hsa-miR-324-5p	SMAD2
hsa-miR-574-5p	SLC7A2	hsa-miR-324-5p	RAPH1
hsa-miR-574-5p	SLITRK3	hsa-miR-324-5p	PCDH9
hsa-miR-574-5p	WAC	hsa-miR-324-5p	NUFIP2
hsa-miR-574-5p	AMER1	hsa-miR-324-5p	RMND5A
hsa-miR-574-5p	RNF152	hsa-miR-324-5p	CCND3
hsa-miR-574-5p	ASH1L	hsa-miR-324-5p	TGIF1
hsa-miR-574-5p	CDKN1A	hsa-miR-324-5p	PRCP
hsa-miR-574-5p	C12orf60	hsa-miR-324-5p	HNRNPDL
hsa-miR-574-5p	NCDN	hsa-miR-324-5p	FYN
hsa-miR-574-5p	SH3TC2	hsa-miR-324-5p	AJUBA
hsa-miR-574-5p	ACVR2B	hsa-miR-324-5p	PPP3CA
hsa-miR-574-5p	APBA1	hsa-miR-324-5p	SOBP
hsa-miR-574-5p	RAB3IP	hsa-miR-324-5p	CTTNBP2NL
hsa-miR-574-5p	VPS36	hsa-miR-324-5p	NDFIP2
hsa-miR-574-5p	HP1BP3	hsa-miR-324-5p	COL14A1
hsa-miR-574-5p	HIPK2	hsa-miR-324-5p	SCD
hsa-miR-574-5p	CLCF1	hsa-miR-324-5p	ETS1
hsa-miR-574-5p	PPP2R1B	hsa-miR-324-5p	WASF2
hsa-miR-574-5p	ZNF621	hsa-miR-324-5p	AP1S2
hsa-miR-671-5p	FMNL3	hsa-miR-324-5p	CCND2
hsa-miR-671-5p	SURF4	hsa-miR-324-5p	NFATC1
hsa-miR-671-5p	SMC1A	hsa-miR-324-5p	DBNL
hsa-miR-671-5p	TBCEL	hsa-miR-324-5p	ZBTB44
hsa-miR-671-5p	IL15RA	hsa-miR-324-5p	TMEM63B
hsa-miR-671-5p	NRG1	hsa-miR-324-5p	NELFB
hsa-miR-671-5p	OSMR	hsa-miR-324-5p	ZNF747
hsa-miR-671-5p	SOD2	hsa-miR-324-5p	EFNB1
hsa-miR-671-5p	WBP2	hsa-miR-324-5p	PBX1
hsa-miR-671-5p	ATF3	hsa-miR-324-5p	UBE2I
hsa-miR-671-5p	RREB1	hsa-miR-324-5p	PDRG1

Table 1: Continued.

ceRNA regulatory network		ceRNA regulatory network	
hsa-miR-671-5p	ODC1	hsa-miR-324-5p	ST3GAL1
hsa-miR-671-5p	ERP29	hsa-miR-324-5p	NME3
hsa-miR-671-5p	CPEB3	hsa-miR-324-5p	GXYLT1
hsa-miR-671-5p	WDR43	hsa-miR-324-5p	DBT
hsa-miR-671-5p	FEM1B	hsa-miR-324-5p	AK3
hsa-miR-671-5p	FNDC3B	hsa-miR-324-5p	CBX3
hsa-miR-671-5p	MRM1	hsa-miR-324-5p	ERLIN2
hsa-miR-671-5p	TC2N	hsa-miR-324-5p	FAT3
hsa-miR-671-5p	SSR1	hsa-miR-324-5p	MMD
hsa-miR-671-5p	TBRG1	hsa-miR-324-5p	NFIX
hsa-miR-671-5p	TNPO1	hsa-miR-324-5p	MGMT
hsa-miR-671-5p	LNPEP	hsa-miR-326	PAQR8
hsa-miR-671-5p	GNS	hsa-miR-326	NUFIP2
hsa-miR-671-5p	NSF	hsa-miR-326	RMND5A
hsa-miR-671-5p	NR4A3	hsa-miR-326	PTPA
hsa-miR-671-5p	MCTS1	hsa-miR-326	SLC39A1
hsa-miR-671-5p	NSUN5	hsa-miR-326	PDE1B
hsa-miR-671-5p	ABHD2	hsa-miR-326	SYNE2
hsa-miR-671-5p	PRKAR1A	hsa-miR-326	SPG7
hsa-miR-671-5p	ANGEL1	hsa-miR-326	KLHDC10
hsa-miR-671-5p	MCL1	hsa-miR-326	SDC1
hsa-miR-671-5p	NAMPT	hsa-miR-326	CCND2
hsa-miR-671-5p	KLHL7	hsa-miR-326	SMPD1
hsa-miR-671-5p	LDLR	hsa-miR-326	ERBB2
hsa-miR-671-5p	RAB3IP	hsa-miR-326	TBL1XR1
hsa-miR-671-5p	HP1BP3	hsa-miR-326	ZBTB4
hsa-miR-671-5p	SERINC3	hsa-miR-326	TAOK1
hsa-miR-671-5p	INSR	hsa-miR-326	CLU
hsa-miR-671-5p	SAA2	hsa-miR-326	GPC4
hsa-miR-671-5p	DDX21	hsa-miR-326	IL10RA
hsa-miR-671-5p	CHI3L1	hsa-miR-326	KDR
hsa-miR-671-5p	NHLRC2	hsa-miR-326	MTHFD2
hsa-miR-885-5p	TBCEL	hsa-miR-326	RECQL5
hsa-miR-885-5p	SOD2	hsa-miR-326	FPR1
hsa-miR-885-5p	ODC1	hsa-miR-326	NREP
hsa-miR-885-5p	CPEB3	hsa-miR-326	PHKA1
hsa-miR-885-5p	RAC1	hsa-miR-326	DUSP7
hsa-miR-885-5p	CD164	hsa-miR-326	ERLIN2
hsa-miR-885-5p	KLF6	hsa-miR-326	PDE3A
hsa-miR-885-5p	TGFBR1	hsa-miR-326	ABCC6
hsa-miR-885-5p	POU2F1	hsa-miR-326	VKORC1
hsa-miR-885-5p	GOLT1B	hsa-miR-326	ARRDC1
hsa-miR-885-5p	HSPA4	hsa-miR-326	LRRC75B
hsa-miR-885-5p	SRSF1	hsa-miR-326	UBE2Z
hsa-miR-885-5p	WDR36	hsa-miR-326	SLC47A1
hsa-miR-885-5p	SULT1B1	hsa-miR-326	FSCN1
hsa-miR-885-5p	CHD8	hsa-miR-331-3p	SRGAP1
hsa-miR-885-5p	ACSS1	hsa-miR-331-3p	NUFIP2

Table 1: Continued.

ceRNA regulatory network		ceRNA regulatory network	
hsa-miR-885-5p	TMC7	hsa-miR-331-3p	PCBP2
hsa-miR-142-3p	AFF1	hsa-miR-331-3p	NFIB
hsa-miR-142-3p	ST6GAL1	hsa-miR-331-3p	QKI
hsa-miR-142-3p	KLF13	hsa-miR-331-3p	PRICKLE1
hsa-miR-142-3p	HECW2	hsa-miR-331-3p	CTDSP1
hsa-miR-142-3p	SRGAP1	hsa-miR-331-3p	AFAP1
hsa-miR-142-3p	NUFIP2	hsa-miR-331-3p	HIC2
hsa-miR-142-3p	RMND5A	hsa-miR-331-3p	SDC1
hsa-miR-142-3p	CLCN5	hsa-miR-331-3p	SCD
hsa-miR-142-3p	CHID1	hsa-miR-331-3p	ETS1
hsa-miR-142-3p	AK4	hsa-miR-331-3p	PITPNA
hsa-miR-142-3p	NFIB	hsa-miR-331-3p	PTPRT
hsa-miR-142-3p	C11orf54	hsa-miR-331-3p	ZBTB38
hsa-miR-142-3p	CREB5	hsa-miR-331-3p	ENTPD1
hsa-miR-142-3p	CCNG1	hsa-miR-331-3p	AP2B1
hsa-miR-142-3p	FAM102A	hsa-miR-331-3p	ZFP36L1
hsa-miR-142-3p	EI24	hsa-miR-331-3p	GUCD1
hsa-miR-142-3p	ZBTB20	hsa-miR-331-3p	SMG6
hsa-miR-142-3p	RGS5	hsa-miR-331-3p	ERBB2
hsa-miR-142-3p	SCD	hsa-miR-331-3p	FBXO44
hsa-miR-142-3p	CLIC4	hsa-miR-331-3p	GCK
hsa-miR-142-3p	ENTPD1	hsa-miR-331-3p	MPLKIP
hsa-miR-142-3p	NR2C1	hsa-miR-331-3p	NRP2
hsa-miR-142-3p	RABGAP1L	hsa-miR-331-3p	PMPCB
hsa-miR-142-3p	ZFP36L1	hsa-miR-331-3p	EXOC6B
hsa-miR-142-3p	VAPA	hsa-miR-331-3p	ZBTB4
hsa-miR-142-3p	CIITA	hsa-miR-331-3p	NUCKS1
hsa-miR-142-3p	CLIC2	hsa-miR-331-3p	TAOK1
hsa-miR-142-3p	SERPINA4	hsa-miR-331-3p	PIK3R3
hsa-miR-142-3p	IFNAR2	hsa-miR-331-3p	MECP2
hsa-miR-142-3p	MPLKIP	hsa-miR-331-3p	ZER1
hsa-miR-142-3p	CUX1	hsa-miR-331-3p	ARSD
hsa-miR-142-3p	RBMS1	hsa-miR-331-3p	IGFBP5
hsa-miR-142-3p	NFIA	hsa-miR-331-3p	RNF146
hsa-miR-142-3p	NELFB	hsa-miR-331-3p	IGF2
hsa-miR-142-3p	TFB1M	hsa-miR-331-3p	APOL6
hsa-miR-142-3p	SLC30A6	hsa-miR-331-3p	FAM126B
hsa-miR-142-3p	NUCKS1	hsa-miR-331-3p	PMAIP1
hsa-miR-142-3p	TAOK1	hsa-miR-331-3p	COTL1
hsa-miR-142-3p	TOB1	hsa-miR-331-3p	ADAMTS5
hsa-miR-142-3p	SF3A1	hsa-miR-331-3p	KREMEN1
hsa-miR-142-3p	ESR1	hsa-miR-331-3p	TMEM254
hsa-miR-142-3p	PBX1	hsa-miR-331-3p	CLDN10
hsa-miR-142-3p	EEF1A1	hsa-miR-331-3p	ADCY1
hsa-miR-142-3p	GPC4	hsa-miR-331-3p	FAT3
hsa-miR-142-3p	ATXN1	hsa-miR-331-3p	EIF2S3
hsa-miR-142-3p	NCK2	hsa-miR-331-3p	LZTS2
hsa-miR-142-3p	ZMYND8	hsa-miR-331-3p	COL6A2

Table 1: Continued.

ceRNA regulatory network		ceRNA regulatory network	
hsa-miR-142-3p	ZNF473	hsa-miR-331-3p	CAMK2G
hsa-miR-142-3p	HMGB1	hsa-miR-331-3p	RRP1B
hsa-miR-142-3p	PIAS2	hsa-miR-331-3p	CDIPT
hsa-miR-142-3p	DPY19L4	hsa-miR-331-3p	WDR33
hsa-miR-142-3p	KRIT1	hsa-miR-331-3p	CREBRF
hsa-miR-142-3p	FBXO7	hsa-miR-331-3p	CD248
hsa-miR-142-3p	CCNE1	hsa-miR-331-3p	ZDHHC8
hsa-miR-142-3p	CCDC28B	hsa-miR-331-3p	HIC1

Figure 3: Venn diagram of overlapping DEGs. Four hundred and eighty-eight overlapping genes were obtained by crossing miRNA-targeted genes and DEGs from the GEO database.

0005303, hsa_circ_0000607, hsa_circ_0036272, hsa_circ_0029403, hsa_circ_0062762, hsa_circ_0080790, hsa_circ_0001191, hsa_circ_0008010, hsa_circ_0023598, hsa_circ_0092319, hsa_circ_0071271, hsa_circ_0008981, hsa_circ_0021928, hsa_circ_0029665, hsa_circ_0083789, hsa_circ_0063583, hsa_circ_0071511, hsa_circ_0011914, hsa_circ_0019917, hsa_circ_0067492, hsa_circ_0000926, hsa_circ_0001971, hsa_circ_0056029), 7 miRNAs (hsa-miR-326, hsa-miR-324-5p, hsa-miR-885-5p, hsa-miR-574-5p, hsa-miR-671 -5p, hsa-miR-142-3p, and hsa-miR-331-3p) and 10 hub genes (KDR, FYN, RAC1, MAPK1, ERBB2, CDKN1A, HSPA4, SMAD2, MCL1, and ESR1).

4. Discussion

We successfully constructed a circRNA-related ceRNA regulatory network by integrating and analyzing the expression differences of NASH-related circRNAs, miRNAs, and mRNAs in the GSE134146, GSE33857, and GSE24807 datasets in the GEO database. We found that 39 circRNAs may indirectly regulate 291 mRNAs (or genes) through competitive binding with 8 miRNAs. Among the regulated genes, the 10 most critical central genes were screened out. Then, a network of circRNAs, miRNAs, and hub genes was constructed, which contained 38 differentially expressed circRNAs, 7 miRNAs, and 10 hub genes. These abnormally expressed ceRNAs in NASH have the potential to be excellent biomarkers.

The importance of NASH is self-evident, as it may promote the occurrence and development of HCC. NAFLD is a pathological manifestation of metabolic syndrome in the liver. Specifically, it is a form of hepatic steatosis caused by accumulation of liver fat and is closely related to metabolic disorders such as obesity, type 2 diabetes, insulin resistance, hypertension, and hyperlipidemia. NASH is the progressive form of NAFLD. Around 20%-27% of the NAFLD patients develop NASH [17]. NASH is characterized by hepatic steatosis, inflammation, hepatocyte damage, and fibrosis, with inflammation playing a key role in its progression. Liver inflammation is a critical factor in the transition from NAFLD to NASH. Therefore, inflammation is a key pathophysiological mechanism of NASH and a target for therapeutic intervention. The KEGG pathway enrichment results in the current study showed that 291 DEGs were mainly involved in the PI3K-Akt signaling pathway, JAK-STAT signaling pathway, Wnt signaling pathway, cGMP-PKG signaling pathway, T cell receptor signaling pathway,

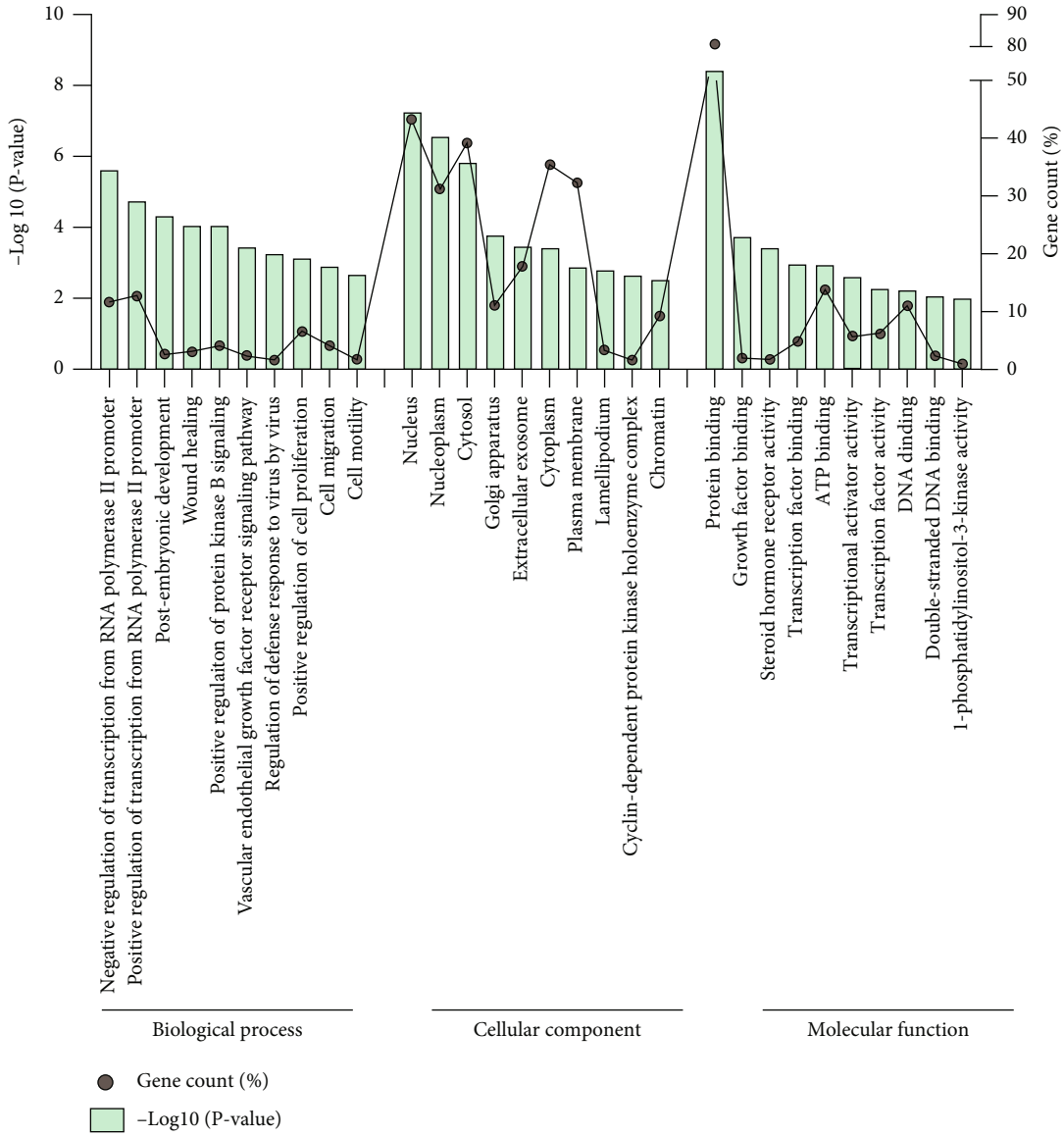

Figure 4: Functional enrichment analysis of 291 DEGs. The enriched Gene Ontology (GO) terms fell into three main GO categories: BP: biological process; CC: cellular component; MF: molecular function.

MAPK signaling pathway, VEGF signaling pathway, etc. Most of these pathways are classical pathways related to inflammation and lipid metabolism.

After multiple screenings, a total of 10 hub genes related to NASH (KDR, FYN, RAC1, MAPK1, ERBB2, CDKN1A, HSPA4, SMAD2, MCL1, and ESR1) in the circRNA–miRNA–mRNA network were identified. Some of them have been linked to liver-related diseases. For example, Zheng et al. identified CDKN1A as a potential key regulator of NASH via dynamic network analysis and dynamic gene coexpression module analysis [18]. Furthermore, studies have shown that the circRNA MAN2B2 promotes the proliferation of hepatoma cells through the miRNA-217/MAPK1 axis [19], which indirectly supports our results. Other studies have shown that HSPA4 is significantly correlated with the prognosis and immune regulation of HCC. Therefore, HSPA4 might be a potential diagnostic and prognostic biomarker as well as a therapeutic target for HCC [20]. In previous studies, these genes, including both MAPK1 and HSPA4, were not reported to be related to NASH but other liver-related diseases. By analyzing the biological processes of these DEGs, we found that these genes may also play an important role in the pathogenesis of NASH.

The importance of ceRNAs in various diseases is emerging, and some ceRNAs have been found to be associated with NASH. There is also evidence that indicates the important regulatory role of miRNAs in NASH [21, 22]. Potential targets of differentially expressed miRNAs were known to play a role in lipid metabolism, cell growth and differentiation, apoptosis, and inflammation. For example, overexpression of miR-142-5p inhibits the progression of NASH by targeting thymic stromal lymphopoietin and inhibiting the

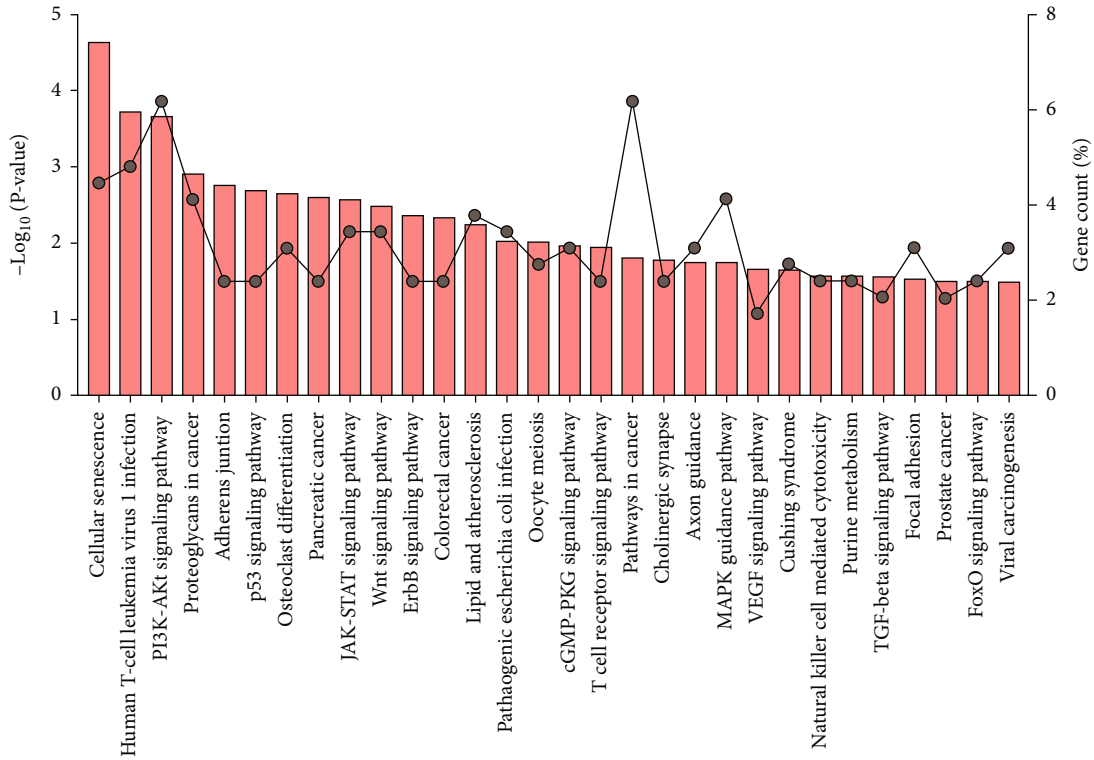

Figure 5: KEGG analysis. KEGG enrichment pathway analysis was performed on 291 differentially expressed genes in the ceRNA network, and the top 30 pathways were visualized. The bars represent *P* values, and the dots represent the percentages of genes included in the process among the 291 genes.

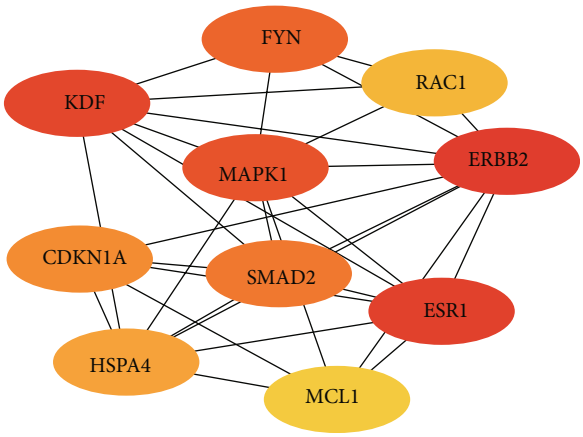

Figure 6: Hub genes in the NASH-associated PPI network. The 10 hub genes were identified from the PPI network using cytoHubba. The line indicates an interaction between two genes.

JAK-STAT signaling pathway. Thus, miR-142-5p might be a novel latent target for NASH therapy [23]. This is consistent with our findings. In addition, miRNA-223 ameliorates NASH by targeting multiple inflammatory genes in hepatocytes [24]. The role for miR-296 is to regulate lipoapoptosis by targeting p53 upregulated modulator of apoptosis. Hepatocyte lipoapoptosis is a key mediator of liver injury in NASH [25], which makes our data more convincing. Emerging studies seem to establish miRNAs as excellent noninvasive tools for the early diagnosis and treatment of various stages of liver diseases [26]. Recent studies suggest that circRNA may be involved in the pathogenesis of NASH [27]. For instance, steatohepatitis-associated circRNA ATP5B regulator, a mitochondria-located circRNA, was demonstrated to play an important role in alleviating NASH by reducing mROS output [10]. In addition, antagonizing the circRNA_

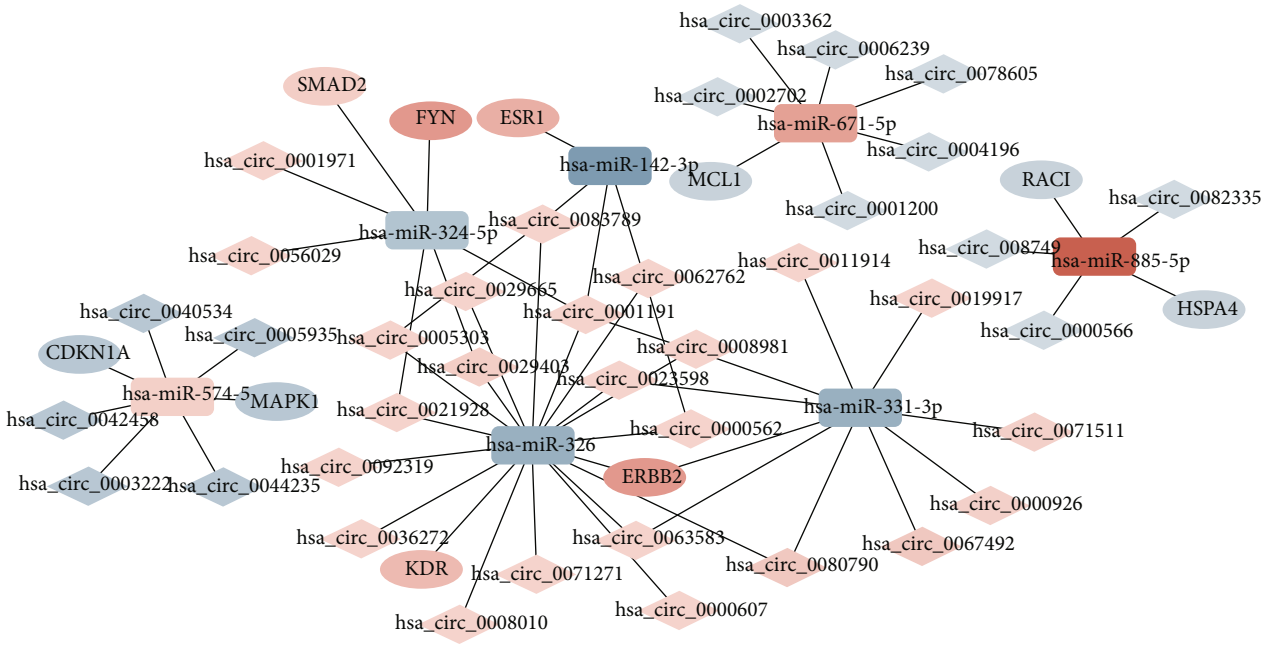

Figure 7: NASH-related circRNA–miRNA–hub gene axis. The key NASH-related circRNA, miRNA, and hub gene axis were composed of 38 circRNAs, 7 miRNAs, and 10 hub genes. Ovals indicate mRNAs, rectangles indicate miRNAs, and diamonds indicate circRNAs. Red indicates upregulation, and blue indicates downregulation. The shade of color indicates the degree of up or down.

002581-miR-122-CPEB1 axis could alleviate NASH by restoring the PTEN-AMPK-mTOR pathway [8]. However, to date, there is no authoritative agency-approved therapeutic drug on the market. The complex pathogenesis, disease heterogeneity, diagnostic barriers, and selection of treatment endpoints also bring great challenges to NASH research. Therefore, research on NASH still has a long way to go.

Certain potential limitations existed in our study. Further evidence from both in vivo and in vitro experiments is needed for verification. Further study on the physiopathologic mechanism of NASH is being performed on the basis of the current bioinformatics analysis.

In this study, bioinformatics methods were used to integrate NASH and normal liver tissue gene chips to screen out DECs and then search for corresponding miRNAs and competing mRNAs to provide a reference for further research on the pathogenesis of NASH. These circRNAs, miRNAs, and mRNAs were found to be abnormally expressed in NASH, and they have the potential to be potential biomarkers for NASH screening. They also have the potential to enter routine clinical practice and be used as predictive markers of the response to NASH-targeted therapies.

5. Conclusions

In this study, we constructed a NASH-related ceRNA network by integrating and analyzing the expression differences of NASH-related circRNAs, miRNAs, and mRNAs in the GEO database. These differentially expressed ceRNAs have the potential to be biomarkers for NASH screening and may provide valuable clues for further research on the pathogenesis of NASH.

Data Availability

All data generated or analyzed in this study are contained in the GEO database and this published article.

Conflicts of Interest

The authors declare no conflicts of interest.

Acknowledgments

This study was supported in part by the National Natural Science Foundation of China (81900793).

References

[1] D. E. Kleiner, E. M. Brunt, M. van Natta et al., "Design and validation of a histological scoring system for nonalcoholic fatty liver disease," *Hepatology*, vol. 41, no. 6, pp. 1313–1321, 2005.

[2] D. Goldberg, I. C. Ditah, K. Saeian et al., "Changes in the prevalence of hepatitis C virus infection, nonalcoholic steatohepatitis, and alcoholic liver disease among patients with cirrhosis or liver failure on the waitlist for liver transplantation," *Gastroenterology*, vol. 152, no. 5, pp. 1090–1099.e1, 2017.

[3] Z. M. Younossi, A. B. Koenig, D. Abdelatif, Y. Fazel, L. Henry, and M. Wymer, "Global epidemiology of nonalcoholic fatty liver disease—meta-analytic assessment of prevalence, incidence, and outcomes," *Hepatology*, vol. 64, no. 1, pp. 73–84, 2016.

[4] M. Zhu, M. Li, W. Zhou et al., "Qianggan extract improved nonalcoholic steatohepatitis by modulating lncRNA/circRNA immune ceRNA networks," *BMC Complementary and Alternative Medicine*, vol. 19, no. 1, p. 156, 2019.

[5] Y. Tay, J. Rinn, and P. P. Pandolfi, "The multilayered complexity of ceRNA crosstalk and competition," *Nature*, vol. 505, no. 7483, pp. 344–352, 2014.

[6] M. Cortés-López and P. Miura, "Emerging Functions of Circular RNAs," *Yale Journal of Biology and Medicine*, vol. 89, no. 4, pp. 527–537, 2016.

[7] X. Jin, C. Feng, Z. Xiang, Y. Chen, and Y. Li, "CircRNA expression pattern and circRNA-miRNA-mRNA network in the pathogenesis of nonalcoholic steatohepatitis," *Oncotarget*, vol. 7, no. 41, pp. 66455–66467, 2016.

[8] X. Jin, J. Gao, R. Zheng et al., "Antagonizing circRNA_002581-miR-122-CPEB1 axis alleviates NASH through restoring PTEN-AMPK-mTOR pathway regulated autophagy," *Cell Death & Disease*, vol. 11, no. 2, p. 123, 2020.

[9] T. Barrett, S. E. Wilhite, P. Ledoux et al., "NCBI GEO: archive for functional genomics data sets—update," *Nucleic Acids Research*, vol. 41, no. D1, pp. D991–D995, 2012.

[10] Q. Zhao, J. Liu, H. Deng et al., "Targeting mitochondria-located circRNA SCAR alleviates NASH via reducing mROS output," *Cell*, vol. 183, no. 1, pp. 76–93.e22, 2020.

[11] D. B. Dudekula, A. C. Panda, I. Grammatikakis, S. de, K. Abdelmohsen, and M. Gorospe, "CircInteractome: a web tool for exploring circular RNAs and their interacting proteins and microRNAs," *RNA Biology*, vol. 13, no. 1, pp. 34–42, 2016.

[12] Y. Fan and J. Xia, "miRNet—Functional Analysis and Visual Exploration of miRNA–Target Interactions in a Network Context," in *Computational Cell Biology*, L. Stechow and A. Santos Delgado, Eds., vol. 1819 of Methods in Molecular Biology, pp. 215–233, Springer, New York, 2018.

[13] Q. Feng, S. S. Baker, W. Liu et al., "Increased apolipoprotein A5 expression in human and rat non-alcoholic fatty livers," *Pathology*, vol. 47, no. 4, pp. 341–348, 2015.

[14] W. Liu, S. S. Baker, R. D. Baker, N. J. Nowak, and L. Zhu, "Upregulation of hemoglobin expression by oxidative stress in hepatocytes and its implication in nonalcoholic steatohepatitis," *PLoS One*, vol. 6, no. 9, article e24363, 2011.

[15] D. W. Huang, B. T. Sherman, and R. A. Lempicki, "Systematic and integrative analysis of large gene lists using DAVID bioinformatics resources," *Nature Protocols*, vol. 4, no. 1, pp. 44–57, 2009.

[16] D. Szklarczyk, A. L. Gable, D. Lyon et al., "STRING v11: protein–protein association networks with increased coverage, supporting functional discovery in genome-wide experimental datasets," *Nucleic Acids Research*, vol. 47, no. D1, pp. D607–D613, 2019.

[17] C. Estes, H. Razavi, R. Loomba, Z. Younossi, and A. J. Sanyal, "Modeling the epidemic of nonalcoholic fatty liver disease demonstrates an exponential increase in burden of disease," *Hepatology*, vol. 67, no. 1, pp. 123–133, 2018.

[18] J. Zheng, H. Wu, Z. Zhang, and S. Yao, "Dynamic co-expression modular network analysis in nonalcoholic fatty liver disease," *Hereditas*, vol. 158, p. 31, 2021.

[19] X. Fu, J. Zhang, X. He et al., "Circular RNA MAN2B2 promotes cell proliferation of hepatocellular carcinoma cells via the miRNA-217/MAPK1 axis," *Journal of Cancer*, vol. 11, no. 11, pp. 3318–3326, 2020.

[20] B.-B. Shang, J. Chen, Z.-G. Wang, and H. Liu, "Significant correlation between HSPA4 and prognosis and immune regulation in hepatocellular carcinoma," *PeerJ*, vol. 9, article e12315, 2021.

[21] G. Szabo and S. Bala, "MicroRNAs in liver disease," *Nature Reviews. Gastroenterology & Hepatology*, vol. 10, no. 9, pp. 542–552, 2013.

[22] X. W. Wang, N. H. H. Heegaard, and H. Ørum, "MicroRNAs in liver disease," *Gastroenterology*, vol. 142, no. 7, pp. 1431–1443, 2012.

[23] C. Zhou, P. Wang, L. Lei, Y. Huang, and Y. Wu, "Overexpression of miR-142-5p inhibits the progression of nonalcoholic steatohepatitis by targeting TSLP and inhibiting JAK-STAT signaling pathway," *Aging*, vol. 12, no. 10, pp. 9066–9084, 2020.

[24] Y. He, S. Hwang, Y. Cai et al., "MicroRNA-223 ameliorates nonalcoholic steatohepatitis and cancer by targeting multiple inflammatory and oncogenic genes in hepatocytes," *Hepatology*, vol. 70, no. 4, pp. 1150–1167, 2019.

[25] S. C. Cazanave, J. L. Mott, N. A. Elmi et al., "A role for miR-296 in the regulation of lipoapoptosis by targeting PUMA[S]," *Journal of Lipid Research*, vol. 52, no. 8, pp. 1517–1525, 2011.

[26] R. Lakshman, R. Shah, K. Reyes-Gordillo, and R. Varatharajalu, "Synergy between NAFLD and AFLD and potential biomarkers," *Clinics and Research in Hepatology and Gastroenterology*, vol. 39, pp. S29–S34, 2015.

[27] Y. Chien, P. H. Tsai, Y. H. Lai et al., "CircularRNA as novel biomarkers in liver diseases," *Journal of the Chinese Medical Association*, vol. 83, no. 1, pp. 15–17, 2020.

Hindawi
Gastroenterology Research and Practice
Volume 2022, Article ID 5259088, 8 pages
https://doi.org/10.1155/2022/5259088

Review Article

Research Progress on the Mechanism of Acupuncture Treatment for Nonalcoholic Fatty Liver Disease

Bai Li[1] and Li Fang[1,2]

[1]*The Acumox and Tuina College, Shandong University of Traditional Chinese Medicine, Jinan, Shandong 250013, China*
[2]*Department of Endocrinology, Shandong Provincial Hospital, Shandong University, Jinan, Shandong 250021, China*

Correspondence should be addressed to Li Fang; fangli19841101@126.com

Received 24 March 2022; Accepted 30 May 2022; Published 22 June 2022

Academic Editor: Enfa Zhao

Nonalcoholic fatty liver disease (NAFLD) represents the most common chronic liver disease worldwide, ranging from simple steatosis and nonalcoholic steatohepatitis to fibrosis, cirrhosis, and hepatocellular carcinoma. Acupuncture is a long-established treatment in traditional Chinese medicine. In recent years, increasing evidence has pointed to the effectiveness of acupuncture in the treatment of NAFLD, and a certain degree of progress has been made in the study of related mechanisms. However, previous systematic reviews have not discussed the characteristics and the related mechanisms of acupuncture in the treatment of NAFLD. Therefore, this review synthesizes the progress in research on acupuncture in the context of NAFLD treatment by the inhibition of inflammatory responses, regulation of lipid metabolism disorder, treatment of insulin resistance, antagonization of oxidative stress injury, and interference with endoplasmic reticulum stress. Overall, we sought to highlight the latest research results, potential applications, and ongoing challenges of this therapy.

1. Introduction

Nonalcoholic fatty liver disease (NAFLD), now known as metabolically associated fatty liver disease, represents a common liver disease affecting approximately 30% of the global population [1]. NAFLD can develop into nonalcoholic steatohepatitis under chronic low-grade aseptic inflammatory conditions, potentially leading to fibrosis, cirrhosis, and ultimately hepatocellular carcinoma [2]. The clinical characteristics of NAFLD mainly consist of abnormal fatty deposition of hepatocytes, hepatic steatosis, severe damage with a characteristic histological appearance, hepatomegaly, and hepatic inflammatory reaction [3, 4]. NAFLD is closely linked to diseases, such as type 2 diabetes, cardiovascular disease, and chronic kidney disease; however, its specific mechanisms remain unknown. Currently, the universally recognized pathogenic mechanisms underpinning NAFLD are associated with inflammatory response, lipid metabolism, oxidative stress, endoplasmic reticulum stress, and insulin resistance (IR). However, there remains no standard therapy specifically for NAFLD, and weight loss is the only intervention that has been proven to be beneficial for patients with NAFLD [5]. Unfortunately, most people find it difficult to lose and to maintain the weight needed to cure NAFLD [6]. Therefore, it is very important to have an in-depth understanding of the pathogenesis of NAFLD and identify new alternative treatments.

Acupuncture is a common complementary and comprehensive therapy in the context of traditional Chinese medicine. It originated in China and has a history of more than 4,000 years. It can be used to promote health or to treat disease via a variety of different techniques. These include hand acupuncture, electricity acupuncture, moxibustion, and finger pressure at specific anatomical positions (acupoints) [7]. Many different studies have shown that acupuncture can effectively treat NAFLD and that it has a powerful therapeutic effect on liver fat, glucolipid metabolism, and IR [8]. In addition, acupuncture may also inhibit the progression of NAFLD by inhibiting inflammation, reducing oxidative stress, and promoting lipid metabolism in liver cells [9]. Since acupuncture is becoming more widely used, the mechanisms involved have been increasingly discussed and

gradually implemented. In this review, we summarize the efficacy and potential mechanisms of acupuncture in the treatment of NAFLD and thereafter highlight its potential applications and challenges.

2. Acupuncture Inhibits Inflammatory Reactions in NAFLD

Inflammation plays a key role in the progression of NAFLD, and continuous inflammation may negatively impact normal physiological activities and eventually lead to liver fibrosis [10]. Low levels of chronic inflammation and lipid accumulation in the liver are considered the core pathogenic underpinnings of NAFLD [11]; the resulting lipid metabolism disorder, IR, and enteric endotoxin contribute to the production and release of proinflammatory factors tumor necrosis factor (TNF)-α, interleukin- (IL-) 1B, and IL-6 [12]. Therefore, inhibiting the expression of relevant inflammatory factors and maintaining the dynamic balance of inflammatory factors may represent an effective strategy for the treatment of NAFLD.

TNF-α plays a core role in the pathogenesis of NAFLD and is the main cytokine leading to liver injury in NAFLD [13]. Zeng Z.H. et al. [14] showed that electroacupuncture of bilateral "PI shu" (BL20), "Shen shu" (BL23), and "Ge shu" (BL17) could effectively reduce the expression level of TNF-α in NAFLD rats so as to further improve the inflammatory state of NAFLD and to reduce the degree of liver injury in NAFLD. In addition, early electroacupuncture of "Zu san li" (ST36), "San yin jiao" (SP6), and "Feng long" (ST40) can inhibit the expression level of TNF-α inflammatory factors, thus effectively regulating the inflammatory state of NAFLD [15]. IL-6 is a proinflammatory cytokine derived from the liver and adipose tissue and is associated with liver and skeletal muscle IR. IL-6 is considered the second core element in the pathophysiology of NAFLD, leading from simple fatty liver to the development of nonalcoholic steatohepatitis [16]. Chen et al. [17] stimulated acupuncture points, such as "Zu san li" (ST36), "San yin jiao" (SP6), and "Feng long" (ST40), by electroacupuncture so as to treat high-fat diet-induced NAFLD in rats and to effectively reduce the expression level of IL-6. This suggests that electroacupuncture can effectively improve the inflammatory state and liver function of NAFLD. Similarly, Yu et al. [18], respectively, intervened in high-fat diet-induced NAFLD in rats by acupuncture "Feng long" (ST40), electroacupuncture "Feng long" (ST40), or electroacupuncture "Zu san li" (ST36), demonstrating that all three methods could effectively inhibit the expression of TNF-α and IL-6, reduce the release of inflammatory mediators, regulate lipid metabolism disorder, and reduce the degeneration of liver lipid deposition. To reduce liver inflammation and injuries, electroacupuncture "Feng long" (ST40) is particularly potent. IL-18 is a proinflammatory cytokine that can be produced by adipocytes, macrophages, Kupffer cells, and endothelial cells, and increased IL-18 can reflect the degree of inflammation and steatosis [19]. Wang et al. [20] showed that acupuncture "Zu san li" (ST36), "Feng long" (ST40), "San yin jiao" (SP6), and "Tai chong" (LR3) in NAFLD rats induced by high-fat diet was found to reduce the expression level of IL-18 in liver tissue and serum, thus improving the degree of steatosis and inflammatory injury in liver tissue.

In addition, nuclear factor- (NF-) κB is a key regulatory factor of liver disease, regulating a variety of pathological processes, such as inflammation, apoptosis, and cell proliferation and differentiation [21], and plays a key role in the development of chronic inflammation in NAFLD. Many studies have shown that increased NF-κB activation promotes the transcription of proinflammatory cytokines, including IL-1β, TNF-α, and IL-6, resulting in inflammatory states in the body [22]. Meanwhile, Sirt1 has been proven to be involved in regulating hepatic steatosis and obesity in obese mice induced by a high-fat diet, suggesting that Sirt is closely related to NAFLD [23]. Therefore, Ma et al. [24] conducted a study based on whether electroacupuncture can participate in NAFLD treatment through the Sirt1/NF-κB signaling pathway, demonstrating that electroacupuncture "Yin ling quan" (SP9), "Feng long" (ST40), and "San yin jiao" (SP6) in rats with NAFLD induced by a high-fat diet can significantly increase the expression of Sirt and decrease the levels of phosphorylated NF-κB (p-NF-κB), p65, pIκBα, pIκB kinase (p-IKK) α, and p-IKK β. These results suggest that electroacupuncture can reduce liver inflammation by regulating the Sirt1/NF-κB pathway, thereby alleviating liver injury in NAFLD rats. In one word, this research shows that acupuncture treatment can effectively improve a NAFLD-associated chronic inflammatory state and degree of steatosis; however, so far, most studies have only discussed the inflammation-related cytokines correlated with NAFLD. There have been fewer studies focused on immune cells and the related signaling pathways. Research on acupuncture through targeted immune cells and inflammatory signaling pathways is warranted. The location and distribution of acupuncture points are detailed in Figure 1.

3. Acupuncture Improves Lipid Metabolism Disorder in NAFLD

The liver is a key organ for lipid metabolism. Whether it deposits or exports fat is determined as a result of fat metabolic flux through the liver. Once the homeostatic status of lipid metabolism is out of balance, excessive fat will accumulate in the liver, which may eventually lead to the development of NAFLD [25]. Lipid metabolism is affected by a variety of biological processes but mainly includes de novo adipogenesis, fatty acid intake, fatty acid oxidation, and very low-density lipoprotein (VLDL) output [26]. Once these processes turn into disorders, liver lipid metabolism will be disturbed, as characterized by the excessive accumulation of liver triglycerides (TGs). High TG deposition results thereafter in hepatic steatosis, making the liver vulnerable to proinflammatory cytokines, mitochondrial dysfunction, oxidative or endoplasmic reticulum stress, and gut microbiota attack, further leading to inflammation, apoptosis, or necrosis and fibrosis [27]. Therefore, improving lipid metabolism to reduce steatosis represents an effective strategy to block the progression of NAFLD.

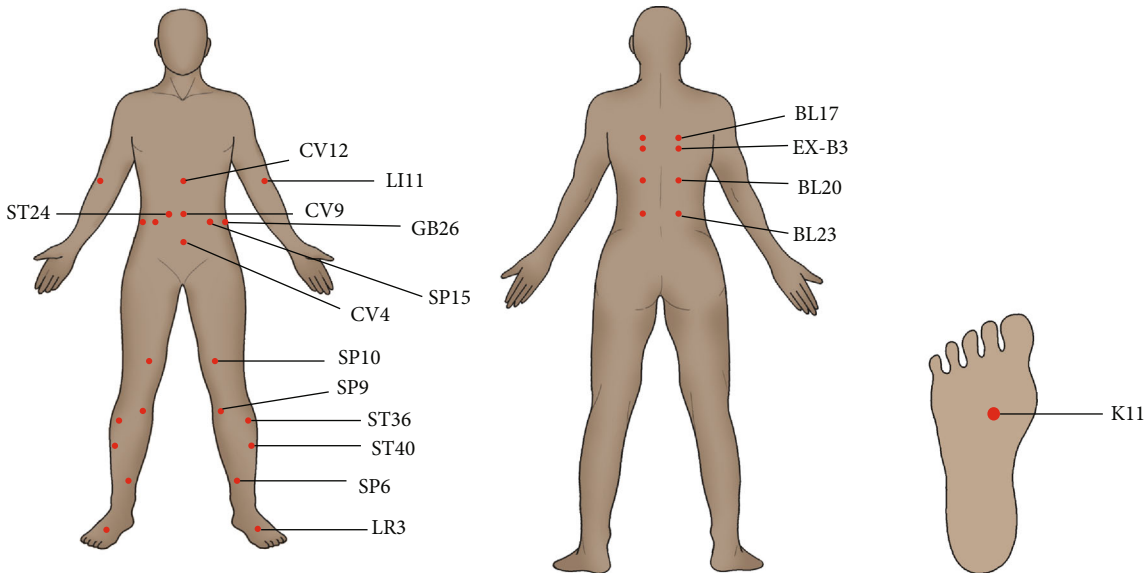

Figure 1: The location and distribution of the acupuncture points.

Several clinical studies have demonstrated that acupuncture can reduce total cholesterol (TC), TG, and low-density lipoprotein cholesterol levels and increase high-density lipoprotein cholesterol levels in patients with dyslipidemia, thus improving the body's lipid metabolism [28] and thereby improving the progression of NAFLD resulting from lipid metabolism disorders. Meng et al. [29] assessed acupuncture at "Zu san li" (ST36), "Guan yuan" (CV4), and "Yong quan" (KI1) acupoints in the NAFLD mouse model with deficient methionine and choline, demonstrating that the levels of TG and free fatty acids (FFAs) in the liver of mice were significantly reduced, while the expression patterns of lipid metabolization-related factors were also altered. These results suggest that acupuncture can reduce lipid deposition in the liver by reducing lipid synthesis and promoting lipid metabolism. In addition, Huang et al. [30] assessed 102 patients with obesity with NAFLD treated by electroacupuncture and found that the electroacupuncture of "Feng long" (ST40) and "Zu san li" (ST36) could improve the hemorheological indices of patients, decrease TC and TG levels, and produce lipolysis, thus regulating their metabolic state. Han et al. [31] assessed the effects of acupuncture "Zu san li" (ST36), "Guan yuan" (CV4), and "Yong quan" (KI1) in the context of a NAFLD mouse model with deficient methionine and choline, demonstrating that acupuncture could reduce the accumulation of abdominal fat, inhibit the absorption of lipids in the small intestine, and downregulate the level of blood lipids in mice, thus proving that acupuncture could reduce the accumulation of abdominal fat in the case of abnormal liver metabolism and may have different beneficial effects on improving lipid metabolism. The above evidence demonstrates that acupuncture treatment can not only regulate the lipid metabolism in the liver but also affect the inhibition of lipid absorption in the small intestine to adjust the lipid metabolism of the body to improve NAFLD; however, the mechanisms underpinning "the inhibition of lipid absorption in the small intestine" remain unclear. For example, it remains unclear how this might be linked to the regulation of the intestinal microbial community in the inhibition of lipid absorption. Therefore, in a future study, acupuncture- and moxibustion-related acupuncture points may be assessed in the context of the treatment of intestinal microbial colonies and regulation of lipid metabolism. This may represent a novel treatment strategy for NAFLD.

4. Acupuncture Antagonizes Oxidative Stress Damage in NAFLD

A normal redox response is essential to cell survival and the maintenance of normal liver function. The excessive lipid accumulation in NAFLD affects redox reactions, and abnormal redox reactions result in an energy metabolism disorder, leading to mitochondrial dysfunction. Reactive oxygen species (ROS) levels are increased as a result of mitochondrial damage, and ROS production is not limited to the mitochondria; the endoplasmic reticulum and peroxisome also produce ROS. Excessive ROS can further accelerate lipid accumulation in hepatocytes, induce an inflammatory response in Kupffer cells, and promote fibrogenesis of hepatic stellate cells [32]. Therefore, restoring the antioxidant levels in cells and antagonizing oxidative stress damage are key to the treatment of NAFLD.

Wang et al. [33] significantly reduced the content of malondialdehyde (MDA), increased the activity levels of total superoxide dismutase (t-SOD) and glutathione peroxidase in liver tissues, and effectively improved the lipid metabolism of rats with abdominal obese NAFLD by acupuncture of bilateral "band veins." Meng et al. [29] observed that after acupuncture of "Zu san li" (ST36), "Yong quan" (KI1), and "Guan yuan" (CV4) acupoints in NAFLD mice induced by a methionine-choline deficiency diet, the levels of oxidative stress markers 8-hydroxyldeoxyguanosine and thiobarbituric acid reactants were significantly decreased, and the

expression patterns of several antioxidant enzymes, including glutathione peroxidase 1, 2, 3, glutathione synthase, and catalase, were significantly increased, thus promoting lipid metabolism. In addition, apoptosis, as the most common mode of programmed cell death, is rather frequent in the context of acute and chronic liver injury. The induction of inflammation, lipotoxicity, mitochondrial dysfunction, or other injuries can lead to the excessive apoptosis of liver cells, in turn stimulating the surrounding hepatic astrocytes and immune cells, leading to the aggravation of hepatitis and fibrosis [25]. Zhang et al. [34] assessed the acupuncture treatment of "Guan yuan" (CV4), "Zu san li" (ST36), and "Yi yu" (EX-B3) to treat high-fat diet-induced obesity model mice and found that following an acupuncture intervention, the MDA content in the liver tissues of mice decreased, the SOD activity increased, and apoptosis-related protein Bax expression levels increased; however, Bcl-2 expression levels decreased. These results suggest that acupuncture can improve liver oxidative stress and inhibit hepatocyte apoptosis, thus playing a protective role in liver cells, suggesting that the cross talk of oxidative stress and apoptosis plays an important role in obesity-induced liver dysfunction and may provide essential insights into the mechanisms of related diseases, such as NAFLD. In conclusion, the above-mentioned studies show that acupuncture treatment can improve the oxidative stress state in the progression of NAFLD, promote the expression of protective antioxidants in the liver, and play a protective role in NAFLD.

5. Acupuncture Improves Endoplasmic Reticulum Stress in NAFLD

The ER is responsible for the correct folding of secreted proteins and transmembrane proteins. To restore homeostasis, the accumulation of misfolded or unfolded proteins leads to UR stress and the activation of the unfolded protein response (UPR) [35]. However, if endoplasmic reticulum stress is too strong or prolonged and the UPR is insufficient to relieve this stress state, abnormal endoplasmic reticulum stress interferes with liver lipid metabolism by activating fat production and limiting VLDL formation and secretion, promoting IR in the liver, and stimulating adipose tissue to indirectly act on TG accumulation. Thereafter, this results in the activation of nuclear transcription factor E2-associated factor 2 (Nrf2), C-Jun amino terminal kinase (JNK), NF-κB, cyclic adenosine phosphate response element binding protein H (CREBH), and transcription factor CCAAT-enhancer binding protein homologous protein (CHOP), eventually promoting subsequent inflammation and cell death [36]. Following endoplasmic reticulum stress, active transcription factor 6 (ATF6) and the precursor form of sterol regulatory element binding protein (SREBP) in the endoplasmic reticulum membrane are translocated to the Golgi apparatus, where they are hydrolyzed and activated by site 1 protease and site 2 protease. Subsequently, the transcriptionally active ATF6 and SREBP are recruited to the nucleus. Although ATF6 plays a protective role by activating genes involved in the UPR, SREBP activates genes involved in adipogenesis and steroid production, which leads to the development of NAFLD [37].

Srebp-1c, a subtype of SREBP, is a major transcription factor upregulated by adipogenic genes in steatosis hepatocytes [38]. By increasing the expression levels of downstream factor fatty acid synthase (FAS) and acetyl-CoA carboxylase, the level of TGs in the liver is regulated; this then acts as a key regulator of fat formation [39]. Li et al. [40] significantly improved the lipid metabolism disorder of insulin-resistant rats by electroacupuncture of "Feng long" (ST40) and "San yin jiao" (SP6), speculating that the underlying mechanisms might be related to a reduction in the expression of SrebP-1c and FAS in liver tissues by electroacupuncture. Similarly, Yu et al. [41] assessed the effects of electroacupuncture of the "Feng long" (ST40) or "Zu san li" (ST36) in NAFLD in rats resulting from a high fat diet; this resulted in a benign regulatory effect on mice. The underlying mechanisms may be related to a downregulation of the expression levels of the SrebP-1C gene and protein, amelioration of endoplasmic reticulum stress, regulation of lipid metabolism disorder, and thus reduction in liver tissue inflammatory injury. Moreover, electroacupuncture of "Feng long" has a better effect. Zhang et al. [42] assessed the effects of electroacupuncture "Zu san li" (ST36) and "San yin jiao" (SP6) on the endoplasmic reticulum stress marker protein disulfide isomerase A3 (ERp57) and SrepP-1C in NAFLD rats induced by a high fat diet, finding that the lipid metabolism of rats was significantly improved by inhibiting the expression of ERp57. It can improve endoplasmic reticulum stress in the liver of NAFLD rats, thus downregulating SREBP-1C levels and reducing lipid synthesis and accumulation. In addition, later studies by this group [43] found that electroacupuncture of "Zu san li" (ST36) and "San yin jiao" (SP6), in addition to dietary control, could inhibit the expression of another endoplasmic reticulum stress marker protein, glucose-binding protein 78, thus effectively improving endoplasmic reticulum stress in NAFLD rats and contributing to the treatment of NAFLD. It has been shown that acupuncture plays an effective role in NAFLD by intervening with endoplasmic reticulum stress. However, current studies are relatively sparse with regard to the intervention of endoplasmic reticulum stress-mediated signaling pathways. Furthermore, it remains unknown whether acupuncture can affect endoplasmic reticulum stress through upregulation of the expression of Nrf2, JNK, NF-κB, CREBH, and CHOP. Further research is needed.

6. Acupuncture Improves Insulin Resistance in NAFLD

IR, especially in adipose tissue, is considered the main driver of NAFLD [44]. The imbalance between the TG inflow rate and clearance rate leads to fat deposition in the liver, and most FFAs stored in the form of TGs are generated from the increase in lipolysis in peripheral tissues, which results from hyperinsulinemia and the increase in IR and fat production induced by dietary fat [32]. Thus, fatty deposition in the liver can lead to metabolic disorders, which further lead to excessive mitochondrial ROS production and endoplasmic reticulum stress, in addition to the eventual development of nonalcoholic steatohepatitis. As a core mechanism in many multifactorial diseases, such as NALFD, type 2 diabetes, metabolic syndrome, and obesity, IR needs to be emphasized in clinical practice.

Feng et al. [45] were the first to demonstrate that electroacupuncture could significantly reduce the levels of fasting blood glucose (FPG) and fasting insulin (FINS) and the IR index (Homeostatic Model Assessment for Insulin Resistance) while improving insulin sensitivity in rats with high-lipid-induced NAFLD by acupuncture at the "Zu san li" (ST36), "Feng long" (ST40), "San yin jiao" (SP6), and "Tai chong" (LR3) acupoints. The concentration of FFAs was significantly reduced, the vicious circle between IR and FFAs was interrupted, and the IR state was further improved. Subsequently, several researchers have demonstrated the remarkable efficacy of acupuncture in IR. For example, Dong [8] found, in a randomized controlled trial of 90 obese NAFLD patients, that acupuncture of the "Zhong wan" (CV12), "Qu chi" (LI11), "Shui fen" (CV9), "Guan yuan" (CV4), "Qi hai" (CV6), "Feng long" (ST40), "San yin Jiao" (SP6), "Tai chong" (LR3), "Xue hai" (SP10), "Hua rou Men" (ST24), and "Da heng" (SP15), combined with lifestyle control, was effective at improving liver function and glucose and lipid metabolism parameters related to human parameters, reducing the levels of FPG and FINS and HOMA-IR, and effectively improving the IR status of obese NAFLD patients. Zeng [46] stimulated acupoints, such as "Feng long" (ST40) and "Tai chong" (LR3), in NAFLD rats induced by a high fat diet by blood prick, assessing the expression patterns of FFAs, leptin (LP), adiponectin (ADP), and cAMP response element binding protein (CREP); he found that the level of ADP in the liver of rats increased significantly, while the levels of LP, FFAs, and CREP decreased significantly, thereby proving that acupuncture and purging can promote the body's ability to improve IR, effectively reduce the accumulation of liver lipids, and prevent the progression of NAFLD. In addition, two recent studies have probed the effect of electricity on IR based on the IKK/NF-κB and SIRT1/ATG7 signaling pathways. Zhang [47] used an electroacupuncture treatment on the "Feng long" and "San-yin" (acupuncture points) in ZDF model rats. This was found to inhibit the activation of the IKK/NF-κB pathway in the liver, kidney, and islet of rats and improve the activity of insulin substrate IRS-1, thereby improving IR status, reducing inflammatory response, and protecting liver and kidney function. IKK β may be a potential target of electroacupuncture for IR. Similarly, Yu [48] used an electroacupuncture treatment of the "Zu san li" (ST36), "Feng long" (ST40), "Zhong wan" (CV12), and "Guan yuan" (CV4) (acupuncture points) to treat IR rats, observing the activation of the SIRT1/ATG7 pathway, thus reducing the level of fat deposition in liver and thereafter improving insulin sensitivity and improving the IR status of rats. It is worth noting that ATG7, as an autophagy related protein, may be involved in the occurrence and development of IR-related diseases; the regulatory effect of electroacupuncture on ATG7 may be further elucidated by studies on acupuncture's involvement in the treatment of NAFLD by regulating autophagy levels. In conclusion, the above studies provide strong evidence that acupuncture can improve IR state and is a key effective way of treating NAFLD. Mechanisms of acupuncture intervention in nonalcoholic fatty liver disease are detailed in Table 1.

7. Discussion

In many cases, acupuncture is often defined as a "macro" treatment option rather than a "specific agent" targeting a particular disease. However, currently, such a comprehensive, multilevel, and multitarget treatment appears to be better aligned with the characteristics of NAFLD, a disease characterized by complex mechanisms. Based on current clinical evidence, acupuncture treatment has been identified as an effective approach to treat NAFLD. Through the intervention of multiple targets and multiple signaling pathways, acupuncture plays a variety of effective roles in the treatment of NAFLD, such as by inhibiting the inflammatory response, regulating lipid metabolism disorder, improving IR, antagonizing oxidative stress injury, and interfering with endoplasm reticulum stress, among others. It provides a practical scientific basis underpinning the mechanisms of acupuncture intervention in NAFLD.

However, there remain certain limitations and deficiencies to current research. First, there are many repeated and low-level controlled studies in clinical practice, which only prove the effectiveness of acupuncture treatment to a certain extent, without providing an in-depth discussion of the specific mechanisms involved. The speculations in some studies have not been followed up, thus compromising the feasibility and reliability of the conclusions as a whole. In contrast, experimental studies with a precise design remain scarce. Most studies are based on the NAFLD model induced by a high fat diet, which does not match clinical reality. The pathways and targets of research are also limited. Second, there remain no unified standards for models, acupoints, acupuncture methods (electroacupuncture or manual acupuncture), and the training levels of acupuncture practitioners, thereby affecting the experimental results to varying degrees. As NAFLD is a chronic progressive disease, the role of acupuncture treatment across various stages of NAFLD also warrants discussion. Whether different acupuncture methods and acupoints play a biased role in the intervention of different pathogenesis of NAFLD has not yet been reported, and corresponding indicators and evaluation of its timeliness and dose-sensitivity are also lacking. In addition, the complex mechanisms underpinning NAFLD have been buoyed by deepened research. Key to determining the fate of cells, autophagy and apoptosis also play an important role in NAFLD [49, 50]. Therefore, it is very important to assess whether acupuncture can alleviate NAFLD by mediating autophagy and apoptosis through related pathways. In addition, new evidence also suggests that NAFLD is closely related to intestinal flora, and acupuncture has been proved to be involved in the treatment of various diseases, including nervous system diseases, endocrine diseases, and digestive system diseases, by regulating intestinal flora [51–53]. The correlation between acupuncture and intestinal flora is also worth exploring. Although some progress has been made in acupuncture treatment of NAFLD, its mechanisms of action remain, to date, insufficiently specific and reliable. More pioneering studies and optimized acupuncture treatments are warranted to shed light on this area of clinical work and ongoing research.

Table 1: Mechanisms of acupuncture intervention in nonalcoholic fatty liver disease.

Category	Research object	Acupuncture points	Mechanism of action	Reference	Year
Inhibit inflammation	Rat	Pi shu (BL20), Shen shu (BL23), and Ge shu (BL17)	Inhibits TNF-α expression	[14]	2014 Y
	Rat	Zu san li (ST36), San yin jiao (SP6), and Feng long (ST40)	Inhibits TNF-α expression	[15]	2018 Y
	Rat	Zu san li (ST36), San yin jiao (SP6), and Feng long (ST40)	Inhibits IL-6 expression	[17]	2014 Y
	Rat	Feng long (ST40), Zu san li (ST36)	Inhibits TNF-α and IL-6 expression	[18]	2018 Y
	Rat	Zu san li (ST36), San yin jiao (SP6), Feng long (ST40), and Tai chong (LR3)	Inhibits IL-18 expression	[20]	2013Y
	Rat	Yin ling quan (SP9), Feng long (ST40), and San yin jiao (SP6)	Regulates Sirt1/NF-κB pathway	[24]	2020Y
Improve lipid metabolism disorder	Mice	Zu san li (ST36), Guan yuan (CV4), and Yong quan (KI1)	Reduces lipid synthesis and promotes lipid metabolism	[29]	2019Y
	Person	Feng long (ST40), Zu san li (ST36)	Improves hemorheological index	[30]	2021Y
	Mice	Zu san li (ST36), Guan yuan (CV4), and Yong quan (KI1)	Inhibits intestinal lipid absorption and reduces lipid accumulation	[31]	2020Y
Antagonize oxidative stress	Rat	Double side tape (GB26)	Decreases MDA content and increases t-SOD and GSH-Px activities	[33]	2019Y
	Mice	Zu san li (ST36), Guan yuan (CV4), and Yong quan (KI1)	Inhibits the expression of 8-OHdG and TBARS and increases the expression of GPX1, 2, 3, and GSS	[29]	2019Y
	Mice	Zu san li (ST36), Guan yuan (CV4), and Yi yu (EX-B3)	Decreases MDA content and increases SOD activity, as well as regulates apoptosis expression of Bax and Bcl-2	[34]	2020Y
Improve endoplasmic reticulum stress	Rat	Feng long (ST40), San yin jiao (SP6)	Inhibits the expression of SrebP-1C and downregulates FAS activity	[40]	2018Y
	Rat	Feng long (ST40), Zu san li (ST36)	Inhibits the expression of SrebP-1C	[41]	2017Y
	Rat	Zu san li (ST36), San yin jiao (SP6)	Inhibits the expression of SrebP-1C Inhibits the expression of ERp57 and SREBP-1C	[42]	2016Y
	Rat	Zu san li (ST36), San yin jiao (SP6)	Inhibits the expression of GRP78	[43]	2016Y
Improve insulin resistance	Rat	Zu san li (ST36), San yin jiao (SP6), Feng long (ST40), and Tai chong (LR3)	Decreases the levels of FPG, FINS and HOMA-IR, and FFA concentration	[45]	2008Y
	Person	Zhong wan (CV12), Qu chi (LI11), Shui fen (CV9), Guan yuan (CV4), Qi hai (CV6), Feng long (ST40), San yin jiao (SP6), Tai chong (LR3), Xue hai (SP10), Hua rou men (ST24), and Da heng (SP15)	Decreases the levels of FPG, FINS, and HOMA-IR	[8]	2020Y
	Rat	Feng long (ST40), Tai chong (LR3)	Increases ADP levels and reduces LP, FFA, and CREP levels	[46]	2018Y
	Rat	Feng long (ST40), San yin jiao (SP6)	Inhibits the IKK/NF-κB pathway and increases irS-1 activity	[47]	2021Y
	Rat	Zu san li (ST36), Feng long (ST40), Zhong wan (CV12), and Guan yuan (CV4)	Activates the SIRT1/ATG7 pathway and reduces liver fat deposition	[48]	2021Y

Data Availability

All analyses were based on previously published studies; thus, no data is required.

Conflicts of Interest

All authors declare that there is no conflict of interest regarding the publication of this article.

Acknowledgments

This study was supported by the National Natural Science Foundation of China (No. 82070087).

References

[1] V. Dorairaj, S. A. Sulaiman, N. Abu, and N. A. Abdul Murad, "Nonalcoholic fatty liver disease (NAFLD): pathogenesis and noninvasive diagnosis," *Biomedicine*, vol. 10, no. 1, p. 15, 2021.

[2] Z. Younossi, M. Stepanova, J. P. Ong et al., "Nonalcoholic steatohepatitis is the fastest growing cause of hepatocellular carcinoma in liver transplant candidates," *Clinical Gastroenterology and Hepatology*, vol. 17, no. 4, pp. 748–755, 2019.

[3] M. H. Kim, J. B. Seong, J. W. Huh, Y. C. Bae, H. S. Lee, and D. S. Lee, "Peroxiredoxin 5 ameliorates obesity-induced nonalcoholic fatty liver disease through the regulation of oxidative stress and AMP-activated protein kinase signaling," *Redox Biology*, vol. 28, p. 101315, 2020.

[4] T. Puengel, H. Liu, A. Guillot, F. Heymann, F. Tacke, and M. Peiseler, "Nuclear receptors linking metabolism, inflammation, and fibrosis in nonalcoholic fatty liver disease," *International Journal of Molecular Sciences*, vol. 23, no. 5, p. 2668, 2022.

[5] E. R. Yoo, S. Sallam, B. J. Perumpail et al., "When to initiate weight loss medications in the NAFLD population," *Diseases*, vol. 6, no. 4, article 91, 2018.

[6] I. Y. Cho, Y. Chang, E. Sung et al., "Weight change and the development of nonalcoholic fatty liver disease in metabolically healthy overweight individuals," *Clinical gastroenterology and hepatology: the official clinical practice journal of the American Gastroenterological Association*, vol. 20, no. 3, pp. e583–e599, 2022.

[7] Y. Zhao, Z. Zhang, S. Qin et al., "Acupuncture for Parkinson's disease: efficacy evaluation and mechanisms in the dopaminergic neural circuit," *Neural Plasticity*, vol. 2021, Article ID 9926445, 23 pages, 2021.

[8] C. Dong, C. R. Zhang, B. Y. Xue et al., "Electroacupuncture combined with lifestyle control on obese nonalcoholic fatty liver disease:a randomized controlled trial," *Zhongguo Zhen jiu= Chinese Acupuncture & Moxibustion*, vol. 40, no. 2, pp. 129–134, 2020.

[9] X. Zang, M. Sun, J. Xian et al., "Effects of acupuncture for nonalcoholic fatty liver disease: a protocol for systematic review and meta-analysis," *Medicine*, vol. 99, no. 47, article e23219, 2020.

[10] Y. Luo and H. Lin, "Inflammation initiates a vicious cycle between obesity and nonalcoholic fatty liver disease," *Immunity, Inflammation and Disease*, vol. 9, no. 1, pp. 59–73, 2021.

[11] S. Ziolkowska, A. Binienda, M. Jabłkowski, J. Szemraj, and P. Czarny, "The interplay between insulin resistance, inflammation, oxidative stress, base excision repair and metabolic syndrome in nonalcoholic fatty liver disease," *International Journal of Molecular Sciences*, vol. 22, no. 20, p. 11128, 2021.

[12] S. Gordon and F. O. Martinez, "Alternative activation of macrophages: mechanism and functions," *Immunity*, vol. 32, no. 5, pp. 593–604, 2010.

[13] F. Wandrer, S. Liebig, S. Marhenke et al., "TNF-receptor-1 inhibition reduces liver steatosis, hepatocellular injury and fibrosis in NAFLD mice," *Cell Death & Disease*, vol. 11, no. 3, p. 212, 2020.

[14] Z. H. Zeng, M. H. Zeng, X. K. Huang, R. Chen, and H. Yu, "Effect of electroacupuncture stimulation of back-shu points on expression of TNF-alpha and lipid peroxidation reaction in the liver tissue in non-alcoholic fatty liver disease rats," *Acupuncture Research*, vol. 39, no. 4, pp. 288–292, 2014.

[15] D. L. Wei, H. L. Zhao, R. Zeng, and B. Zhang, "Effects of blood-pricking therapy on inflammatory cytokines IL-6, IL-18 and TNF-α of nonalcoholic fatty liver disease," *China Journal of Traditional Chinese Medicine and Pharmacy*, vol. 4, pp. 1631–1633, 2018.

[16] R. Jamali, M. Razavizade, A. Arj, and M. H. Aarabi, "Serum adipokines might predict liver histology findings in nonalcoholic fatty liver disease," *World Journal of Gastroenterology*, vol. 22, no. 21, pp. 5096–5103, 2016.

[17] X. L. Chen, C. L. Tang, H. Xie, and N. Z. Tang, "Interventional effect of electro-acupuncture on the lipid metabolism and inflammation factor of nonalcoholic fatty liver in rats," *Journal Chongqing Medical University*, vol. 8, pp. 1119–1123, 2014.

[18] M. Yu, C. L. Tang, Q. T. Feng, R. Q. Gao, and J. Cao, "Effects of electroacupunctrue stimulation at"Feng Long"on expression of P-perk P-IRE1α and inflammatory cytokines in rats with nonalcoholic fatty liver disease," *Chinese Journal of Basic Medicine in Traditional Chinese Medicine*, vol. 5, pp. 651–655, 2018.

[19] E. Tarasów, M. Wojtkowska, I. Białokoz-Kalinowska, and D. M. Lebensztejn, "Predictive role of interleukin-18 in liver steatosis in obese children," *Canadian Journal of Gastroenterology & Hepatology*, vol. 2018, article 3870454, 9 pages, 2018.

[20] L. Wang, B. Gong, L. L. Zhu et al., "Influence of electroacupuncture stimulation on serum and hepatic interleukin-18 expression in nonalcoholic fatty liver rats," *Acupuncture Research*, vol. 38, no. 3, pp. 208–213, 2013.

[21] K. Jin, Y. Liu, Y. Shi et al., "PTPROt aggravates inflammation by enhancing NF-κB activation in liver macrophages during nonalcoholic steatohepatitis," *Theranostics*, vol. 10, no. 12, pp. 5290–5304, 2020.

[22] A. Wullaert, G. van Loo, K. Heyninck, and R. Beyaert, "Hepatic tumor necrosis factor signaling and nuclear factor-kappaB: effects on liver homeostasis and beyond," *Endocrine Reviews*, vol. 28, no. 4, pp. 365–386, 2007.

[23] Y. H. Choi, J. K. Bae, H. S. Chae et al., "α-Mangostin regulates hepatic steatosis and obesity through SirT1-AMPK and PPARγ pathways in high-fat diet-induced obese mice," *Journal of Agricultural and Food Chemistry*, vol. 63, no. 38, pp. 8399–8406, 2015.

[24] B. Ma, P. Li, H. An, and Z. Song, "Electroacupuncture attenuates liver inflammation in nonalcoholic fatty liver disease rats," *Inflammation*, vol. 43, no. 6, pp. 2372–2378, 2020.

[25] Z. Fang, G. Dou, and L. Wang, "MicroRNAs in the pathogenesis of nonalcoholic fatty liver disease," *International Journal of Biological Sciences*, vol. 17, no. 7, pp. 1851–1863, 2021.

[26] X. Wang, H. Rao, F. Liu, L. Wei, H. Li, and C. Wu, "Recent advances in adipose tissue dysfunction and its role in the pathogenesis of non-alcoholic fatty liver disease," *Cell*, vol. 10, no. 12, p. 3300, 2021.

[27] T. H. Kim, D. G. Hong, and Y. M. Yang, "Hepatokines and non-alcoholic fatty liver disease: linking liver pathophysiology to metabolism," *Biomedicine*, vol. 9, no. 12, p. 1903, 2021.

[28] Q. Peng, X. Yao, J. Xiang, Y. Wang, and X. Lin, "Acupuncture for hyperlipidemia: protocol for a systematic review and meta-analysis," *Medicine*, vol. 97, no. 50, article e13041, 2018.

[29] X. Meng, X. Guo, J. Zhang et al., "Acupuncture on ST36, CV4 and KI1 suppresses the progression of methionine- and choline-deficient diet-induced nonalcoholic fatty liver disease in mice," *Metabolites*, vol. 9, no. 12, p. 299, 2019.

[30] Z. Huang, S. L. Song, and Z. Di, "Clinical observation on acupoint catgut embedding combined with electroacupuncture in the treatment of obese patients with nonalcoholic fatty liver disease," *Indian Journal of Pharmaceutical Sciences*, vol. 83, pp. 62–67, 2021.

[31] J. Han, X. Guo, X. J. Meng et al., "Acupuncture improved lipid metabolism by regulating intestinal absorption in mice," *World Journal of Gastroenterology*, vol. 26, no. 34, pp. 5118–5129, 2020.

[32] Y. Ma, G. Lee, S. Y. Heo, and Y. S. Roh, "Oxidative stress is a key modulator in the development of nonalcoholic fatty liver disease," *Antioxidants*, vol. 11, no. 1, article 91, 2021.

[33] H. Y. Wang, C. M. Liang, J. W. Cui, L. Pan, H. Hu, and H. J. Fang, "Acupuncture improves hepatic lipid metabolism by suppressing oxidative stress in obese nonalcoholic fatty liver disease rats," *Acupuncture Research*, vol. 44, no. 3, pp. 189–194, 2019.

[34] S. Y. Zhang, L. L. Li, X. Hu, and H. T. Tang, "Effect of acupuncture on oxidative stress and apoptosis-related proteins in obese mice induced by high-fat diet," *Chinese Acupuncture & Moxibustion*, vol. 40, no. 9, pp. 983–988, 2020.

[35] C. M. Flessa, I. Kyrou, N. Nasiri-Ansari et al., "Endoplasmic reticulum stress and autophagy in the pathogenesis of non-alcoholic fatty liver disease (NAFLD): current evidence and perspectives," *Current Obesity Reports*, vol. 10, no. 2, pp. 134–161, 2021.

[36] X. Q. Zhang, C. F. Xu, C. H. Yu, W. X. Chen, and Y. M. Li, "Role of endoplasmic reticulum stress in the pathogenesis of nonalcoholic fatty liver disease," *World Journal of Gastroenterology*, vol. 20, no. 7, pp. 1768–1776, 2014.

[37] J. Fujii, T. Homma, S. Kobayashi, and H. G. Seo, "Mutual interaction between oxidative stress and endoplasmic reticulum stress in the pathogenesis of diseases specifically focusing on non-alcoholic fatty liver disease," *World Journal of Biological Chemistry*, vol. 9, no. 1, pp. 1–15, 2018.

[38] A. Gnoni, B. Di Chiara Stanca, L. Giannotti, G. V. Gnoni, L. Siculella, and F. Damiano, "Quercetin reduces lipid accumulation in a cell model of NAFLD by inhibiting de novo fatty acid synthesis through the acetyl-CoA carboxylase 1/AMPK/PP2A Axis," *International Journal of Molecular Sciences*, vol. 23, no. 3, p. 1044, 2022.

[39] B. Yang, J. Sun, S. Liang et al., "Prediction of Srebp-1 as a key target of Qing Gan San against MAFLD in rats via RNA-sequencing profile analysis," *Frontiers in Pharmacology*, vol. 12, p. 680081, 2021.

[40] Z. X. Li, H. H. Zhang, D. C. Lan, H. T. Zhang, X. Z. Chen, and J. Sun, "Effect of eletroacupuncture intervention on insulin resistance, lipid metabolic disorder and expression of hepatic SREBP-1 c and fatty acid synthase proteins in rats with hyperlipidemia," *Acupuncture Research*, vol. 43, no. 1, pp. 8–13, 2018.

[41] M. Yu, G. Li, C. L. Tang, R. Q. Gao, Q. T. Feng, and J. Cao, "Effect of electroacupunctrue stimulation at "Fenglong"(ST 40) on expression of SREBP-1 c in non-alcoholic fatty liver disease rats," *Acupuncture Research*, vol. 42, no. 4, pp. 308–314, 2017.

[42] Y. Zhang, C. L. Tang, Y. Tian et al., "Effect of electroacupunctrue on ERp57 in NAFLD rats," *Journal of Sichuan University (Medical Sciences)*, vol. 47, no. 2, pp. 208–213, 2016.

[43] Y. Zhang, "Effects of electroacupuncture combined with dietary control on liver endoplasmic reticulum stress in rats with non-alcoholic fatty liver disease," *Zhongguo Zhen jiu= Chinese Acupuncture & Moxibustion*, vol. 36, no. 9, pp. 951–956, 2016.

[44] S. Guerra, G. Mocciaro, and A. Gastaldelli, "Adipose tissue insulin resistance and lipidome alterations as the characterizing factors of non-alcoholic steatohepatitis," *European Journal of Clinical Investigation*, vol. 52, no. 3, article e13695, 2022.

[45] W. Q. Feng, Z. H. Zeng, and L. S. Zhuo, "Influence of electroacupuncture on insulin-resistance in nonalcoholic fatty liver rats," *Acupuncture Research*, vol. 33, no. 2, pp. 111–115, 2008.

[46] R. Zeng, *Exploring the effect of pricking blood intervention on nonalcoholic fatty liver disease based on insulin resistance theory*, University of Chinese Medicine, Beijing, 2018.

[47] L. Z. Zhang, *Effect of electroacupuncture on insulin resistance of ZDF rats by inhibitingIKK/NF-κB pathway, [Ph.D thesis]*, Guangzhou University of Chinese Medicine, China, 2021.

[48] Y. G. Yu, *Electroacupuncture Ameliorates Insulin Resistance Via the Hepatic SIRT1/ATG7 Pathway*, Master Dissertation, Hubei University of Chinese Medicine, 2021.

[49] S. Rajak, S. Raza, and R. A. Sinha, "ULK1 signaling in the liver: autophagy dependent and independent actions," *Frontiers in Cell and Development Biology*, vol. 10, article 836021, 2022.

[50] L. Parlati, M. Régnier, H. Guillou, and C. Postic, "New targets for NAFLD," *JHEP Rep.*, vol. 3, no. 6, p. 100346, 2021.

[51] H. Xiang, D. Sun, X. Liu, Z. G. She, and Y. Chen, "The role of the intestinal microbiota in nonalcoholic steatohepatitis," *Frontiers in Endocrinology*, vol. 13, article 812610, 2022.

[52] Z. Liu, Y. Jiao, T. Yu et al., "A review on the immunomodulatory mechanism of acupuncture in the treatment of inflammatory bowel disease," *Evidence-based Complementary and Alternative Medicine*, vol. 2022, Article ID 8528938, 9 pages, 2022.

[53] J. Jiang, H. Liu, Z. Wang et al., "Electroacupuncture could balance the gut microbiota and improve the learning and memory abilities of Alzheimer's disease animal model," *PLoS One*, vol. 16, no. 11, article e0259530, 2021.

Hindawi
Gastroenterology Research and Practice
Volume 2022, Article ID 5403423, 16 pages
https://doi.org/10.1155/2022/5403423

Research Article

Identification and Validation of a Novel Immune Infiltration-Based Diagnostic Score for Early Detection of Hepatocellular Carcinoma by Machine-Learning Strategies

Xuli Guo, Hailin Xiong, Shaoting Dong, and Xiaobing Wei

Department of Oncology, Huizhou Central Hospital, Huizhou, Guangdong, China 516001

Correspondence should be addressed to Xiaobing Wei; wxb13421612887@163.com

Received 16 March 2022; Accepted 11 May 2022; Published 14 June 2022

Academic Editor: Xiude Fan

Objective. To investigate the diagnostic gene biomarkers for hepatocellular carcinoma (HCC) and identify the immune cell infiltration characteristics in this pathology. *Methods*. Five gene expression datasets were obtained through Gene Expression Omnibus (GEO) portal. After batch effect removal, differentially expressed genes (DEGs) were conducted between 209 HCC and 146 control tissues and functional correlation analyses were performed. Two machine learning algorithms were used to develop diagnostic signatures. The discriminatory ability of the gene signature was measured by AUC. The expression levels and diagnostic value of the identified biomarkers in HCC were further validated in three independent external cohorts. CIBERSORT algorithm was adopted to explore the immune infiltration of HCC. A correlation analysis was carried out between these diagnostic signatures and immune cells. *Results*. A total of 375 DEGs were identified. GPC3, ACSM3, SPINK1, COL15A1, TP53I3, RRAGD, and CLDN10 were identified as the early diagnostic signatures of HCC and were all validated in external cohorts. The corresponding results of AUC presented excellent discriminatory ability of these feature genes. The immune cell infiltration analysis showed that multiple immune cells associated with these biomarkers may be involved in the development of HCC. *Conclusion*. This study indicates that GPC3, ACSM3, SPINK1, COL15A1, TP53I3, RRAGD, and CLDN10 are potential biomarkers associated with immune infiltration in HCC. Combining these genes can be used for early detection of HCC and evaluating immune cell infiltration. Further studies are needed to explore their roles underlying the occurrence of HCC.

1. Introduction

Hepatocellular carcinoma (HCC) is a highly aggressive malignant solid tumors and remains the major cause of cancer death across the world [1]. The development of HCC is closely associated with the infection of hepatitis B virus (HBV) and/or hepatitis C virus (HCV) [2]. There are multiple therapy strategies for various clinical characteristics of HCC. Hepatectomy, transplantation, ablation, immunotherapy, transarterial chemoembolization, and chemotherapy have been indicated to yield survival benefits [3, 4]. Among these, surgical resection can only be conducted in early-stage HCC patients. However, its mortality is still high, which largely due to early-stage tumors symptoms which are typically asymptomatic and limited treatments for individuals with advanced HCC [5]. The high morbidity and mortality rates make early screening and diagnosis of HCC even more important. The optimal curative therapy strategies for early HCC individuals include surgical resection and liver transplantation, and individuals who finished those treatments generally show a favorable outcome, with a five-year overall survival (OS) rate between 60% and 80% [6]. From a clinical perspective, improving early screening for HCC will provide the patients more opportunity for curative treatment. Thus, developing a stable and precise model for the diagnosis of individuals with early HCC will present a considerable influence on clinical outcomes. Presently, application of ultrasonography as well as serum α-fetoprotein (AFP) is a commonly noninvasive approach for HCC supervision. However, the

sensitivity and specificity for early-stage HCC diagnosing is unsatisfactory [7]. Thus, identification of reliable and robust diagnostic biomarkers is urgent for HCC treatment.

With the increasing development in genome-sequencing technologies as well as bioinformatic algorithms, numerous molecular signatures and genetic biomarkers have been developed to enhance the diagnosis and prognosis prediction in individuals with HCC [8–10]. Recently, immunotherapy has presented promising findings [11]. Tumor-infiltrating immune cells (TIICs) are involved in the prognosis and treatment of multiple cancer types, including HCC [12–14]. However, diagnostic gene biomarkers associated with immune cell infiltration in HCC were still limited. Thus, it is still a great need to identify novel gene biomarkers for the diagnosis of HCC, especially for early-stage HCC, in clinical practice. Machine learning (ML) belongs to a subset of artificial intelligence that is widely used to solve prediction problems in human diseases by providing the machine the ability to learn from data without giving specific instructions [15, 16].

Therefore, in this study, we downloaded multiple large-scale datasets diagnosed with HCC from the GEO portal and merged into a discovery cohort after batch effect was removed. After performing differentially expressed gene (DEG) analysis, ML algorithms, including support vector machine-recursive feature elimination (SVM-RFE) and LASSO, were applied to screen candidate diagnostic genes between HCC and controls. The shared genes identified by the two methods were validated in three external validation cohorts and were used to construct the diagnostic score for early-stage HCC screening using a logistic regression method. Then, the putative abundance of immune cell subtypes via CIBERSORT algorithm was calculated. Further, the association between the gene markers and infiltrating immune cells was explored to present a reference for future research in HCC.

2. Materials and Methods

2.1. HCC Datasets. We searched and downloaded five HCC microarray expression profile datasets (GSE121248, GSE45267, GSE65372, GSE51401, and GSE14520-GPL571) from the GEO portal (http://www.ncbi.nlm.nih.gov/geo) for DEG analysis, which is a public functional genomics data repository. The characteristics of the multiple cohorts utilized in the study are presented in Table 1. GSE14520-GPL3921 cohort contained 225 HCC samples and 220 controls; gene expression data was used for external validation of the diagnostic score. Gene expression matrix of 374 HCC tissues and 50 control tissues collected from The Cancer Genome Atlas (TCGA) was used for another external validation. To yield robust diagnostic performance, the Japan Project from International Cancer Genome Consortium (ICGC-LIRI-JP) collected the RNA-Seq data of 243 HCC patients and 202 controls which was used as the third external validation cohort. Next, the probes' ID in every cohort was annotated and transformed into gene symbols according to platform annotation documents, and the probes falling to match any gene symbols were excluded. If multiple probes match to a same gene symbol, average value was used value. The gene expression files of the five datasets (GSE121248, GSE45267, GSE65372, GSE51401, and GSE14520-GPL571) were merged into a discovery cohort for subsequent analysis. The batch effects between different datasets were corrected by the R package "SVA" containing the "Combat" function [17].

2.2. DEG Identification. Five datasets were combined, and batch effects were eliminated by using the "Combat" algorithm. Then, these datasets were merged into a discovery cohort. There are 209 patients with HCC and 146 normal individuals in the cohort. The present study analyzed differentially expressed gene (DEG) by the "limma" R package via the comparison of the expression matrixes of HCC and control samples. The volcano plot was plotted to show the DEGs, which with thresholds of adjusted $P < 0.05$ and $|\log_2 \mathrm{FC}| > 1$ being statistically significant.

2.3. Functional Correlation Analysis. Gene Ontology (GO) enrichment was conducted and visualized using the "ClusterProfiler" R packages. Disease Ontology (DO) enrichment was implemented via the "ClusterProfiler" and DOSE packages [18, 19]. Gene set enrichment analysis (GSEA) was performed to seek the foremost regulated pathways and functional terms between the HCC and normal samples [20]. The "c2.cp.kegg.v7.0.symbols.gmt" was adopted as the reference gene set. The cutoff point of significance was deemed as notably enriched if a $P < 0.05$ as well as false discovery rate < 0.025.

2.4. Identification and Validation of Candidate Biomarkers. To construct a gene-based diagnostic score using the discovery cohort, two machine learning algorithms were selected to perform the disease status predictions. A LASSO-based algorithm, which is a regression analysis algorithm, was used for data dimensionality reduction. LASSO runs a covariate selection, which contributes to the prediction accuracy as well as the interpretability through regularization. LASSO was implemented with the "glmnet" R package to investigate the variables notably related to the discrimination of HCC and controls [21]. SVM is a supervised machine learning classification algorithm that has been commonly utilized for disease classification through predicting the extent of an individual belonging to a specific class [22]. To identify the set of genes with highest discriminative power, SVM-RFE was used to choose the suitable feature genes. The intersection genes identified by the two ML procedures were used as candidate biomarkers, and the expression values of these genes were additional confirmed in three independent external datasets.

2.5. Feature Gene Biomarker Selection and Diagnostic Score Construction. The validated biomarkers were used for model construction. The gene-based diagnostic score was developed via logistic regression model analysis in the discovery cohort using the following formula: $\text{diagnostic score} = (\beta_1 * \text{Expgene}_1) + (\beta_2 * \text{of Expgene}_2) + \cdots + (\beta \text{n} * \text{Expgene}_\text{n})$. The predictive significance of the diagnostic score was measured using receiver operating curve (ROC) analysis. The diagnostic scores in three external cohorts were calculated

using the same formula, respectively. ROC curve was generated based on the gene expression value from HCC and normal tissues in the discovery cohort and three validation cohorts. The AUC was adopted to measure the diagnostic efficiency in separating HCC from normal samples and further verified in the validation cohorts. Moreover, the effectiveness of the diagnostic score in identifying early stage of HCC individuals (stage I) from control ones was additionally quantified in three validation cohorts via the AUCs.

2.6. Analysis of Immune Cell Infiltration. Infiltrating immune cells derived from the gene expression matrix in the discovery cohort in HCC were calculated by the CIBERSORT algorithm (https://cibersortx.stanford.edu/). To infer the relative abundance of infiltrating immune cells, a reference set with 22 sorted kinds of immune cell subtypes (LM22) with 1,000 permutations was adapted [23]. The R package "corrplot" was used to analyze the correlation analysis and visualize the 22 kinds of infiltrating immune cells. The "vioplot" package in R was adapted to plot violin plots and visualize the differences of immune cell infiltration between the HCC and normal tissues.

2.7. Investigating the Link between Selected Biomarkers and Infiltrating Immune Cells. We used CIBERSORT in R language to analyze the differences in the infiltration of 22 immune cells between the HCC and normal tissues. Spearman's rank correlation analysis was adapted to obtain the relationship between each diagnostic gene and immune cell infiltration and was visualized with "ggplot2" package.

2.8. Statistical Analysis. The LASSO regression analysis was implemented using the "glmnet" R package, and the SVM algorithm was carried out using the "e1071" R package. ROC curve analysis was performed to quantify the diagnostic efficacy of the diagnostic score. All statistical analyses were performed using R software (version 3.6.1), and a $P < 0.05$ was deemed statistically significant.

3. Results

3.1. Screening of Predictive Genes in HCC. DEGs were performed between 146 normal individuals and 209 patients with HCC in the discovery cohort after eliminating the batch effects (Figure 1(a)). Initially, 375 DEGs were acquired, which included 130 significantly upregulated genes and 245 significantly downregulated genes (Figure 1(b)).

3.2. Functional Enrichment Analysis of DEGs. The GO and KEGG analysis results show that DEGs are significantly enriched in cellular senescence, cell cycle, tubulin binding, mitotic spindle, and mitotic nuclear division (Figure 2(a)). Moreover, the functional enrichment demonstrated that diseases enriched by DEGs were generally related to non-small-cell lung carcinoma, liver cirrhosis, kidney cancer, bile duct adenocarcinoma, renal carcinoma, and breast carcinoma (Figure 2(b)). The GSEA results revealed that changed genes were enriched in several common pathways that are mainly involved in DNA replication, mismatch repair, proteasome, pyrimidine metabolism, and progesterone-mediated oocyte maturation (Figure 2(c)). These findings strongly suggest that cell cycle and cancer-related pathways play an essential role in the pathogenesis of HCC.

3.3. Development and Confirmation of an Immune-Related Diagnostic Gene Biomarker-Based Diagnostic Score. We performed two different bioinformatic algorithms to screen the potential biomarkers of HCC. By using the LASSO regression algorithm, DEGs were narrowed down to 29 variables as diagnostic biomarkers for HCC (Figure 3(a)). By using the SVM-RFE algorithm, we identified a subset of 40 genes among the DEGs (Figure 3(b)). The 8 overlapping feature genes (GPC3, ACSM3, SPINK1, COL15A1, TP53I3, RRAGD, CLDN10, and GPR88) were finally identified (Figure 3(c)). Moreover, in order to yield precise and reliable gene expression results, the GSE14520-GPL3921 dataset, ICGC, and TCGA-HILC cohorts were adapted to check the expression values of the 8 genes. Finally, the expression values of GPC3, ACSM3, SPINK1, COL15A1, TP53I3, RRAGD, and CLDN10 in HCC samples were particularly lower than individuals in the control cohort (Figures 4(a)–4(c); all $P < 0.05$), while the expression values of GPR88 in HCC samples were not greatly higher than individuals in the control group in GSE14520-GPL3921 dataset and ICGC ($P > 0.05$). Thus, the seven selected biomarkers were adapted to construct a diagnostic score via a logistic regression procedure. After obtaining the coefficients via multivariate logistic regression algorithm, the diagnostic score was established. Diagnostic score = $(0.6325 * \text{GPC3}) + (-0.9191 * \text{ACSM3}) + (0.2633 * \text{SPINK1}) + (0.7349 * \text{COL15A1}) + (0.8170 * \text{TP53I3}) + (0.4756 * \text{RRAGD}) + (-0.8263 * \text{CLDN10})$. Therefore, the diagnostic scores in four cohorts were obtained, respectively.

3.4. Diagnostic Effectiveness of the Diagnostic Score in HCC. We further quantified the discrimination ability by the area under a ROC curve (AUC). As demonstrated in Figure 5(a), the diagnostic capability of the seven genes in separating HCC from the normal tissues presented an excellent diagnostic performance, with all AUCs > 0.8. Considering the discriminatory ability of the diagnostic score, ROC curve analysis was performed. The AUC was 0.980 (95%CI = 0.960 − 0.990), demonstrating a high prediction efficacy of the diagnostic score gene signature for HCC. The robustness of the seven-gene diagnostic score was further confirmed in three validation cohorts for predicting diagnosis in individuals with HCC with an AUC of 0.962 in GSE14520 validation cohort (Figure 5(b)), AUC of 0.963 in ICGC cohort (Figure 5(c)), and AUC of 0.942 in TCGA-HILC cohort (Figure 5(d)), suggesting that the identified gene biomarkers had a high and strong diagnostic ability.

Additionally, we further calculated the diagnostic role of the diagnostic score gene signature for HCC at early stage (stage I). The detailed stage information was available in three validation cohorts. Surprisingly, the diagnostic score displayed high discriminability for early-stage HCC in the GSE14520 validation cohort (HCC-stage I vs. non-HCC, AUC = 0.955, Figure 6(a)), ICGC cohort (HCC-stage I vs. non-HCC, AUC = 0.952, Figure 6(b)), and TCGA-HILC cohort (HCC-stage I vs. non-HCC, AUC = 0.944, Figure 6(c)). These results demonstrate that the selected gene biomarkers presented a high diagnostic power for the early diagnosis of HCC.

Table 1: Details of the multiple datasets included in this study.

Datasets	Platform	Sample size (tumor/control)	Application
GSE121248	GPL570 [HG-U133_Plus_2] Affymetrix Human Genome U133 Plus 2.0 Array	107 (70/37)	Identification of DEGs
GSE45267	GPL570 [HG-U133_Plus_2] Affymetrix Human Genome U133 Plus 2.0 Array	87 (48/39)	Identification of DEGs
GSE65372	GPL14951 Illumina HumanHT-12 WG-DASL V4.0 R2 expression beadchip	54 (39/15)	Identification of DEGs
GSE51401	GPL570 [HG-U133_Plus_2] Affymetrix Human Genome U133 Plus 2.0 Array	64 (30/34)	Identification of DEGs
GSE14520	GPL571 [HG-U133A_2] Affymetrix Human Genome U133A 2.0 Array	43 (22/21)	Identification of DEGs
GSE14520	GPL3921 [HT_HG-U133A] Affymetrix HT Human Genome U133A Array	445 (225/220)	Validation of DEGs
ICGC-JP cohort		445 (243/202)	Validation of DEGs
TCGA-HILC		424 (374/50)	Validation of DEGs

3.5. Investigation of Immune Cell Infiltration. We explored the composition of immune cells in HCC cases and healthy controls using the CIBERSORT algorithm. The abundance of 22 immune cells in HCC and control samples was shown using a bar plot (Figure 7(a)). The proportions of $CD8^+$ T cell ($P = 0.004$), resting memory $CD4^+$ T cells ($P = 0.006$), gamma delta T cells ($P < 0.001$), resting NK cell ($P = 0.001$), monocytes ($P = 0.004$), M2 macrophages ($P = 0.021$), and neutrophils ($P < 0.001$) in HCC were significantly lower than in healthy controls (Figure 7(b)). However, the proportion of regulatory T cells ($P < 0.001$), activated NK cell ($P < 0.001$), M0 macrophages ($P < 0.001$), resting dendritic cell ($P < 0.001$), and activated mast cell in HCC was significantly higher than that in healthy controls (Figure 7(b)).

3.6. Association between the Seven Gene and Infiltrating Immune Cells. As exhibited in Figure 8, CLDN10 was positively associated with naive $CD4^+$ T cells ($r = 0.132$, $P = 0.049$), $CD8^+$ T cells ($r = 0.147$, $P = 0.003$), neutrophils ($r = 0.149$, $P = 0.025$), and gamma delta T cells ($r = 0.246$, $P = 0.0002$) and negatively correlated with M0 macrophages ($r = -0.366$, $P < 0.001$), activated mast cells ($r = -0.212$, $P = 0.001$), regulatory T cells ($r = -0.199$, $P = 0.003$), and activated NK cells ($r = -0.137$, $P = 0.042$). GPC3 was positively correlated with regulatory T cells ($r = 0.145$, $P = 0.031$), activated memory $CD4^+$ T cells ($r = 0.151$, $P = 0.025$), activated NK cells ($r = 0.208$, $P = 0.002$), and M0 macrophages ($r = 0.487$, $P < 0.001$) and negatively correlated with resting NK cells ($r = -0.259$, $P < 0.001$), M2 macrophages ($r = -0.252$, $P = 0.0001$), monocytes ($r = -0.248$, $P = 0.0001$), gamma delta T cells ($r = -0.225$, $P = 0.0007$), and neutrophils ($r = -0.221$, $P = 0.0009$). ACSM3 was positively correlated with $CD8^+$T cells ($r = 0.136$, $P = 0.043$), resting memory $CD4^+$ T cells ($r = 0.156$, $P = 0.020$), M1 macrophages ($r = 0.204$, $P = 0.002$), resting NK cells ($r = 0.259$, $P < 0.001$), and delta gamma T cells ($r = 0.321$, $P < 0.001$) and negatively correlated with naive $CD4^+$ T cells ($r = -0.144$, $P = 0.032$), plasma cells ($r = -0.151$, $P = 0.024$), activated NK cells ($r = -0.221$, $P = 0.001$), regulatory T cells ($r = -0.267$, $P < 0.001$), and M0 macrophages ($r = -0.385$, $P < 0.001$). SPINK1 was positively correlated with M0 macrophages ($r = 0.346$, $P < 0.001$), activated NK cells ($r = 0.205$, $P = 0.002$), and regulatory T cells ($r = 0.163$, $P = 0.015$) and negatively correlated with monocytes ($r = -0.144$, $P = 0.033$), resting NK cells ($r = -0.162$, $P = 0.016$), $CD8^+$ T cells ($r = -0.245$, $P = 0.0001$), and delta gamma T cells ($r = -0.258$, $P = 0.0001$). COL15A1 was positively correlated with regulatory T cells ($r = 0.134$, $P = 0.047$), resting dendritic cells ($r = 0.175$, $P = 0.009$), activated NK cells ($r = 0.175$, $P = 0.009$), and M0 macrophages ($r = 0.415$, $P < 0.001$) and negatively correlated with delta gamma T cells ($r = -0.307$, $P < 0.001$), resting NK cells ($r = -0.305$, $P < 0.001$), neutrophils ($r = -0.261$, $P < 0.001$), and $CD8^+$ T cells ($r = -0.243$, $P < 0.001$). TP53I3 was positively correlated with M1 macrophages ($r = 0.161$, $P = 0.016$), resting dendritic cells ($r = 0.189$, $P = 0.005$), regulatory T cells ($r = 0.226$, $P < 0.001$), activated NK cells ($r = 0.315$, $P < 0.001$), and M0 macrophages ($r = 0.424$, $P < 0.001$) and negatively correlated with delta gamma T cells ($r = -0.361$, $P < 0.001$), resting NK cells ($r = -0.323$, $P < 0.001$), $CD8^+$ T cells ($r = -0.258$, $P < 0.001$), resting memory $CD4^+$ T cells ($r = -0.221$, $P < 0.001$), neutrophils ($r = -0.217$, $P = 0.001$), and activated dendritic cells ($r = -0.170$, $P = 0.011$). RRAGD was positively correlated with M0 macrophages ($r = 0.439$, $P < 0.0001$), activated NK cells ($r = 0.241$, $P < 0.001$), regulatory T cells (r = 0.202, $P = 0.003$), plasma cells ($r = 0.161$, $P = 0.017$), and activated mast cells ($r = 0.146$, $P = 0.030$) and negatively correlated with neutrophils ($r = -0.148$, $P = 0.028$), resting NK cells ($r = -0.188$, $P = 0.005$), resting memory $CD4^+$ T cells ($r = -0.211$, $P = 0.002$), $CD8^+$ T cells ($r = -0.301$, $P < 0.001$), and delta gamma T cells ($r = -0.472$, $P < 0.001$).

4. Discussion

In recent years, numerous reports have endeavored to demonstrate the pathogenesis and pathomechanism of HCC.

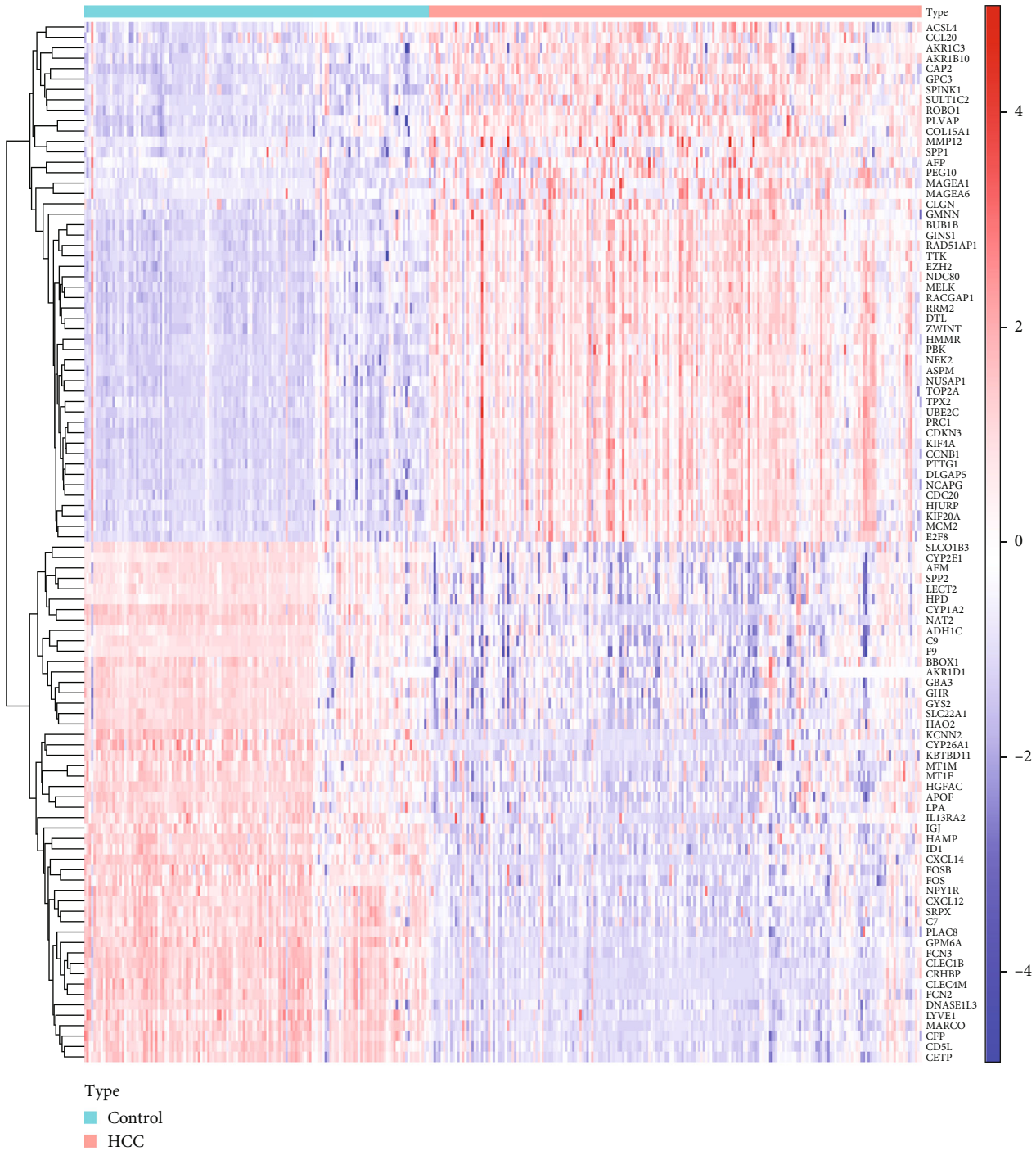

(a)

Figure 1: Continued.

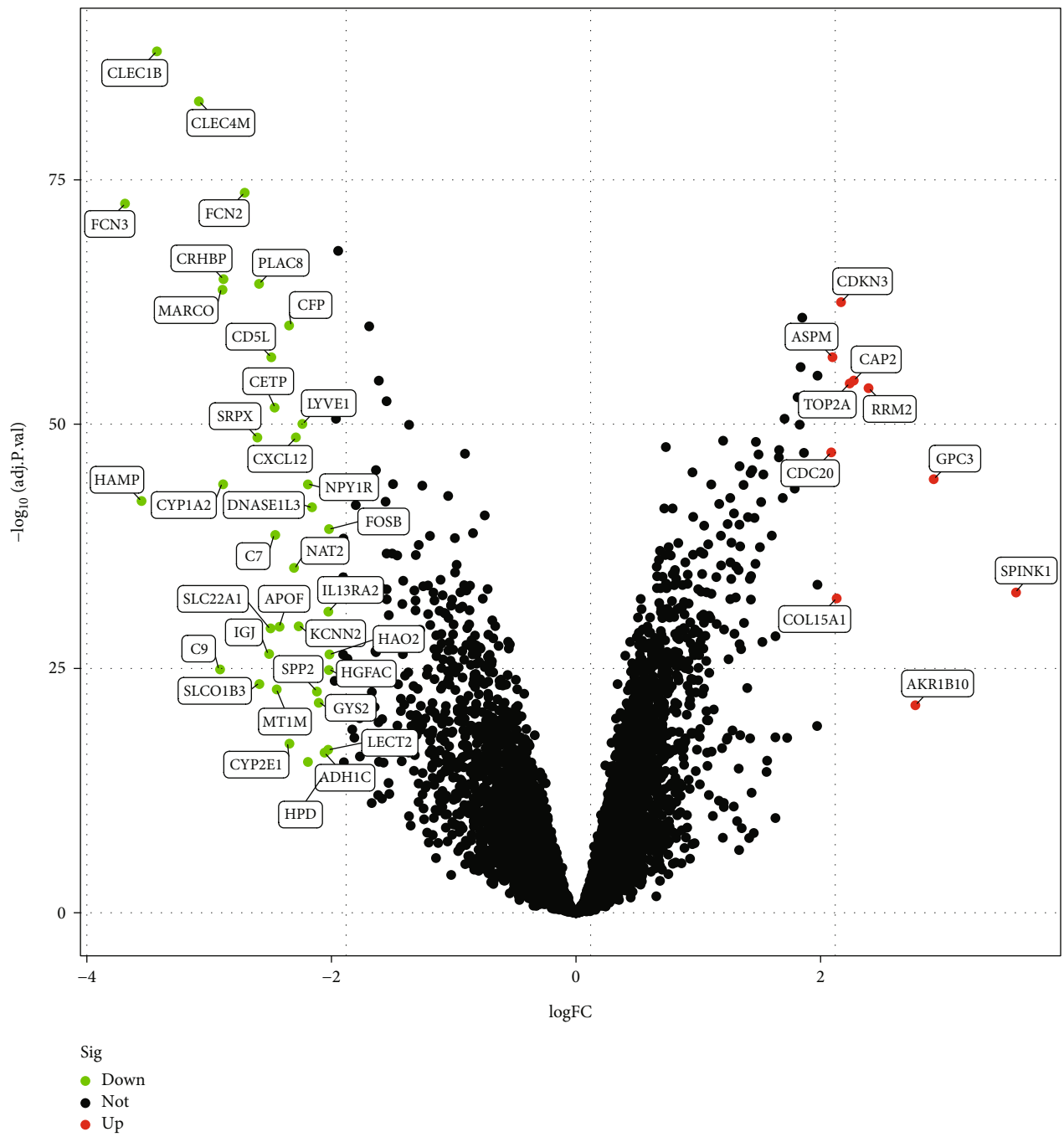

(b)

Figure 1: Differentially expressed genes (DEGs) identified between HCC and control samples. (a) Heatmap of DEG distribution and (b) volcano plots of DEG distribution.

Despite that huge development on surgical treatment and drug therapy has been acquired, the outcome of HCC is still unsatisfactory. Without powerful diagnosis approach on the early stage often results in poor progression of HCC. Therefore, developing stable prognostic biomarkers that reveal the biological progression of the HCC will be vital for its prevention and treatment.

In the current study, we constructed an integrated bioinformatic analysis to determine diagnostic genes that are involved in immune cell infiltration in individuals with HCC. Seven potential immune-related diagnostic gene biomarkers (GPC3, ACSM3, SPINK1, COL15A1, TP53I3, RRAGD, and CLDN10) were identified for HCC using two machine learning algorithms. In addition, these candidate biomarkers were strongly related to multiple immune cells. These feature genes and immune cells may offer new promising early diagnostic and immunotherapeutic strategies for HCC. The diseases enriched by DEGs were observed to be

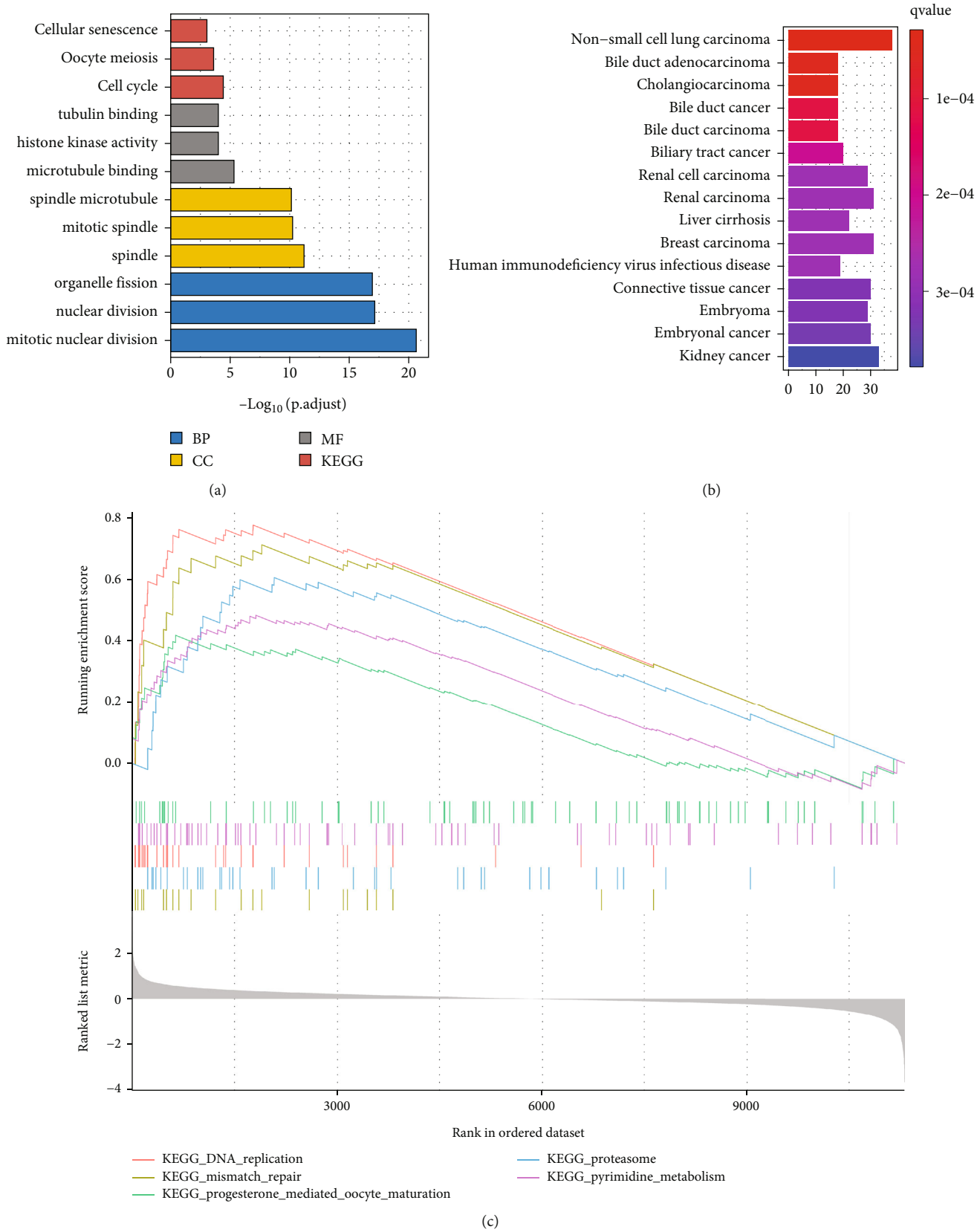

Figure 2: Functional enrichment analysis. (a) GO and KEGG functional enrichment analyses of the DEGs. (b) Disease Ontology enrichment analysis of the DEGs between HCC and control samples. (c) Enriched gene set enrichment analysis (GSEA) terms between HCC and controls.

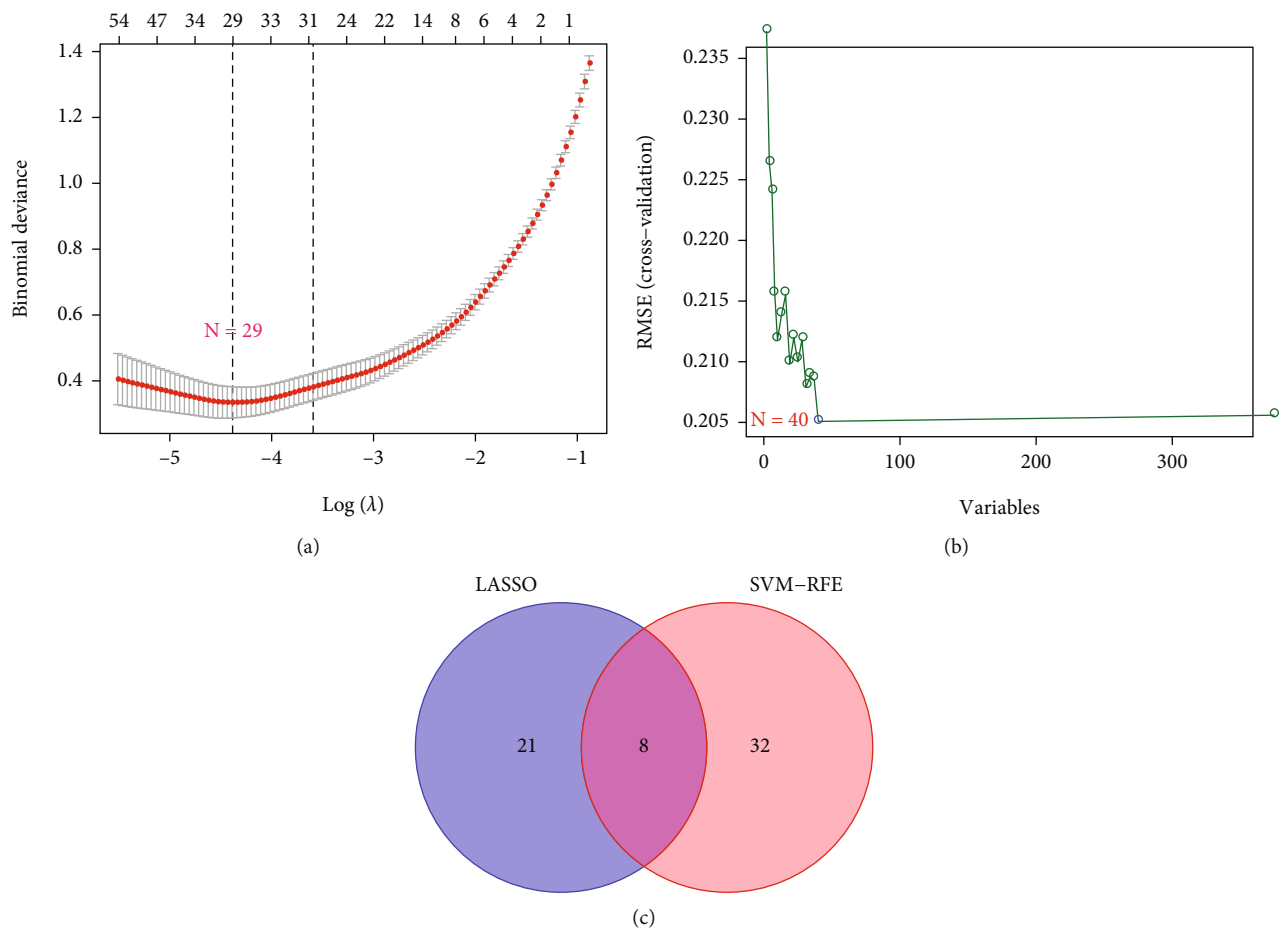

Figure 3: Screening for potential diagnostic gene biomarkers of HCC by two machine learning strategies. (a) Screening diagnostic gene biomarkers using the least absolute shrinkage and selection operator (LASSO). (b) The optimal gene biomarker selection via support vector machine-recursive feature elimination (SVM-RFE) algorithm. (c) Venn diagram displaying eight diagnostic biomarkers shared by LASSO and SVM-RFE algorithms.

mainly associated with cancer-related pathways. GO and KEGG analysis results show that DEGs are significantly enriched in cell cycle, tubulin binding, mitotic spindle, and mitotic nuclear division, highly associated with HCC oncological diseases, suggesting cell cycle exerts a strong influence on the development and homeostasis of HCC. Deregulated cell cycle process is a hallmark of malignancy, and targeting CDKs to inhibit cell proliferation has been approved as a helpful anticancer therapy [24] [25]. Abnormalities in cell cycle mechanisms often accompany HCC carcinogenesis. Based on these findings, the results in our study may present potential targets for the therapy of HCC.

HCC is a highly heterogeneous malignant solid tumor. Cells of the immune system are indispensable regulators for tumor microenvironment (TME) homeostasis. The TME comprises the stromal as well as immune cells which interact with or infiltrate a particular cancer [26]. Among the TME, immune cells are the key factors of tumor progression. At the same time, immunotherapy is a promising tumor-killing method. The degree of infiltration of immune cells can reflect the response of HCC cells to immunotherapy, as well as different prognoses. However, despite the development of immunotherapy for HCC, the results have not been satisfactory. Immune cell infiltration and distribution are highly heterogeneous and complex, and the search for factors driving immune infiltration or key biomarkers is crucial to reveal this heterogeneity. In HCC, TME is immunosuppressive and contributes to immune tolerance and evasion via multiple processes, boosting cancer proliferation, invasion, and metastasis [26]. Presently, increasing investigations have illustrated that the effector of CD8+, regulatory T cells, $CD4^+$ cells, and dendritic cells could affect the effectiveness of immune checkpoint inhibitors [27, 28]. In this present study, by using CIBERSOTR algorithm, a great diversity of the infiltrated immune cells was found to be participating in the process of HCC. In detail, regulatory T cell, activated NK cells, M0 macrophages, resting dendritic cell, and activated mast cell were decreased in HCC cohort. This evidence is in general agreement with our results that multiple immune cells are associated with these biomarkers, suggesting that a substantial amount of immune cell is involved in HCC. Therefore, identifying potential gene biomarkers correlated with immune cell infiltration for HCC will contribute to its diagnosis and treatment.

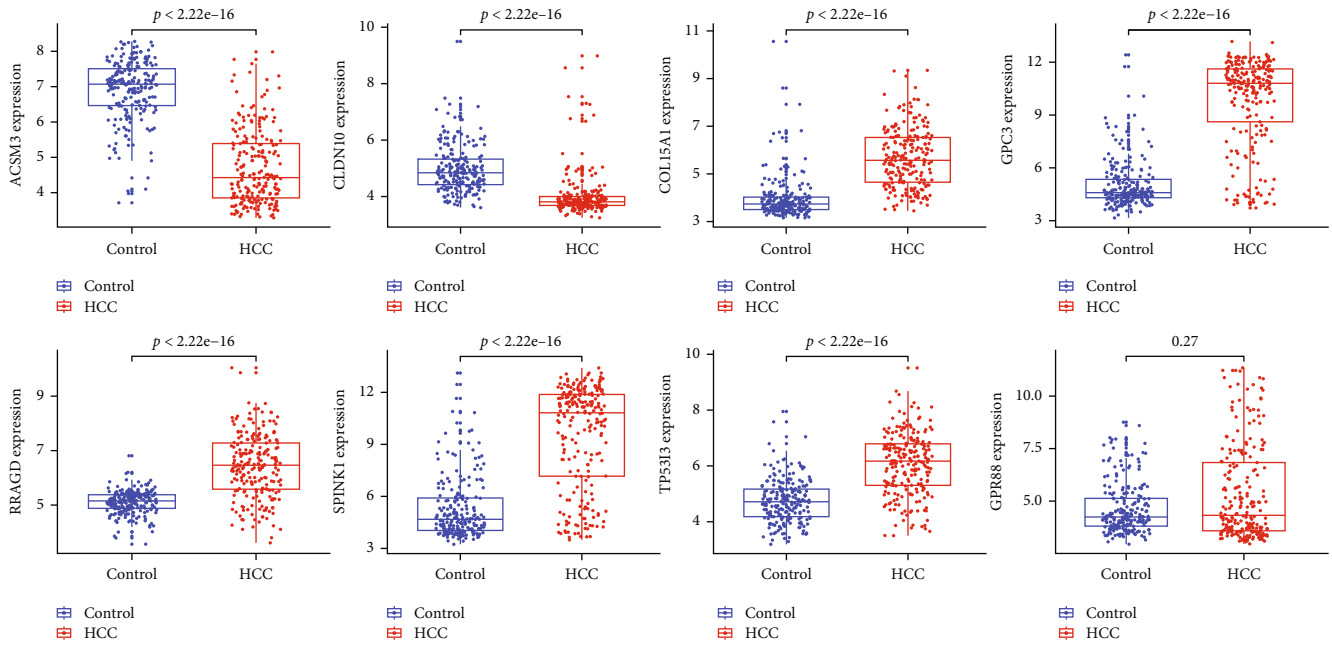

(a)

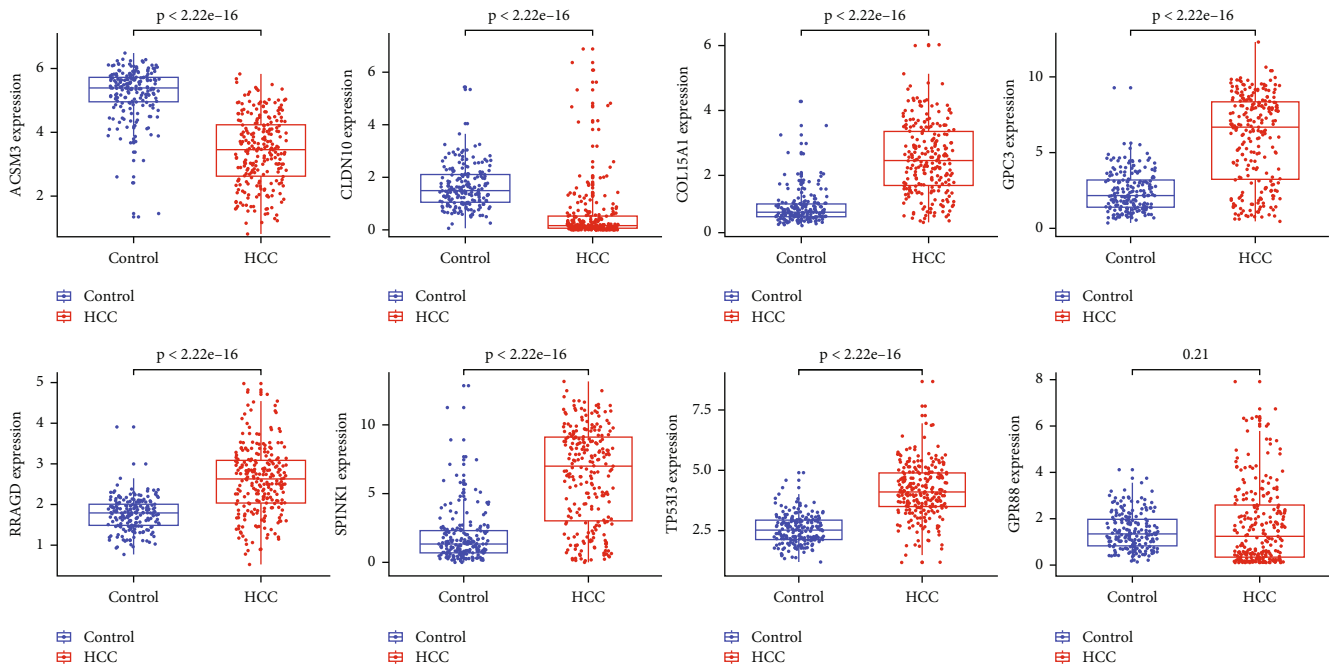

(b)

Figure 4: Continued.

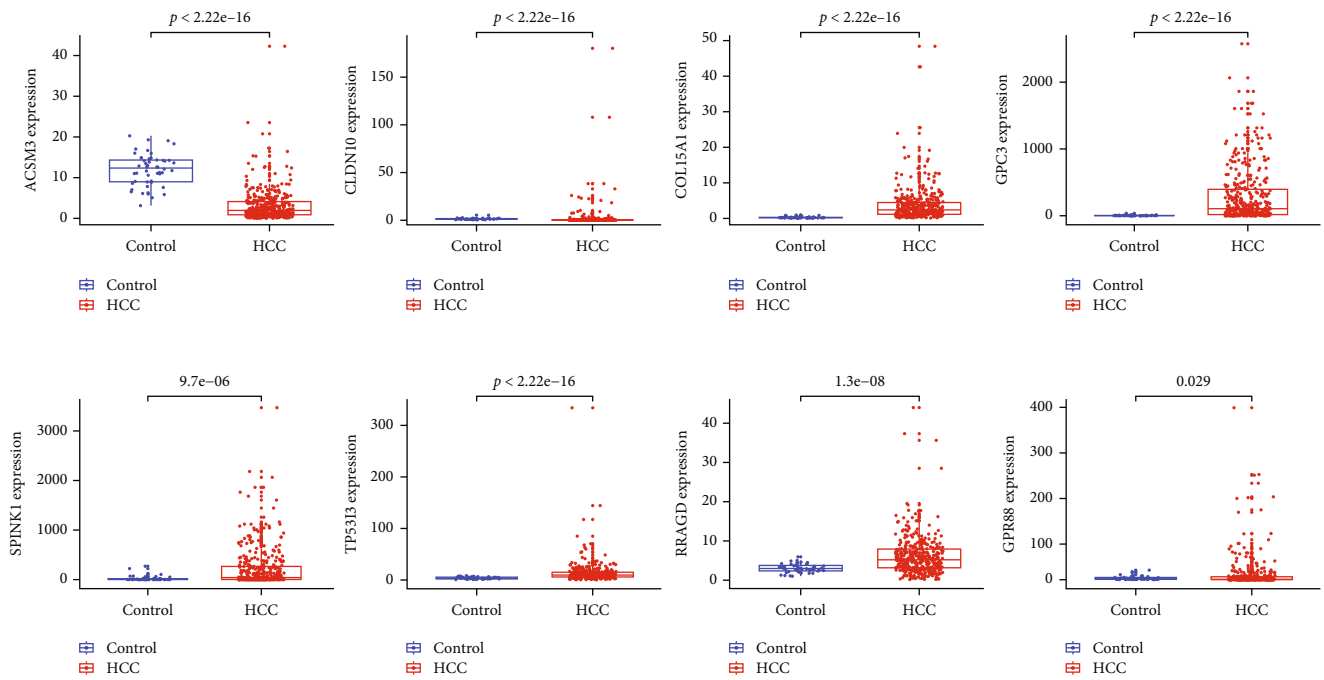

(c)

Figure 4: Verification of the expression levels of selected diagnostic gene markers in three validation cohorts. (a) GSE14520-GPL3921 cohort. (b) ICGC-LIRI-JP cohort. (c) TCGA cohort.

GPC3, ACSM3, SPINK1, COL15A1, TP53I3, RRAGD, and CLDN10 were identified as potential new immune-related diagnostic biomarkers with high diagnostic value, which may serve as ideal biomarkers for the diagnosis of HCC, as well as for the early stage of HCC. In recent years, machine learning has been applied to various fields of biomedicine. Compared with most traditional statistical methods, the advantage of machine learning is that it can identify potential rules through massive data learning. Machine learning algorithms have been applied to identify cancer prognostic characteristic genes and tumor classification [29]. Machine learning is a crucial discipline of artificial intelligence, utilizes procedures that identify patterns within existing data, and trains itself to perform predictions on other data [30]. Glypican-3 (GPC3) belongs to a member of the glypican family, which has been utilized as a potential diagnostic biomarker for HCC owning to its preferential expression in HCC [31]. GPC3 was highly expressed in HCC samples than in benign liver lesions, which may play an important role in HCC diagnosis than alpha-fetoprotein (AFP) [32]. ACSM3 was downregulated in HCC, and individuals with little expression of ACSM3 presented miserable prognosis. High expression of ACSM3 weakened migration and invasion of HCC cells *in vitro* and *in vivo* as well as downregulated the phosphorylation of WNK1 and AKT [33]. SPINK1 is highly expressed and contributes to cancer progress in multiple cancers, including HCC. It has been proved that SPINK1 increased proliferation and promoted migration and invasion capability of HCC cell lines [34]. CLDN10 expressed highly in HCC cells, and growing evidence demonstrates that CLDN10 is functionally involved in HCC invasion and is a possible target for HCC therapy [35]. Furthermore, knockdown of CLDN10 by siRNA reduced HCC cell migration [36]. COL15A1 is a novel atherosclerosis gene that is involved in vascular smooth muscle cell phenotype, which is regulated by epigenetic state in passaged cells and located in atherosclerotic tissue [37]. However, the diagnostic and prognostic role of COL15A1 in HCC remains unknown. TP53I3, one of the p53-induced genes, is an oxidoreductase-like protein that is transcriptionally activated by the tumor suppressor TP53 and involved in TP53-mediated apoptosis as well as DNA damage response [38]. As we know, TP53 mutation is one of the common alterations in multiple cancers, including HCC. Mutations in the TP53 gene could yield genetic instability and result in cancer progression [39]. RRAGD encodes a small Rag guanosine triphosphatase, which is an important component of the nutrient-sensing pathway that activates mTOR signaling [40]. The relationship between mTOR signaling pathway and the pathogenesis of HCC has been widely confirmed previously [41, 42].

To deeply evaluate the diagnostic performance of the model, this signature was sufficiently validated and evaluated in multiple different external validation datasets, revealing the robustness and reliability of the diagnostic score. Despite the use of bioinformatics and machine learning algorithms in our study and the discovery of the diagnostic value of key genes in HCC patients, several limitations still exist in present study. First, the findings concluded from bioinformatics analysis need RT-PCR in clinical tissues to additional

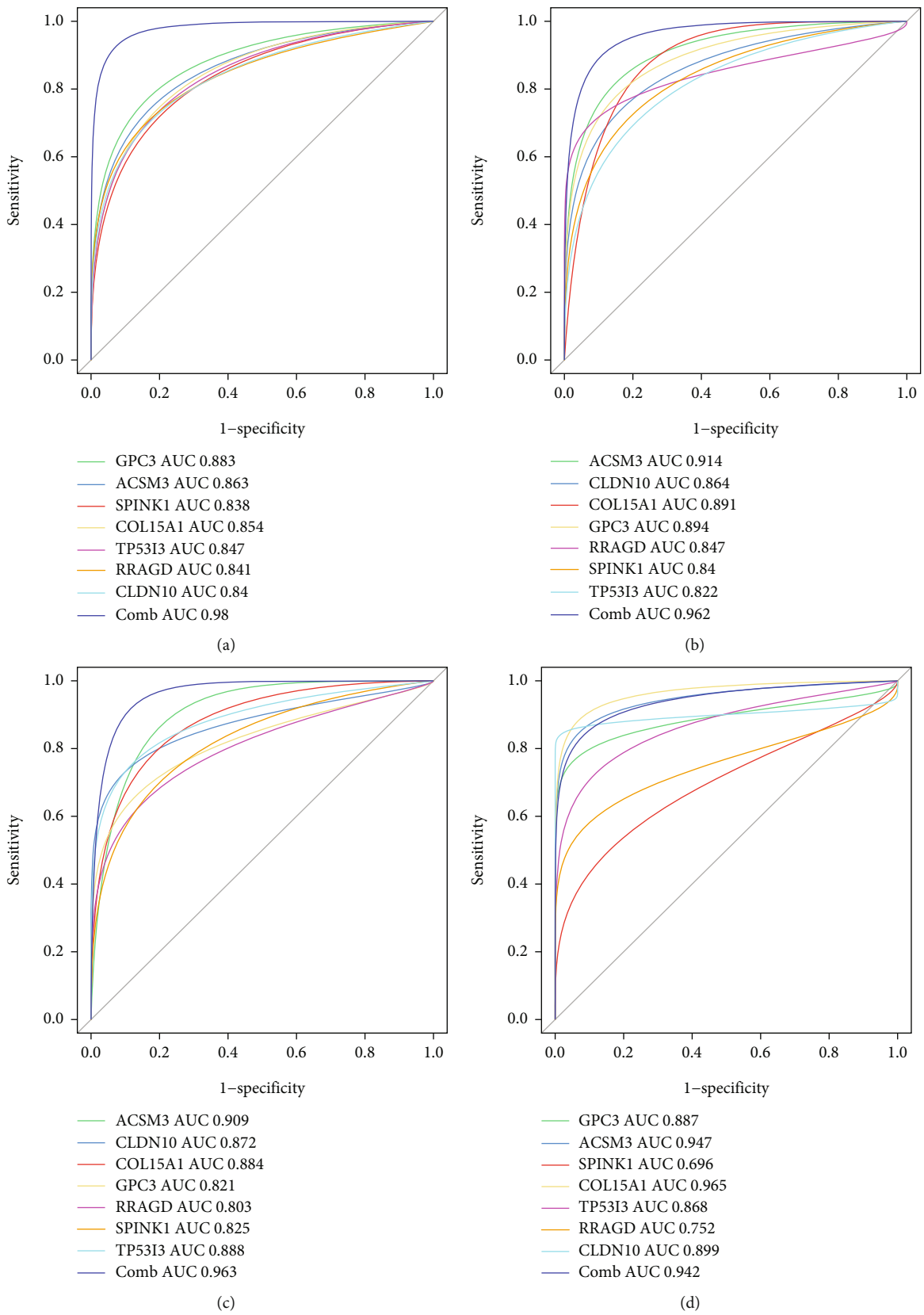

Figure 5: The ROC curve of the discrimination ability of the seven identified diagnostic gene biomarkers in different cohorts. (a) The discovery cohort. (b) GSE14520-GPL3921 cohort. (c) ICGC-LIRI-JP cohort. (d) The TCGA cohort.

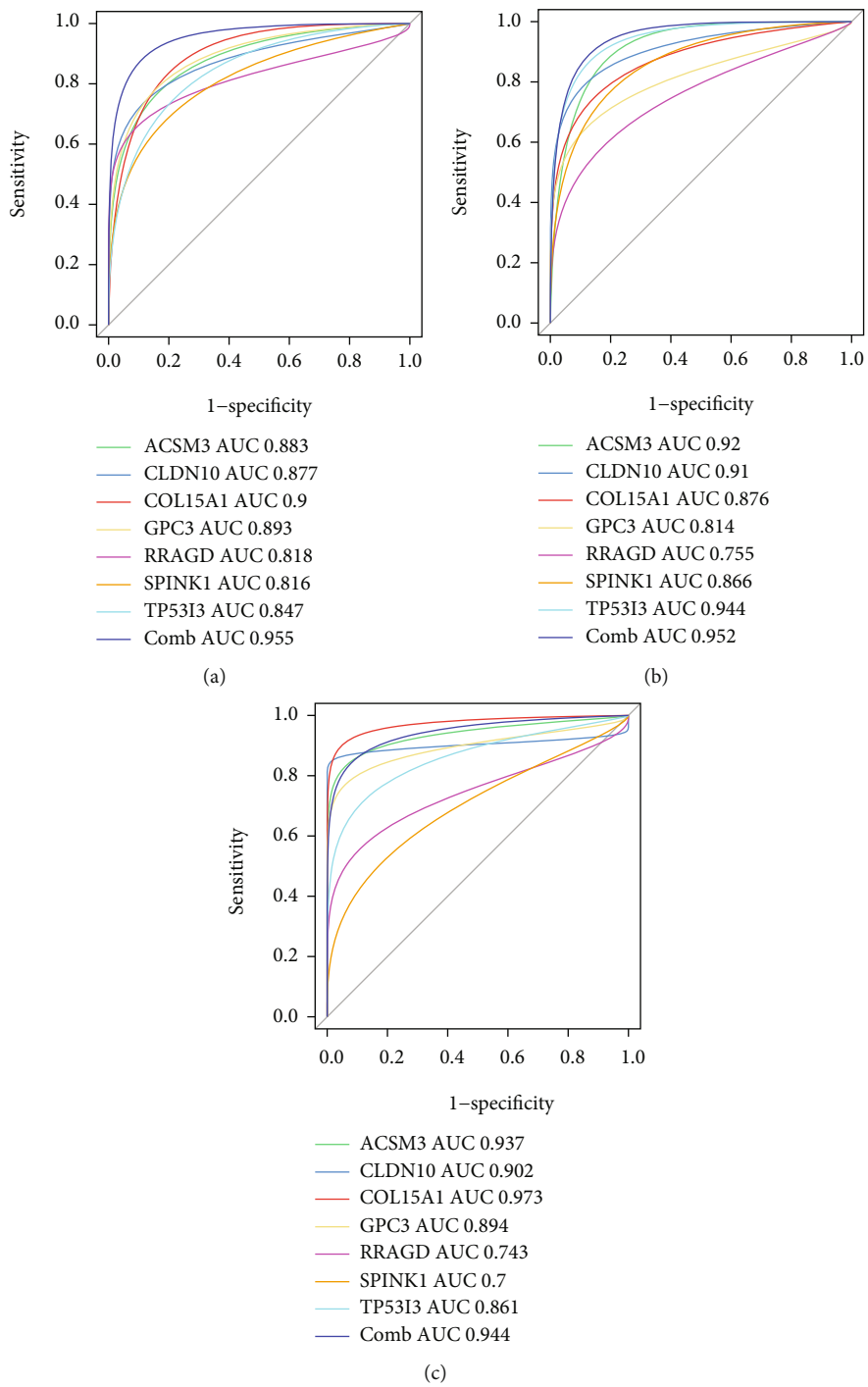

Figure 6: The ROC curve of the discrimination ability of the seven identified diagnostic gene biomarkers for early-stage HCC in cohorts. (a) GSE14520-GPL3921 cohort. (b) ICGC-LIRI-JP cohort. (c) The TCGA cohort.

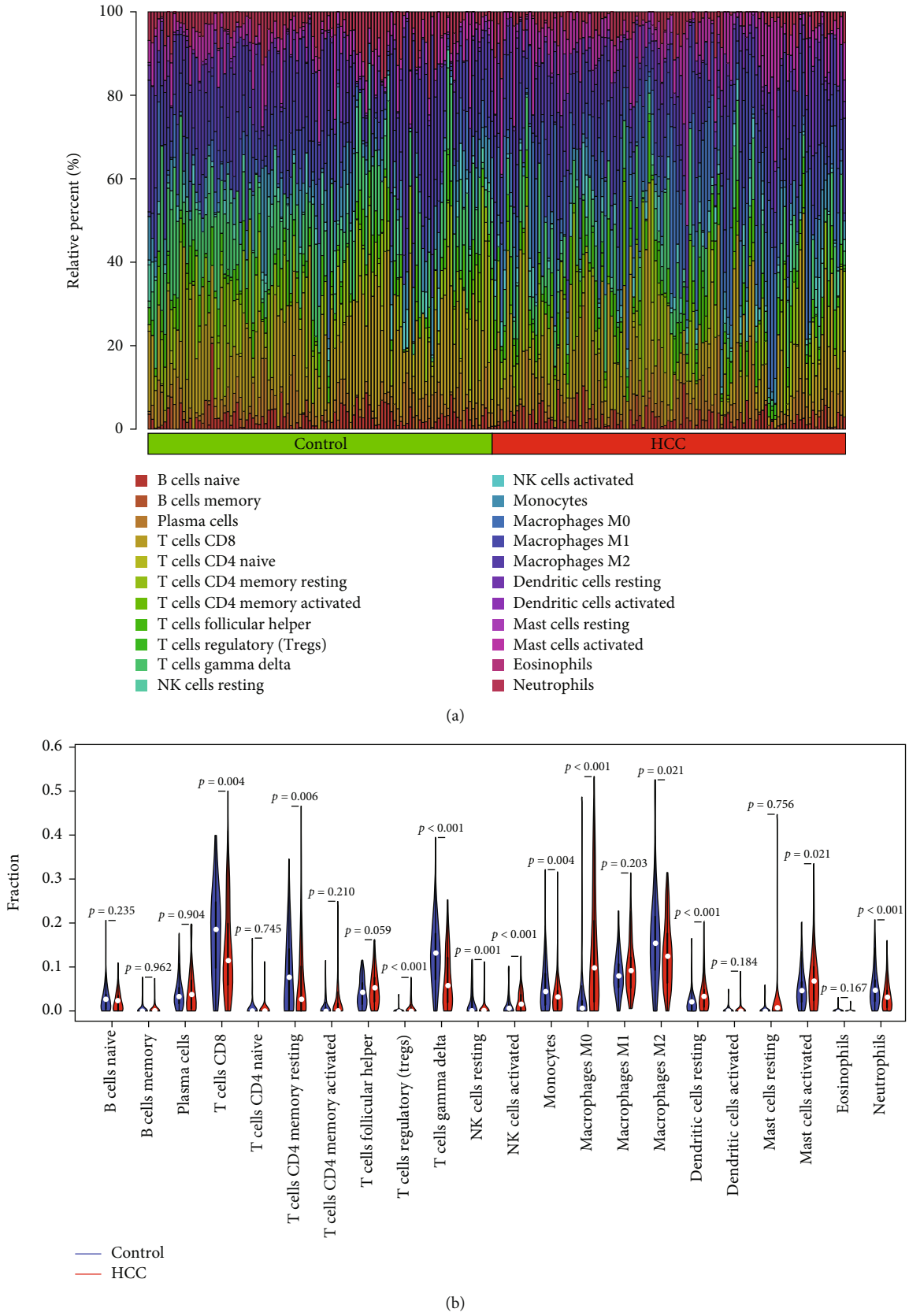

Figure 7: The view of immune infiltration between HCC and controls. (a) Violin diagram of the proportion of 20 types of immune cells between HCC and normal controls. (b) The difference of immune infiltration between HCC and normal controls.

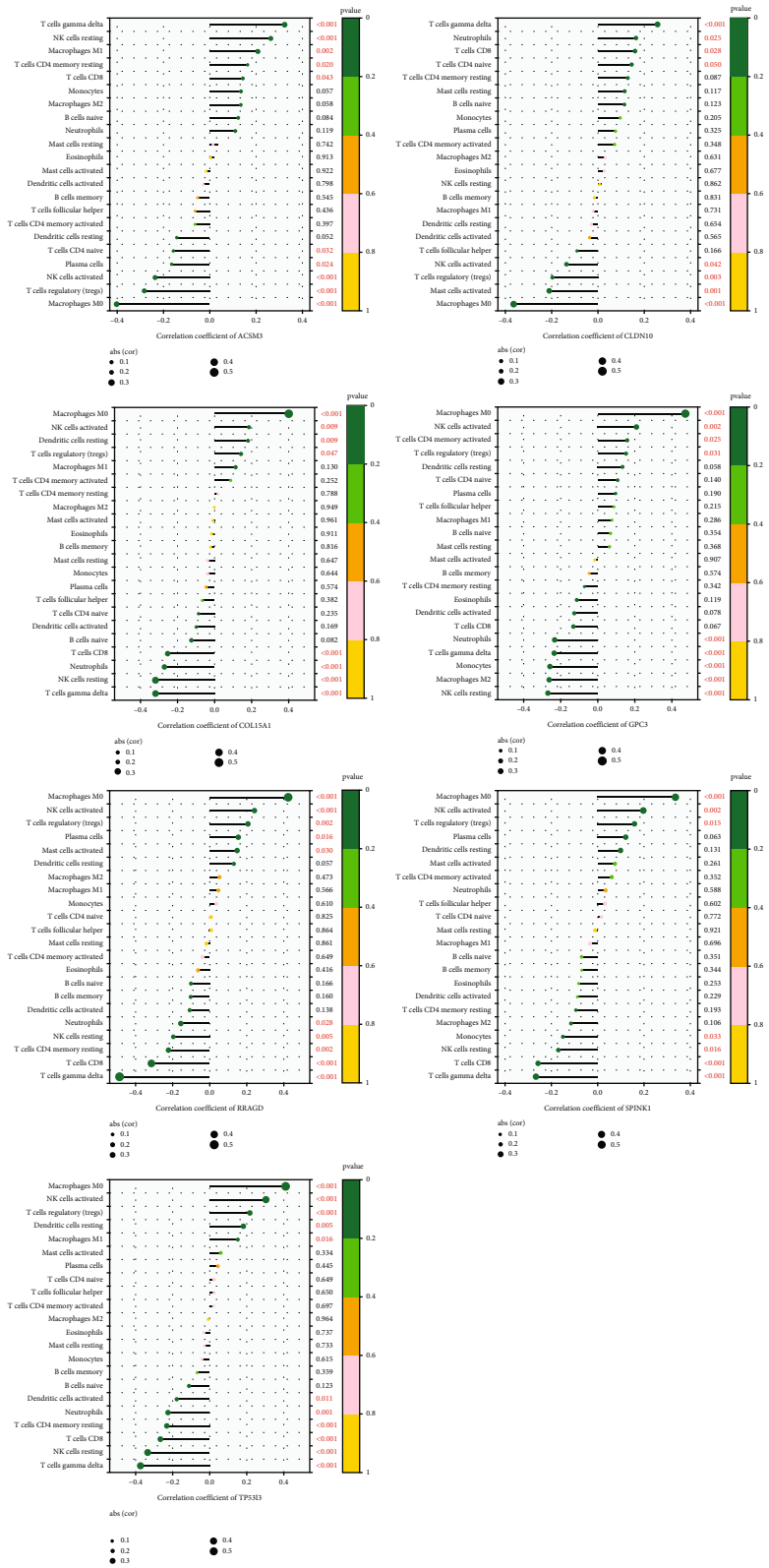

Figure 8: Correlation analyses between diagnostic gene biomarkers and infiltrating immune cells in HCC. Correlation between GPC3, ACSM3, SPINK1, COL15A1, TP53I3, RRAGD, CLDN10, and infiltrating immune cells. The size of the dots represents the strength of the correlation between feature genes and immune cells; the larger the dots, the stronger the correlation.

verify. Besides, most of the identified genes need *in vitro* and *in vivo* validation experiments in HCC, and further evidence provided by a well-designed study is required.

5. Conclusion

In summary, we identified GPC3, ACSM3, SPINK1, COL15A1, TP53I3, RRAGD, and CLDN10 as diagnostic immune-related biomarkers with potential clinical utility, which might have the ability to accurately early diagnosis of HCC, enable earlier access to intervention, and improve the clinical outcomes. Moreover, multiple immune cells may be involved in the occurrence and development of HCC and could be used as potential targets for future immunotherapy in patients with HCC that warrant further investigations.

Data Availability

Multiple publicly cohort data were used in the present study. The data utilized in present study are downloaded from the open GEO data database (https://www.ncbi.nlm.nih.gov/geo/; accession numbers: GSE14520, GSE45267, GSE51401, GSE65372, and GSE121248), TCGA data portal (https://portal.gdc.cancer.gov/), and ICGC data portal (https://dcc.icgc.org/).

Conflicts of Interest

The authors declare that they have no conflicts of interest.

References

[1] H. Sung, J. Ferlay, R. L. Siegel et al., "Global cancer statistics 2020: GLOBOCAN estimates of incidence and mortality worldwide for 36 cancers in 185 countries," *CA: A Cancer Journal for Clinicians*, vol. 71, no. 3, pp. 209–249, 2021.

[2] J. F. Perz, G. L. Armstrong, L. A. Farrington, Y. J. Hutin, and B. P. Bell, "The contributions of hepatitis B virus and hepatitis C virus infections to cirrhosis and primary liver cancer worldwide," *Journal of Hepatology*, vol. 45, no. 4, pp. 529–538, 2006.

[3] J. M. Llovet and J. Bruix, "Systematic review of randomized trials for unresectable hepatocellular carcinoma: chemoembolization improves survival," *Hepatology*, vol. 37, no. 2, pp. 429–442, 2003.

[4] K. T. Wu, C. C. Wang, L. G. Lu et al., "Hepatocellular carcinoma: clinical study of long-term survival and choice of treatment modalities," *World Journal of Gastroenterology*, vol. 19, no. 23, pp. 3649–3657, 2013.

[5] J. D. Yang and J. K. Heimbach, "New advances in the diagnosis and management of hepatocellular carcinoma," *BMJ*, vol. 371, article m3544, 2020.

[6] J. Bruix, M. Reig, and M. Sherman, "Evidence-based diagnosis, staging, and treatment of patients with hepatocellular carcinoma," *Gastroenterology*, vol. 150, no. 4, pp. 835–853, 2016.

[7] K. Tzartzeva, J. Obi, N. E. Rich et al., "Surveillance imaging and alpha fetoprotein for early detection of hepatocellular carcinoma in patients with cirrhosis: a meta-analysis," *Gastroenterology*, vol. 154, no. 6, pp. 1706–1718.e1, 2018.

[8] J. Zucman-Rossi, A. Villanueva, J. C. Nault, and J. M. Llovet, "Genetic landscape and biomarkers of hepatocellular carcinoma," *Gastroenterology*, vol. 149, no. 5, pp. 1226–1239.e4, 2015.

[9] B. Yu, S. Zhou, H. Liang, Q. Ye, and Y. Wang, "Development and Validation of a Novel Circulating miRNA-Based Diagnostic Score for Early Detection of Hepatocellular Carcinoma," *Digestive Diseases and Sciences*, 2021.

[10] X. Gan, Y. Luo, G. Dai et al., "Identification of gene signatures for diagnosis and prognosis of hepatocellular carcinomas patients at early stage," *Frontiers in Genetics*, vol. 11, p. 857, 2020.

[11] L. Silva, J. Egea, L. Villanueva et al., "Cold-inducible RNA binding protein as a vaccination platform to enhance immunotherapeutic responses against hepatocellular carcinoma," *Cancers*, vol. 12, no. 11, p. 3397, 2020.

[12] S. Yang, Y. Cheng, X. Wang, P. Wei, H. Wang, and S. Tan, "Identification of the immune cell infiltration landscape in hepatocellular carcinoma to predict prognosis and guide immunotherapy," *Frontiers in Genetics*, vol. 12, article 777931, 2021.

[13] E. Zhao, S. Chen, and Y. Dang, "A novel signature based on pairwise PD-1/PD-L1 signaling pathway genes for predicting the overall survival in patients with hepatocellular carcinoma," *Clinical and Translational Medicine*, vol. 11, no. 5, article e431, 2021.

[14] Q. Sun, Y. Li, X. Yang et al., "Identification and validation of 17-lncRNA related to regulatory T cell heterogeneity as a prognostic signature for head and neck squamous cell carcinoma," *Frontiers in Immunology*, vol. 12, article 782216, 2021.

[15] N. T. Issa, V. Stathias, S. Schürer, and S. Dakshanamurthy, "Machine and deep learning approaches for cancer drug repurposing," *Seminars in Cancer Biology*, vol. 68, pp. 132–142, 2021.

[16] A. Rajkomar, J. Dean, and I. Kohane, "Machine learning in medicine," *The New England Journal of Medicine*, vol. 380, no. 14, pp. 1347–1358, 2019.

[17] J. T. Leek, W. E. Johnson, H. S. Parker, A. E. Jaffe, and J. D. Storey, "The sva package for removing batch effects and other unwanted variation in high-throughput experiments," *Bioinformatics*, vol. 28, no. 6, pp. 882-883, 2012.

[18] G. Yu, L. G. Wang, Y. Han, and Q. Y. He, "clusterProfiler: an R package for comparing biological themes among gene clusters," *OMICS*, vol. 16, no. 5, pp. 284–287, 2012.

[19] G. Yu, L. G. Wang, G. R. Yan, and Q. Y. He, "DOSE: an R/Bioconductor package for disease ontology semantic and enrichment analysis," *Bioinformatics*, vol. 31, no. 4, pp. 608-609, 2015.

[20] A. Subramanian, H. Kuehn, J. Gould, P. Tamayo, and J. P. Mesirov, "GSEA-P: a desktop application for gene set enrichment analysis," *Bioinformatics*, vol. 23, no. 23, pp. 3251–3253, 2007.

[21] J. Friedman, T. Hastie, and R. Tibshirani, "Regularization paths for generalized linear models via coordinate descent," *Journal of Statistical Software*, vol. 33, no. 1, pp. 1–22, 2010.

[22] M. R. Daliri, "Feature selection using binary particle swarm optimization and support vector machines for medical diagnosis," *Biomedizinische Technik Biomedical Engineering*, vol. 57, no. 5, pp. 395–402, 2012.

[23] A. M. Newman, C. L. Liu, M. R. Green et al., "Robust enumeration of cell subsets from tissue expression profiles," *Nature Methods*, vol. 12, no. 5, pp. 453–457, 2015.

[24] X. Shi, M. Ma, and S. Lin, "Cell cycle-dependent expression dynamics of G1/S specific cyclin, cellulose synthase and cellulase in the dinoflagellate Prorocentrum donghaiense," *Frontiers in Microbiology*, vol. 8, p. 1118, 2017.

[25] T. Otto and P. Sicinski, "Cell cycle proteins as promising targets in cancer therapy," *Nature Reviews. Cancer*, vol. 17, no. 2, pp. 93–115, 2017.

[26] Y. Xiao and D. Yu, "Tumor microenvironment as a therapeutic target in cancer," *Pharmacology & Therapeutics*, vol. 221, article 107753, 2021.

[27] K. C. Barry, J. Hsu, M. L. Broz et al., "A natural killer-dendritic cell axis defines checkpoint therapy-responsive tumor microenvironments," vol. 24, no. 8, pp. 1178–1191, 2018.

[28] D. Lambrechts, E. Wauters, B. Boeckx et al., "Phenotype molding of stromal cells in the lung tumor microenvironment," *Nature Medicine*, vol. 24, no. 8, pp. 1277–1289, 2018.

[29] E. Zhao, H. Xie, and Y. Zhang, "Predicting diagnostic gene biomarkers associated with immune infiltration in patients with acute myocardial infarction," *Frontiers in Cardiovascular Medicine*, vol. 7, article 586871, 2020.

[30] T. Badrick, G. Banfi, A. Bietenbeck, M. A. Cervinski, T. P. Loh, and K. Sikaris, "Machine learning for clinical chemists," *Clinical Chemistry*, vol. 65, no. 11, pp. 1350–1356, 2019.

[31] H. C. Hsu, W. Cheng, and P. L. Lai, "Cloning and expression of a developmentally regulated transcript MXR7 in hepatocellular carcinoma: biological significance and temporospatial distribution," *Cancer Research*, vol. 57, no. 22, pp. 5179–5184, 1997.

[32] M. Wu, Z. Liu, A. Zhang, and N. Li, "Associated measurement of fucosylated levels of AFP, DCP, and GPC3 for early diagnosis in hepatocellular carcinoma," *The International Journal of Biological Markers*, vol. 34, no. 1, pp. 20–26, 2019.

[33] H. Y. Ruan, C. Yang, X. M. Tao et al., "Downregulation of ACSM3 promotes metastasis and predicts poor prognosis in hepatocellular carcinoma," *American Journal of Cancer Research*, vol. 7, no. 3, pp. 543–553, 2017.

[34] K. Huang, W. Xie, S. Wang et al., "High SPINK1 expression predicts poor prognosis and promotes cell proliferation and metastasis of hepatocellular carcinoma," *Journal of Investigative Surgery*, vol. 34, no. 9, pp. 1011–1020, 2021.

[35] Y. C. Ip, S. T. Cheung, Y. T. Lee, J. C. Ho, and S. T. Fan, "Inhibition of hepatocellular carcinoma invasion by suppression of claudin-10 in HLE cells," *Molecular Cancer Therapeutics*, vol. 6, no. 11, pp. 2858–2867, 2007.

[36] H. Sun, C. Cui, F. Xiao et al., "miR-486 regulates metastasis and chemosensitivity in hepatocellular carcinoma by targeting CLDN10 and CITRON," *Hepatology Research*, vol. 45, no. 13, pp. 1312–1322, 2015.

[37] J. J. Connelly, O. A. Cherepanova, J. F. Doss et al., "Epigenetic regulation of COL15A1 in smooth muscle cell replicative aging and atherosclerosis," *Human Molecular Genetics*, vol. 22, no. 25, pp. 5107–5120, 2013.

[38] J. L. Lopes, S. Chaudhry, G. S. Lopes, N. K. Levin, and M. A. Tainsky, "FANCM, RAD1, CHEK1 and TP53I3 act as BRCA-like tumor suppressors and are mutated in hereditary ovarian cancer," *Cancer Genetics*, vol. 235-236, pp. 57–64, 2019.

[39] M. Shi, Y. Wang, W. Tang et al., "Identification of TP53 mutation associated-immunotype and prediction of survival in patients with hepatocellular carcinoma," *Annals of Translational Medicine*, vol. 8, no. 6, p. 321, 2020.

[40] K. P. Schlingmann, F. Jouret, K. Shen et al., "mTOR-activating mutations inRRAGDAre causative for kidney tubulopathy and cardiomyopathy," *Journal of the American Society of Nephrology*, vol. 32, no. 11, pp. 2885–2899, 2021.

[41] Y. Zhang, P. Qin, X. Xu et al., "Mediator complex subunit 19 promotes the development of hepatocellular carcinoma by regulating the AKT/mTOR signaling pathway," *Frontiers in Oncology*, vol. 11, article 792285, 2021.

[42] L. Yao, Y. Xuan, H. Zhang et al., "Reciprocal REGγ-mTORC1 regulation promotes glycolytic metabolism in hepatocellular carcinoma," *Oncogene*, vol. 40, no. 3, pp. 677–692, 2021.

Hindawi
Gastroenterology Research and Practice
Volume 2022, Article ID 2021066, 14 pages
https://doi.org/10.1155/2022/2021066

Research Article

Identifying the Mechanism of Polygoni Cuspidati Rhizoma et Radix in Treating Acute Liver Failure Based on Network Pharmacology and Molecular Docking

Jing Hong,[1,2] **Jie Ding**,[2,3] **Han-han Hong**,[4] **Xiao-wan Xu**,[1] **Bo Pan**,[1] **Yi Ruan**,[2] **and Xiao-feng Zhai**[1,2]

[1]*Department of Integrative Oncology, Changhai Hospital, Naval Medical University, Shanghai 200433, China*
[2]*School of Traditional Chinese Medicine, Naval Medical University, Shanghai 200433, China*
[3]*Gynecology of Traditional Chinese Medicine, Changhai Hospital, Naval Medical University, Shanghai 200433, China*
[4]*Department of Nursing, Chengjiaqiao Community Health Service Center of Changning District, Shanghai 201103, China*

Correspondence should be addressed to Bo Pan; pb453275454@126.com, Yi Ruan; ruanyi@smmu.edu.cn, and Xiao-feng Zhai; zhaixfch@163.com

Received 10 January 2022; Revised 6 March 2022; Accepted 10 March 2022; Published 8 April 2022

Academic Editor: Xiude Fan

Background and Objective. Acute liver failure (ALF) is a rare clinical syndrome with a poor prognosis and leads to multiple organ failure. Polygoni Cuspidati Rhizoma et Radix (PCRR) is a commonly used Chinese medicine, which is recognized as a potential therapeutic herb against ALF. This study aimed to explore the pharmacological mechanisms of the therapeutic effect of PCRR in ALF via network pharmacology and molecular docking. *Materials and Methods.* The potential bioactive compounds of PCRR and their targets were collected from TCMSP, TCMID, and BATMAN-TCM databases with absorption, distribution, metabolism, and excretion protocols (oral bioavailability ≥30% and drug-likeness ≥0.18). The ALF-related target genes were identified using the GeneCards and OMIM databases. A protein-protein interaction (PPI) network among these targets was constructed using the Cytoscape software to obtain the core targets. The genes associated with ALF were analyzed via Gene Ontology (GO) and Kyoto Encyclopedia of Genes and Genomes (KEGG) enrichment analyses to identify the signaling pathways related to the therapeutic effect of PCRR in ALF. *Results.* In total, 10 bioactive compounds of PCRR and 200 targets related to them were obtained, and 2913 ALF-related target genes were identified. PPI network analysis pinpointed 15 core targets, namely, TP53, AKT1, JUN, HSP90AA1, MAPK1, RELA, TNF, ESR1, IL6, MYC, MAPK14, FOS, RB1, CDKN1A, and EGFR. GO enrichment and KEGG pathway analyses revealed that the therapeutic mechanisms of PCRR in ALF are related to cell metabolism, oxidative stress, inflammation, and hepatocyte apoptosis. *Conclusion.* This is the first study to explore the therapeutic mechanisms of PCRR in ALF via network pharmacology and molecular docking. This study provides a research platform with candidate ALF-related targets of PRCC for the development of therapeutics against ALF.

1. Introduction

Acute liver failure (ALF) is a serious decompensation disorder caused by various factors, including hepatic synthesis, detoxification, excretion, and biotransformation [1]. In developed countries, the incidence of ALF is higher than 10 cases per million persons per year [2]. Hepatitis virus infection and acetaminophen are the main causes of ALF in developing [3] and developed countries [4], respectively. Although the worldwide survival rate in ALF has steadily improved from approximately 20% to more than 60% over the past few decades [5], there are still no specific drugs for the treatment of this disorder.

Traditional Chinese medicine (TCM) uses natural sources and thereby provides unique advantages in the treatment of liver injury [6]. Polygoni Cuspidati Rhizoma et Radix (PCRR) is a popular Chinese herb used to treat various liver diseases. PCRR has been reported to have more than 67 bioactive components, including quinones, stilbenes, flavonoids, and lignans

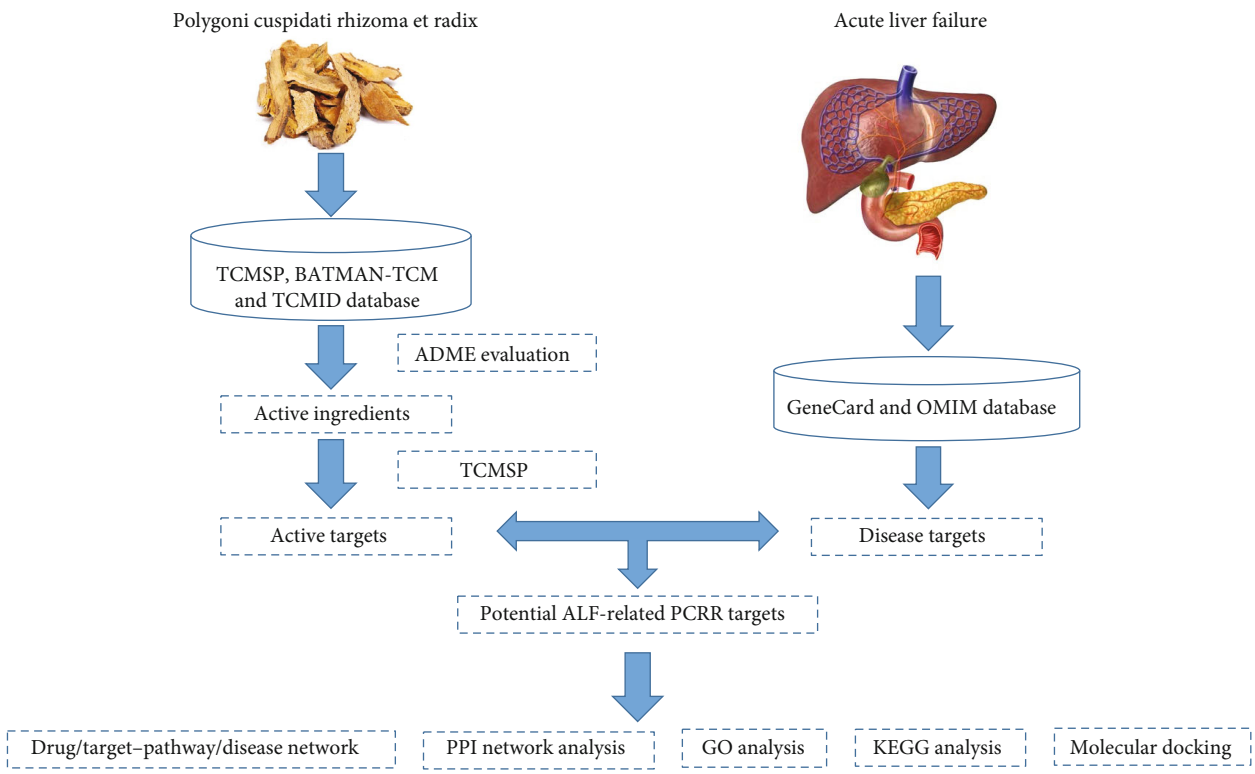

Figure 1: Detailed flowchart of the study design.

Table 1: Active pharmaceutical components of PCRR.

Molecule ID	Molecule name	OB	DL
MOL000006	Luteolin	36.16	0.25
MOL000098	Quercetin	46.43	0.28
MOL000358	β-Sitosterol	36.91	0.75
MOL000492	(+)-Catechin	54.83	0.24
MOL002259	Physcion diglucoside	41.65	0.63
MOL002268	Rhein	47.07	0.28
MOL002280	Torachrysone-8-O-β-D-(6-oxayl)-glucoside	43.02	0.74
MOL013281	6,8-Dihydroxy-7-methoxyxanthone	35.83	0.21
MOL013287	Physovenine	106.10	0.19
MOL013288	Picralinal	58.01	0.75

PCRR: Polygoni Cuspidati Rhizoma et Radix; OB: oral bioavailability; DL: drug-likeness.

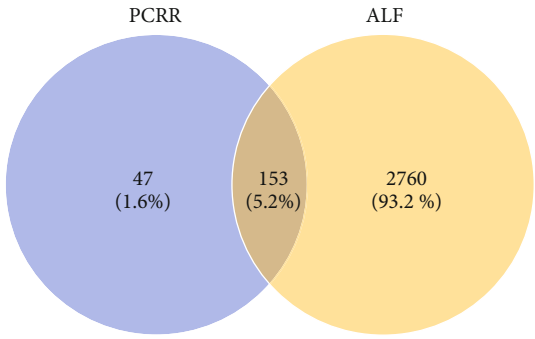

Figure 2: The candidate target genes of Polygoni Cuspidati Rhizoma et Radix (PCRR) and/or in acute liver failure (ALF).

[7]. Acute-on-chronic liver failure refers to acute decompensation in liver injury and has a similar prognosis as ALF [8, 9]. The Guidelines for Clinical Diagnosis and Treatment of Acute-on-chronic Liver Failure in TCM recommends PCRR as one of the main components of the prescription in treating acute-on-chronic liver failure [10]. The results of many clinical observations are in line with this recommendation [11, 12]. A study has confirmed the protective effect of the PCRR against carbon tetrachloride-induced liver injury in mice [13]. However, only a few studies on the therapeutic mechanisms of PCRR in ALF have been reported.

The therapeutics of TCM generally involve multiple components, targets, and pathways, and thus characterization of therapeutic mechanisms is highly challenging in TCM.

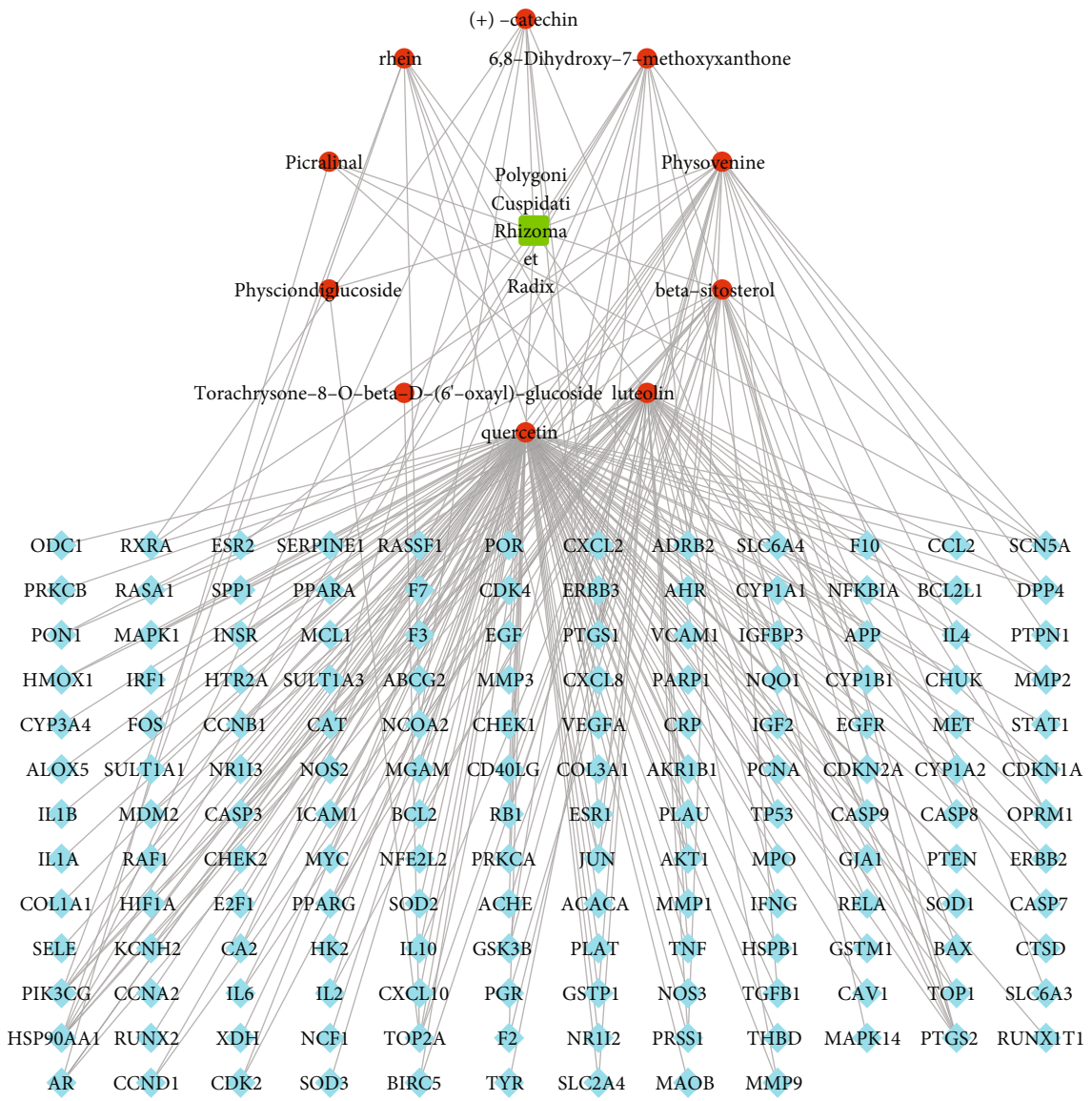

Figure 3: Drug-components–target genes network. The red circle nodes represent the bioactive components of Polygoni Cuspidati Rhizoma et Radix (PCRR), the blue diamond-shaped nodes represent the candidate targets, and the green square represents PCRR.

Network pharmacology is very useful to this end. In this approach, a multilevel network of "disease/phenotype–gene/drug" is constructed to explore the correlation between drugs and diseases from a holistic perspective, whereby drug targets can be identified or new drugs can be developed [14, 15].

This study sought to identify the bioactive compounds of PCRR against ALF and the involving key genes and pathways via network pharmacology and molecular docking methods. The flowchart of this study is shown in Figure 1.

2. Materials and Methods

2.1. Collection of Potential Bioactive Compounds and Related Targets of PCRR. The corresponding compounds and related information were obtained using the Traditional Chinese Medicine Systems Pharmacology (TCMSP, https://tcmspw.com/tcmsp.php) database [16], Bioinformatics Analysis Tool for Molecular mechANism of Traditional Chinese Medicine (BATMAN-TCM, http://bionet.ncpsb.org/batman-tcm/) [17], and Traditional Chinese Medicine Integrated Database (TCMID, http://www.megabionet.org/tcmid/) [18]. TCMSP also provides absorption, distribution, metabolism, and excretion (ADME)-related parameters, such as oral bioavailability (OB) and drug-likeness (DL), of herbal components. OB indicates the relative amount and rate of oral absorption of a drug into the circulation of the body. DL is a concept based on the physicochemical properties and molecular structure of existing drugs. Generally, only compounds with OB ≥30% and DL ≥0.18 are considered potential bioactive compounds [19]. The target information analysis function of the TCMSP platform was used to obtain the gene targets of the anti-ALF bioactive components of PCRR. For the components with no corresponding targets in the TCMSP platform, a similarity ensemble approach (SEA, https://sea.bkslab.org/) was used to

Table 2: Core pharmaceutical components of PCRR.

Molecule ID	Molecule name	OB	DL	2D structure	PubChem CID
MOL000006	Luteolin	36.16	0.245	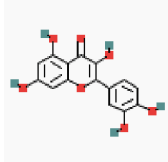	5280445
MOL000098	Quercetin	46.43	0.28	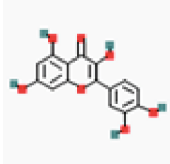	5280343
MOL000358	β-Sitosterol	36.91	0.75	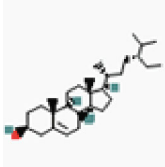	222284
MOL013287	Physovenine	106.21	0.19	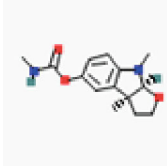	442113

PCRR: Polygoni Cuspidati Rhizoma et Radix; OB: oral bioavailability; DL: drug-likeness.

predict the targets. The target protein species was set as *Homo sapiens*, and the obtained target information was unified using UniProt (https://www.uniprot.org).

2.2. Acquisition of ALF-Related Targets. Keywords such as "acute liver failure", "acute hepatic failure", and "ALF" were used to search ALF-related targets from the GeneCards (https://www.genecards.org) [20] and OMIM (https://omim.org/) [21] databases. PCRR-related targets and ALF-related targets were input into an online Venn tool (https://bioinfogp.cnb.csic.es/tools/venny/) to obtain the intersection genes, which were considered candidate targets of PCRR against ALF

2.3. Analysis of the Drug/Target–Pathway/Disease Network. The relationship between potential bioactive compounds of PRCC and intersection genes was constructed using the Cytoscape software (version 3.8.0) as a drug-components-target-disease network. The average value of the degree value of the network nodes was calculated (average value), and the components with the degree value of the network node ≥ average value were considered as core components.

2.4. Gene Ontology (GO) and Kyoto Encyclopedia of Genes and Genomes (KEGG) Analyses. The candidate targets of PCRR against ALF obtained were used to explore the potential mechanism of PCRR in ALF via GO and KEGG analyses. The GO and KEGG pathway enrichment analyses were performed using the Database for Annotation, Visualization, and Integrated Discovery tool (DAVID, https://david.ncifcrf.gov/home.jsp). The biological processes (BPs), cellular components (CCs), molecular functions (MFs), and key signaling pathways were obtained to explore PCRR-related biological pathways. The functional annotations with P-values < 0.05 were further analyzed.

2.5. Construction of a Protein-Protein Interaction (PPI) Network. Search Tool for the Retrieval of Interacting Genes (STRING, https://string-db.org/) was used to identify possible PPIs by uploading the candidate targets from the Venn diagram. Species was limited to *Homo sapiens* with a confidence score > 0.9. The analysis plugin of Cytoscape 3.8.0 was used to visualize the PPI network, in which the target of the height value plays a pivotal role. The HUBBA plug-in was used to calculate the degree of hub nodes and to select out hub nodes with degree higher than the average degree as the core targets.

2.6. Molecular Docking Simulation. The top 15 target genes were selected. The protein crystal structures corresponding to the core target genes were accessed from the Protein Data Bank (PDB, https://www.rcsb.org) database, and the structures of the bioactive components were downloaded from the TCMSP database. The AutoDock 4.2.6 software was employed to perform molecular docking between receptors and ligands. Eventually, the results were visualized using the PyMOL software.

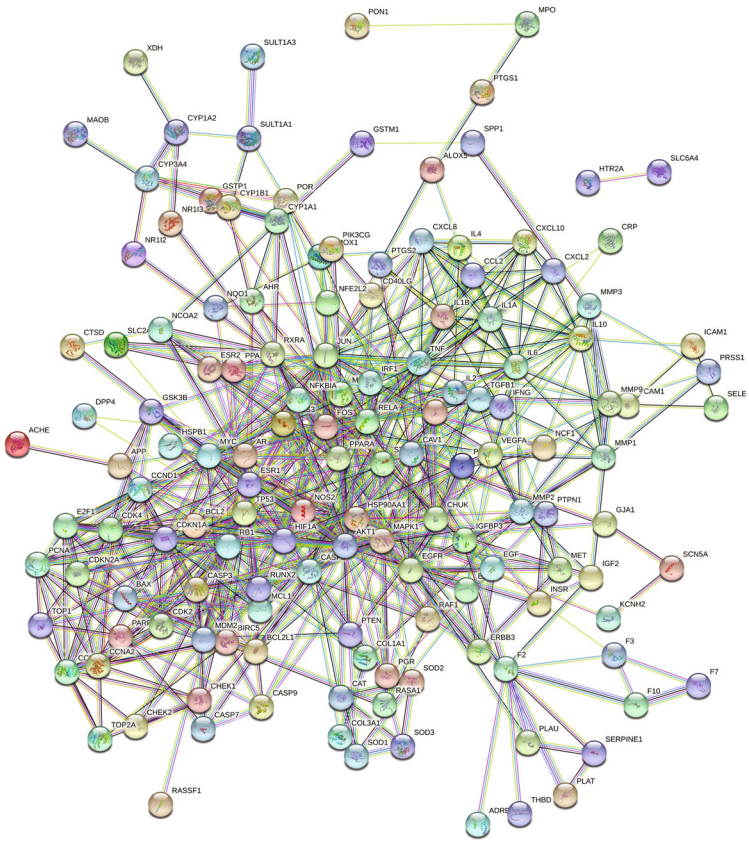

(a)

Figure 4: Continued.

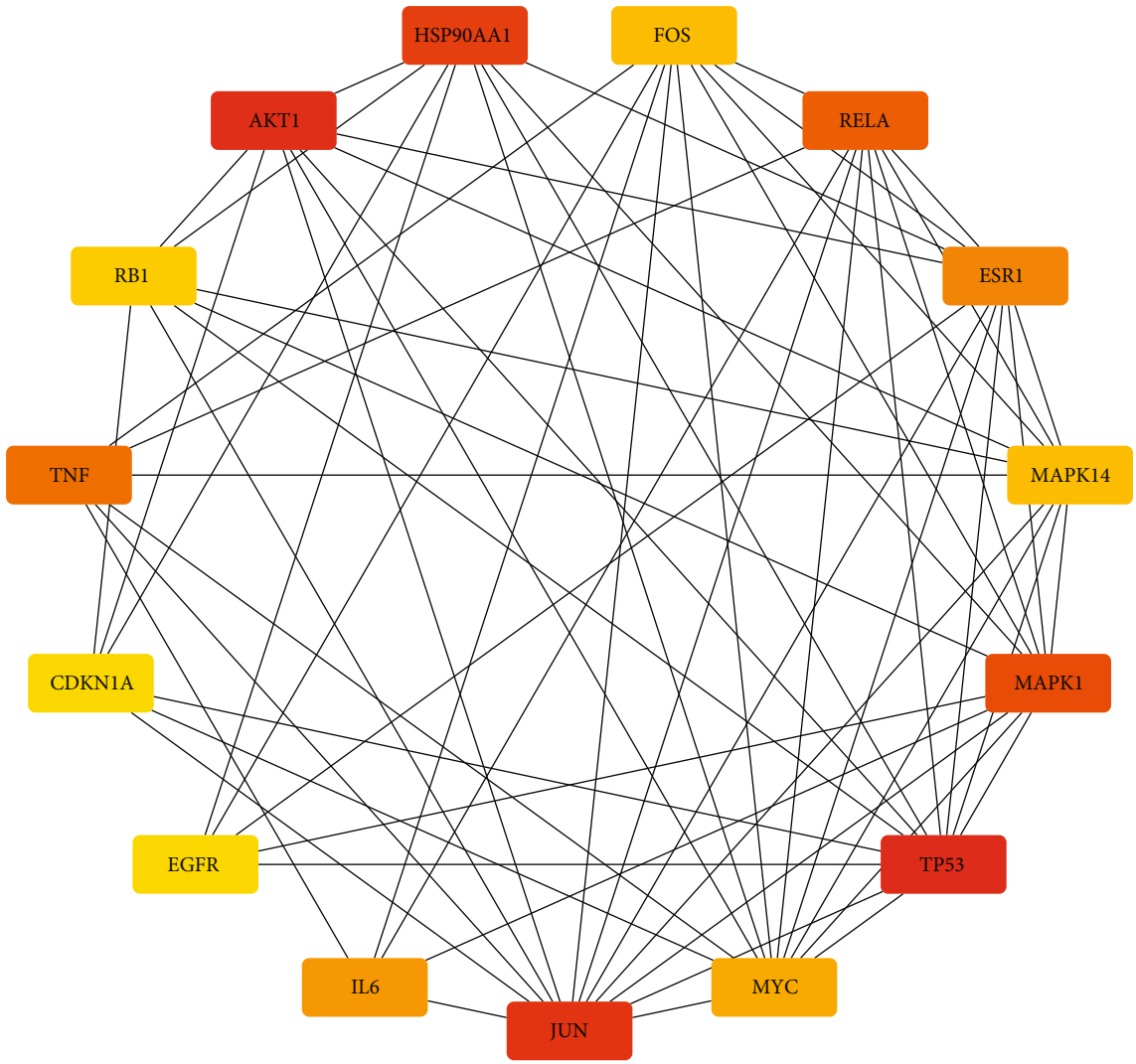

(b)

Figure 4: Protein-protein interaction (PPI) network based on the candidate target genes of Polygoni Cuspidati Rhizoma et Radix against acute liver failure. (a) PPI network of the candidate target genes. Each node represents the protein product of an associated target gene. The degree values of the proteins are represented by the node sizes. Colors indicate the connection sources. (b) The top 15 core target genes were identified based on the degree values. The protein with the darkest color has the highest degree value, indicating that it plays the most significant role in the regulation of the network.

3. Results

3.1. Bioactive Compounds and Potential Targets of PCRR. After searching, filtering, and duplicate removal in the TCMSP, TCMID, and BATMAN-TCM databases, 10 bioactive components of PCRR with OB ≥ 30% and DL ≥ 0.18 were collected, including luteolin, quercetin, β-sitosterol, (+)-catechin, physcion diglucoside, rhein, torachrysone-8-O-β-D-(6′-oxayl)-glucoside, 6,8-dihydroxy-7-methoxyxanthone, physovenine, and picralinal (Table 1). Additionally, 200 target genes interacting with these 10 bioactive components were identified (Supplementary file, Table S1).

3.2. Potential ALF-Related PCRR Targets. In total, 2913 ALF-related target genes were obtained by searching the GeneCards and OMIM databases (Supplementary file, Table S2). The Venn diagram tool was used to identify the genes found among both ALF-related targets and PCRR targets. Consequently, 153 ALF-related PCRR target candidates were identified (Figure 2 and Supplementary file, Table S3).

3.3. Analysis of the Drug/Target–Pathway/Disease Network. The 10 bioactive components of PCRR and 153 candidate targets of PCRR against ALF were imported into the Cytoscape 3.8.0 software to illustrate the interaction between the two groups (Figure 3). We identified the core components among the 153 ALF-related PCRR target candidates by calculating the degree values of the network nodes. In the order from high to low degrees, the core components were quercetin (degree = 131), luteolin (degree = 51), β-sitosterol (degree = 22), and physovenine (degree = 22) (Table 2). According to the network analysis, multiple bioactive

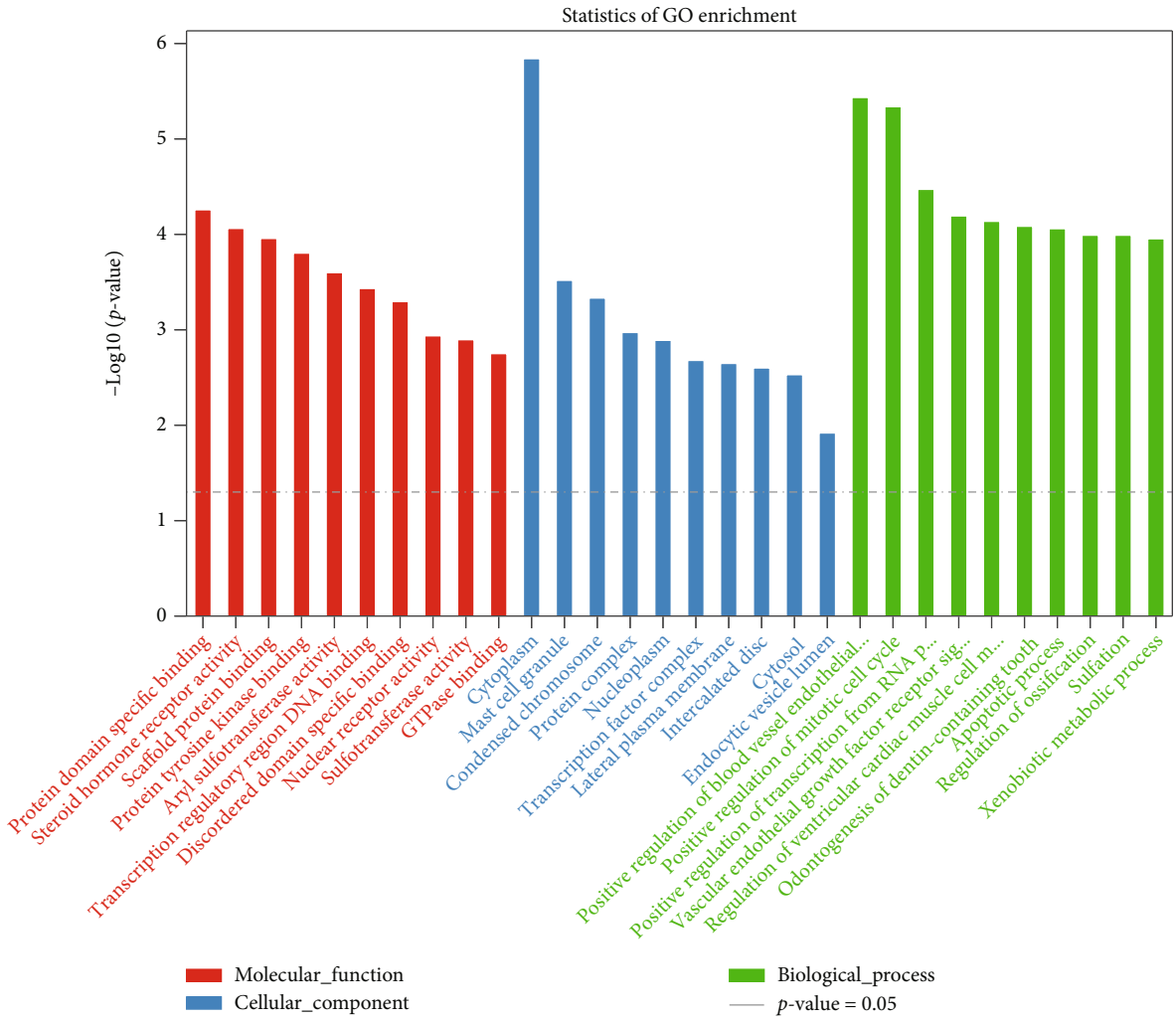

(a)

Figure 5: Continued.

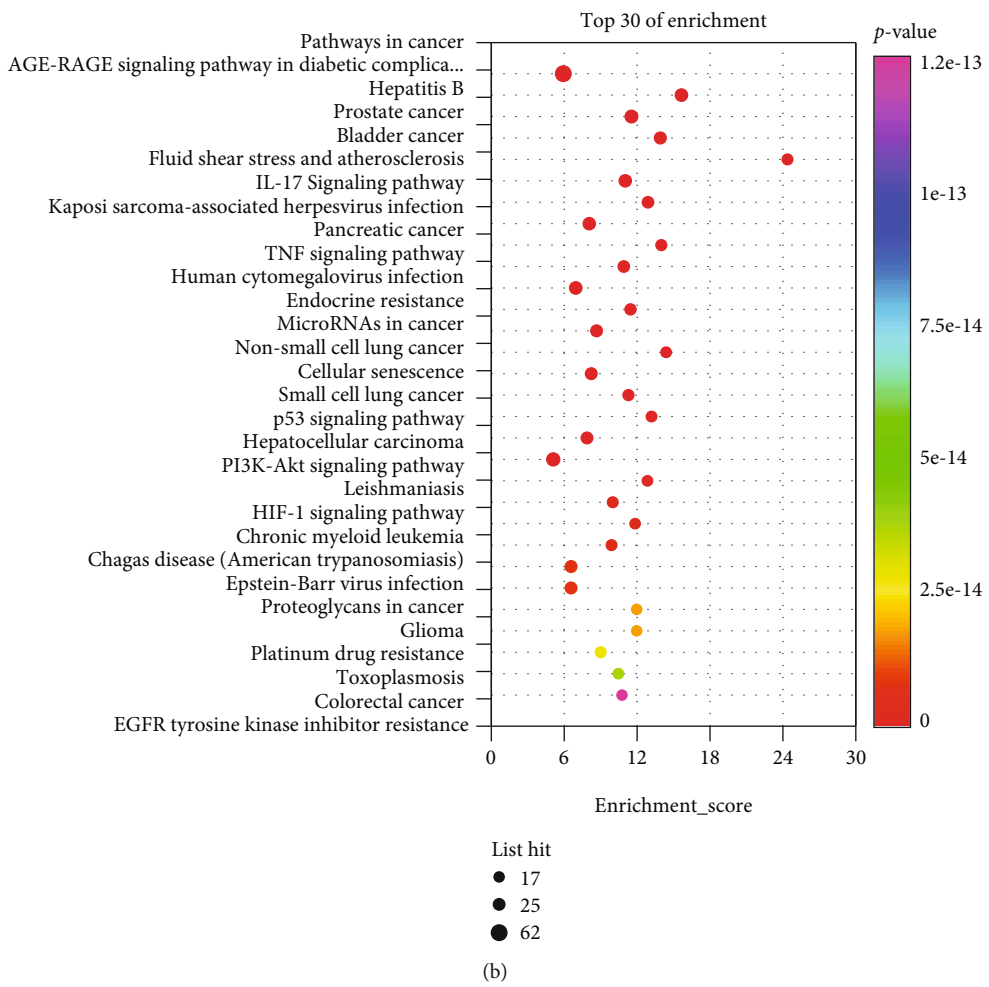

Figure 5: Gene ontology (GO) and Kyoto Encyclopedia of Genes and Genomes (KEGG) analyses. Different colors represent different *P*-values, and circle size represents the counts. (a) The top 10 GO terms. Red, blue, and green bars represent molecular function, cellular component, and biological process, respectively. (b) The top 30 KEGG pathways.

Table 3: Core targets of PCRR in the treatment of ALF and the topological parameters.

Uniport ID	Gene symbol	Degree	Betweenness	Closeness
P04637	TP53	40	0.11	0.49
P31749	AKT1	39	0.11	0.49
P05412	JUN	36	0.09	0.50
P07900	HSP90AA1	35	0.08	0.48
P28482	MAPK1	34	0.12	0.50
Q04206	RELA	33	0.06	0.49
P01375	TNF	28	0.06	0.46
P03372	ESR1	26	0.04	0.46
P05231	IL6	25	0.04	0.44
P01106	MYC	24	0.03	0.46
Q16539	MAPK14	23	0.02	0.46
P01100	FOS	23	0.04	0.46
P06400	RB1	22	0.02	0.45
P38936	CDKN1A	21	0.01	0.43
P00533	EGFR	21	0.03	0.44

PCRR: Polygoni Cuspidati Rhizoma et Radix; ALF: acute liver failure.

components of PCRR act on at least one core target gene. The results showed that the therapeutic effect of PCRR in ALF has multicomponent and multitarget characteristics.

3.4. GO Functional and KEGG Pathway Enrichment Analysis. To elucidate the biological processes involved in the ALF-related PCRR candidates targets, GO enrichment analysis was performed. A total of 320 significantly enriched GO terms were identified (*P*-value <0.05, Supplementary file, Table S4). The top 10 significantly enriched terms, including BPs, MFs, and CCs are presented in Figure 4(a). In the order from low to high adjusted *P*-values, the top three GO-MC terms were mainly enriched in protein domain-specific binding (GO:0019904), steroid hormone receptor activity (GO:0003707), and scaffold protein binding (GO:0097110); the top three GO-CC terms were mainly enriched in cytoplasm (GO:0005737), mast cell granule (GO:0042629), and condensed chromosome (GO:0000793); and the top three GO-BP terms were mainly enriched in positive regulation of blood vessel endothelial cell migration (GO:0043536), positive regulation of mitotic cell cycle (GO:0045931), and positive

Table 4: Results of 15 core target genes and related bioactive compounds of molecular docking.

No.	Targets	PDB ID	Compound	Binding affinity(kcal/Mol)
1	AKT1	3O96	Luteolin	-9.8
			Physovenine	-8.6
			Quercetin	-9.7
			β-Sitosterol	-10.9
2	CDKN1A	6P8H	Luteolin	-6.4
			Physovenine	-5.9
			Quercetin	-6.0
			β-Sitosterol	-6.9
3	EGFR	1 M17	Luteolin	-8.4
			Physovenine	-7.2
			Quercetin	-8.5
			β-Sitosterol	-8.5
4	ESR1	1A52	Luteolin	-8.7
			Physovenine	-7.6
			Quercetin	-8.4
			β-Sitosterol	-4.2
5	FOS	1A02	Luteolin	-5.6
			Physovenine	-4.9
			Quercetin	-5.0
			β-Sitosterol	-5.5
6	HSP90AA1	7L7I	Luteolin	-9.8
			Physovenine	-8.0
			Quercetin	-10.2
			β-Sitosterol	-7.2
7	IL-6	1ALU	Luteolin	-8.0
			Physovenine	-6.4
			Quercetin	-7.9
			β-Sitosterol	-6.6
8	JUN	1JNM	Luteolin	-5.4
			Physovenine	-4.8
			Quercetin	-5.4
			β-Sitosterol	-5.4
9	MAPK1	1PME	Luteolin	-9.2
			Physovenine	-7.5
			Quercetin	-8.5
			β-Sitosterol	-8.8
10	MAPK14	1A9U	Luteolin	-7.5
			Physovenine	-6.9
			Quercetin	-7.2
			β-Sitosterol	-8.2
11	MYC	5I4Z	Luteolin	-6.5
			Physovenine	-5.6
			Quercetin	-6.1
			β-Sitosterol	-6.9
12	RB1	4EIJ	Luteolin	-8.5
			Physovenine	-7.0
			Quercetin	-8.4
			β-Sitosterol	-6.9
13	RELA	1NFI	Luteolin	-7.4
			Physovenine	-6.4
			Quercetin	-7.0
			β-Sitosterol	-7.0
14	TNF	1TNF	Luteolin	-7.0
			Physovenine	-5.7
			Quercetin	-6.9
			β-Sitosterol	-6.6
15	TP53	TP53	Luteolin	-7.1
			Physovenine	-6.0
			Quercetin	-7.3
			β-Sitosterol	-6.0

regulation of transcription from RNA polymerase II promoter (GO:0045944).

KEGG enrichment analysis was performed to elucidate the pathways involved in the therapeutic effect of PCRR in the treatment of ALF. Consequently, 160 enriched KEGG pathways were identified (P-value <0.05, Supplementary file, Table S5). The top 30 significant signaling pathways are shown in Figure 4(b). The top 10 ALF-related signaling pathways were identified as pathway in cancer (path:hsa05200), AGE-RAGE signaling pathway in diabetic complications (path:hsa04933), hepatitis B (path:hsa05161), prostate cancer (path:hsa05215), bladder cancer (path:hsa05219), fluid shear stress and atherosclerosis (path: hsa05418), interlukin (IL)-17 signaling pathway (path:hsa04657), Kaposi sarcoma-associated herpesvirus infection (path:hsa05167), pancreatic cancer (path:hsa05212), and tumor necrosis factor (TNF) signaling pathway (path:hsa04668). These pathways suggest that the therapeutic effect of PCRR in ALF is related to cell metabolism, oxidative stress, inflammation, and hepatocyte apoptosis.

3.5. PPI Network Analysis. To assess the synergism between the bioactive components of PCRR, the 153 candidate target genes were imported into the STRING database to construct an initial PPI network with the minimum required interaction score > 0.9 (Figure 5(a)). The Cytoscape 3.8.0 software was used to reconstruct the STRING graph, and the HUBBA plug-in was used to select the top 15 targets for plotting (Figure 5(b)). The core targets, which may play important anti-ALF roles, were TP53, AKT1, JUN, HSP90AA1, MAPK1, RELA, TNF, ESR1, IL6, MYC, MAPK14, FOS, RB1, CDKN1A, and EGFR (Table 3).

3.6. Validation through Molecular Docking. Molecular docking is used to verify the interaction between ligands and their receptors. Here, we applied this strategy for the 4 bioactive compounds of PCRR and the 15 core target genes by using AutoDock Vina (Table 4). A minimum binding potential energy of < 0 between a molecule and its target indicates that

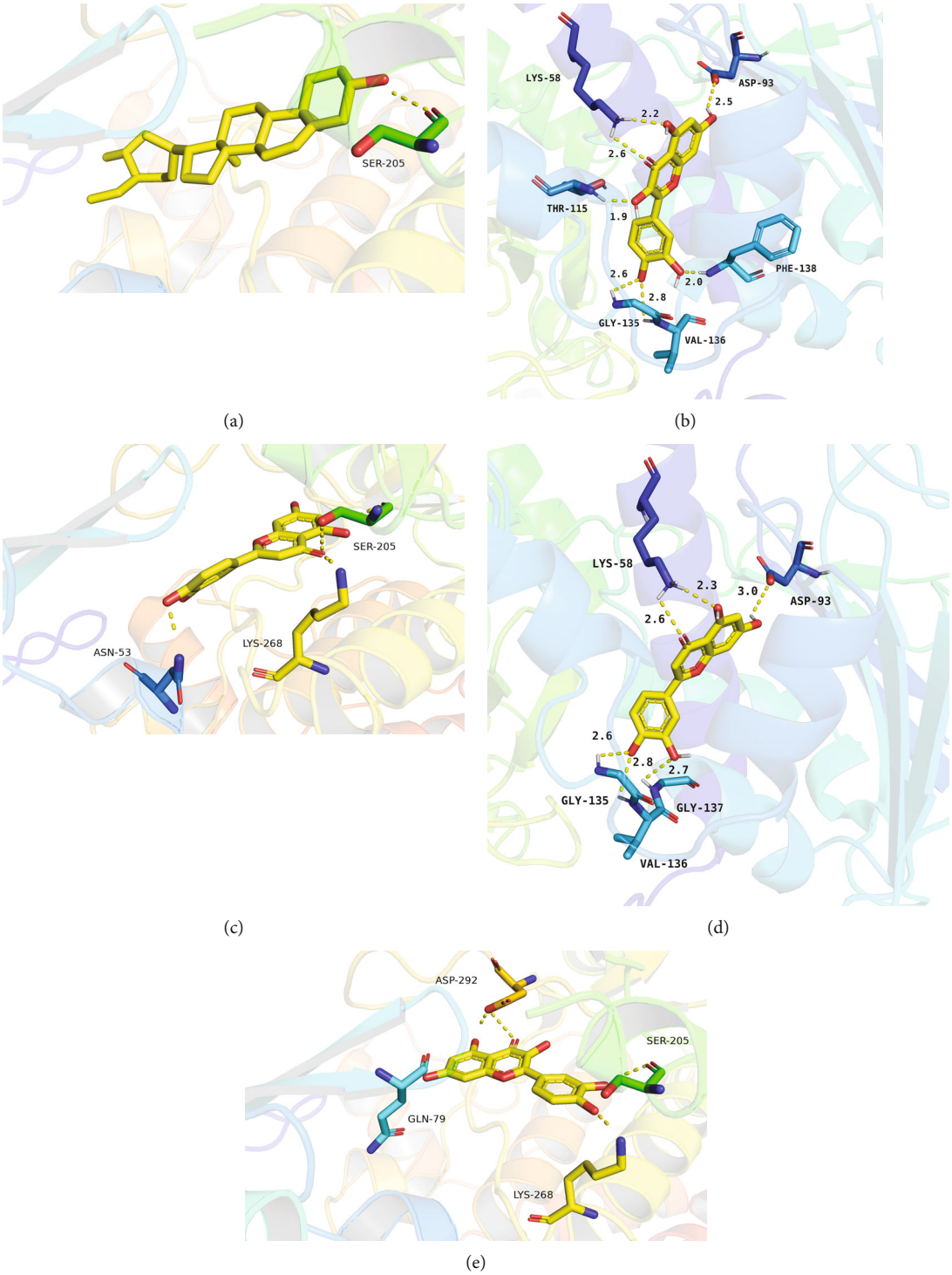

Figure 6: Molecular docking of the receptors and their ligands: (a) β-sitosterol to AKT1; (b) quercetin to HSP90AA1; (c) luteolin to AKT1; (d) luteolin to HSP90AA1; (e) quercetin to AKT1.

the two molecules can spontaneously bind to each other [22]. The lowest binding-free energies of β-sitosterol to AKT1, quercetin to HSP90AA1, luteolin to AKT1, luteolin to HSP90AA1, and quercetin to AKT1 were estimated at −10.9, −10.2, −9.8, −9.8, and −9.7 kcal/mol, respectively (See Figure 6).

4. Discussion

ALF is a rare but serious clinical syndrome involving hepatocyte damage and progresses rapidly, with a possibility of causing multiple organ dysfunction [23]. For patients with

ALF, there is no specific treatment. With the advent of liver transplantation, the survival rate of ALF has greatly improved [24]. However, the lack of donors and high treatment costs limited the application of this approach. PCRR is a classical TCM therapeutic with a highlighted effect in the prevention and treatment of various liver diseases. TCM comprises multicomponent and multitarget therapeutics, which are difficult to mechanistically characterize. Network pharmacology is a simple and feasible method that solves this difficulty. In this study, the bioactive components and potential targets of PCRR in the treatment of ALF were predicted via network pharmacology and molecular docking.

According to ADME protocols (OB $\geq 30\%$, DL ≥ 0.18) and the principle of target correspondence, four bioactive components were screened out. Of them, the flavonoid luteolin is found in various types of plants, including fruits, vegetables, and herbs, worldwide [25]. Previous studies have suggested that the protective effect of luteolin on acetaminophen-induced liver failure in mice may be related to the inhibition of lipid peroxidation, oxidative stress, and estrogen-receptor stress [26, 27]. Quercetin is a bioactive flavonoid in the class of polyphenols [28], which can prevent and treat liver injury by preventing oxidative stress, inhibiting the release of inflammatory factors, and promoting the synthesis of antioxidant enzymes [29, 30].

Based on the PPI network analysis, we predicted that the ALF-related genes most commonly targeted by the PCRR bioactive compounds are TP53, AKT1, JUN, HSP90AA1, MAPK1, RELA, TNF, ESR1, IL6, MYC, MAPK14, FOS, RB1, CDKN1A, and EGFR. The tumor suppressor gene TP53 encodes P53 [31, 32], whose transient activation helps prevent progression of acetaminophen-induced liver injury, and continued activation of P53 may affect regeneration and recovery of the liver [33, 34]. AKT1 has been reported to regulate fibrogenesis and proliferation in hepatocytes and hepatic stellate cells [35, 36]. Additionally, previous studies have shown that HSP90 can promote proinflammatory cytokines and its inhibition can attenuate alcohol-induced liver injury [37, 38]. MAPK1 (extracellular signal-regulated kinase 2, ERK2) is involved in the regulation of cellular physiology and pathology [39]. Altering the ERK signaling pathway through ERK2 deficiency can reduce liver fibrosis and inflammation [40]. ESR1-mediated signaling inhibits liver regeneration after chemical-induced liver injury by suppressing the Wnt signaling pathway, resulting in lower cyclin D1 activation [41]. During the development of acute liver failure, TNF-mediated over-immune cascade response may contribute to massive hepatocyte apoptosis and impaired hepatocyte proliferation [42, 43].

To explore the therapeutic mechanism of PCRR in ALF, GO and KEGG pathway enrichment analyses were performed. According to the adjusted P-values, the top three GO-MC terms were mainly enriched in protein domain-specific binding, steroid hormone receptor activity, and scaffold protein binding; the top three GO-CC terms were mainly enriched in cytoplasm, mast cell granule, and condensed chromosome; and the top three GO-BP terms were mainly enriched in positive regulation of blood vessel endothelial cell migration, positive regulation of mitotic cell cycle, and positive regulation of transcription from RNA polymerase II promoter. The 10 crucial pathways that may be regulated by PCRR in the treatment of ALF by the KEGG pathway enrichment analysis included pathway in cancer, AGE-RAGE pathway in diabetic complications, hepatitis B, prostate cancer, bladder cancer, fluid shear stress and atherosclerosis, IL-17 pathway, Kaposi sarcoma-associated herpesvirus infection, pancreatic cancer, and TNF. The pathway enrichment results suggested that the anti-ALF therapeutic effect of PCRR mainly results from the regulation of immune and inflammatory responses and cell metabolism. Cancer mechanisms are known to be relevant with ALF since neoplastic infiltration is one of the courses of ALF progression [44–46]. Chronic hepatitis B virus infection is one of the important causes of acute liver failure in developing countries, including China [47]. AGE-RAGE interaction contributes to fat accumulation in the liver, increases oxidative stress and chronic inflammation, and may be involved in liver injury [48–50]. IL-17 plays an important role in the pathogenesis of immune-mediated liver injury; IL-17 is significantly upregulated in the liver and serum of BALB/cJ mice infected with mouse hepatitis virus strain 3 [51]. The PI3K-Akt signaling affects cell migration, mobilization, differentiation, and apoptosis [52, 53] and has also been found to affect early liver regeneration and improve survival in a mouse model of acetaminophen-induced acute liver injury [52, 54]. Excessive reactive oxygen species (ROS) can directly lead to oxidative stress, which plays an important role in liver damage [55]. Activation of the PI3K/Akt signaling can alleviate liver injury by reducing ROS levels, inhibiting apoptosis, and accelerating hyoxia-inducible factor-1α [56].

5. Conclusion

This is the first study that has predicted the therapeutic mechanisms of PCRR in ALF by using network pharmacology and molecular docking. The results suggest that the therapeutic effect of PCRR in ALF involves multiple components, targets, and pathways. Luteolin, quercetin, β-sitosterol, and physovenine are likely the major bioactive compounds of PCRR against ALF. Accordingly, this study provides a research platform with candidate ALF-related targets of PRCC for the development of therapeutics against ALF. However, it has several limitations as well. First, the potential bioactive components are screened primarily by databases using ADME protocols [58], and some components may be overlooked. Second, the study lacks experimental verification, which should be addressed in biologically relevant platforms in the future.

Abbreviations

ALF: Acute liver failure
PCRR: Polygoni Cuspidati Rhizoma et Radix
TCM: Traditional Chinese medicine
TCMSP: Traditional Chinese medicine systems pharmacology
OB: Oral bioavailability
DL: Drug-likeness
PPI: Protein-protein interaction

GO: Gene ontology
KEGG: Kyoto Encyclopedia of Genes and Genomes.

Data Availability

All data obtained or analyzed during this work are included within the article.

Conflicts of Interest

The authors have no conflict of interests related to this study.

Authors' Contributions

Jing Hong, Jie Ding, and Han-han Hong contributed equally to this work.

Acknowledgments

This research was funded by the Major Clinical Research Project on Traditional Chinese Medicine of Shanghai Municipal Health and Family Planning Commission (No. ZY[2018-2020]-CCX-4003) and "234 Discipline Climbing Plan" of Changhai Hospital, Naval Medical University (No.2019YXK029).

Supplementary Materials

The 200 target genes interacting with the 10 bioactive components of PCRR, and the 2913 ALF-related target genes are provided in supplementary Tables S1 and S2, respectively. The 153 ALF-related PCRR target candidates are provided in supplementary Table S3. The results of the GO and KEGG pathway enrichment analyses are provided in supplementary Tables S4 and S5, respectively. *(Supplementary Materials)*

References

[1] Y. Wang, Q. Chen, C. Shi, F. Jiao, and Z. Gong, "Mechanism of glycyrrhizin on ferroptosis during acute liver failure by inhibiting oxidative stress," *Molecular Medicine Reports*, vol. 20, no. 5, pp. 4081–4090, 2019.

[2] M. R. Kappus, "Acute hepatic failure and nutrition," *Nutrition in Clinical Practice*, vol. 35, no. 1, pp. 30–35, 2020.

[3] S. Vento and F. Cainelli, "Acute liver failure," *Lancet*, vol. 395, no. 10240, p. 1833, 2020.

[4] P. Zhao, C. Wang, W. Liu et al., "Causes and outcomes of acute liver failure in China," *PLoS One*, vol. 8, no. 11, article e80991, 2013.

[5] M. A. Arshad, N. Murphy, and M. N. Bangash, "Acute liver failure," *Clinical Medicine (London, England)*, vol. 20, no. 5, pp. 505–508, 2020.

[6] A. Wang, L. Lin, and Y. Wang, "Traditional Chinese herbal medicine Penthorum chinense Pursh: a phytochemical and pharmacological review," *The American Journal of Chinese Medicine*, vol. 43, no. 4, pp. 601–620, 2015.

[7] W. Peng, R. Qin, X. Li, and H. Zhou, "Botany, phytochemistry, pharmacology, and potential application of Polygonum cuspidatum Sieb.et Zucc.: a review," *Journal of Ethnopharmacology*, vol. 148, no. 3, pp. 729–745, 2013.

[8] J. S. Bajaj, R. Moreau, P. S. Kamath et al., "Acute-on-chronic liver failure: getting ready for prime time?," *Hepatology*, vol. 68, no. 4, pp. 1621–1632, 2018.

[9] R. Hernaez, E. Solà, R. Moreau, and P. Ginès, "Acute-on-chronic liver failure: an update," *Gut*, vol. 66, no. 3, pp. 541–553, 2017.

[10] China Association of Chinese Medicine, "Guidelines for clinical diagnosis and treatment of acute-on-chronic liver failure in traditional Chinese medicine," *Lin Chuang Gan Dan Bing Za Zhi*, vol. 35, no. 3, pp. 494–503, 2019.

[11] X. Y. Hu, Y. Zhang, G. Chen, S. Zhong, and X. J. Fan, "A prospective cohort study on the influence of high doses of herbs for clearing heat and resolving stasis on survival rates in patients with hepatitis B related acute–on-chronic liver failure," *Journal of Chinese Integrative Medicine*, vol. 10, no. 2, pp. 176–185, 2012.

[12] Z. Q. Dang, G. H. Yang, Y. J. Ma et al., "Synergistic effect of multi-ways Chinese medication on routine therapy for hepatitis B virus related acute-on-chronic liver failure," *Zhong Yi Za Zhi*, vol. 53, no. 24, pp. 2109–2111, 2012.

[13] H. Zhang, C. H. Yu, Y. P. Jiang et al., "Protective effects of polydatin from Polygonum cuspidatum against carbon tetrachloride-induced liver injury in mice," *PLoS One*, vol. 7, no. 9, article e46574, 2012.

[14] S. Li and B. Zhang, "Traditional Chinese medicine network pharmacology: theory, methodology and application," *Chinese Journal of Natural Medicines*, vol. 11, no. 2, pp. 110–120, 2013.

[15] A. L. Hopkins, "Network pharmacology: the next paradigm in drug discovery," *Nature Chemical Biology*, vol. 4, no. 11, pp. 682–690, 2008.

[16] J. Ru, P. Li, J. Wang et al., "TCMSP: a database of systems pharmacology for drug discovery from herbal medicines," *Journal of Cheminformatics*, vol. 6, no. 1, 2014.

[17] Z. Liu, F. Guo, Y. Wang et al., "BATMAN-TCM: a Bioinformatics Analysis Tool for Molecular mechANism of Traditional Chinese Medicine," *Scientific Reports*, vol. 6, no. 1, 2016.

[18] L. Huang, D. Xie, Y. Yu et al., "TCMID 2.0: a comprehensive resource for TCM," *Nucleic Acids Research*, vol. 46, no. D1, pp. D1117–D1120, 2018.

[19] S. J. Huang, F. Mu, F. Li et al., "Systematic elucidation of the potential mechanism of Erzhi pill against drug-induced liver injury via network pharmacology approach," *Evidence-based Complementary and Alternative Medicine*, vol. 2020, Article ID 6219432, 2020.

[20] G. Stelzer, I. Dalah, T. I. Stein et al., "In-silico human genomics with GeneCards," *Human Genomics*, vol. 5, no. 6, pp. 709–717, 2011.

[21] J. S. Amberger, C. A. Bocchini, F. Schiettecatte, A. F. Scott, and A. Hamosh, "OMIM.org: Online Mendelian Inheritance in Man (OMIM®), an online catalog of human genes and genetic disorders," *Nucleic Acids Research*, vol. 43, no. Database issue, 2015.

[22] M. Wei, H. Li, Q. Li et al., "Based on network pharmacology to explore the molecular targets and mechanisms of Gegen Qinlian decoction for the treatment of ulcerative colitis," *BioMed Research International*, vol. 2020, 2020.

[23] S. Krawitz, V. Lingiah, and N. T. Pyrsopoulos, "Acute liver failure: mechanisms of disease and multisystemic involvement," *Clinics in Liver Disease*, vol. 22, no. 2, pp. 243–256, 2018.

[24] R. Olivo, J. V. Guarrera, and N. T. Pyrsopoulos, "Liver transplantation for acute liver failure," *Clinics in Liver Disease*, vol. 22, no. 2, pp. 409–417, 2018.

[25] M. Imran, A. Rauf, T. Abu-Izneid et al., "Luteolin, a flavonoid, as an anticancer agent: a review," *Biomedicine & Pharmacotherapy*, vol. 112, article 108612, 2019.

[26] M. Tai, J. Zhang, S. Song et al., "Protective effects of luteolin against acetaminophen-induced acute liver failure in mouse," *International Immunopharmacology*, vol. 27, no. 1, pp. 164–170, 2015.

[27] Y. He, Z. Xia, D. Yu et al., "Hepatoprotective effects and structure-activity relationship of five flavonoids against lipopolysaccharide/d-galactosamine induced acute liver failure in mice," *International Immunopharmacology*, vol. 68, pp. 171–178, 2019.

[28] S. Liu, L. Tian, G. Chai, B. Wen, and B. Wang, "Targeting heme oxygenase-1 by quercetin ameliorates alcohol-induced acute liver injury via inhibiting NLRP3 inflammasome activation," *Food & Function*, vol. 9, no. 8, pp. 4184–4193, 2018.

[29] F. Q. Zhao, G. F. Wang, D. Xu, H. Y. Zhang, Y. L. Cui, and Q. S. Wang, "Glycyrrhizin mediated liver-targeted alginate nanogels delivers quercetin to relieve acute liver failure," *International Journal of Biological Macromolecules*, vol. 168, pp. 93–104, 2021.

[30] J. Fang and W. Liang, "ASCs -derived exosomes loaded with vitamin A and quercetin inhibit rapid senescence-like response after acute liver injury," *Biochemical and Biophysical Research Communications*, vol. 572, pp. 125–130, 2021.

[31] W. Hu, S. Chen, R. F. Thorne, and M. Wu, "TP53, TP53 target genes (DRAM, TIGAR), and autophagy," *Advances in Experimental Medicine and Biology*, vol. 1206, pp. 127–149, 2019.

[32] P. Monti, P. Menichini, A. Speciale et al., "Heterogeneity of TP53 mutations and P53 protein residual function in cancer: does it matter?," *Frontiers in Oncology*, vol. 10, article 593383, 2020.

[33] P. Borude, B. Bhushan, S. Gunewardena, J. Akakpo, H. Jaeschke, and U. Apte, "Pleiotropic role of p53 in injury and liver regeneration after acetaminophen overdose," *The American Journal of Pathology*, vol. 188, no. 6, pp. 1406–1418, 2018.

[34] D. Chen, H. M. Ni, L. Wang et al., "p53 up-regulated modulator of apoptosis induction mediates acetaminophen- induced necrosis and liver injury in mice," *Hepatology*, vol. 69, no. 5, pp. 2164–2179, 2019.

[35] D. Wang, Y. Ma, Z. Li et al., "The role of AKT1 and autophagy in the protective effect of hydrogen sulphide against hepatic ischemia/reperfusion injury in mice," *Autophagy*, vol. 8, no. 6, pp. 954–962, 2012.

[36] K. Reyes-Gordillo, R. Shah, J. Arellanes-Robledo, Y. Cheng, J. Ibrahim, and P. L. Tuma, "Akt1 and Akt2 isoforms play distinct roles in regulating the development of inflammation and fibrosis associated with alcoholic liver disease," *Cell*, vol. 8, no. 11, p. 1337, 2019.

[37] A. Choudhury, D. Bullock, A. Lim et al., "Inhibition of HSP90 and activation of HSF1 diminish macrophage NLRP3 inflammasome activity in alcohol-associated liver injury," *Alcoholism, Clinical and Experimental Research*, vol. 44, no. 6, pp. 1300–1311, 2020.

[38] A. Ambade, D. Catalano, A. Lim, A. Kopoyan, S. A. Shaffer, and P. Mandrekar, "Inhibition of heat shock protein 90 alleviates steatosis and macrophage activation in murine alcoholic liver injury," *Journal of Hepatology*, vol. 61, no. 4, pp. 903–911, 2014.

[39] D. Sun, L. Chen, H. Lv, Y. Gao, X. Liu, and X. Zhang, "Circ_0058124 upregulates MAPK1 expression to promote proliferation, metastasis and metabolic abilities in thyroid cancer through sponging miR-940," *Oncotargets and Therapy*, vol. - Volume 13, pp. 1569–1581, 2020.

[40] K. S. Jeng, S. J. Lu, C. H. Wang, and C. F. Chang, "Liver fibrosis and inflammation under the control of ERK2," *International Journal of Molecular Sciences*, vol. 21, no. 11, 2020.

[41] S. R. McGreal, K. Rumi, M. J. Soares, B. L. Woolbright, H. Jaeschke, and U. Apte, "Disruption of estrogen receptor alpha in rats results in faster initiation of compensatory regeneration despite higher liver injury after carbon tetrachloride treatment," *International Journal of Toxicology*, vol. 36, no. 3, pp. 199–206, 2017.

[42] Y. Xu, H. Wang, S. Bao et al., "Amelioration of liver injury by continuously targeted intervention against TNFRp55 in rats with acute-on-chronic liver failure," *PLoS One*, vol. 8, no. 7, article e68757, 2013.

[43] S. A. E. Bashandy, S. A. El Awdan, S. M. Mohamed, and E. A. A. Omara, "Allium porrum and Bauhinia variegata mitigate acute liver failure and nephrotoxicity induced by thioacetamide in male rats," *Indian Journal of Clinical Biochemistry*, vol. 35, no. 2, pp. 147–157, 2020.

[44] C. Yin, K. J. Evason, K. Asahina, and D. Y. Stainier, "Hepatic stellate cells in liver development, regeneration, and cancer," *The Journal of Clinical Investigation*, vol. 123, no. 5, pp. 1902–1910, 2013.

[45] E. Mogrovejo, P. Manickam, M. Amin, and M. S. Cappell, "Characterization of the syndrome of acute liver failure caused by metastases from breast carcinoma," *Digestive Diseases and Sciences*, vol. 59, no. 4, pp. 724–736, 2014.

[46] W. Bernal and J. Wendon, "Acute liver failure," *The New England Journal of Medicine*, vol. 369, no. 26, pp. 2525–2534, 2013.

[47] H. Lin, Q. Zhang, X. Li, Y. Wu, Y. Liu, and Y. Hu, "Identification of key candidate genes and pathways in hepatitis B virus-associated acute liver failure by bioinformatical analysis," *Medicine (Baltimore)*, vol. 97, no. 5, article e9687, 2018.

[48] K. A. Moy, L. Jiao, N. D. Freedman et al., "Soluble receptor for advanced glycation end products and risk of liver cancer," *Hepatology*, vol. 57, no. 6, pp. 2338–2345, 2013.

[49] K. Asadipooya, K. B. Lankarani, R. Raj, and M. Kalantarhormozi, "RAGE is a potential cause of onset and progression of nonalcoholic fatty liver disease," *International Journal of Endocrinology*, vol. 2019, Article ID 2151302, 2019.

[50] N. M. E. Abo El-Nasr, D. O. Saleh, S. S. Mahmoud et al., "Olmesartan attenuates type 2 diabetes-associated liver injury: cross-talk of AGE/RAGE/JNK, STAT3/SCOS3 and RAS signaling pathways," *European Journal of Pharmacology*, vol. 874, article 173010, 2020.

[51] L. Zhu, T. Chen, Y. Lu, D. Wu, X. Luo, and Q. Ning, "Contribution of IL-17 to mouse hepatitis virus strain 3-induced acute liver failure," *Journal of Huazhong University of Science and Technology. Medical Sciences*, vol. 32, no. 4, pp. 552–556, 2012.

[52] M. Martini, M. C. De Santis, L. Braccini, F. Gulluni, and E. Hirsch, "PI3K/AKT signaling pathway and cancer: an updated review," *Annals of Medicine*, vol. 46, no. 6, pp. 372–383, 2014.

[53] Y. Xie, X. Shi, K. Sheng et al., "PI3K/Akt signaling transduction pathway, erythropoiesis and glycolysis in hypoxia

(review)," *Molecular Medicine Reports*, vol. 19, no. 2, pp. 783–791, 2019.

[54] H. Y. Wu, X. C. Zhang, B. B. Jia et al., "Exosomes derived from human umbilical cord mesenchymal stem cells alleviate acetaminophen-induced acute liver failure through activating ERK and IGF-1R/PI3K/AKT signaling pathway," *Journal of Pharmacological Sciences*, vol. 147, no. 1, pp. 143–155, 2021.

[55] H. Cichoż-Lach and A. Michalak, "Oxidative stress as a crucial factor in liver diseases," *World Journal of Gastroenterology*, vol. 20, no. 25, pp. 8082–8091, 2014.

[56] L. Tang, F. Wang, L. Xiao et al., "Yi-Qi-Jian-Pi formula modulates the PI3K/AKT signaling pathway to attenuate acute-on-chronic liver failure by suppressing hypoxic injury and apoptosis _in vivo_ and _in vitro_," *Journal of Ethnopharmacology*, vol. 280, article 114411, 2021.

Hindawi
Gastroenterology Research and Practice
Volume 2022, Article ID 4745042, 17 pages
https://doi.org/10.1155/2022/4745042

Research Article

Explore the Mechanism of Astragalus mongholicus Bunge against Nonalcoholic Fatty Liver Disease Based on Network Pharmacology and Experimental Verification

Lili Fu,[1,2,3] **Zhongming Wu**,[2] **Yanjun Chu**,[1,2,3] **Wenbin Chen**,[4] **Ling Gao**,[2,3,4,5,6] **Shumin Mu**,[7] **and Jiajun Zhao**[1,2,3,5,6]

[1]*Shandong University of Traditional Chinese Medicine, Jinan, Shandong 250355, China*
[2]*Department of Endocrinology, Shandong Provincial Hospital Affiliated to Shandong First Medical University, Jinan, Shandong 250021, China*
[3]*Shandong Key Laboratory of Endocrinology and Lipid Metabolism, Jinan, Shandong 250021, China*
[4]*Scientific Center, Shandong Provincial Hospital Affiliated to Shandong First Medical University, Jinan, Shandong 250021, China*
[5]*Shandong Clinical Research Center of Diabetes and Metabolic Diseases, Jinan, Shandong 250021, China*
[6]*Shandong Prevention and Control Engineering Laboratory of Endocrine and Metabolic Diseases, Jinan, Shandong 250021, China*
[7]*The Affiliated Hospital of Shandong University of Traditional Chinese Medicine, Jinan, Shandong, China*

Correspondence should be addressed to Shumin Mu; yaya2009@126.com and Jiajun Zhao; jjzhao@sdu.edu.cn

Received 9 February 2022; Accepted 8 March 2022; Published 5 April 2022

Academic Editor: Enfa Zhao

Objective. Astragalus mongholicus Bunge [Fabaceae] (AMB), a traditional Chinese medicine (TCM), has been widely used to treat liver diseases in the clinic. However, the efficacy and mechanism of AMB in the treatment of nonalcoholic fatty liver disease (NAFLD) remain unclear. The purpose of this study was to systematically investigate the active components and mechanisms of AMB against NAFLD based on network pharmacology, molecular docking, and experimental verification. *Methods*. First, the bioactive components and relevant targets of AMB were screened from the Traditional Chinese Medicine Systematic Pharmacology (TCMSP) database, and NAFLD-related targets were obtained from the GeneCards database. Then, the AMB-NAFLD protein target interaction network was built by the STRING database. GO and KEGG pathway enrichment analyses were performed using the DAVID database. The component targets were visualized using Cytoscape software. Finally, molecular docking and experiments were used to verify the results of network pharmacological prediction. *Results*. Network pharmacology predicted that quercetin may be the main active component in AMB, and the TNF and MAPK signaling pathways may be the key targets of AMB against NAFLD. Molecular docking validation results demonstrated that quercetin, as the main active component of AMB, had the highest binding affinity with TNF. Furthermore, quercetin played a distinct role in alleviating NAFLD through in vitro experiments. Quercetin upregulated the phosphorylation levels of AMPK and inhibited the expression of p-MAPK and TNF-α. In addition, we further discovered that quercetin could increase ACC phosphorylation and CPT1α expression in PA-induced HepG2 cells. *Conclusions*. Our results indicated that quercetin, as the main active component in AMB, exerts an anti-NAFLD effect by regulating the AMPK/MAPK/TNF-α and AMPK/ACC/CPT1α signaling pathways to inhibit inflammation and alleviate lipid accumulation.

1. Introduction

Nonalcoholic fatty liver disease (NAFLD) refers to excessive lipid deposition in hepatocytes that has become a leading cause of chronic liver disease worldwide, with a prevalence of 25% in adults [1, 2]. NAFLD has a wide range of hepatic pathological features that range from simple hepatic lipid accumulation to nonalcoholic steatohepatitis (NASH) and even progress to cirrhosis and hepatocellular carcinoma. Due to this progressive feature, even NAFLD patients with

simple steatosis may eventually lead to an increase in all-cause mortality [3]. Multiple parallel hits have been widely used to explain the pathogenesis of NAFLD, including inflammation, insulin resistance, and oxidative stress [4]. NAFLD has become a global public health issue that cannot be ignored. However, there are currently no approved drugs to treat NAFLD. Paying attention to a healthy diet and regular exercise are the primary therapeutic modalities for NAFLD, but few adherents have been successful [5]. Therefore, developing natural products with clinical therapeutic potential is of great significance and has received widespread attention from society in recent years.

Astragalus mongholicus Bunge [Fabaceae] (ABM) is one of the most widely used traditional Chinese medicines (TCMs) in clinics and is widely distributed in Northeast, North, and Northwest China as well as in Mongolia and Korea [6]. The root of AMB [Fabaceae] is medicinal and has been used for many years in traditional Chinese medicine to treat chronic fatigue, weakness, anemia, loss of appetite, uterine bleeding, and uterine prolapses [7]. Modern pharmacology has confirmed that this herb possesses a variety of activities, including regulating immunity [8], anti-inflammatory [9], antioxidant [10], and antihyperglycemic [9] activities. To date, it has been reported that more than 100 compounds have been isolated and identified in AMB, such as saponins, flavonoids, polysaccharide amino acids, and trace elements with various biological activities [11]. Previous studies suggested that AMB possessed hepatoprotective effects. For example, Huang-Qi San had a significant effect on improving glucose, lipid metabolism, and liver steatosis in high-fat rats [12]. Notwithstanding extensive research efforts, the main active components in AMB and their anti-NAFLD mechanisms have thus far unclear.

Due to the characteristics of multicomponents and multitargets, traditional experimental methods cannot systematically explain the pharmacological mechanism of TCM. Thus, we adopted network pharmacology analysis based on bioinformatics and systems biology to carry out the research [13]. Network pharmacology systematically reveals the complex relationship between drugs and diseases by constructing biological networks and visualizing the network to analyze potential active ingredients, pivotal targets, signaling pathways, and diseases [14]. It is a powerful tool to improve drug efficacy and accelerate drug research and development. The holistic and systematic features of network pharmacology are consistent with the holistic view of TCM and the principles of syndrome differentiation and treatment. Molecular docking is a computational method used to study the interactions between molecules [15]. The purpose is to predict the binding model of small molecule drugs and large molecule proteins. It is also commonly used to verify the accuracy of network pharmacological predictions.

In this study, we first predicted the bioactive compounds and mechanisms of ABM in ameliorating NAFLD based on network pharmacology. Then, molecular docking technology and experiments were utilized to verify the reliability and accuracy of the above results. To our knowledge, this study is the first to reveal the effect and mechanisms of AMB against NAFLD based on network pharmacology, molecular docking, and experimental validation. This research was carried out to provide a theoretical basis for AMB in the treatment of NAFLD. The workflow is shown in Figure 1.

2. Materials and Methods

2.1. Screening Active Components and Targets of AMB. The related chemical components of AMB were obtained from the Chinese Medicine System Pharmacology Database (TCMSP, http://lsp.nwu.edu.cn/tcmsp.php). Then, oral bioavailability (OB) ≥ 30% and drug – like quality (DL) ≥ 0.18 were defined as important ADME-related pharmacokinetic parameters for identifying active ingredients in AMB [16]. OB refers to the amount of medicine that reaches the blood circulation after oral administration [17]. DL represents the similarity between components and known drugs that can optimize pharmacokinetics [18]. Subsequently, the compound-related protein targets screened above were searched in TCMSP.

2.2. Predicting NAFLD-Related Targets. Information on NAFLD-related targets were obtained from the GeneCards database (https://www.genecards.org/), a comprehensive functional database that contains genomics, proteomics, and transcriptomics [19]. "nonalcoholic fatty liver disease" was selected as a keyword to search disease targets for the subsequent study. A Venn diagram was drawn based on the intersection targets of AMB and NAFLD.

2.3. Protein-Protein Interaction (PPI) Network Construction. The PPI network was constructed based on the STRING database (https://string-db.org/). Its function is to visually present the direct or indirect interactions between proteins. First, the common component-disease targets were entered into the STRING database and selected within the scope of "Homo sapiens". PPI information was exported in tab-separated value (TSV) format with confidence score set to 0.4. Then, the results in TSV format were imported into Cytoscape (version 3.7.2; https://www.cytoscape.org/) software to visualize the protein interactions.

2.4. Network Construction. Cytoscape 3.7.2 software can be used to generate a visual network that reflects the interaction between the active compounds, potential targets, and pathways [20]. The network was composed of dots and lines. The nodes represent active ingredients, targets, or pathways, and the lines represent the interaction between them [14].

2.5. GO and KEGG Enrichment Pathway Analysis. Gene Ontology (GO) Knowledgebase and Kyoto Encyclopedia of Genes and Genomes (KEGG) pathway enrichment analyses of the common AMB-NAFLD targets were performed using the DAVID database (https://david.ncifcrf.gov/, ver. 6.8). GO analysis was used for gene functional classification analysis, including biological process (BP), molecular function (MF), and cell component (CC). A P value < 0.05 was employed for further analysis.

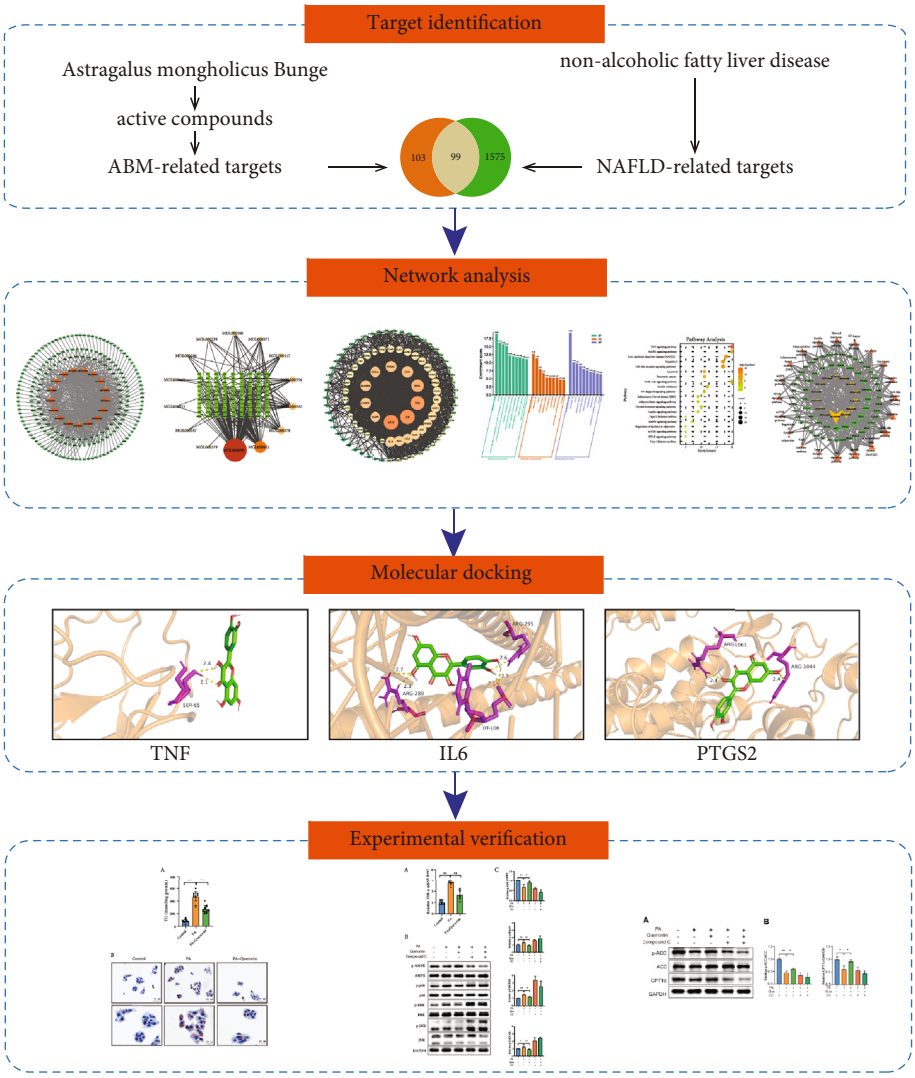

Figure 1: Flow chart of the pharmacological mechanisms of AMB against NAFLD.

2.6. Molecular Docking Validation. To validate the binding affinities of ingredient targets, molecular docking was performed using AutoDock Vina 1.5.6. [21]. First, quercetin, the main component in AMB, was used as a ligand. The key targets in the PPI network include AKT1, IL6, TNF, TP53, JUN, PTGS2, CXCL8, MAPK8, MMP9, and CASP3, which are used as protein receptors. On the one hand, for small-molecule compound components (compounds of AMB), their 2D structures (SDF format) were downloaded from the PubChem Database (https://pubchem.ncbi.nlm.nih.gov). Then, the SDF format was transformed to PDB format by minimizing energy using ChemBio3D software. Finally, they were preprocessed and saved in PDBQT format as docking ligands in AutoDock Tools software. On the other hand, for protein receptors, their X-ray crystal structures were obtained from the Protein Data Bank (PDB) (https://www1.rcsb.org/), including AKT1 (PDB ID: 1unq), IL6 (PDB ID: 6 mg1), TNF (PDB ID: 6q00), TP53 (PDB ID: 4cz5), JUN (PDB ID: 6osn), PTGS2 (PDB ID: 1pxx), CXCL8 (PDB ID: 4xdx), MAPK8 (PDB ID: 2xrw), MMP9 (PDB ID: 6esm), and CASP3 (PDB ID: 2dko). Afterwards, solvent and organic protein receptors were removed using PyMOL software and converted to pdbqt format through AutoDock Tools [22]. Finally, the location of the grid box was determined, and molecular docking results were visualized using AutoDock Vina. The binding activity between ligand and protein was evaluated by Vina score; the lower the Vina score was, the higher the binding affinity. The docking results were visualized by PyMOL software.

2.7. Chemicals and Reagents. Quercetin (C15H10O7, CAS No. 117-39-5, Cat No. A0083) were purchased from Chengdu Must Biotechnology Co. Ltd. (Chengdu, China). The purity of quercetin was >98% and kept protected from light and refrigerated at 4°C. Palmitic acid (PA) was dissolved in ethanol and mixed with fatty acid-free bovine serum albumin (BSA) to prepare stock solutions. The AMPK inhibitor compound C (P5499) was purchased from Sigma-Aldrich.

2.8. Cell Culture and Treatment. HepG2 cells were cultured in DMEM containing 10% fetal bovine serum (FBS) and

1% 100 U/mL penicillin–streptomycin at 37°C in a 5% CO_2 atmosphere. To mimic the NAFLD model in vitro, HepG2 cells were grown in medium containing palmitic acid (PA) at a concentration of 0.4 mM. The experiment was divided into three groups: the control group (BSA+DMSO), PA group (0.4 mM PA+DMSO), and PA+quercetin group (0.4 mM PA+25 μM quercetin). The overall experimental time was 24 hours. Moreover, HepG2 cells were cultured in the absence or presence of compound C (20 μM) to verify the specificity of quercetin in AMPK activation.

2.9. Cell Lipid Content Assay. Hepatocyte TG content was quantified using a commercial kit (Applygen Technologies Inc., Beijing, China). All experimental manipulations were performed in accordance with the manufacturer's instructions. In addition, oil red O staining was also used to assess lipid accumulation in cells. The cells were immobilized in 10% paraformaldehyde and then stained shielded from light. All pathological images were observed using a light microscope.

2.10. Quantitative Real-Time PCR. Total RNA was isolated from cell cultures using RNAiso plus reagent (TaKaRa) according to the manufacturer's instructions. Reverse transcription was performed using the PrimeScript RT reagent kit (TaKaRa). Real-time PCR was performed on a Roche LightCycler 480 (Roche, Mannheim, Germany) using SYBR Green (Bestar qPCR Mastermix, DBI, Germany). Relative gene expression levels were calculated by the $2^{-\triangle\triangle CT}$ method, and the results are expressed as the fold change relative to the control. The PCR primers used are shown in Table 1.

2.11. Western Blot Analysis. Total proteins were extracted from HepG2 cells using protease inhibitors and phosphatase inhibitors (Bimake, Houston, USA). Protein concentrations were measured using a BCA Protein Quantitative Assay Kit. The target proteins were blotted with the following antibodies: anti-phospho-p38 (CST, 4511), anti-p38 (CST, 9212), anti-phospho-ERK (CST, 4376), anti-ERK (CST, 4695), anti-phospho-JNK (CST, 4668), anti-JNK (CST, 9252), anti-phospho-AMPK (CST, 2535), anti-AMPK (CST, Thr172, 2532S), anti-phospho-ACC (CST, Ser79, 11818), anti-ACC (CST, 3662), anti-CPT1α (Abcam, ab128568), and anti-GAPDH (Proteintech, 60004-1-Ig). The appropriate secondary antibodies conjugated to horseradish peroxidase (HRP) (Amersham, Little Chalfont Bucks, UK) were used at a 1 : 5000 dilution. An Alpha Q detection system was used to visualize the bound primary antibodies.

2.12. Statistical Analysis. The data are presented as the mean ± standard deviation (SD). Statistical analysis was performed in GraphPad Prism 8.0 software. One-way analysis of variance (ANOVA) was performed to examine differences between multiple groups. A P value < 0.05 was considered statistically significant.

3. Results

3.1. The Active Compounds and Targets in AMB. Eighty-seven components of AMB were acquired from TCMSP. According to the screening standards of OB ≥ 30% and DL ≥ 0.18, 20 active components of AMB were finally obtained for subsequent research and analysis (Table 2). Then, 450 active component-targets of AMB were screened using the TCMSP database, and 202 component-targets were finally identified after the deletion of duplicates (Supplementary Table S1). To elucidate intuitive interactions between the components of AMB and their targets, we constructed a compound-target network using Cytoscape 3.7.2 (Figure 2(a)). The network contains 219 nodes and 465 edges, which means that one compound can correspond to multiple targets. The top three active ingredients were quercetin, kaempferol, and 7-O-methylisomucronulatol, which correspond to 142, 61, and 44 targets, respectively. The network suggested that these components may serve as the main therapeutic ingredients of AMB anti-NAFLD.

3.2. Potential Targets and Active Components of AMB in Anti-NAFLD. A total of 1674 NAFLD-related protein targets were downloaded from the GeneCards database (Supplementary Table S2). Furthermore, the 202 active component targets of AMB intersected with the NAFLD-related targets. Finally, 99 common targets were obtained and are shown in the form of a Venn diagram (Figure 2(b) and Supplementary Table S3). The 99 common targets mentioned above may be key potential targets for the treatment of NAFLD.

To identify the main anti-NAFLD effective component in AMB, we constructed a component-NAFLD target network (Figure 2(c)). The circular nodes represent potential active components in AMB, and the square represents the 99 common targets of AMB and NAFLD. The larger the node area is, the darker the color, indicating the more important components. As shown in Figure 2(d), quercetin (MOL000098) had the highest degree, suggesting that quercetin may be the most important active component of AMB against NAFLD.

3.3. PPI Network Analysis. To assess the protein-protein interactions, 99 common targets were uploaded to the STRING database. Then, Cytoscape 3.7.2 was used to build a visual PPI network (Figure 3). There were 97 nodes and 1476 edges in the PPI network. The larger and darker the color of nodes, the denser the lines indicating that the protein is more important. Finally, 10 hub targets were screened out according to betweenness (BC), and closeness (CC) values were ≥2 × median. [23] The top ten targets were AKT1, IL6, TNF, TP53, JUN, PTGS2, CXCL8, MAPK8, MMP9, and CASP3 (Table 3). These targets are likely to be the key targets of AMB in the treatment of NAFLD. Notably, these key targets were predicted mainly from quercetin.

3.4. GO Enrichment Analysis. To elucidate the biological function of therapeutic targets, 99 common component targets were uploaded to the DAVID database. A total of 486 GO terms were enriched according to the value of the

Table 1: Primer sequences of TNF-α and GAPDH.

Genes	Forward primer	Reverse primer
TNF-α	CACGCTCTTCTGCCTGCTG	GGCTTGTCACTCGGGGTTC
GAPDH	GGAGCGAGATCCCTCCAAAAT	GGCTGTTGTCATACTTCTCATGG

Table 2: Characteristics of active ingredients in ABM.

No.	Molecule ID	Molecule name	OB (%)	DL
1	MOL000098	Quercetin	46.43334812	0.27525
2	MOL000422	Kaempferol	41.88224954	0.24066
3	MOL000378	7-O-methylisomucronulatol	74.68613752	0.29792
4	MOL000392	Formononetin	69.67388061	0.21202
5	MOL000354	Isorhamnetin	49.60437705	0.306
6	MOL000371	3,9-Di-O-methylnissolin	53.74152673	0.47573
7	MOL000296	Hederagenin	36.91390583	0.75072
8	MOL000380	(6aR,11aR)-9,10-dimethoxy-6a,11a-dihydro-6H-benzofurano[3,2-c]chromen-3-ol	64.25545452	0.42486
9	MOL000417	Calycosin	47.75182783	0.24278
10	MOL000239	Jaranol	50.82881677	0.29148
11	MOL000387	Bifendate	31.09782391	0.66553
12	MOL000442	1,7-Dihydroxy-3,9-dimethoxy pterocarpene	39.04541112	0.47943
13	MOL000379	9,10-Dimethoxypterocarpan-3-O-β-D-glucoside	36.73668801	0.9243
14	MOL000433	FA	68.96043622	0.7057
15	MOL000033	(3S,8S,9S,10R,13R,14S,17R)-10,13-dimethyl-17-[(2R,5S)-5-propan-2-yloctan-2-yl]-2,3,4,7,8,9,11,12,14,15,16,17-dodecahydro-1H-cyclopenta[a]phenanthren-3-ol	36.22847056	0.78288
16	MOL000439	Isomucronulatol-7,2′-di-O-glucosiole	49.28105539	0.62065
17	MOL000211	Mairin	55.37707338	0.7761
18	MOL000374	5′-Hydroxyiso-muronulatol-2′,5′-di-O-glucoside	41.71766574	0.69251
19	MOL000398	Isoflavanone	109.9866565	0.29572
20	MOL000438	(3R)-3-(2-hydroxy-3,4-dimethoxyphenyl)chroman-7-ol	67.6674794	0.26479

OB, oral bioavailability; DL, drug-likeness.

parameter ($P \leq 0.05$). Among them, 383 GO terms were biological processes (BP) (Supplementary Table S4), 40 GO terms were cellular components (CC) (Supplementary Table S5), and 63 GO terms were molecular functions (MF) (Supplementary Table S6). The top 10 GO terms of BP, MF, and CC are shown in (Figure 4(a)).

3.5. KEGG Pathway Enrichment Analysis and Compound-Target-Pathway Network Construction. To further explore the signaling pathway of AMB against NAFLD, we performed KEGG pathway enrichment analysis based on 99 common component targets. After deleting the unrelated broad-spectrum pathway [24], we identified the top 20 pathways based on a P value < 0.05 (Figure 4(b)). Data analysis showed that targets were significantly enriched in multiple pathways, such as the TNF signaling pathway, MAPK signaling pathway, nonalcoholic fatty liver disease (NAFLD), and Toll-like receptor signaling pathway. The most significantly enriched pathway was the TNF signaling pathway.

Moreover, to further systematically clarify the molecular mechanism of AMB against NAFLD, the top 20 significantly enriched pathways, corresponding targets, and components were used to complete a component-target-pathway network (Figure 5). The size of the graph area is proportional to the degree value. Quercetin exhibits the highest number of genes and is considered the most represented active component among AMB. The TNF and MAPK signaling pathways were significantly enriched by the corresponding targets. Collectively, these results indicate that the therapeutic effects of AMB on NAFLD are achieved in a multitarget and multipathway manner.

3.6. Molecular Docking Verification. To further verify the potential targets of AMB against ANFLD, ten hub genes in the PPI were screened for molecular docking analysis with quercetin. Ten key genes were AKT1, IL6, TNF, TP53, JUN, PTGS2, CXCL8, MAPK8, MMP9, and CASP3. The results are shown in Table 4. The affinity value is a vital parameter for evaluating the binding strength between receptors and ligands. The lower the affinity value is, the stronger the binding force. Generally, an affinity value < −5 kcal/mol indicates good binding affinity, and an affinity score value <−7 kcal/mol indicates stronger adhesion of the receptor to ligands. The results revealed that quercetin docked well with all the key targets, which also demonstrates the accuracy of network pharmacology. In addition,

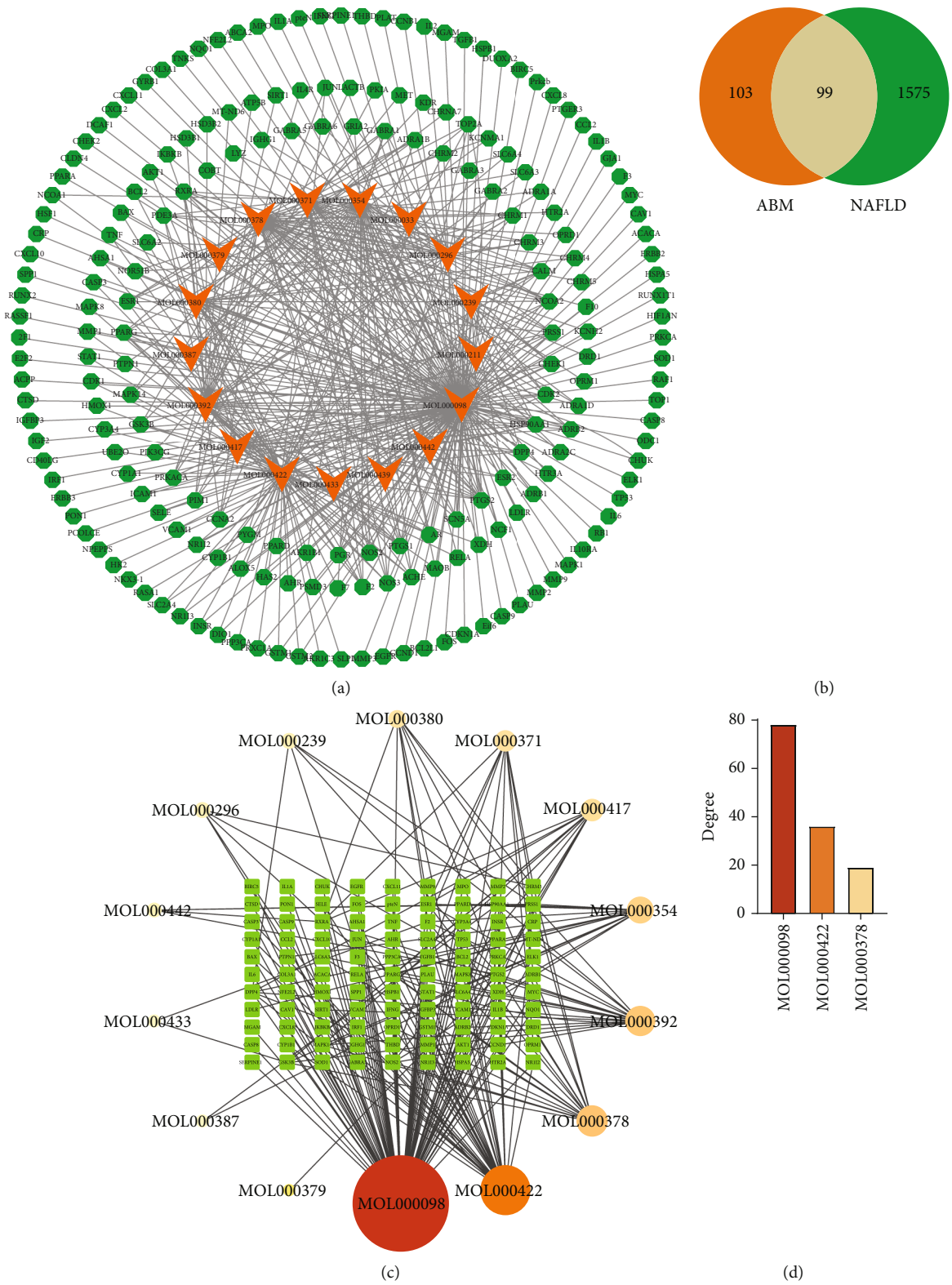

Figure 2: Compound-target network construction. (a) The component-target network of AMB. The orange triangles represent active compounds, and the green nodes represent component-related targets. (b) Venn diagram. The orange part represents the number of AMB targets, and the green part represents the number of NAFLD targets. (c) Compound-NAFLD targets network. The circular nodes represent potential active components in AMB, and the square represents the 99 common targets of AMB and NAFLD. (d) Degree of potential active compounds.

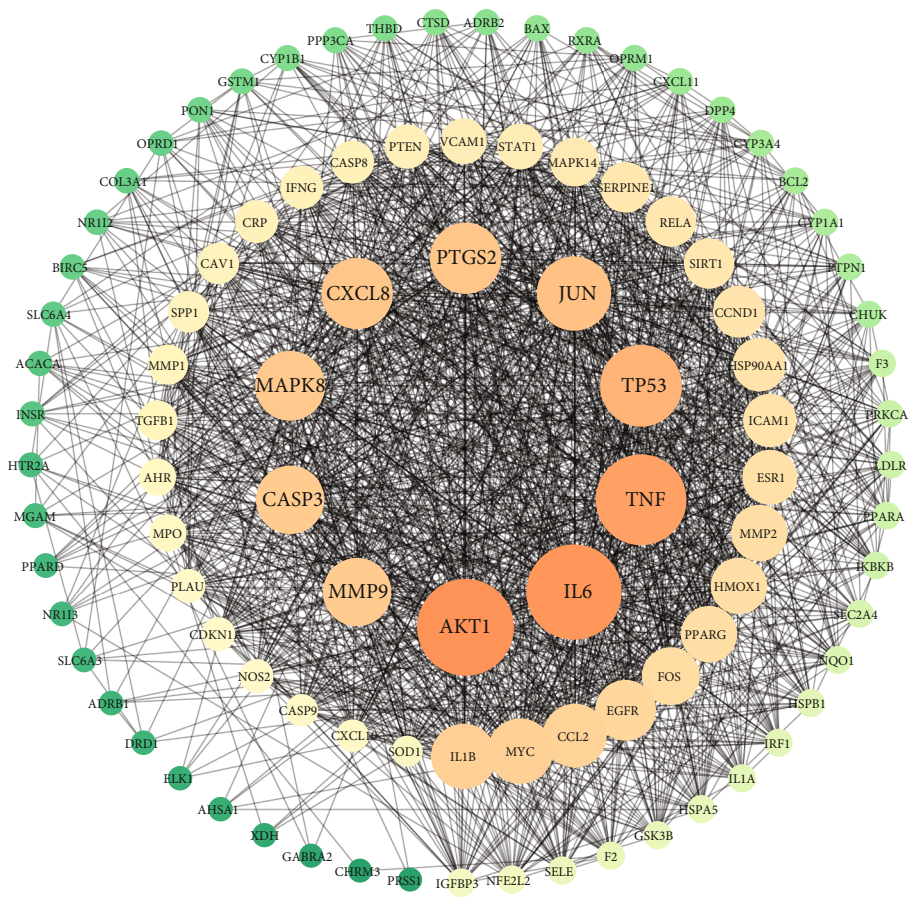

Figure 3: The protein-protein interaction (PPI) network analyze of overlapping targets. The color and depth of the nodes (orange → yellow → green) are in descending order of degree values, and node sizes are proportional to their degree.

Table 3: Ten key targets of ABM in treating NAFLD.

No.	Gene symbol	Description	Degree (DC)	Betweenness centrality (BC)
1	AKT1	RAC-alpha serine/threonine-protein kinase	76	0.09007483
2	IL6	Interleukin-6	75	0.06038545
3	TNF	Tumor necrosis factor	72	0.04427747
4	TP53	Cellular tumor antigen p53	66	0.02811782
5	JUN	Transcription factor AP-1	61	0.01848417
6	PTGS2	Prostaglandin G/H synthase 2	59	0.01631192
7	CXCL8	Interleukin-8	59	0.01898645
8	MAPK8	Mitogen-activated protein kinase 8	58	0.01679413
9	MMP9	Matrix metalloproteinase-9	57	0.02436033
10	CASP3	Caspase-3	57	0.01529514

quercetin had the highest binding affinity with TNF (-8.3 kcal/mol), while it had the second and third highest binding affinity with IL6 and PTGS2 (-7.6 and -7.5 kcal/mol). Therefore, the above results indicated that TNF is expected to be the most critical target of AMB against NAFLD. Moreover, 3 pairs with the highest docking scores were selected for 3D visualization (Figure 6). The binding of quercetin to TNF mainly occurs through hydrogen bond interactions with SER-65 (Figure 6(a)). Quercetin binds to IL-6 mainly through hydrogen bonding with ARG-295, DT-106, and ARG-289 (Figure 6(b)). The combination of quercetin and PTGS2 occurs mainly through hydrogen bonding interactions of ARG-1061 and ARG-1044 (Figure 6(c)). In addition, the accuracy of network pharmacology was confirmed by molecular docking.

3.7. Quercetin Exhibits the Anti-NAFLD Effect in PA-Induced HepG2 cells. To investigate the effect of quercetin on NAFLD, HepG2 cells were treated with quercetin (25 μM) in the presence or absence of PA (0.4 mM) for 24 h. PA-

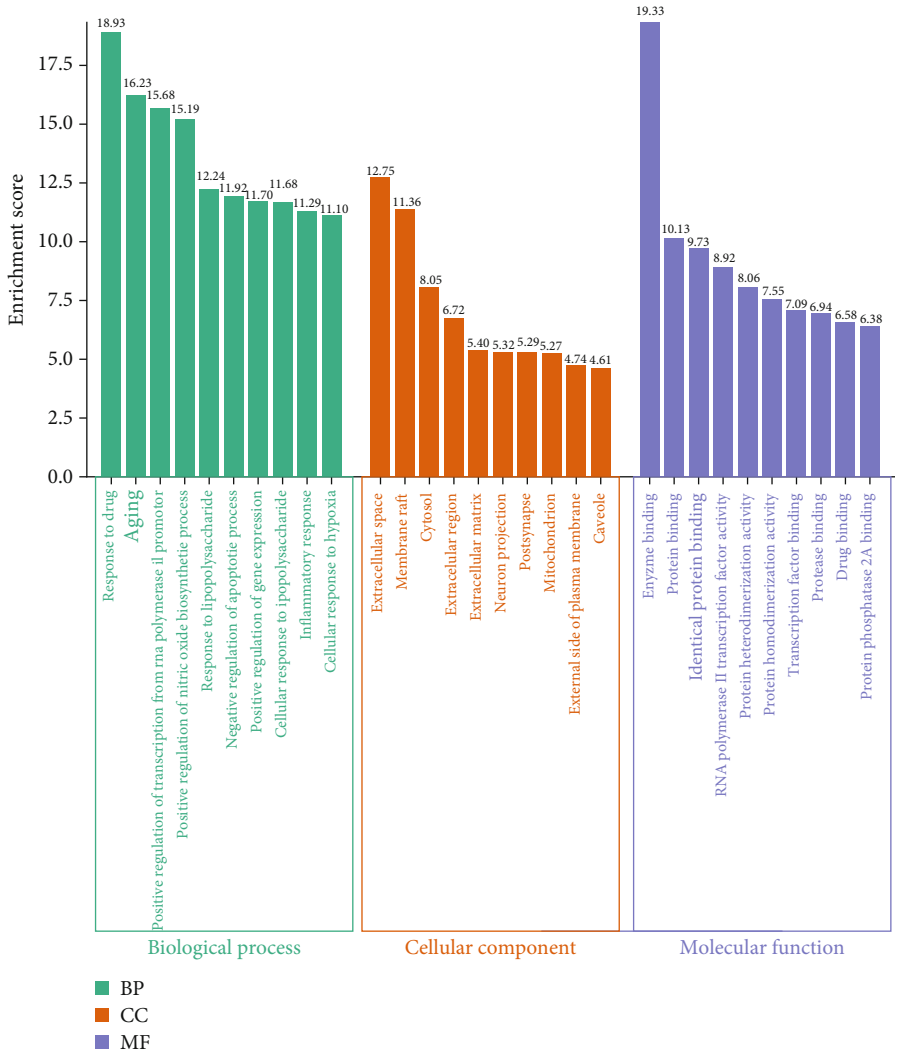

(a)

Figure 4: Continued.

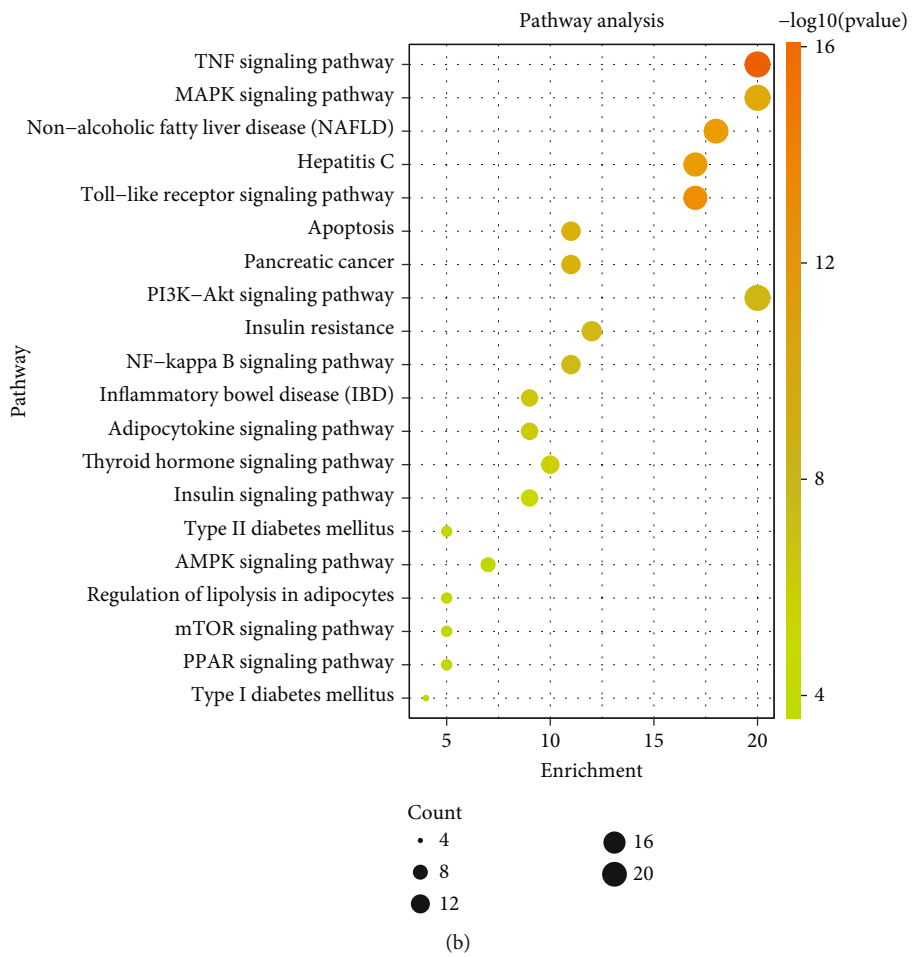

Figure 4: Overlapped term-based analysis. (a) GO enrichment analysis for the major targets of AMB against NAFLD. The green, orange, and purple color rectangles represent biological process (BP), cellular component (CC), and molecular function (MF), respectively. (b) The top 20 KEGG pathway analysis for the major targets of AMB against NAFLD.

induced HepG2 cells were used as the NAFLD model. The cell TG content results showed that TG levels were markedly higher in the PA group than in the control group. However, quercetin treatment significantly reduced cell TG levels (Figure 7(a)). The effect of quercetin on alleviating lipid accumulation in HepG2 cells was further confirmed by oil red O staining (Figure 7(b)). In summary, these studies suggested that quercetin exerts an anti-NAFLD effect in PA-induced HepG2 cells. Moreover, these results further highlighted that quercetin is the main active ingredient in AMB against NAFLD.

3.8. Quercetin Suppresses Inflammation by Regulating the AMPK/MAPK/TNF-α Signaling Pathway. To explore the mechanism of AMB against NAFLD, we first tested the idea that TNF might be a key therapeutic target for NAFLD predicted by network pharmacology and molecular docking. The real-time qPCR results showed that PA significantly increased TNF-α mRNA expression, while quercetin remarkably decreased PA-induced TNF-α mRNA levels in HepG2 cells (Figure 8(a)).

TNF-α is known to be regulated by MAPK signaling pathways [25, 26]. In addition, the MAPK signaling pathway was regarded as a significant pathway with the highest number of enriched genes in KEGG enrichment analysis. Thus, we investigated whether quercetin influences the expression of the MAPK signaling pathway. Consistent with previous reports, PA treatment enhanced the expression of p-p38, p-ERK, and p-JNK. However, this expression trend was reversed after quercetin treatment. No significant changes were observed in total p38, ERK, or JNK levels. Furthermore, we found that quercetin upregulated the phosphorylation levels of AMPK. To determine whether AMPK activation inhibited the expression of MAPK, we applied the AMPK inhibitor compound C to PA-induced HepG2 cells. The inhibitory effect of quercetin on the MAPK pathway was abolished by compound C (Figures 8(b) and 8(c)). Together, these data suggested that the AMPK/MAPK/TNF-α signaling pathways are involved in the anti-inflammatory effect of quercetin in PA-induced HepG2 cells.

3.9. Quercetin Alleviates Lipid Accumulation by Regulating the AMPK/ACC/CPT1α Signaling Pathway. To further elucidate the mechanism by which quercetin alleviates lipid accumulation, we detected the expression of proteins related to the fatty acid β-oxidation pathway. Acetyl-CoA carboxylase (ACC) is a

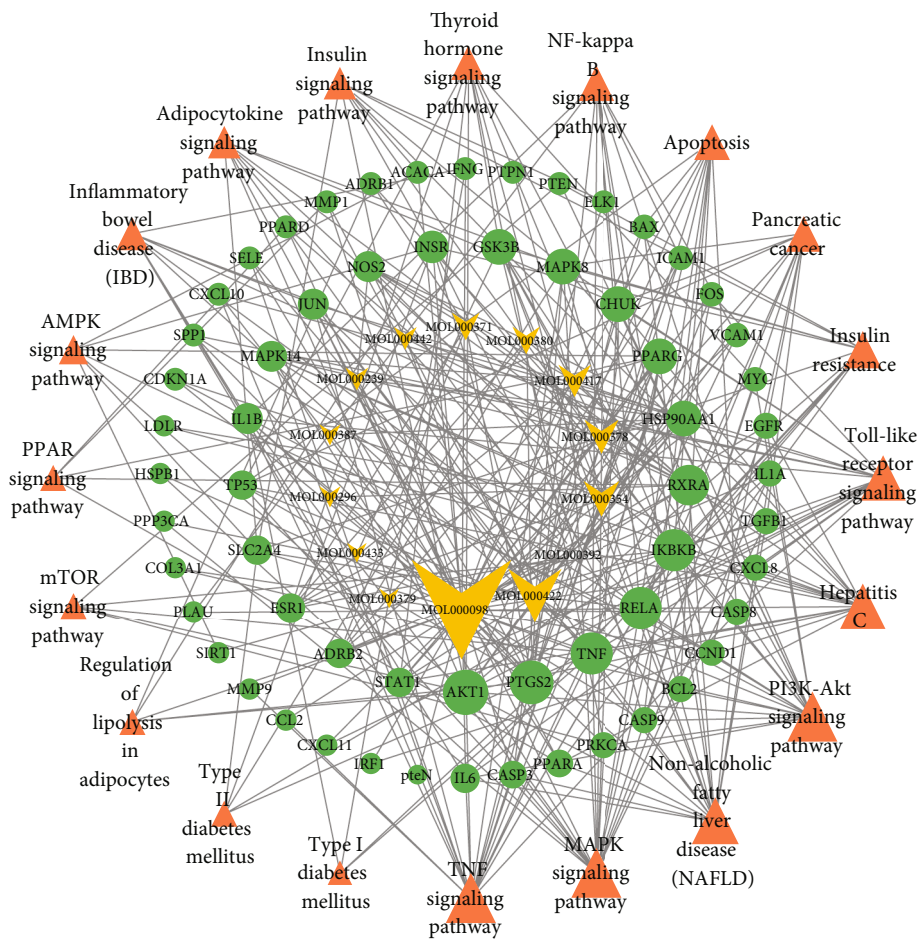

Figure 5: The component-target-pathway network constructed by Cytoscape. The yellow arrows represent active components of AMB, the green nodes represent the targets, and the orange triangles represent signaling pathways. Node sizes are proportional to their degree.

Table 4: Molecular docking parameters and results of ten key targets with quercetin.

Compounds	Target	PDB ID	Affinity (kcal/mol)
Quercetin	TNF	6q00	-8.3
Quercetin	IL6	6mg1	-7.6
Quercetin	PTGS2	1pxx	-7.5
Quercetin	TP53	4cz5	-7.3
Quercetin	CXCL8	4xdx	-7.3
Quercetin	MAPK8	2xrw	-7.2
Quercetin	CASP3	2dko	-6.8
Quercetin	JUN	6osn	-6.6
Quercetin	AKT1	1unq	-6.2
Quercetin	MMP9	6esm	-5.7

direct substrate of AMPK, and its phosphorylation level was increased after quercetin treatment. Quercetin also significantly enhanced the level of CPT1α. However, the upregulation of p-ACC and CPT1α was abrogated by compound C (Figure 9). In conclusion, these results indicated that quercetin alleviates lipid accumulation by activating AMPK/ACC/CPT1α signaling to increase fatty acid β-oxidation.

4. Discussion

NAFLD is a progressive disease. NAFLD refers to simple liver steatosis, which often occurs in the initial stage of the disease. NASH is defined as a more serious process accompanied by inflammation and liver cell damage, which can progress to liver cirrhosis and eventually liver cancer [27]. The complexity of the pathogenesis of NAFLD leads to significant challenges in its treatment. There are currently no relevant therapeutic drugs for NAFLD approved by the FDA [28]. To date, treatment targets focus on improving insulin resistance, reducing lipid deposition, and reducing inflammatory responses. According to relevant reports, AMB exhibits excellent hepatoprotective efficacy in clinical treatment by relieving inflammation and antioxidants [6]. However, the bioactive components and pharmacological mechanism of ABM against NAFLD have not been completely elucidated due to its multicomponent and multi-target features. Network pharmacology screens out numerous active components of TCM and comprehensively predicts multiple targets and pathways by building a systematic network [29]. Therefore, in the present study, we aimed to explore the active components and mechanisms of AMB in ameliorating NAFLD by integrating network pharmacology, molecular docking, and experimental verification.

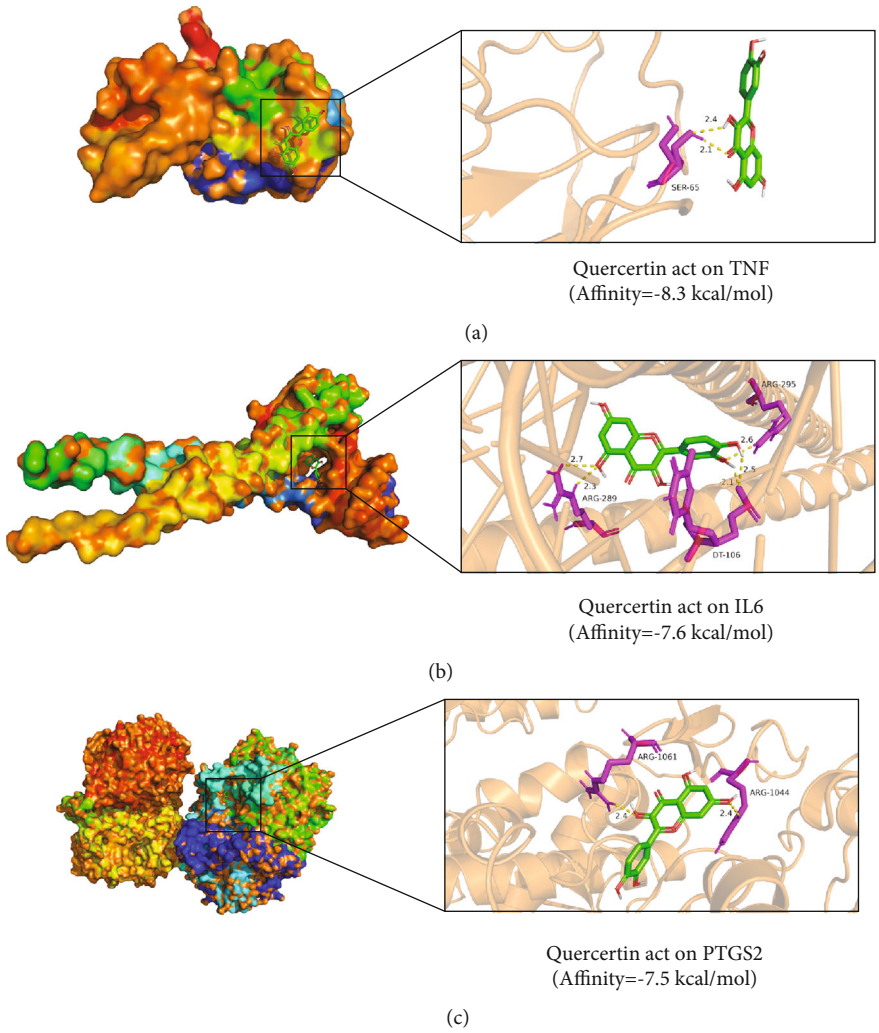

Figure 6: Molecular docking model of the top 3 key target proteins with the highest docking scores docked with quercetin. (a) TNF, (b) IL6, and (c) PTGS2.

First, network pharmacology predicted that ABM has the ability to improve NAFLD, and this effect is closely related to the regulation of the TNF-α and MAPK signaling pathways. Specifically, 20 active components of AMB and 202 component targets were screened from the TCMSP database. According to the topological value in the component-target network, the top three components in AMB were quercetin, kaempferol, and 7-O-methylisomucronulatol, suggesting that they are the key components of AMB anti-NAFLD. Quercetin was recognized as the component with the highest degree related to several NAFLD targets. Therefore, quercetin was selected as the most representative component of AMB for the follow-up study. Studies have indicated that quercetin protects the liver by promoting hepatic VLDL assembly [30]. Besides, quercetin improved NAFLD induced by T2DM, which was characterized by restoring abnormal liver enzymes and reducing hepatic lipid deposition in db/db mice [31]. Furthermore, quercetin not only improved liver steatosis but also alleviated liver fibrosis. The expression of proinflammatory factors and fibrogenic genes is decreased [32]. Despite numerous studies, the anti-NAFLD mechanisms remain ambiguous.

For other compounds studied, evidence showed that CYP2b9, Cyp4a12b, Mup17, Mup7, and Mup16 were differentially expressed genes for NASH treated with kaempferol through integrating transcriptomics and metabolomics [33]. Similarly, studies have confirmed that kaempferol can effectively alleviate the formation and development of liver fibrosis by selectively binding receptor–like kinase 5 and downregulating the TGF-β1/Smad pathway [34]. In general, several main active ingredients of AMB have different degrees of therapeutic effects on NAFLD.

PPI network analysis showed that the key genes of ABM against NAFLD were mainly related to inflammatory factors. The correlations of 99 common component-disease targets were presented in the PPI network, of which 10 hub genes were AKT1, IL6, TNF, TP53, JUN, PTGS2, CXCL8, MAPK8, MMP9, and CASP3. These genes play significant roles in glucose and lipid metabolism, the inflammatory response, and cell apoptosis. Meanwhile, the PPI network showed that

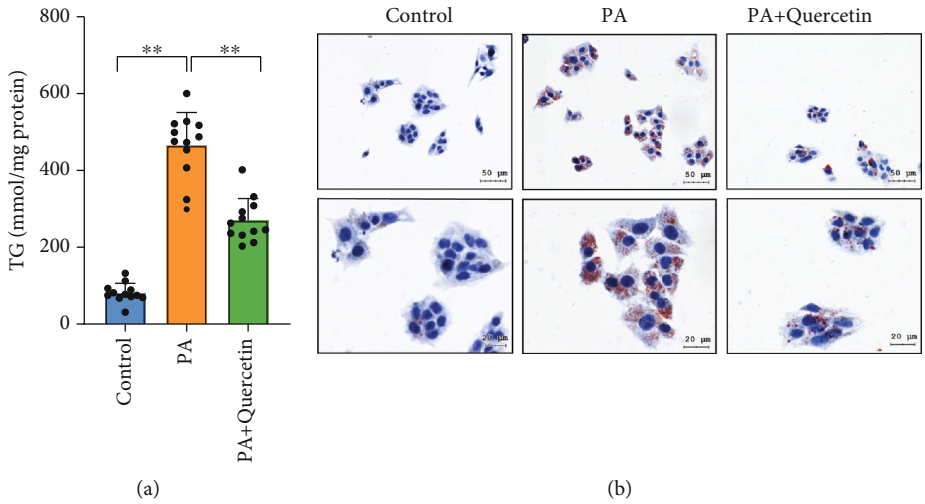

Figure 7: Anti-NAFLD effect of quercetin in PA-induced HepG2 cells. (a) TG contents in HepG2 cells treated with DMSO or 25 μM quercetin in response to BSA or 0.4 mM PA stimulation for 24 h ($n = 12$). Data are presented as the mean ± S.E.M. $^{*}P < 0.05$ and $^{**}P < 0.01$. (b) Oil red O staining showing that PA induced lipid accumulation, which was suppressed after quercetin treatment for 24 h in HepG2 cells ($n = 4$).

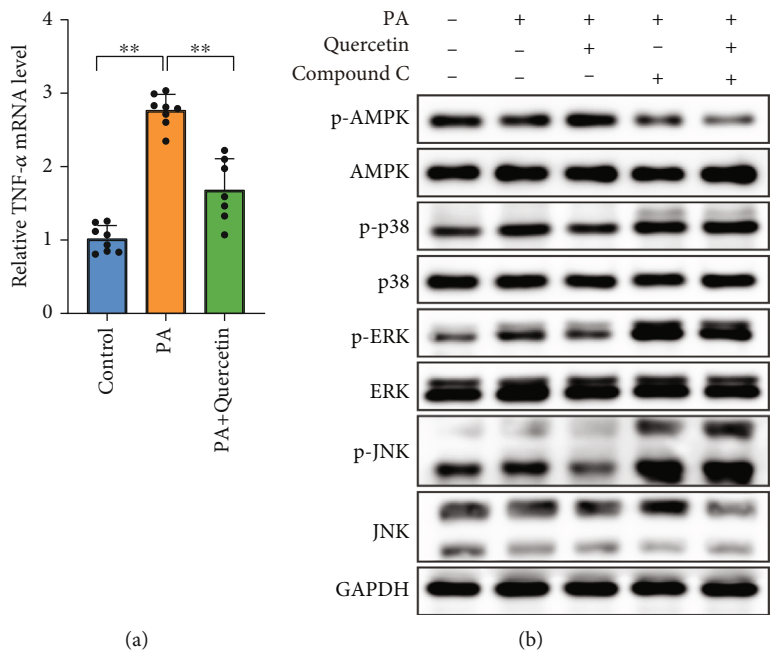

Figure 8: Continued.

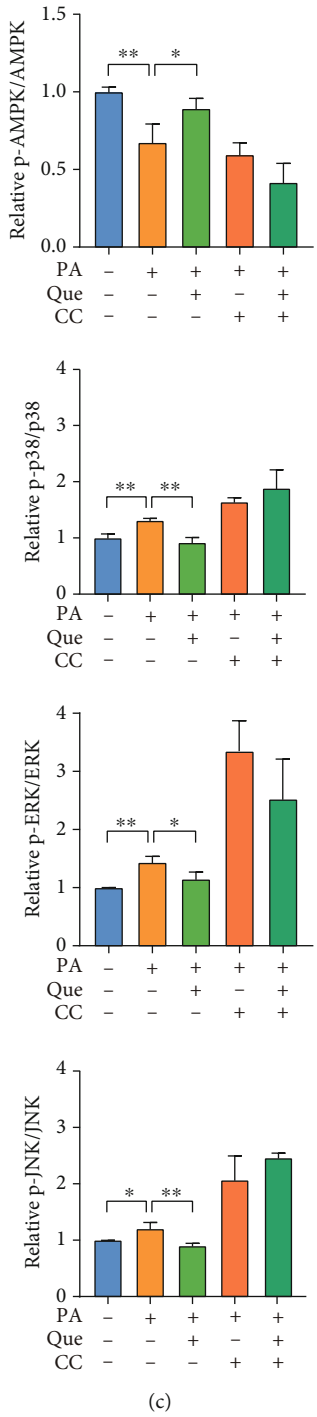

Figure 8: Quercetin suppresses inflammation by regulating the AMPK/MAPK/TNF-α signaling pathway in PA-induced HepG2 cells. (a) qPCR analyses of TNF-α mRNA levels in HepG2 cells stimulated by 0.4 mM PA with DMSO or 25 μM quercetin for 24 h ($n = 7 - 8$). (b) Western blot analysis of p-AMPK, AMPK, p-p38, p38, p-ERK, ERK, p-JNK, and JNK levels in HepG2 cells stimulated by PA with quercetin ($n = 3$). (c) Gray value analysis of p-AMPK/AMPK, p-p38/p38, p-ERK/ERK, and p-JNK/JNK. Data are presented as the mean ± S.E.M. $^{*}P < 0.05$ and $^{**}P < 0.01$.

99 common targets were not independent but interacted, suggesting that AMB treated NAFLD by regulating multiple proteins.

KEGG enrichment analysis indicated that ABM may exert its anti-NAFLD effect by regulating inflammation and metabolism-related pathways, such as the TNF signaling pathway, MAPK signaling pathway, Toll-like receptor signaling pathway, PI3K-Akt signaling pathway, insulin resistance, NF-kappa B signaling pathway, AMPK signaling pathway, and other signaling pathways. Hepatic lipid accumulation is the initial pathological hallmark of NAFLD, which can lead to inflammation, oxidative stress, and

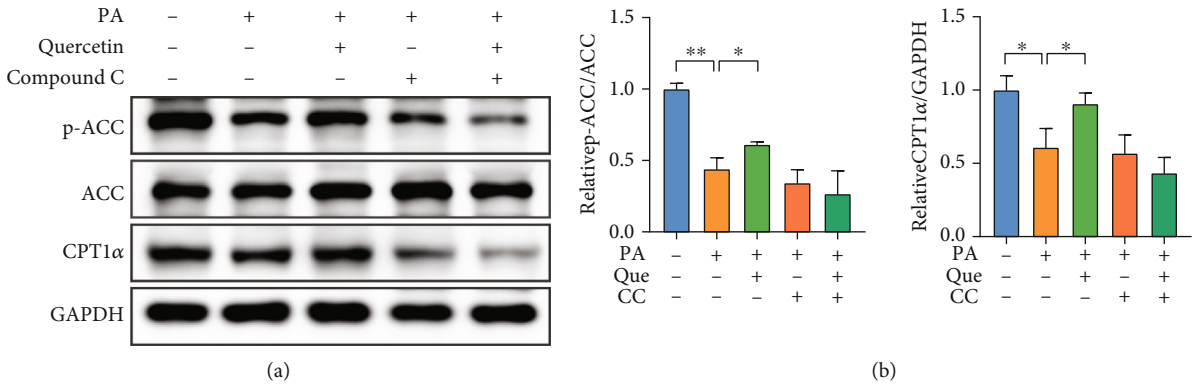

Figure 9: Quercetin increases fatty acid β-oxidation by regulating AMPK/ACC/CPT1α signaling in PA-induced HepG2 cells. (a) The protein expression levels of p-ACC, ACC, and CPT1α were examined by Western blot analysis in HepG2 cells ($n = 3$). (b) The gray value analysis of p-ACC, ACC, and CPT1α. Data are presented as the mean ± S.E.M. $^{*}P < 0.05$ and $^{**}P < 0.01$.

eventually liver cancer in the absence of effective interventions [35]. Here, we selected pathways with good correlation to discuss the mechanism of AMB in the treatment of NAFLD. The TNF signaling pathway was the most significantly enriched pathway, and the results were further verified by molecular docking. In recent years, as a convenient and effective emerging technology, molecular docking has been commonly used to predict the binding force between components and targets. All these results suggested that the TNF signaling pathway may be a potential effective target for AMB against NAFLD through network pharmacology analysis and molecular docking.

To further validate the results predicted by network pharmacology, in vitro experiments were performed. First, HepG2 cells were induced with PA to form a NAFLD model. NAFLD is characterized by excessive lipid deposition in hepatocytes, mainly triglycerides [36]. Our in vitro experimental results showed that quercetin significantly reduced the triglyceride content in HepG2 cells, which was further supported by oil red O staining. Based on the above evidence, we believe that quercetin has a role in ameliorating NAFLD.

Next, we examined the mechanism of AMB against NAFLD. Excessive lipid accumulation in hepatocytes is the pathological feature of NAFLD in the initial stage. Excessive fatty acids produce lipotoxic species that lead to inflammasome activation, oxidative stress, and ER stress. Inflammation, which plays a critical role in the pathogenesis of NASH, can promote the progression of liver fibrosis to cirrhosis [4]. In this study, we found that the TNF-α mRNA level was also significantly decreased by quercetin treatment compared to the PA group. TNF is an inflammatory cytokine with multiple biological effects, including promoting cell growth, differentiation, and apoptosis and inducing inflammation [37]. TNF is composed of TNF-α secreted by macrophages and TNF-β produced by T lymphocytes, of which TNF-α accounts for 70% to 95% of the total activity [38]. TNF-α is the accelerator that promotes the progression of hepatic steatosis to steatohepatitis and ultimately to liver fibrosis. A study including 52 obese patients demonstrated that the liver TNF-α mRNA level was higher in NASH patients than in the control group. Next, NASH patients were further classified according to the presence or absence of fibrosis. It was found that liver TNF-α mRNA expression in NASH patients with liver fibrosis was stronger than that in NASH patients without fibrosis. In addition, TNF-α mRNA expression in the adipose tissue of NASH patients with inflammation was strikingly elevated [39]. Another study revealed that TNF-α can activate stellate cells and accelerate the progression of NASH. Moreover, TNF also promoted insulin resistance and ultimately led to increased hepatic steatosis in patients with NAFLD [40]. Therefore, the development of a TNF-α inhibitor may be an effective therapeutic strategy for NAFLD. In an experiment, NASH model mice were given intraperitoneal injection of infliximab. As a result, anti-TNF-α reduced AST and ALT levels and ameliorated hepatic inflammation, necrosis, and fibrosis compared to the control group intraperitoneally injected with sterile saline solution [41]. Similarly, another study indicated that HFD-induced mice that received injection of infliximab had lower liver levels of IL-6, IL-1β, and IL-10 than HFD model mice. Furthermore, infliximab also improved insulin resistance and inhibited hepatic lipid deposition and fibrosis [42]. Altogether, the above results verified that TNF is a key target of AMB in the treatment of NAFLD, which also confirmed the accuracy of network pharmacology and molecular docking technology.

Interestingly, we also discovered that quercetin could downregulate the expression of MAPK signaling pathways, including ERK, p38, and JNK. The MAPK signaling pathway is closely related to cell growth, differentiation, apoptosis, and inflammation and consists of extracellular signal-regulated kinase (ERK), Jun N-terminal kinase (JNK), and p38 [43, 44]. The MAPK signaling pathway has attracted wide attention due to its involvement in regulating the expression of multiple genes related to NAFLD. Liver lipid deposition, inflammation, and fibrosis can be improved by suppressing the MAPK pathway in HFD-induced mice [45]. AMB extract can effectively inhibit the secretion and expression of IL-1β and TNF-α in macrophages. The mechanism is closely related to the regulation of the p38 MAPK and NF-κB signaling pathways [46]. In addition, the MAPK

signaling pathway was another significant pathway with the highest number of enriched genes in KEGG enrichment analysis.

Furthermore, in the present study, we found that quercetin could increase AMPK phosphorylation levels and that the inhibitory effect of quercetin on the MAPK signaling pathway was abolished by the AMPK inhibitor compound C in PA-induced HepG2 cells. These results indicate that the AMPK signaling pathway regulates the expression of MAPK and that MAPK is a downstream protein of AMPK. In addition, previous studies have illustrated that TNF-α can be activated by MAPK signaling pathways [47]. In summary, these data demonstrated that quercetin could ameliorate NAFLD by regulating the AMPK/MAPK/TNF-α signaling pathway to inhibit the inflammatory response.

Beyond this, we further explored the mechanism by which quercetin improves lipid metabolism because quercetin alleviates lipid accumulation in HepG2 cells, which was also consistent with literature reports [31, 48]. Hepatic lipid deposition is caused by an imbalance between lipogenesis and lipolysis. Mitochondrial fatty acid β-oxidation accelerates lipolysis, which contributes to reducing lipid deposition in hepatocytes. AMPK is regarded as a key factor that regulates energy metabolism homeostasis, and AMPK signaling pathway activation has been confirmed to have a protective effect on NAFLD [49]. ACC catalyzes the production of malonyl-CoA, which is an allosteric inhibitor of CPT1 [50]. Phosphorylation of ACC by AMPK inactivates ACC, which enhances the activity of CPT1 and fatty acid β-oxidation. In our current study, quercetin treatment significantly increased AMPK and ACC phosphorylation levels, which inhibited ACC activity, and ultimately, the expression of CPT1α was upregulated. However, this effect was abolished by the AMPK inhibitor compound C. Altogether, quercetin alleviated hepatic lipid accumulation by enhancing fatty acid β-oxidation through activating the AMPK/ACC/CPT1α signaling pathway in PA-induced HepG2 cells.

However, there were several limitations in the present study. First, although quercetin was considered to be the main component of AMB proven to have an anti-NAFLD effect, it could not fully represent AMB. Therefore, to elucidate the mechanism of AMB in the treatment of NAFLD, further experiments are essential. Second, this study only confirmed the effect and mechanism of quercetin against NAFLD in vitro. Thus, further in vivo experiments and clinical trials are needed to verify our conclusions.

5. Conclusion

In conclusion, this study adopted an integrated strategy that combined network pharmacology, molecular docking, and experimental verification to illustrate novel mechanisms of AMB in the treatment of NAFLD. Our findings revealed that quercetin, as the main active component of AMB, could inhibit the inflammatory response, enhance fatty acid β-oxidation, and alleviate hepatic lipid accumulation via the AMPK/MAPK/TNF-α and AMPK/ACC/CPT1α signaling pathways to exert its anti-NAFLD effect (Figure 10). This discovery not only provides a scientific basis for revealing the molecular mechanism of AMB in the treatment of NAFLD but also suggests a novel promising therapeutic strategy for anti-NAFLD.

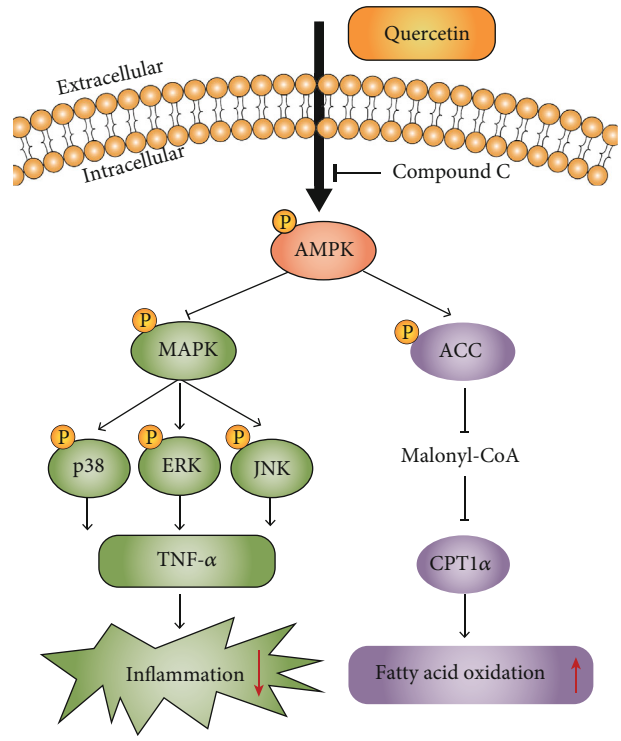

Figure 10: Quercetin exerts an anti-NAFLD effect by regulating the AMPK/MAPK/TNF-α and AMPK/ACC/CPT1α signaling pathways to inhibit inflammation and enhance fatty acid β-oxidation. Activation of AMPK by quercetin leads to downregulation of MAPK signaling pathways and decreases the expression of TNF-α, which may contribute to relieve inflammation. In addition, phospho-AMPK phosphorylates ACC, the rate-limiting enzyme of de novo lipogenesis. This decrease in ACC activity limits malonyl CoA production, relieving the inhibition of CPT-1α activity and enhancing fatty acid β-oxidation.

Data Availability

The original contributions presented in the study are included in the article/Supplementary Material, and further inquiries can be directed to the corresponding authors.

Conflicts of Interest

The authors declare no conflicts of interest for this work.

Authors' Contributions

The design of the study was performed by JJZ, SMM, and LLF, the study was performed by LLF, and technical assistance was performed by ZMW, YJC, WBC, and LG. All authors read and approved the final manuscript.

Acknowledgments

This work was supported by the Project of "Special Diseases Construction of Integrated Traditional Chinese and Western Medicine of Shandong Provincial Health and Family Planning Commission" (2019-2021), National Natural Science Foundation of China (82070819), Natural Science Foundation of Shandong Province (ZR2020MH103), and Jinan Science and Technology Plan (201907038).

Supplementary Materials

Table S1: the bioactive components and corresponding targets of ABM. Table S2: information of NAFLD-related targets collected from the GeneCards database. Table S3: the common targets of ABM and NAFLD. Table S4: the 383 biological process terms. Table S5: the 40 cellular component terms. Table S6: the 63 molecular function terms. *(Supplementary Materials)*

References

[1] Z. Younossi, Q. M. Anstee, M. Marietti et al., "Global burden of NAFLD and NASH: trends, predictions, risk factors and prevention," *Nature Reviews. Gastroenterology & Hepatology*, vol. 15, no. 1, pp. 11–20, 2018.

[2] G. Vernon, A. Baranova, and Z. M. Younossi, "Systematic review: the epidemiology and natural history of non-alcoholic fatty liver disease and non-alcoholic steatohepatitis in adults," *Alimentary Pharmacology & Therapeutics*, vol. 34, no. 3, pp. 274–285, 2011.

[3] H. Tilg and G. Targher, "NAFLD-related mortality: simple hepatic steatosis is not as 'benign' as thought," *Gut*, vol. 70, no. 7, pp. 1212-1213, 2021.

[4] S. L. Friedman, B. A. Neuschwander-Tetri, M. Rinella, and A. J. Sanyal, "Mechanisms of NAFLD development and therapeutic strategies," *Nature Medicine*, vol. 24, no. 7, pp. 908–922, 2018.

[5] W. N. Hannah Jr. and S. A. Harrison, "Lifestyle and dietary interventions in the management of nonalcoholic fatty liver disease," *Digestive Diseases and Sciences*, vol. 61, no. 5, pp. 1365–1374, 2016.

[6] J. Fu, Z. Wang, L. Huang et al., "Review of the botanical characteristics, phytochemistry, and pharmacology of Astragalus membranaceus (Huangqi)," *Phytotherapy Research*, vol. 28, no. 9, pp. 1275–1283, 2014.

[7] C. Kim, H. Ha, J. S. Kim, Y. T. Kim, S. C. Kwon, and S. W. Park, "Induction of growth hormone by the roots of Astragalus membranaceus in pituitary cell culture," *Archives of Pharmacal Research*, vol. 26, no. 1, pp. 34–39, 2003.

[8] E. Bedir, N. Pugh, I. Calis, D. S. Pasco, and I. A. Khan, "Immunostimulatory effects of cycloartane-type triterpene glycosides from astragalus species," *Biological & Pharmaceutical Bulletin*, vol. 23, no. 7, pp. 834–837, 2000.

[9] J. Y. Chan, F. C. Lam, P. C. Leung, C. T. Che, and K. P. Fung, "Antihyperglycemic and antioxidative effects of a herbal formulation of Radix Astragali, Radix Codonopsis and Cortex Lycii in a mouse model of type 2 diabetes mellitus," *Phytotherapy Research*, vol. 23, no. 5, pp. 658–665, 2009.

[10] D. H. Yu, Y. M. Bao, C. L. Wei, and L. J. An, "Studies of chemical constituents and their antioxidant activities from Astragalus mongholicus Bunge," *Biomedical and Environmental Sciences*, vol. 18, no. 5, pp. 297–301, 2005.

[11] F. Xu, Y. Zhang, S. Xiao et al., "Absorption and metabolism of Astragali radix decoction: in silico, in vitro, and a case study in vivo," *Drug Metabolism and Disposition*, vol. 34, no. 6, pp. 913–924, 2006.

[12] Y. Li, C. Wang, Y. Jin et al., "Huang-Qi San improves glucose and lipid metabolism and exerts protective effects against hepatic steatosis in high fat diet-fed rats," *Biomedicine & Pharmacotherapy*, vol. 126, article 109734, 2020.

[13] J. Zhang, R. Liang, L. Wang, and B. Yang, "Effects and mechanisms of Danshen-Shanzha herb-pair for atherosclerosis treatment using network pharmacology and experimental pharmacology," *Journal of Ethnopharmacology*, vol. 229, pp. 104–114, 2019.

[14] X. Shen, R. Yang, J. An, and X. Zhong, "Analysis of the molecular mechanisms of the effects of Prunella vulgaris against subacute thyroiditis based on network pharmacology," *Evidence-based Complementary and Alternative Medicine*, vol. 2020, Article ID 9810709, 13 pages, 2020.

[15] J. H. Wang, L. F. Zhao, H. F. Wang et al., "GenCLiP 3: mining human genes' functions and regulatory networks from PubMed based on co-occurrences and natural language processing," *Bioinformatics*, vol. 36, 2019.

[16] S. J. Yue, J. Liu, W. W. Feng et al., "System pharmacology-based dissection of the synergistic mechanism of Huangqi and Huanglian for diabetes mellitus," *Frontiers in Pharmacology*, vol. 8, p. 694, 2017.

[17] X. Xu, W. Zhang, C. Huang et al., "A novel chemometric method for the prediction of human oral bioavailability," *International Journal of Molecular Sciences*, vol. 13, no. 6, pp. 6964–6982, 2012.

[18] W. P. Walters and M. A. Murcko, "Prediction of 'drug-likeness'," *Advanced Drug Delivery Reviews*, vol. 54, no. 3, pp. 255–271, 2002.

[19] S. Paolacci, V. Precone, F. Acquaviva et al., "Genetics of lipedema: new perspectives on genetic research and molecular diagnoses," *European Review for Medical and Pharmacological Sciences*, vol. 23, no. 13, pp. 5581–5594, 2019.

[20] T. Qin, L. Wu, Q. Hua, Z. Song, Y. Pan, and T. Liu, "Prediction of the mechanisms of action of Shenkang in chronic kidney disease: a network pharmacology study and experimental validation," *Journal of Ethnopharmacology*, vol. 246, article 112128, 2020.

[21] O. Trott and A. J. Olson, "AutoDock Vina: improving the speed and accuracy of docking with a new scoring function, efficient optimization, and multithreading," *Journal of Computational Chemistry*, vol. 31, no. 2, pp. 455–461, 2010.

[22] S. Yuan, H. C. S. Chan, S. Filipek, and H. Vogel, "PyMOL and Inkscape bridge the data and the data visualization," *Structure*, vol. 24, no. 12, pp. 2041-2042, 2016.

[23] W. Song, S. Ni, Y. Fu, and Y. Wang, "Uncovering the mechanism of _Maxing Ganshi_ Decoction on asthma from a systematic perspective: A network pharmacology study," *Scientific Reports*, vol. 8, no. 1, p. 17362, 2018.

[24] X. Q. Shi, S. J. Yue, Y. P. Tang et al., "A network pharmacology approach to investigate the blood enriching mechanism of Danggui buxue decoction," *Journal of Ethnopharmacology*, vol. 235, pp. 227–242, 2019.

[25] G. Ye, C. Lin, Y. Zhang et al., "Quercetin alleviates neuropathic pain in the rat CCI model by mediating AMPK/MAPK pathway," *Journal of Pain Research*, vol. 14, pp. 1289–1301, 2021.

[26] S. Kempe, H. Kestler, A. Lasar, and T. Wirth, "NF-kappa B controls the global pro-inflammatory response in endothelial cells: evidence for the regulation of a pro-atherogenic program," *Nucleic Acids Research*, vol. 33, no. 16, pp. 5308–5319, 2005.

[27] Q. M. Anstee, G. Targher, and C. P. Day, "Progression of NAFLD to diabetes mellitus, cardiovascular disease or cirrhosis," *Nature Reviews. Gastroenterology & Hepatology*, vol. 10, no. 6, pp. 330–344, 2013.

[28] Z. M. Younossi, R. Loomba, M. E. Rinella et al., "Current and future therapeutic regimens for nonalcoholic fatty liver disease and nonalcoholic steatohepatitis," *Hepatology*, vol. 68, no. 1, pp. 361–371, 2018.

[29] S. Zheng, J. P. Baak, S. Li et al., "Network pharmacology analysis of the therapeutic mechanisms of the traditional Chinese herbal formula Lian Hua Qing Wen in Corona virus disease 2019 (COVID-19), gives fundamental support to the clinical use of LHQW," *Phytomedicine*, vol. 79, article 153336, 2020.

[30] X. Zhu, T. Xiong, P. Liu et al., "Quercetin ameliorates HFD-induced NAFLD by promoting hepatic VLDL assembly and lipophagy via the IRE1a/XBP1s pathway," *Food and Chemical Toxicology*, vol. 114, pp. 52–60, 2018.

[31] H. Yang, T. Yang, C. Heng et al., "Quercetin improves nonalcoholic fatty liver by ameliorating inflammation, oxidative stress, and lipid metabolism in db/db mice," *Phytotherapy Research*, vol. 33, no. 12, pp. 3140–3152, 2019.

[32] E. Marcolin, B. San-Miguel, D. Vallejo et al., "Quercetin treatment ameliorates inflammation and fibrosis in mice with nonalcoholic steatohepatitis," *The Journal of Nutrition*, vol. 142, no. 10, pp. 1821–1828, 2012.

[33] Y. Lu, M. Shao, H. Xiang, P. Zheng, T. Wu, and G. Ji, "Integrative transcriptomics and metabolomics explore the mechanism of kaempferol on improving nonalcoholic steatohepatitis," *Food & Function*, vol. 11, no. 11, pp. 10058–10069, 2020.

[34] T. Xu, S. Huang, Q. Huang et al., "Kaempferol attenuates liver fibrosis by inhibiting activin receptor-like kinase 5," *Journal of Cellular and Molecular Medicine*, vol. 23, no. 9, pp. 6403–6410, 2019.

[35] G. N. Dalekos, N. K. Gatselis, K. Zachou, and G. K. Koukoulis, "NAFLD and autoimmune hepatitis: do not judge a book by its cover," *European Journal of Internal Medicine*, vol. 75, pp. 1–9, 2020.

[36] M. Park, J. H. Yoo, Y. S. Lee, and H. J. Lee, "Lonicera caerulea extract attenuates non-alcoholic fatty liver disease in free fatty acid-induced HepG2 hepatocytes and in high fat diet-fed mice," *Nutrients*, vol. 11, no. 3, p. 494, 2019.

[37] J. Holbrook, S. Lara-Reyna, H. Jarosz-Griffiths, and M. F. McDermott, "Tumour necrosis factor signalling in health and disease," *F1000Research*, vol. 8, 2019.

[38] W. Li, X. Yang, T. Zheng et al., "TNF-α stimulates endothelial palmitic acid transcytosis and promotes insulin resistance," *Scientific Reports*, vol. 7, no. 1, p. 44659, 2017.

[39] J. Crespo, A. Cayon, P. Fernandez-Gil et al., "Gene expression of tumor necrosis factor alpha and TNF-receptors, p 55 and p 75, in nonalcoholic steatohepatitis patients," *Hepatology*, vol. 34, no. 6, pp. 1158–1163, 2001.

[40] D. Cai, M. Yuan, D. F. Frantz et al., "Local and systemic insulin resistance resulting from hepatic activation of IKK-beta and NF-kappa B," *Nature Medicine*, vol. 11, no. 2, pp. 183–190, 2005.

[41] S. S. Koca, I. H. Bahcecioglu, O. K. Poyrazoglu, I. H. Ozercan, K. Sahin, and B. Ustundag, "The treatment with antibody of TNF-alpha reduces the inflammation, necrosis and fibrosis in the non-alcoholic steatohepatitis induced by methionine- and choline-deficient diet," *Inflammation*, vol. 31, no. 2, pp. 91–98, 2008.

[42] R. Barbuio, M. Milanski, M. B. Bertolo, M. J. Saad, and L. A. Velloso, "Infliximab reverses steatosis and improves insulin signal transduction in liver of rats fed a high-fat diet," *The Journal of Endocrinology*, vol. 194, no. 3, pp. 539–550, 2007.

[43] L. Chang and M. Karin, "Mammalian MAP kinase signalling cascades," *Nature*, vol. 410, no. 6824, pp. 37–40, 2001.

[44] L. Santarpia, S. M. Lippman, and A. K. El-Naggar, "Targeting the MAPK-RAS-RAF signaling pathway in cancer therapy," *Expert Opinion on Therapeutic Targets*, vol. 16, no. 1, pp. 103–119, 2012.

[45] L. Wu, J. Sun, L. Liu et al., "Anti-toll-like receptor 2 antibody ameliorates hepatic injury, inflammation, fibrosis and steatosis in obesity-related metabolic disorder rats via regulating MAPK and NF-κB pathways," *International Immunopharmacology*, vol. 82, article 106368, 2020.

[46] Q. Qin, J. Niu, Z. Wang, W. Xu, Z. Qiao, and Y. Gu, "Astragalus membranaceus inhibits inflammation via phospho-P38 mitogen-activated protein kinase (MAPK) and nuclear factor (NF)-κB pathways in advanced glycation end product-stimulated macrophages," *International Journal of Molecular Sciences*, vol. 13, no. 7, pp. 8379–8387, 2012.

[47] C. Wu, W. Chen, J. He et al., "Interplay of m6A and H3K27 trimethylation restrains inflammation during bacterial infection," *Science Advances*, vol. 6, no. 34, article eaba0647, 2020.

[48] M. Wang, Y. Mao, B. Wang et al., "Quercetin improving lipid metabolism by regulating lipid metabolism pathway of ileum mucosa in broilers," *Oxidative Medicine and Cellular Longevity*, vol. 2020, Article ID 8686248, 17 pages, 2020.

[49] D. G. Hardie, F. A. Ross, and S. A. Hawley, "AMPK: a nutrient and energy sensor that maintains energy homeostasis," *Nature Reviews. Molecular Cell Biology*, vol. 13, no. 4, pp. 251–262, 2012.

[50] J. S. V. Lally, S. Ghoshal, D. K. DePeralta et al., "Inhibition of acetyl-CoA carboxylase by phosphorylation or the inhibitor ND-654 suppresses lipogenesis and hepatocellular carcinoma," *Cell Metabolism*, vol. 29, no. 1, pp. 174–182.e5, 2019.